

UNIVERSITAT POLITÈCNICA DE VALÈNCIA

INSTITUTO INTERUNIVERSITARIO DE RECONOCIMIENTO MOLECULAR Y

DESARROLLO TECNOLÓGICO - HOSPITAL UNIVERSITARI I POLITÈCNIC LA FE



**DEVELOPMENT OF RAPID DETECTION TESTS FOR
SARS-COV-2 AND OTHER PATHOGENS BASED ON
MATERIALS WITH MOLECULAR GATES**

PhD. THESIS

Submitted by

María Isabel Caballos Gómez

PhD. Supervisors:

Prof. Ramón Martínez Máñez

Prof. Elena Aznar Gimeno

València

November 2024



UNIVERSITAT
POLITÈCNICA
DE VALÈNCIA

RAMÓN MARTÍNEZ MÁÑEZ, Ph.D. in Chemistry and Professor at the *Universitat Politècnica de València* and ELENA AZNAR GIMENO, Ph.D. in Chemistry and Professor at the *Universitat Politècnica de València*.

CERTIFY:

That the work ***“Development of rapid detection tests for SARS-CoV-2 and other pathogens based on materials with molecular gates”*** has been developed by MARÍA ISABEL CABALLOS GÓMEZ under their supervision in the Instituto Interuniversitario de Investigación de Reconocimiento Molecular y Desarrollo Tecnológico (IDM) of the *Universitat Politècnica de València*, forming part of the Unidad Mixta UPV-IISLAFE de Nanomedicina y Sensores, as a Thesis Project in order to obtain the degree of Ph.D. in Biotechnology at the *Universitat Politècnica de València*.

Valencia, December 2024

Prof. Ramón Martínez Máñez

Prof. Elena Aznar Gimeno

Director

Directora

*A mis padres y a todas las personas que me
sostuvieron desde la distancia*

“In every job that must be done, there is an element of fun.”

- Mary Poppins

Agradecimientos

Acknowledgements

Aunque parecía que no llegaría ya estamos aquí, porque al final, poco a poco, todo se resuelve o como me gusta siempre pensar, “el tiempo ordena todo en su lugar”, y ahora no puedo más que pensar en los sentimientos agridulces que se me despiertan al ver que este momento de mi vida llega a su fin.

Para mí esta etapa predoctoral ha sido mucho más que un logro académico. Ha sido la formación de mi personalidad adulta, mi primer sueldo, mis primeras experiencias en una ciudad completamente nueva a la que a día de hoy puedo llamar hogar y, sobre todo, ha sido una etapa de autoconocimiento individual que la Isa de 24 años recién cumplidos no podía ni siquiera imaginar.

Estoy orgullosa, y por eso me gustaría también agradecerme a mí misma: por haber sido perseverante con mis objetivos, por haber sido capaz de adaptarme a un sitio completamente nuevo, por haber formado una familia y una red de apoyo desde cero y por supuesto por haber trabajado duro en cada proyecto científico y honrar a la niña que siempre soñó con investigar y crear cosas que pudieran ayudar a la sociedad.

Dicho esto, obviamente los siguientes agradecimientos van a mi familia: mis padres, mi hermano y mi tía Lole, que me han descolgado el teléfono al primer toque siempre que los he necesitado y que la semana de antes de ir de visita ya se empezaban a poner nerviosos. Aunque a veces soy demasiado independiente y paso un poco del móvil, sé que ellos saben todo lo que les quiero y que, obviamente, no podría haber llegado a ser la persona que soy hoy sin sus enseñanzas. El orgullo de mí que proyectan hace que me obligue a mejorar cada día.

AGRADECIMIENTOS

También tengo que agradecer a todas las personas que desde la distancia siempre han sabido mantenerse cerca, de una forma u otra, y han sacado siempre un hueco para vernos cuando se podía o escuchar cualquier problema de forma remota. Mis amigas del pueblo, Ana Mari, Ángela, Eva y en especial Marina, que todavía tiene la esperanza de que me mude a Carmona en algún momento y poder ir los viernes al Leo a tomarnos una cervecita. Tu cariño incondicional siempre me ha llegado intacto pese a estos 600 km que nos separan, no puedo ser más feliz de haber estado juntas en este crecimiento. Estoy esperando con ansias febrero.

A mis amigas de Sevilla (o de la uni mejor dicho): Carmen, Clara, Gara, María y Miryam, que son un salvavidas en este mundo precario e inestable llamado ciencia. Las biotecnólogas más brillantes que han salido de la Pablo de Olavide, y no porque sean mis amigas. Carmen, siempre me reconforta cuando estás incluida en cualquier plan porque al menos sé que hay alguien a los mandos, mamá pato por naturaleza siempre nos has cuidado incluso al borde de la exasperación. Clara, no sabes cuanto bien me haces cada día, siempre en las gracias y en las desgracias, porque a dramáticas no nos gana nadie, pero a simpáticas tampoco. Gara, es impresionante cómo pese a estar a tanta distancia, siempre te he sentido cerca y accesible cuando te he necesitado. María, gracias por tu sinceridad, por haberme enseñado a preparar un potaje de garbanzos en Trieste y porque sé que siendo más desastre aún que yo con la comunicación online siempre estás ahí. Miryam, tu futuro es brillante, todas confiamos en que nos vas a sacar de pobres, sigue así.

Por supuesto no puede faltar hacer mención especial a mi familia valenciana, aunque de valencianas tenemos poco. Ellas han sido el motivo principal de mi felicidad y de que me haya encontrado tan a gusto y tan en casa todos estos años. Mari Nieves, no sabes lo afortunada que me siento de haberte conocido, me acogiste en tu casa el primer día de conocernos y pusiste mi vida patas arriba. Si yo soy un poco polvorilla tú eres la chispa que faltaba para la explosión. Gracias por tantas charlas, por tu apoyo

incondicional, por seguirme en todas mis locuras y yo en las tuyas. Por tantos viajes y experiencias. Me llevo una hermana para toda la vida. Valencia no es lo mismo sin ti, aunque me reconforta saber que Santander te trata bien y que estando lejos siempre tendremos la excusa de un viajecito para vernos.

A mis chicas CIPF, Blanca y Elena, porque son el punto de cordura que a veces me falta. Blanca, eres calma, gracias por tu risa contagiosa y por haber estado siempre ahí en los momentos más importantes. Elena, como bien dijiste en los agradecimientos de tu tesis: “Lo que empezó en el gym fue mucho más allá” y pasamos de ser “gymsis” a ser “sis” a secas. Gracias por ser una tía tan guay, con tantas ganas de hacer cualquier plan inesperado, sé que siempre voy a poder contar contigo para una cervecita en el Cedro acompañada de charlita existencial, porque Nietzsche se queda en pañales al lado de nosotras. Te admiro infinito.

Gracias Marina, por ser la voz de la razón cuando me dejaba arrastrar por la desesperación, tanto con la tesis como con todo lo demás. Siempre he valorado muchísimo tus consejos y cómo nos has cuidado siempre a todas. Gracias por esas primeras clases de esquí, por tu paciencia y serenidad.

Gracias Alba y, sobre todo, perdona por tantos años de tocarte las narices siempre a tu derecha sentada (en el fondo no me arrepiento de nada). Hemos compartido más tiempo juntas estos cuatro años que literalmente con cualquier otra persona y solo puedo pensar en la suerte que he tenido de llamarte amiga y compañera. El laboratorio (y fuera de él) no hubiera sido lo mismo sin ti, en todos mis buenos recuerdos estás presente.

Y por supuesto quiero agradecer a nuestro último fichaje estrella, Andrea, por ser la guinda del pastel. Eres luz, cuando llegas a cualquier sitio la habitación se ilumina con tu alegría. Tus ganas y tu motivación me han ayudado mucho en esta última etapa predoctoral. Gracias por ser como eres, por abrirme las puertas de tu casa y por dejarme

AGRADECIMIENTOS

probar la paella más buena de toda Valencia. Sé que me llevo a una amiga para toda la vida.

Gracias a tantas otras personas, que han pasado a lo largo de estos cuatro años por mi vida, ya sea para quedarse o no, por todas las experiencias y sobre todo por tantas enseñanzas que han hecho que sea lo que soy hoy.

Con respecto a nuestro equipazo investigador no puede faltar dar las gracias a mis directores. Gracias Ramón, por confiar en mí y en mis ganas de hacer ciencia. Estos cuatro años de trabajo me han permitido desarrollarme como investigadora y aprender en un entorno privilegiado lleno de grandes investigadores y proyectos muy ambiciosos. Mi CV y yo te estamos eternamente agradecidos.

Gracias Elena, por el aire maternal con el que siempre nos has tratado, por dejarme meter mi coche en tu garaje cuando no sabía qué hacer con él durante la estancia y sobre todo por guiarme y aportar luz en mi investigación además de meterme en cualquier proyecto que pensaras que iba a ser bueno para mi futuro.

Gracias a la infinita lista de personas que conforman nuestro equipo, y es que las comidas y cenas de Navidad/Fallas son maravillosas con tanta gente. Gracias al resto de integrantes (y exintegrantes) de la Unidad Mixta de La Fe: Mari Carmen, Moloud, Sara, Luis, Estela, Ana y Clara por haberme guiado en mis primeros pasos y/o ayudarme hoy en día con cualquier cosa que necesite.

Mil gracias a los chicos y chicas del resto de “labs”, a los que entraron conmigo allá por el 2020 e inicios de 2021, Guille, Javi H., Javi M., los Davides, Miguel, Yoel, Juanjo, Giovanni y a los que ya estaban: Eva, Paula, Toni, Alba G., Andrea B., Angy, Serena, Marcia, Juanfran, Xente, Andrea E. y el resto. Especial mención a Andy por su infinita ayuda a lo largo de la tesis: siempre serás una chica de la Fe más.

Gracias a las personas que pasaron por el grupo dejando un buen recuerdo tras de sí, a Ale y Ara, así como a Gema, mi *roomie* en los últimos tiempos, me encantan nuestras cenas con charlita.

Mil gracias a las chicas de gestión, Tania y Eva B., por estar siempre accesibles y por su ayuda incondicional con todos los documentos y asuntos burocráticos que me costaba entender, así como a Laura, por ser tan paciente cuando la liamos un poco con las compras.

Y por supuesto no me puedo olvidar de las nuevas incorporaciones, el futuro del grupo está en vuestras manos: Carol, Carla, Víctor, las Sandras, Rocío, Paula, Alba O., las Marías, Lucía, Lara, Jordi, Jenni, Jessi, Isa, Guille F., Eva C., Edu y Pablo. Espero no dejarme a nadie.

Por último, pero no menos importante, gracias a todas las personitas que hicieron de mis tres meses de estancia una de las épocas más felices de mi vida. *Firenze sempre sarà nel mio cuore.*

Que esta tesis sirva como ejemplo de cómo con dedicación, constancia, trabajo duro y perseverancia se pueden conseguir grandes cosas.

Os quiero mucho a todos.

Isa.

AGRADECIMIENTOS

Resumen

La presente tesis doctoral titulada “**Development of rapid detection tests for SARS-CoV-2 and other pathogens based on materials with molecular gates**” se centra en el desarrollo de materiales avanzados de detección, diseñados para la identificación rápida de patógenos como SARS-CoV-2, *Xylella fastidiosa* y *Mycobacterium tuberculosis*. Para lograr este objetivo general, la investigación se estructura en cuatro metas específicas, las cuales se desarrollan a lo largo de los capítulos de esta tesis.

En el **primer capítulo**, se presenta el desarrollo de un sistema de detección basado en el soporte de alúmina anódica nanoporosa (NAA) combinado con puertas moleculares de ADN complementario para la detección del ADN genómico de *Xylella fastidiosa*. Este sistema aprovecha estas hebras como agente de bloqueo de los poros de la NAA, lo que permite una detección específica de este patógeno de gran relevancia en ecología y agricultura.

En el **segundo capítulo** se explora la creación de un sistema basado en materiales de alúmina con anticuerpos como puertas moleculares para la detección de *Mycobacterium tuberculosis*, el patógeno responsable de la tuberculosis. Este dispositivo busca brindar una detección específica mediante la implementación de anticuerpos que actúan como agentes de bloqueo de los poros a la vez que elemento reconocedor en el sistema.

El **tercer capítulo**, aborda el diseño, síntesis y evaluación de los sistemas de NAA funcionalizados con aptámeros para la detección temprana de SARS-CoV-2. El proyecto de investigación se enfoca en obtener una alta sensibilidad y selectividad para identificar el virus, dado su impacto en la salud pública y la importancia de su detección temprana para controlar la propagación del COVID-19.

Por último, el **cuarto capítulo** se desarrolló un novedoso sistema de detección para material genético de SARS-CoV-2, combinando el sistema CRISPR-Cas con el soporte de NAA funcionalizado con ADN de cadena simple. Esta metodología integró la especificidad de CRISPR-Cas con la amplificación de señal de los materiales de NAA, logrando detectar secuencias de oligonucleótidos específicos con alta precisión.

Todos los capítulos profundizan en la síntesis y caracterización de estos materiales con puertas moleculares, que se han diseñado para detectar biomoléculas de diferente naturaleza como pueden ser proteínas o secuencias específicas de ADN. Además, se estudian las dinámicas de liberación del indicador encapsulado en los poros en presencia de sus respectivos analitos e interferentes, lo cual es crucial para evaluar la eficiencia y viabilidad práctica de los materiales en aplicaciones reales. Los estudios demuestran cómo la interacción entre el analito y la puerta molecular desplaza a esta última dando lugar a la liberación controlada del colorante, funcionando como una señal medible que confirma la presencia del patógeno.

Estos avances en el diseño de sistemas de detección con puertas moleculares representan un importante progreso en los campos de reconocimiento y diagnóstico, ofreciendo métodos rápidos, altamente sensibles, selectivos y adaptables a la detección de un amplio rango de patógenos de importancia en la actualidad.

Resum

La present tesi doctoral titulada "**Development of rapid detection tests for SARS-CoV-2 and other pathogens based on materials with molecular gates**" se centra en el desenvolupament de materials avançats de detecció, dissenyats per a la identificació ràpida de patògens com SARS-CoV-2, *Xylella fastidiosa* i *Mycobacterium tuberculosis*. Per a assolir aquest objectiu general, la investigació s'estructura en quatre metes específiques, les quals es desenvolupen al llarg dels capítols d'aquesta tesi.

En el **primer capítol**, es presenta el desenvolupament d'un sistema de detecció basat en el suport d'alúmina anòdica nanoporosa (NAA) combinat amb portes moleculars d'ADN complementari per a la detecció de l'ADN genòmic de *Xylella fastidiosa*. Aquest sistema aprofita aquestes cadenes com a agent de bloqueig dels porus de la NAA, la qual cosa permet una detecció específica d'aquest patògen de gran rellevància en ecologia i agricultura.

En el **segon capítol** s'explora la creació d'un sistema basat en materials d'alúmina amb anticossos com a portes moleculars per a la detecció de *Mycobacterium tuberculosis*, el patògen responsable de la tuberculosi. Aquest dispositiu busca proporcionar una detecció específica mitjançant la implementació d'anticossos que actuen com a agents de bloqueig i reconeixement en el sistema.

El **tercer capítol** aborda el disseny, síntesi i avaluació dels sistemes de NAA funcionalitzats amb aptàmers per a la detecció primerenca de SARS-CoV-2. El projecte de recerca se centra en obtenir una alta sensibilitat i selectivitat per a identificar el virus, donat el seu impacte en la salut pública i la importància de la seua detecció primerenca per a controlar la propagació de la COVID-19.

Finalment, el **quart capítol** desenvolupa un innovador sistema de detecció per a material genètic de SARS-CoV-2, combinant el sistema CRISPR-Cas amb el suport de NAA funcionalitzat amb ADN de cadena simple. Aquesta metodologia integra l'especificitat de CRISPR-Cas amb l'amplificació de senyal dels materials de NAA, aconseguint detectar seqüències específiques d'oligonucleòtids amb alta precisió.

Tots els capítols profunditzen en la síntesi i caracterització d'aquests materials amb portes moleculars, que s'han dissenyat per a detectar diferents tipus d'analits, des de cèl·lules i proteïnes fins a seqüències específiques d'ADN. A més, s'estudien les dinàmiques d'alliberament de l'indicador encapsulat en els porus en presència dels seus respectius analits, la qual cosa és crucial per a avaluar l'eficiència i viabilitat pràctica dels materials en aplicacions reals. Els estudis demostren com la interacció entre l'analit i la porta molecular desplaça aquesta última, donant lloc a l'alliberament controlat del colorant i funcionant com un senyal mesurable que confirma la presència del patogen.

Aquests avanços en el disseny de sistemes de detecció amb portes moleculars representen un important progrés en els camps del reconeixement i diagnòstic, oferint mètodes ràpids, altament sensibles, selectius i adaptables per a la detecció d'un ampli rang de patògens d'importància actual.

Abstract

This doctoral thesis, titled "**Development of rapid detection tests for SARS-CoV-2 and other pathogens based on materials with molecular gates,**" focuses on the development of advanced detection materials, designed for the rapid identification of pathogens such as SARS-CoV-2, *Xylella fastidiosa*, and *Mycobacterium tuberculosis*. To achieve this aim, the research is structured into four specific goals, which are developed throughout the chapters of this thesis.

The **first chapter** presents the development of a detection system based on nanoporous anodic alumina (NAA) combined with complementary DNA molecular gates to detect the genomic DNA of *Xylella fastidiosa*. This system leverages these DNA strands as pore-blocking agents in the NAA, allowing a specific detection of this pathogen, which is highly relevant in ecology and agriculture.

The **second chapter** explores the development of a system based on alumina materials with antibodies as molecular gates to recognize *Mycobacterium tuberculosis*, the pathogen responsible for tuberculosis. This device aims to provide specific detection by implementing antibodies that act as blocking and recognition agents in the system.

The **third chapter** addresses the design, synthesis, and evaluation of NAA systems functionalized with aptamers for the early detection of SARS-CoV-2. This research project focuses on achieving high sensitivity and selectivity to identify the virus, given its impact on public health and the importance of early detection to control the spread of COVID-19.

Finally, the **fourth chapter** develops an innovative detection system for SARS-CoV-2 genetic material, combining the CRISPR-Cas system with an NAA support functionalized with single-stranded DNA. This methodology integrates the specificity of

ABSTRACT

CRISPR-Cas with the signal amplification of NAA materials, achieving highly precise detection of specific oligonucleotide sequences.

All chapters explore the synthesis and characterization of these gated materials, designed to detect analytes from different nature, from proteins to specific DNA sequences. In addition, the dynamics of the encapsulated indicator release within the pores are studied in the presence of their respective analytes, which is crucial for evaluating the efficiency and practical feasibility of these materials in real-world applications. The studies demonstrate how the interaction between the analyte and the molecular gate displaces the latter, resulting in the controlled release of the dye, acting as a measurable signal that confirms the presence of the pathogen.

These advances in the design of detection systems with molecular gates represent a significant step forward in the fields of recognition and diagnostics, offering rapid, highly sensitive, selective, and adaptable methods for detecting a wide range of pathogens of current importance.

Publications

Results of this PhD thesis and other contributions have resulted in the following scientific publications.

- Caballos, I.; Aranda, M.N.; López-Palacios, A.; Pla, L.; Santiago-Felipe, S.; Hernández-Montoto, A.; Tormo-Mas, M.A.; Pemán, J.; Gómez-Ruiz, M.D.; Calabuig, E.; Sánchez-Sendra, B.; Francés-Gómez, C.; Geller, R.; Aznar, E.; Martínez-Máñez, R. Aptamer-Capped Nanoporous Anodic Alumina for SARS-CoV-2 Spike Protein Detection. *Adv. Mater. Technol.* 2023, 8, 2201913. <https://doi.org/10.1002/admt.202201913>

- Submitted: Caballos, I.; Román-Écija, M.; Landa, B.B.; Aznar, E.; Martínez-Máñez, R. Advancements in Nanomaterial-Enhanced Biosensing for the Detection of *Xylella fastidiosa*.

- Submitted: Caballos, I.; Requena-Menéndez, A.; Montagud-Martínez, R.; Hernández-Montoto, A.; Navarro, D.; Martínez-Máñez, R.; Aznar, E.; Rodrigo, G. Nucleic Acid Detection with Gated Nanoporous Anodic Alumina and CRISPR-Cas12a.

- Under development: Caballos, I.; Gil-Brusola, A.; Martínez-Máñez, R.; Aznar, E. Targeted Detection of *Mycobacterium tuberculosis* Using an Antibody-Coated Nanoporous Anodic Alumina Biosensor for MPT64 Antigen: A Novel Approach for Tuberculosis Screening.

- Hernández-Montoto, M. N. Aranda, I. Caballos, A. López-Palacios, M. Á. Tormo-Mas, J. Pemán, M. P. Rodríguez, C. Picornell, E. Aznar, R. Martínez-Máñez, Human Papilloma Virus DNA Detection in Clinical Samples Using Fluorogenic Probes Based on Oligonucleotide Gated Nanoporous Anodic Alumina Films. *Adv. Healthcare Mater.* 2023, 12, 2203326. <https://doi.org/10.1002/adhm.202203326>

- Nieves, O.; Ortiz de Zárate, D.; Aznar, E.; Caballos, I.; Garrido, E.; Martínez-Máñez, R.; Dortu, F.; Bernier, D.; Mengual-Chuliá, B.; López-Labrador, F.X.; et al.

Development of Photonic Multi-Sensing Systems Based on Molecular Gates Biorecognition and Plasmonic Sensors: The PHOTONGATE Project. *Sensors* 2023, 23, 8548. <https://doi.org/10.3390/s23208548>

- Ortega-Reig, M.; Abarca, JM.; Aragón, P.; Aznar, E.; Bayón, A.; Caballos, I.; Escribano, S.... (2023). Fotovoz: Integrando la fotografía participativa en diferentes contextos docentes. Editorial Universitat Politècnica de València. 1152-1165. <https://doi.org/10.4995/INRED2023.2023.16687>

Abbreviations and Acronyms

A

- Abs.** Absorbance
- AFB1.** Aflatoxin B1
- AFM.** Atomic Force Microscopy
- ALD.** Atomic Layer Deposition
- APTES.** (3-Aminopropyl)triethoxysilane
- AU.** Arbitrary Units
- AuNR.** Gold NanoRods

B

- BCG.** Bacille Calmette-Guérin
- BSA.** Bovine serum albumin

C

- CBPQT⁴⁺.** Cyclobis(paraquat-p-phenylene)
- CD.** Carbon Dot
- CDC.** Centers of Disease Control and Prevention
- CECT.** Colección Española de Cultivos Tipo
- CM.** Competitive Media
- COVID-19.** Coronavirus Disease-19
- CRISPR.** Clustered Regularly Interspaced Short Palindromic Repeat
- crRNA.** CRISPR RNA
- CTAB.** Cetyltrimethylammonium bromide
- CVC.** Colorful Chlorosis
- CVD.** Chemical Vapor Deposition

D

DAS-ELISA. Double Antibody Sandwich Enzyme-linked immunosorbent assay

DETECTR. Cas12a-based DNA Endonuclease-Targeted CRISPR Technology

DNA. Deoxyribonucleic acid

DNase. Deoxyribonuclease

DNP. 1,5-dioxynaphthalene

DAS-ELISA. Double Antibody Sandwich Enzyme-linked immunosorbent assay

DETECTR. Cas12a-based DNA Endonuclease-Targeted CRISPR Technology

DNA. Deoxyribonucleic acid

DNase. Deoxyribonuclease

DNP. 1,5-dioxynaphthalene

E

EIDs. Emerging Infectious Diseases

EDXS. Energy Dispersive X-ray spectroscopy

ELISA. Enzyme-linked immunosorbent assay

EPPO. European and Mediterranean Plant Protection Organization

F

FBS. Fetal Bovine Serum

FRET. Fluorescence Resonance Energy Transfer

H

HIV. Human Immunodeficiency Virus

HPLC. High-performance liquid chromatography

HR-FESEM. High resolution field emission scanning electron microscopy

I

Ig. Immunoglobulin

IUPAC. International Union of Pure and Applied Chemistry

ICPTS. (3-isocyanatopropyl)triethoxysilane

L

LAMP. Loop-mediated Isothermal Amplification

LC. Liquid chromatography

LFA. Lateral Flow Assay

LOD. Limit of Detection

LRTIs. Lower Respiratory Tract Infections

M

MSNs. Mesoporous silica nanoparticles

mPCR. Multiplex Polymerase Chain Reaction

MOF. Metal Organic Framework

MRM. Multiple Reaction Monitoring

MSN. Mesoporous Silica Nanoparticles

NAA. Nanoporous Anodic Alumina

NBP. Nanobipyramid

N

NCBI. National Center for Biotechnology Information

NGS. Next Generation Sequencing

NPs. Nanoparticles

NPV. Negative Predictive Value

PAA. Porous Anodic Alumina

PAM. Protospacer Adjacent Motif

P

PBS. Phosphate Buffered Saline

PCR. Polymerase Chain Reaction

PD. Pierce's Disease

POC. Point of Care

PPD. Brazilian Pseudopeach Disease

PPV. Positive Predictive Value

Q

QD. Quantum Dot

RBD. Receptor Binding Domain

RBITC. Rhodamine B isothiocyanate

RhB. Rhodamine B

RNA. Ribonucleic acid

R

ROC. Receiver Operating Characteristics

RPA. Recombinase Polymerase Amplification

RPM. Revolutions per minute

RTIs. Respiratory Tract Infections

RT-PCR. Reverse Transcription Polymerase Chain Reaction

RSV. Respiratory Syncytial Virus

SAM. Self-Assembled Monolayer

SARS. Severe Acute Respiratory Syndrome

SELEX. Systematic Evolution of Ligands by Exponential Enrichment

S

SEM. Scanning electron microscopy

SPR. Surface Plasmon Resonance

ssDNA. Single-stranded DNA

STEM. Scanning transmission electron microscopy

SME. Small medium-sized Enterprises

- T**
- TB.** Tuberculosis
 - TEA.** Triethylamine
 - TEM.** Transmission electron microscopy
 - TEOS.** Tetraethylorthosilicate
 - TFF.** Tetrathiafulvalene
 - TGA.** Thermogravimetric analysis
- U**
- URTIs.** Upper Respiratory Tract Infections
 - UV.** Ultraviolet
- V**
- VEGF.** Vascular endothelial growth factor
 - VSV.** Vesicular Stomatitis Virus
- W**
- WGA.** Wheat Germ Agglutinin
 - WHO.** World Health Organization
 - WST-1.** Water-soluble tetrazolium salt

General index

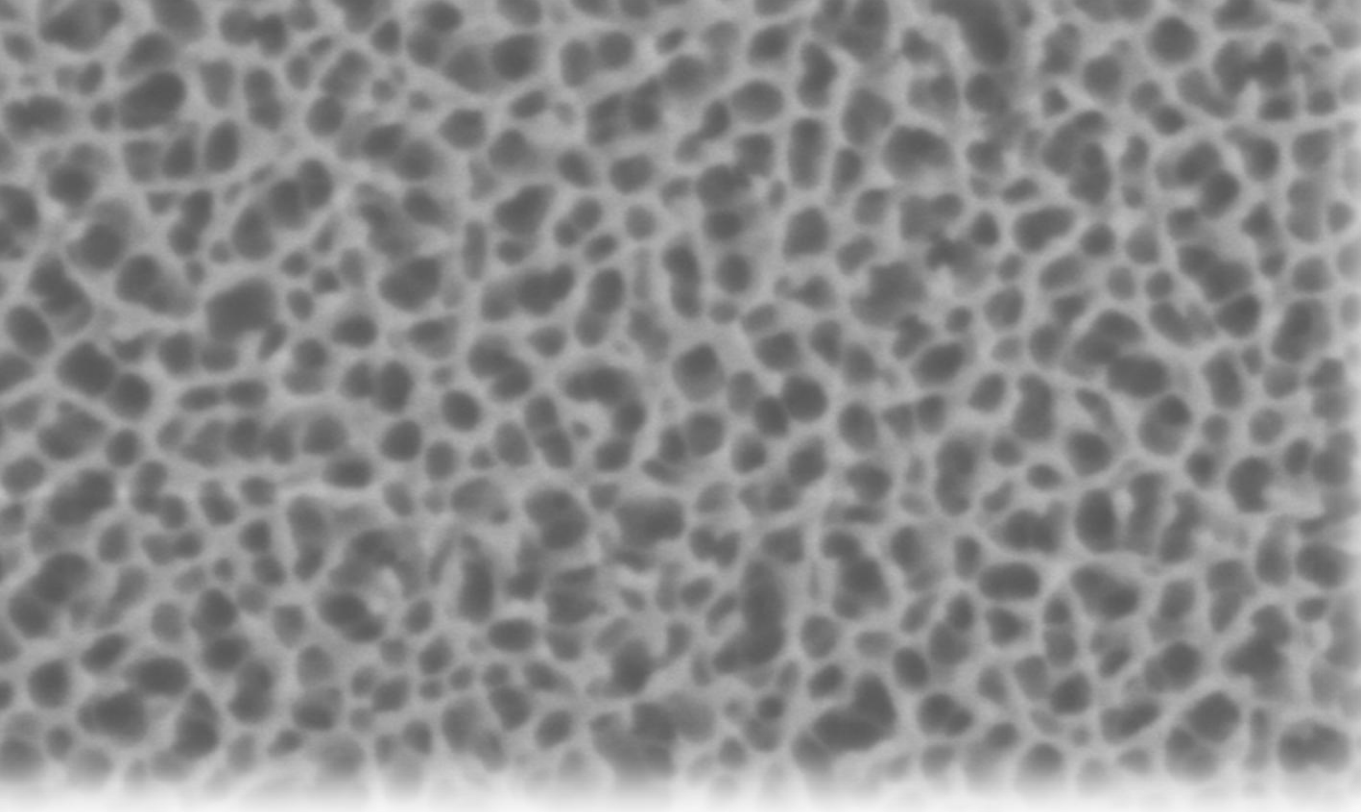
GENERAL INTRODUCTION	1
1. MOLECULAR RECOGNITION	4
1.1. <i>Sensors as an application of molecular recognition</i>	7
1.2. <i>Biosensors: Characteristics and classification</i>	15
1.3. <i>Current tendencies in biosensing</i>	24
2. NANOTECHNOLOGY	25
3. ORGANIC-INORGANIC HYBRID POROUS MATERIALS	28
3.1. <i>Types of porous materials</i>	30
3.2. <i>Porous anodic alumina (PAA)</i>	31
3.3. <i>Anodic alumina functionalization</i>	33
4. GATED MATERIALS	41
5. IMPORTANCE OF GLOBAL INFECTIOUS DISEASE CONTROL	49
5.1. <i>Vegetal-infecting pathogens</i>	50
5.2. <i>Animal-infecting pathogens</i>	54
5.2.1. <i>Pathogens and respiratory diseases</i>	56
6. REFERENCES	59
OBJECTIVES	83
CHAPTER I ADVANCEMENTS IN NANOMATERIAL-ENHANCED BIOSENSING FOR THE DETECTION OF XYLELLA FASTIDIOSA.....	87
1. ABSTRACT.....	90
2. INTRODUCTION.....	90
3. RESULTS AND DISCUSSION	96

3.1. Release assays	100
3.2. Stability evaluation in blank and inoculated competitive media	102
3.3. Sensitivity studies.....	103
3.4. Study of the system behavior with different sub-species of <i>Xylella fastidiosa</i>	105
3.5. Detection of <i>Xylella fastidiosa</i> in real field samples.....	106
4. CONCLUSION.....	109
5. MATERIALS AND METHODS.....	110
5.1. General techniques	110
5.2. Chemicals.....	110
5.3. Oligonucleotides design	110
5.4. Synthesis of support S_1	111
5.5. Synthesis of support S_2	111
5.6. Synthesis of support S_3	111
5.7. Synthesis of support S_3-O_2	111
5.8. Characterization of the prepared supports	112
5.9. Release experiments of support S_3-O_2	112
5.10. Plant extracts preparation	112
5.11. Samples validation.....	113
5.12. Statistical analysis.....	113
6. REFERENCES.....	114
CHAPTER II TARGETED DETECTION OF <i>MYCOBACTERIUM TUBERCULOSIS</i> USING AN ANTIBODY-COATED NANOPOROUS ANODIC ALUMINA BIOSENSOR FOR MPT64 ANTIGEN: A NOVEL APPROACH FOR TUBERCULOSIS SCREENING	121
1. ABSTRACT.....	124

2. INTRODUCTION	124
3. RESULTS AND DISCUSSION	131
3.1. <i>Design, synthesis and characterization of gated NAA materials</i>	131
3.2. <i>Purified antigen-triggered cargo release</i>	136
3.3. <i>Specificity and sensitivity assays</i>	136
3.4. <i>Detection of M. tuberculosis in competitive media and clinical samples</i>	139
4. CONCLUSIONS	144
5. MATERIALS AND METHODS	145
5.1. <i>Reagents</i>	145
5.2. <i>Material characterization</i>	146
5.3. <i>Linker peptide design</i>	146
5.4. <i>ELISA peptides assay</i>	146
5.5. <i>Synthesis of solids</i>	147
5.6. <i>Cargo quantification</i>	148
5.7. <i>Detection protocol</i>	148
5.8. <i>Quantification curve of MPT64 protein recognition</i>	149
5.9. <i>Specificity</i>	149
5.10. <i>Validation in competitive media</i>	150
5.11. <i>MPT64 detection in patient samples</i>	150
6. REFERENCES	151
CHAPTER III APTAMER-CAPPED NANOPOROUS ANODIC ALUMINA FOR SARS-COV-2 SPIKE PROTEIN DETECTION	157
1. ABSTRACT	161
2. INTRODUCTION	161

3. RESULTS AND DISCUSSION	165
3.1. <i>Synthesis and characterization of gated NAA</i>	165
3.2. <i>Release assays</i>	168
3.3. <i>Sensitivity and specificity studies</i>	170
3.4. <i>Detection of VSV-S in competitive media and inoculated clinical samples</i>	173
3.5. <i>Study of the system behavior with different S proteins from different SARS-CoV-2 variants of concern</i>	175
4. CONCLUSION.....	176
5. MATERIALS AND METHODS	177
5.1. <i>General Techniques</i>	177
5.2. <i>Reactives and reagents</i>	177
5.3. <i>Oligonucleotides Design</i>	177
5.4. <i>Synthesis of solids</i>	177
5.5. <i>Cargo quantification</i>	178
5.6. <i>Virus obtention</i>	178
5.7. <i>Detection protocol</i>	179
5.8. <i>Quantification curve of SARS-CoV-2 spike protein recognition</i>	180
5.9. <i>Selectivity</i>	180
5.10. <i>Validation in competitive media</i>	180
5.11. <i>Study of the system behavior with different VSV-S variants</i>	181
6. REFERENCES	181
7. SUPPORTING INFORMATION.....	186

CHAPTER IV NUCLEIC ACID DETECTION WITH GATED NANOPOROUS ANODIC ALUMINA AND CRISPR-CAS12A	191
1. ABSTRACT.....	194
2. INTRODUCTION.....	194
3. RESULTS AND DISCUSSION	198
3.1. <i>Design, synthesis, and characterization of gated NAA materials</i>	<i>198</i>
3.2. <i>CRISPR-Cas12a regulation of cargo release</i>	<i>202</i>
3.3. <i>Specificity and sensitivity assays.....</i>	<i>207</i>
3.4. <i>Detection of SARS-CoV-2 in clinical samples.....</i>	<i>209</i>
4. CONCLUSIONS.....	211
5. MATERIALS AND METHODS	212
5.1. <i>Reagents</i>	<i>212</i>
5.2. <i>Material characterization</i>	<i>213</i>
5.3. <i>Material preparation for release assays</i>	<i>213</i>
5.4. <i>CRISPR-Cas12a-based detection</i>	<i>214</i>
5.5. <i>Patient samples.....</i>	<i>215</i>
5.6. <i>Nucleic acid amplification by RT-RP.....</i>	<i>215</i>
5.7. <i>SARS-CoV-2 detection in patient samples.....</i>	<i>215</i>
5.8. <i>RT-qPCR validation.....</i>	<i>216</i>
6. REFERENCES.....	216
7. SUPPORTING INFORMATION	222
DISCUSSION	227
CONCLUSIONS.....	235



General Introduction

**Cover: FESEM image of raw NAA (self-produced image)*

Chemistry is one of the oldest and most productive sciences in enhancing the quality of human life. Everything that surrounds us, all that we perceive through our senses—whether by sight, sound, taste, smell, or touch—is the result of chemistry or some form of chemical reaction. As a fundamental science, chemistry impacts every aspect of our daily lives. From the food we consume to the personal hygiene products we use, and the medications that keep us healthy, chemistry lies at the heart of many technological innovations and scientific advances that improve our quality of life. Chemical products have enabled the development of stronger and lighter materials, cleaner and more efficient energy sources, and more sustainable and less polluting industrial processes. Chemistry intersects with a vast array of fields, including agriculture, biochemistry, geology, medicine, metallurgy, mineralogy, molecular biology, physics, and many others. Its interdisciplinary position between physics and biology allows for its application in numerous practical developments for humanity.

One of the most prominent fields in the application of chemistry is medicine and public health. The synthesis of new drugs and the development of advanced therapeutic treatments have extended life expectancy and significantly improved the quality of life for millions of people worldwide. Furthermore, chemistry has played a crucial role in agriculture by providing fertilizers and pesticides that increase crop productivity and ensure global food security.

To truly understand the world we live in and how we interact with it, we must dive into the vast ocean of chemistry, descending from the surface of simple certainties to the depths of the unknown. Chemistry revolves around the formation or destruction of molecular entities in pursuit of achieving a more stable state. The driving force behind all chemical processes is the attainment of the lowest energy state, which may involve the formation of new chemical bonds or the breaking of existing ones.

In 1960, researchers Pedersen, Cram, and Lehn introduced the groundbreaking concept of "Supramolecular Chemistry," which was later recognized with the Nobel Prize in 1987 (Lehn, 1988). Supramolecular chemistry explores the intricate formations that arise when two or more chemical species come together through intermolecular forces. These forces, which include hydrogen bonding, hydrophobic interactions, metal coordination, van der Waals forces, electrostatic effects, and π - π stacking interactions, are weak, non-covalent, and reversible, and can be tailored to meet specific objectives (J. L. Atwood, 2004).

Nature serves as a remarkable source of inspiration for advancing supramolecular chemistry. The complex nanostructures found in biological systems—such as enzymatic reactions, protein interactions, antigen-antibody associations, neurotransmission, genetic code processes, and oxygen transport—have been emulated in synthetic systems. However, the progress in this field cannot be attributed solely to nature's influence. From the outset, researchers have recognized the potential applications of supramolecular chemistry and molecular recognition in areas such as nanotechnology, particularly in the design of sensors and medical diagnostics, which has greatly contributed to its study.

1. MOLECULAR RECOGNITION

Molecular recognition is a fundamental concept in chemistry and biology, involving specific noncovalent interactions between molecules that enable the formation of complex structures. This concept, which gained popularity in the 1980s, underpins many processes in biological systems and has become a central theme in modern chemical research. The development of new technologies through the design of molecular recognition systems has expanded our understanding and capability to manipulate chemical and biological systems. Although the term "molecular recognition" may seem less innovative in contemporary chemistry, its significance remains profound, as it encompasses both intermolecular and intramolecular processes (Gellman, 1997).

Supramolecular chemistry has played a crucial role in advancing our understanding and application of molecular recognition. At its core, molecular recognition occurs when a receptor molecule identifies and interacts with a guest molecule in a manner that minimizes the total free energy of the resulting supramolecular structure. This interaction is highly selective and is driven by noncovalent forces such as hydrogen bonding, van der Waals forces, and electrostatic interactions. The principle of complementarity, often illustrated by the "lock and key" model (as shown in Figure 1), is central to this process, where the spatial and electronic alignment of binding sites between the host (receptor) and guest (substrate) molecules determines the specificity of recognition.

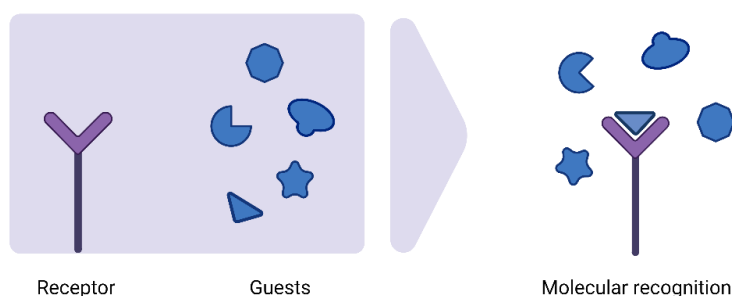


Figure 1. Molecular recognition interaction between molecules based on the lock-and-key model.

The concept of molecular recognition is not limited to simple binary interactions. It extends to the formation of larger supramolecular assemblies, where multiple molecules associate through specific recognition processes to design materials with well-defined internal structures. For instance, the formation of hydrogen bonds or coordination bonds in multiple binding sites can lead to the formation of highly ordered materials such as metal-organic frameworks (MOFs) and porous polymers. These structures are characterized by their regularity and have significant applications in areas such as catalysis, gas storage, and drug delivery.

Conversely, when molecular recognition involves weaker interactions, such as hydrophobic interactions in aqueous environments, it leads to the formation of more flexible and dynamic assemblies. A prime example of this is the self-assembly of amphiphilic molecules, which contain both hydrophilic and hydrophobic regions. These molecules can spontaneously organize into structures like micelles or lipid bilayers, where the hydrophobic parts are shielded from water, resulting in a reduction of the system's free energy. Such assemblies are not only fundamental in biological membranes but also serve as the basis for various nanotechnological applications.

These concepts in the science of molecular assemblies have its roots in discoveries such as A.D. Bangham and R. W. Horne's work in 1964 on lipid bilayers (Bangham & Horne, 1964), which laid the groundwork for understanding how molecules self-assemble into complex structures. These spontaneous processes are often combined with intentional techniques for nanostructure formation, such as self-assembled monolayers and Langmuir–Blodgett films. These methods have evolved to powerful tools for modifying material surfaces and constructing hierarchical structures, making them invaluable in the development of functional materials for biomedical applications, including controlled release systems as described later in this chapter.

Supramolecular systems share many working principles with biological systems, as both rely heavily on molecular interactions. Consequently, artificial supramolecular systems that mimic biological processes have been extensively studied. These systems have been applied in various fields, including molecular transport, information transmission and conversion, energy conversion, and enzymatic function. In this context, it is often said that the best supramolecular system is the living organism itself, as it represents the perfect example of successful molecular assembly. This analogy underscores the importance of supramolecular chemistry in developing biomaterials and nanotechnologies, particularly in the realm of biomedical applications.

In summary, molecular recognition is a fundamental process that drives the formation of complex supramolecular structures, with wide-ranging applications in chemistry, biology, and materials science. The ability to design and manipulate these interactions has led to significant advancements in various fields, particularly in the development of new materials and biomedical technologies. As we continue to explore the potential of molecular recognition, the next logical step is to consider its role in the development of molecular sensors. These sensors, which rely on the principles of molecular recognition, are crucial for detecting and responding to specific chemical or biological signals, paving the way for new innovations in diagnostics, environmental monitoring, and beyond.

1.1. Sensors as an application of molecular recognition

The development of sensors represents a critical application of molecular recognition and supramolecular chemistry. These sensors, broadly defined, are devices engineered to detect, record, and indicate specific physical or chemical properties. Molecular sensors, also referred to as chemosensors, are chemical systems designed to recognize and measure the presence of particular analytes, often at extremely low concentrations. These sensors translate chemical data into an analytically relevant signal, which can range from identifying the concentration of a particular component to conducting a comprehensive analysis of the sample's overall composition. The conceptual framework for designing these sensors is heavily influenced by natural processes observed in biological organisms, using the principles of supramolecular chemistry. When talking about recognition in living systems, it serves as a fundamental mechanism by which organisms can identify the presence of analytes, a concept that forms the foundation for the design of molecular sensors, often termed biosensors. These natural recognition systems are highly specialized, enabling organisms to detect a broad spectrum of molecules, including essential nutrients, harmful toxins, and intricate biomolecular interactions such as those involved in antibody-antigen binding, DNA recognition,

enzymatic activities, and cellular communication processes. As a result, biosensors play a crucial role in the detection and analysis of various biological phenomena, contributing significantly to fields like diagnostics, environmental monitoring, and food safety (Naresh & Lee, 2021).

These biological systems often inspire the design of sensors, applying natural processes of molecular recognition observed in living organisms. These systems employ sophisticated recognition mechanisms to identify and interact with a wide range of molecules, from essential nutrients to hazardous toxins, as well as monitor critical biomolecular interactions, such as those involved in glucose metabolism, hormone regulation, and immune responses (J. X. J. Zhang & Hoshino, 2018). The relevance and utility of molecular sensors or biosensors are further emphasized by substantial investments from small and medium-sized enterprises (SMEs) and large pharmaceutical and chemical corporations, all of which are heavily invested in the advancement of chemosensor technologies. These investments highlight the significant potential of these sensors in various applications as mentioned before, including medical diagnostics, environmental protection, and industrial process monitoring. A comprehensive overview of their primary applications is outlined in Table 1 (Que et al., 2008).

Table 1. Sensors' primary application areas.

Biomedical, diagnostic (<i>in vivo</i>)	<ul style="list-style-type: none"> • Glucose monitoring in diabetes patients. • Body fluids screening for disease detection. • Other physical parameters that are related to activities of molecules (temperature, voltage, pressure, light intensity).
Biomedical (<i>ex vivo</i>)	<ul style="list-style-type: none"> • Blood screening. • Drug discovery and evaluation. • Protein engineering in biosensors.
Environmental and safety	<ul style="list-style-type: none"> • River water (detection of pesticides, heavy metal ions). • Air pollution (gas, particulate matter). • Explosive detection. • Gas monitoring.
Food related	<ul style="list-style-type: none"> • Drinking water. • Allergens (egg, wheat, gluten, milk, tree, nuts, shellfish, soy). • Determination of drug residues (antibiotic, growth promoters).

Chemosensors or biosensors (when talking about biomolecules) integrate molecular recognition with signal generation to detect the presence of specific analytes (Akine et al., 2016; Rogers & Wolf, 2002). Typically, they consist of at least two distinct subunits, as illustrated in Figure 2.

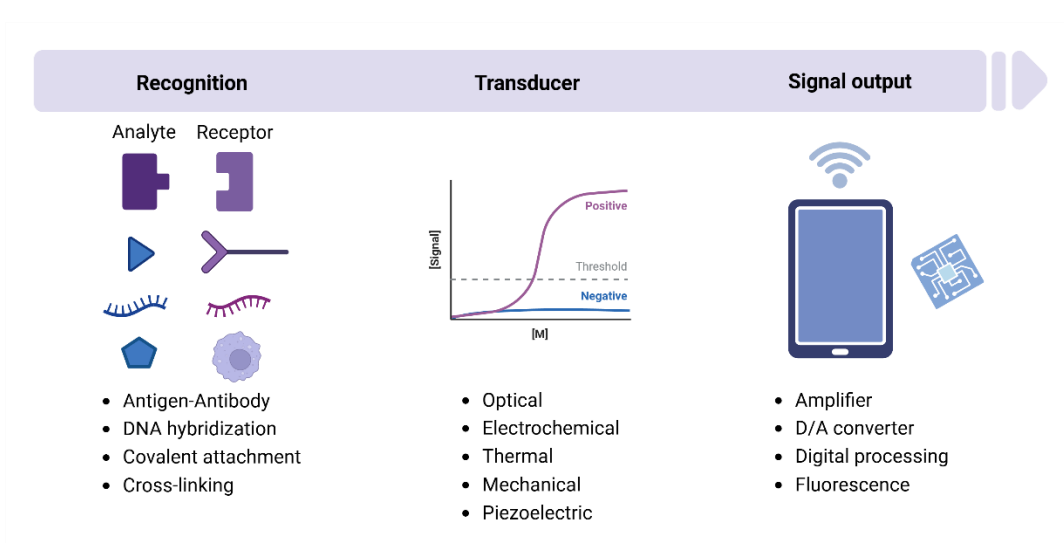


Figure 2. General components of a chemosensor.

- **Recognition subunit:** This component is specifically designed for molecular interactions, ensuring the specificity and sensitivity of the recognition process. The binding event initiates the sensing process and requires a high degree of complementarity between the receptor and the target in terms of size, shape, electrostatic charge, and other factors. Ideally, this subunit should provide: (a) selectivity, interacting only with the target analyte; (b) sensitivity, inducing significant changes in the signalling unit at minimal target concentrations; (c) resolution, where changes correlate directly with the target analyte amount; and (d) a wide dynamic range, operating effectively across various concentrations.

- **Signalling subunit:** This component converts the molecular recognition event (at the microscopic level) into a measurable signal (at the macroscopic level). The signal may manifest as changes in physical or chemical parameters, such as variations in absorption or fluorescence, redox processes, or electrochemical reactions. The most effective chemical sensors are those with high sensitivity and resolution.

Among the diverse signalling approaches utilized in chemical sensor development, chromo-fluorogenic (optical) techniques stand out as particularly significant and of great utility. These sensors operate by inducing changes in the absorption or emission spectra of the signalling subunit, manifesting as shifts in wavelength or variations in band intensity (Balzani, 1990; Turro et al., 2012). Optical chemosensors can be categorized into two types: colorimetric sensors, which rely on changes in ground-state energy (absorption), and luminescent sensors, which depend on changes in excited-state energy (fluorescence or phosphorescence). Both types require spectrophotometers for signal detection, a standard instrument available in most scientific laboratories.

Fluorescence-based sensors often achieve detection limits below 10^{-6} M, making them highly competitive compared to colorimetric sensors. Additionally, fluorogenic sensors typically offer greater sensitivity and specificity because they allow for precise selection of absorption and emission bands, thus achieving lower detection limits compared to colorimetric methods.

The literature describes numerous optical chemosensors incorporating various binding sites (specific to cations, anions, or neutral molecules) and signalling units (dyes and/or fluorophores). These sensors are generally constructed using three established paradigms, as illustrated in Figure 3: (a) the binding site-signalling subunit approach, (b) the displacement approach, and (c) the chemodosimeter approach (Martínez-Máñez & Sancenón, 2006). Each paradigm differs in how it integrates the binding/reactive sites with the signalling components.

- **Binding Site – Signalling Subunit Approach:** This widely used method involves chemically bonding the binding site to the signalling unit. Target binding alters the electronic properties of the signalling subunit, causing detectable fluorescence or absorption changes. However, this approach requires complex synthesis and

relies on weak supramolecular interactions, limiting effectiveness in aqueous environments.

- **Displacement Approach:** Here, the binding site and signalling unit form a non-covalent complex. The target analyte preferentially binds to the site, displacing the signalling unit, which changes its optical properties upon release. This produces observable colour or emission shifts.
- **Chemodosimeter Approach:** This strategy involves chemical reactions between the sensor and target analyte, causing fluorescence or colorimetric changes. Chemodosimeters offer greater selectivity and function well in aqueous conditions, making them ideal for real-time, in situ measurements.

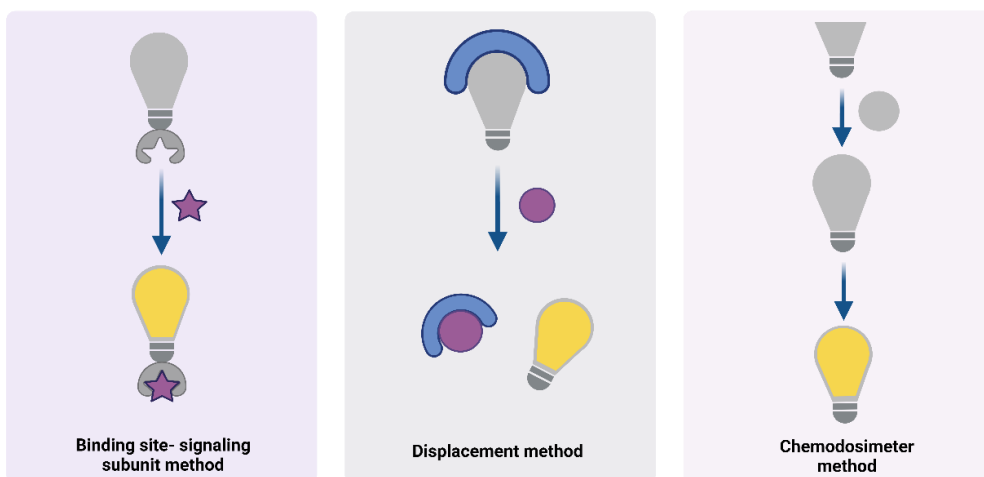


Figure 3. Illustration of three methodologies employed in optical chemosensors.

Given the considerations mentioned before, there has been a significant increase in the design and development of optical chemosensors for detecting target analytes across various research domains, including healthcare, the food industry, and environmental monitoring. Currently, chemosensors for identifying bioanalytes such as pathogens, amino acids, and enzymes are emerging as valuable tools for the rapid

exploration and monitoring of disease pathogenesis (see Figure 4). Advances in optical chemosensors for point-of-care applications are very soon offering potential improvements in patient monitoring. Additionally, integrating chemical sensors with nanomaterials promises to build innovative sensing nanodevices with superior selectivity, sensitivity, and applicability compared to traditional molecular-based probes.

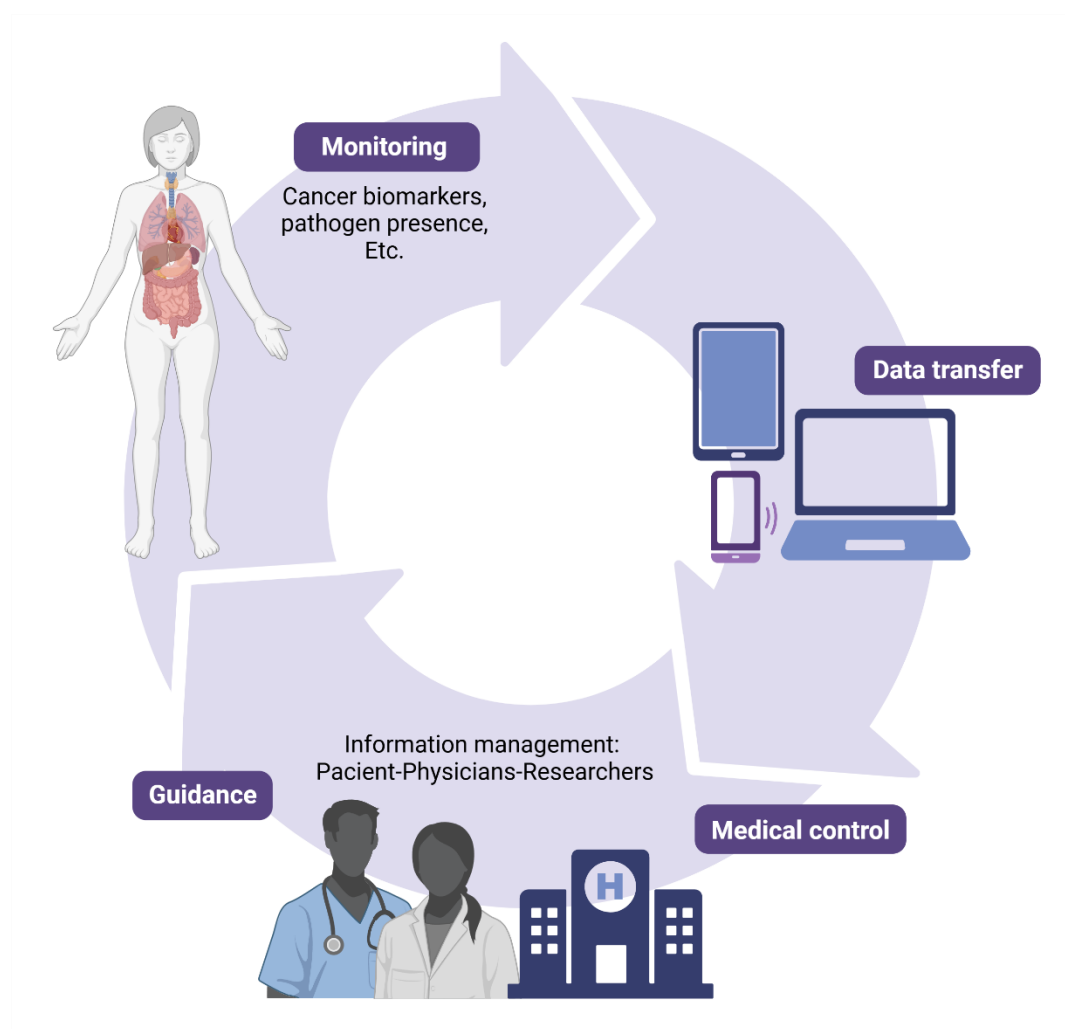


Figure 4. Prospective use of chemosensors for continuous and remote disease monitoring in medical applications

The field of diagnostics is undergoing a significant transformation with the integration of this kind of chemosensors, which offer a promising alternative to current detection methods. At the core of effective diagnostics lies the ability to accurately identify the target, such as pathogenic bacteria, considering key analytical performance factors like sensitivity, selectivity, stability, response time, and cost. Presently, the most widely used methods for detecting pathogenic bacteria in clinical diagnostics rely heavily on DNA-based polymerase chain reaction (PCR) or mass spectrometry for phenotypic identification of bacteria cultivated in chromogenic media. While these technologies are regarded as the most systematically sensitive and reliable for pathogen detection, they are encumbered by complex pre-treatment and analysis procedures. These processes are labor-intensive, require highly skilled personnel, and are time-consuming, which limits their efficiency in rapid diagnostics.

In contrast, immunoassays like ELISA (enzyme-linked immunosorbent assay) and LFIA (lateral flow immunoassay) offer faster detection with good selectivity and stability. However, these immunological assays also have their limitations. They typically involve expensive materials, require complex antibody labelling, and multiple washing steps, making them less cost-effective. Furthermore, the sensitivity of immunoassays is relatively low, which can easily lead to false positives. More critically, immunological methods generally target a single pathogen, making it challenging to detect multiple pathogens simultaneously. Although the multiplex polymerase chain reaction (mPCR) assay provides a more effective solution for simultaneous detection of multiple pathogens by amplifying DNA or RNA from different bacteria in a single PCR system, it still suffers from the complexities of pre-treatment and analysis, which can lead to false negatives.

This new concept of chemosensor emerge as a powerful alternative to these traditional methods, particularly for rapid, accurate, and simultaneous detection of multiple pathogens. These chemical sensors are designed to detect specific analytes, such as pathogens, at very low concentrations by converting chemical information into

analytically useful signals. Unlike traditional methods, chemosensors offer the potential for high sensitivity and selectivity without the need for extensive pre-treatment or complex procedures. They can be engineered to detect multiple pathogens at once, addressing a significant gap in current diagnostic capabilities.

The adoption of chemosensors in diagnostics could dramatically improve the current state-of-the-art by overcoming the limitations of existing methods. These sensors promise faster detection times, higher sensitivity and selectivity, and the ability to monitor multiple targets simultaneously. Additionally, the simplicity of chemosensors reduces the need for expensive materials and complicated procedures, making them more accessible and cost-effective. As a result, chemosensors could play a crucial role in enhancing public and environmental safety by enabling quicker, more accurate detection of pathogens, ultimately leading to better disease prevention and control. The advancement of chemosensor technology not only holds the potential to revolutionize diagnostics but also paves the way for the development of more sophisticated and versatile molecular sensors in the future (Shen et al., 2021)

1.2. Biosensors: Characteristics and classification

A biosensor is a device or probe that integrates a biological component, such as an enzyme or antibody, with a reading component to produce a measurable signal. The biosensor is the biological version of the chemosensors explained before (based on biological processes). The reading component detects, records, and transmits information regarding physiological changes or the presence of various chemical or biological substances in the environment. Biosensors come in various sizes and shapes and can detect and measure even low concentrations of specific pathogens, toxic chemicals, and pH levels.

The development of biosensors can be classified into three generations based on the integration method of the biorecognition element (bioreceptor) with the transducer.

1. **First Generation (1st Gen):** In this initial phase, biosensors detect the content of analytes and the products of bioreceptor reactions that diffuse to the surface of the transducer, resulting in an electric response. These sensors are also known as mediator-less amperometric biosensors. The components of a biosensor were first described by Leland Charles Clark Jr., who is considered the father of biosensors, in a report published in 1953 (Clark et al., 1953). This seminal report detailed an electrode capable of measuring oxygen concentration in blood.

2. **Second Generation (2nd Gen):** The biosensor evolution continued with the second generation, where the bioreceptor is covalently linked to the transducer. This integration improves the specificity and sensitivity of the sensor, allowing for a more direct and stable interaction between the biorecognition event and the signal transduction.

3. **Third Generation (3rd Gen):** In this most advanced phase, the bioreceptor is directly integrated with the transducer in a manner that eliminates the need for diffusion. This generation leverages the advantages of nanotechnology and advanced materials to design highly sensitive and selective biosensors capable of real-time monitoring and analysis in various applications.

These advancements highlight the progressive refinement in the design and functionality of biosensors, leading to increasingly accurate and efficient detection methods for a wide range of applications.

To develop a highly effective and efficient biosensor system, it is essential to meet specific static and dynamic requirements. These specifications are crucial for optimizing biosensor performance for commercial applications. The key characteristics we should include in our criteria are:

I. **Selectivity:** The ability of the bioreceptor to specifically detect the target analyte in a complex mixture containing various other substances and contaminants.

II. **Sensitivity:** The capacity to accurately identify and quantify very low concentrations of the analyte (in ng/mL or fg/mL) with minimal steps, ensuring the detection of even trace amounts.

III. **Linearity:** Ensures the accuracy of the biosensor by maintaining a direct proportional relationship between the substrate concentration and the signal produced, resulting in higher detection accuracy at varying concentrations.

IV. **Response Time:** The duration required to achieve 95% of the final measurement, indicating the speed at which the biosensor can deliver results.

V. **Reproducibility:** The ability of the biosensor to produce consistent results upon repeated measurements of the same sample, characterized by precision (consistent outputs) and accuracy (mean values close to the true value).

VI. **Stability:** Critical for continuous monitoring applications, stability refers to the biosensor's resistance to environmental disturbances. Stability is influenced by the bioreceptor's affinity for the analyte and its degradation over time.

These characteristics ensure that biosensors are reliable, precise, and suitable for various commercial and practical applications. The classification of biosensors spans various disciplines and involves multiple criteria. The classification scheme is illustrated in Table 2.

1. **Based on Bioreceptors:** Bioreceptors are the primary component in biosensor construction. Biosensors can be classified according to the type of bioreceptor used:

- **Enzymatic Biosensors:** The most common class, utilizing enzymes as bioreceptors.
- **Immunosensors:** Known for high specificity and sensitivity, particularly useful in diagnostics.
- **Aptamer or Nucleic Acid-based Biosensors:** High specificity for microbial strains and nucleic acid-containing analytes.
- **Microbial or Whole-cell Biosensors:** Employ entire cells or microorganisms as bioreceptors.

2. **Based on Transducers:** Another classification is based on the type of transducer employed:

- **Electrochemical Biosensors:** Further subdivided into potentiometric, amperometric, impedance, and conductometric sensors. As a result of electrochemical or immunological responses, electrochemical SRs produce electrical signals such as voltage, current, conductance, or impedance via transducers.
- **Electronic Biosensors:** Utilize electronic transduction methods.
- **Thermal Biosensors:** Measure changes in temperature.
- **Optical Biosensors:** Detect changes in light properties.
- **Fluorescent Biosensors:** Detect changes in the sample fluorescence.
- **Mass-based or Gravimetric Biosensors:** Measure changes in mass.

3. **Based on Bioreceptor-Analyte Combinations:** This classification includes specific combinations of bioreceptors and analytes, though these are more limited in number.

4. **Based on Detection Systems:** Sensors can also be categorized by the detection system used:

- **Optical Sensors**
- **Electrical Sensors**
- **Electronic Sensors**
- **Thermal Sensors**
- **Mechanical Sensors**
- **Magnetic Sensors**

5. **Based on Technology:** Classification can also be based on the technology integrated into the biosensor:

- **Nanotechnology-based Biosensors**
- **Surface Plasmon Resonance (SPR) Biosensors**
- **Biosensors-on-Chip (Lab-on-Chip)**
- **Electrometers**
- **Deployable Biosensors**

These classifications help in understanding the diverse applications and technological integrations of biosensors in various fields.

Table 2. Classification of biosensors based on various bioreceptors the different approaches used.

Based on bioreceptors	Enzyme-based	
	Antibody-based	
	Aptamer-based	
	Whole cells biosensors	
	Nanobiosensors	
Based on transducers	Electrochemical	Amperometric
		Potentiometric
		Voltametric
		Conductometric
		Impedimetric
	Optical	
	Fluorescent	
	Electronic	
	Thermal	
	Gravimetric	
Acoustic		
Based on detection system	Optical	
	Electrical	
	Thermal	
	Magnetic	
	Electronic	
	Mechanical	
Based on technology	Nanobiosensors	
	SRP Biosensors	
	Biosensors-on-chip	
	Electrometers	

Having reviewed the general classifications of biosensors based on different criteria, it is important to narrow the focus to a specific subset: affinity-based biosensors. These belong to the broader category of biosensors that utilize bioreceptors, as discussed previously. Unlike other types, affinity-based biosensors operate through specific interactions between a bioreceptor and its target analyte, offering high selectivity and

precision. This type of sensor usually comprises antibodies, cell receptors, and nucleic acids as the biorecognition element for detection (Naresh & Lee, 2021). In this thesis we are going to focus on this kind of coating as it represents a powerful tool for biomolecular recognition.

- **Antibody-Based Biosensors**

Antibodies, known for their high affinity and specificity, have been utilized in biosensors for over twenty years due to their versatile applications and robust antigen-antibody interactions. Antibodies are immunoglobulins (Ig) with a distinctive "Y" shape structure, consisting of two heavy and two light polypeptide chains linked by disulfide bonds. They are categorized into five classes based on variations in their heavy chains: IgG, IgM, IgA, IgD, and IgE.

Biosensors incorporating antibodies as ligands or relying on antigen-antibody interactions are termed immunosensors. These immunosensors can be divided into two types: (i) non-labelled and (ii) labelled depending on if there is a label attached that allows a direct quantification of the complex formation.

For instance, de Castro et al. developed a label-free immunosensor for ovarian cancer detection, which demonstrated a linear response to anti-CA125 concentrations ranging from 5 to 80 U/mL, with a detection limit of 1.45 U/mL (A. C. H. de Castro et al., 2020). Similarly, Bhardwaj et al. developed electrical and optical biosensors for label-free detection of Aflatoxin B1 (AFB1) using gold (Au) nanobipyramids (NBPs). Their surface plasmon resonance (SPR)-based detection showed a linear range of 0.1–500 nM with a detection limit of 0.4 nM, while impedimetric detection covered a linear range of 0.1–25 nM with a detection limit of 0.1 nM (Bhardwaj et al., 2021).

- **Oligonucleotides-Based Biosensors**

Unlike conventional approaches like antibody-based biosensors, oligonucleotide-based biosensors rely on the complementary base pairing of oligonucleotides. The hybridization process between nucleic acids offers both stability and a high degree of specificity. Oligonucleotide-based biosensors also utilize aptamers, which are short oligonucleotides with a strong binding affinity for specific target molecules. Unlike the sequence-specific hybridization seen with DNA or RNA, the binding mechanism between aptamers and their target molecules varies depending on the system. This binding is typically driven by electrostatic and hydrophobic interactions, and many aptamers achieve selective binding through their unique structural designs in addition to their nucleotide sequences.

Aptamers are synthetic single-stranded nucleic acids (either DNA or RNA) engineered to bind selectively to target molecules, adopting either two-dimensional (2D) or three-dimensional (3D) conformations. These conformations enhance binding efficiency by increasing surface density and reducing spatial obstruction (Odeh et al., 2020). Aptamers are stable over a broad range of temperatures and storage conditions due to their nucleic acid nature. Unlike antibodies, which require biological systems for production, aptamers are chemically synthesized, maintain stability across a pH range of 2–12, and exhibit thermal refolding capabilities. Additionally, aptamers can be chemically modified to meet specific detection requirements (Adachi & Nakamura, 2019; Odeh et al., 2020).

Aptamers are isolated from oligonucleotide libraries using a process known as SELEX (Systematic Evolution of Ligands by EXponential enrichment). Various SELEX techniques have been developed, including cell-SELEX, capillary electrophoresis-based SELEX, microfluidics-SELEX, FACS-based SELEX, microtiter plate-SELEX, magnetic bead-SELEX, and *in vivo* SELEX where a pool of oligonucleotides is repeatedly tested for its

binding with the selected analyte. Through this cyclic process the oligonucleotide capable of binding to the target is amplified and then sequenced to obtain the nucleotide sequence of the aptamer (process detailed in Figure 5).

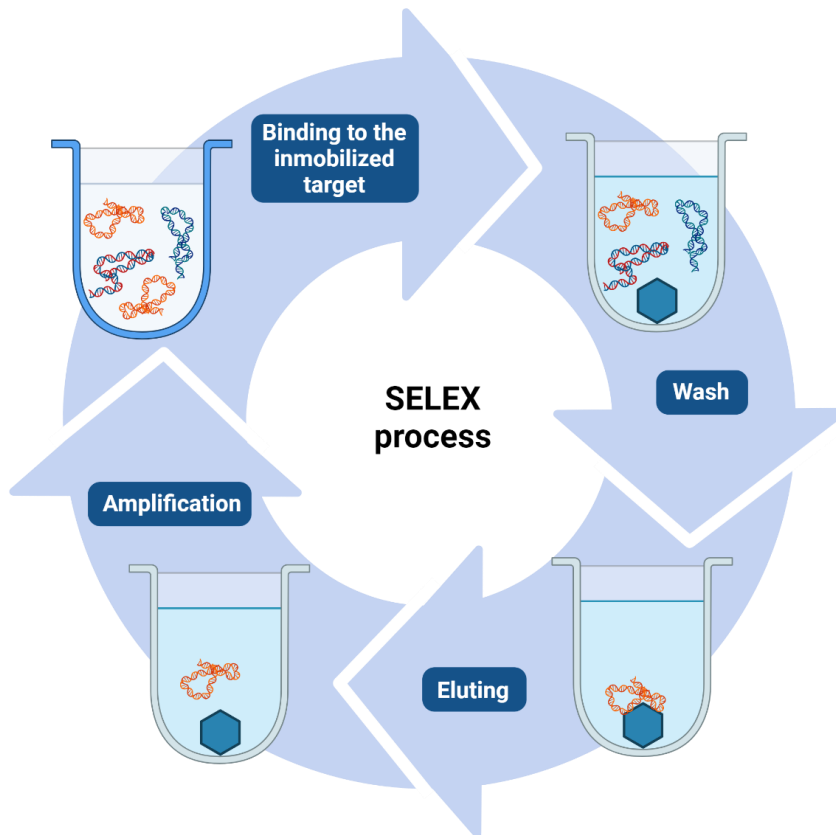


Figure 5. a) Diagrammatic overview of aptamer SELEX preparation. b) Illustration of the aptamer-target interaction mechanism.

Aptamer-based biosensors are commonly categorized based on their transduction methods, which include optical, electrochemical, and piezoelectric techniques. These biosensors can be further classified into labelled and label-free aptasensors. Surface plasmon resonance (SPR) is frequently employed for label-free

optical detection, while fluorescent dyes, such as fluorescein, are used for label-based optical aptasensors (Zeng et al., 2020).

Aptamers are particularly valuable for detecting proteins, heavy metals, and other chemicals that lack sequence-specific hybridization properties. As a result, oligonucleotide-based biosensors offer significant flexibility in design, making them suitable for a wide range of applications. Their high specificity, stability, and adaptability in base-pairing hybridization have made them widely used tools in clinical diagnostics and genome mutation detection. However, these biosensors do have some limitations. Temperature control during detection is essential as it cannot exceed biocompatibility. Additionally, the detection process often requires a fluorescent dye system, adding further steps and equipment to the procedure (Goyal et al., 2019; Jung et al., 2016; N. Verma & Kaur, 2019).

1.3. Current tendencies in biosensing

Recent years have witnessed the successful development of various bio-nanosensors as an alternative approach for the rapid, accurate, affordable, and on-site monitoring of diverse analytes. Current demands include point-of-care devices that are reliable, robust, and easy to use. These devices must not only meet but exceed the sensitivity standards of traditional methods, providing faster and more reliable results. Conventional methods, such as nucleic acid applications and immunoassay-based techniques, face limitations including the need for expensive, bulky equipment, complex sample preparation, and access to advanced research facilities. These drawbacks hinder their application for rapid and on-site food safety testing. Consequently, there is an urgent need for sensitive and practical methods to detect pathogens and their toxins that are portable, cost-effective, and rapid.

As a result, current analytical research focuses predominantly on the development of real-time, simple, reliable, and affordable point-of-care analytical

devices. In this context, bio- and nanotechnology-based detection techniques have emerged as cost-effective alternatives to conventional, expensive methods used to analyze a wide range of substances. The primary advantage lies in their operational simplicity, where the focus is solely on converting biological responses into detectable signals. Extensive research on various aspects of bio/nanosensors has led to numerous biotechnological advancements and innovations, particularly in bacterial and viral detection and monitoring.

Newly-emerging optical biosensors based on innovative structural architectures and materials—including emerging metamaterials, hybrid plasmonic-2D metasurfaces, metal/dielectric nanostructures, and all-dielectric metasurfaces—can generate a variety of novel supports for these devices. Their characteristics can be utilized to dramatically improve the sensitivity of current label-free biosensing technology and offer new attractive functionalities such as imaging and multi-sensing options, super-resolution, spectral tunability, size selectivity, and new functionalization strategies. (Kabashin et al., 2023)

Furthermore, the integration of computer science and artificial intelligence with nanobiosensors could make new biosensors smarter and more convenient. With continuous research and development, nanomaterials are expected to bring higher performance levels and more application possibilities to biosensor technology (L. Li et al., 2023)

2. NANOTECHNOLOGY

The term "nanotechnology" was first defined by Professor Norio Taniguchi in 1974, who described it as: *"production technology to achieve extremely high accuracy and ultra-fine dimensions, specifically on the order of 1 nm, or 10⁻⁹ meters in length."*(Taniguchi, 1974)

Since that time, the exploration and use of nanotechnology have remarkably progressed, with its definition evolving to “*the construction and use of functional structures designed from the atomic or molecular scale, with at least one characteristic dimension measured in nanometers.*” (Kumar & Kumbhat, 2016) The unique size of these structures (between 1-100 nm scale, see in Figure 6) enables them to exhibit novel and significantly enhanced physical, chemical, and biological properties, phenomena, and processes.

This field encompasses research and development that involves measuring and manipulating matter at atomic, molecular, and supramolecular levels, with at least one dimension comparable to the size of antibodies and viruses as depicted in Figure 6.

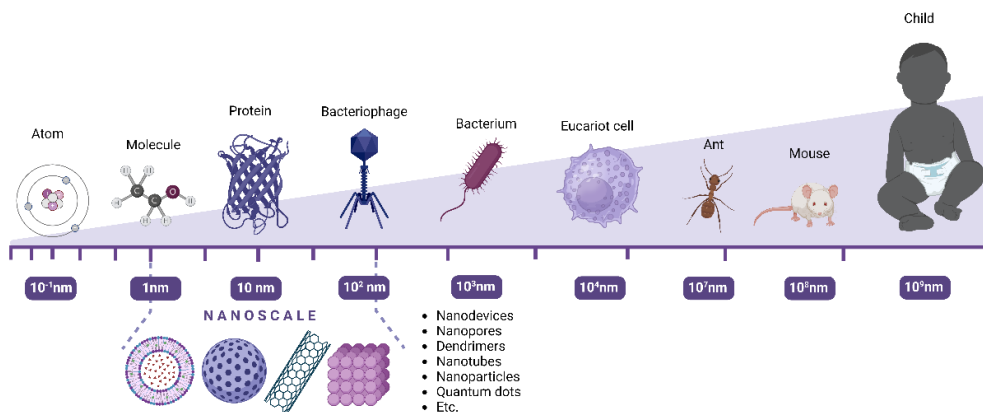


Figure 6. Size comparison of different organisms (pluricellular, unicellular), biomolecules and nanomaterials.

As observed previously, nanotechnology operates at the nanoscale, a size range that offers significant advantages due to the emergence of quantum mechanical effects. This unique scale enables a wide array of applications across numerous scientific disciplines, including materials science, electrical and electronic engineering, catalysis,

metallurgy, chemical engineering, drug delivery, polymer science, medicine, biotechnology, forensics, and environmental and food control. Among the various elements within nanotechnology, nanomaterials stand out as particularly significant.

Nanomaterials include a diverse group of substances such as nanoparticles, nanofibers, nanotubes, nanocomposites, nanofoams, and nanoporous materials. Of these, nanoporous materials are particularly notable for their nanostructured systems that feature porous networks with pore sizes ranging from 1 to 100 nanometers. These materials are finding applications in nearly every research field and industrial sector, with their utility being largely determined by their structural characteristics. Key structural parameters like pore size, porosity, functionalization, and specific surface area play crucial roles in defining the material's final properties, including hydrophilicity or hydrophobicity, conductivity, charge distribution, and catalytic activity (Ameen et al., 2020).

The broader field of nanotechnology encompasses any technology that operates at the nanoscale with practical real-world applications. Advances in this field have led to the development of bio-nanosensors that incorporate advanced nanomaterials, offering significant potential to improve both sensitivity and selectivity. These cutting-edge biosensors are set to revolutionize diagnostics and other applications. Supramolecular chemistry and molecular recognition have further enhanced this area by introducing additional functionalities to nano-objects, leading to the continuous development of various nanosystems. These include nanoparticles, nanotubes, and nanostructured surfaces, which are being utilized in areas such as nanobiotechnology, nanomaterials, nanoelectronics, nanomagnetism, and nanophotonics. The progress in these fields underscores the transformative potential of nanotechnology across diverse scientific and industrial domains (Abedi-Firoozjah et al., 2024). Among these nanomaterials, researchers have explored the use of nanoporous materials in the development of reliable, miniaturized, and portable sensing devices as those described in this thesis. These devices are designed by loading the pores of the nanoporous support with a

signalling reporter and functionalizing the external surface with supramolecular or biochemical architectures. These systems remain inactive until they encounter a specific molecule, which triggers the release of the signalling reporter, making them highly effective in sensing applications.

3. ORGANIC-INORGANIC HYBRID POROUS MATERIALS

Since the start of the industrial era, the fusion of organic and inorganic substances to develop materials with unique properties has been a significant challenge. The term "hybrid organic-inorganic material" has been relatively recently coined, as this field has demonstrated its wide array of applications. Today, it is recognized as a rapidly expanding and dynamic research discipline.

Hybrid materials combine their components in a synergistic manner, resulting in properties that surpass the sum of their individual parts. (Callan et al., 2005; Gale & Quesada, 2006; Mohr, 2005) As Professor Clément Sanchez explains, "*hybrid organic-inorganic materials are not simple mixtures. They can be broadly defined as molecular or nanocomposites with (bio)organic and inorganic components, intimately mixed where at least one of the component domains has a dimension ranging from a few Å to several nanometers. Consequently, the properties of hybrid materials are not only the sum of the individual contributions of both phases, but the role of their inner interfaces could be predominant*". (Callan et al., 2005; Gale & Quesada, 2006; Mohr, 2005) The final structure and properties of these nanocomposites are determined by the chosen inorganic support, the organic groups attached to its surface, and the specific reaction conditions used during synthesis (Livage et al., 1988).

Some hybrid materials are formed by anchoring functional organic groups onto nanoscopic materials composed primarily of inorganic structures serving as scaffolds (Rurack & Martínez-Máñez, 2010). This approach is central to the design and development of new hybrid organic-inorganic materials, as explored in this thesis. Covalent bonding for

anchoring or functionalizing solid supports offers several advantages for molecular recognition processes, which include:

- Receptors are organized into compact monolayers on the surface (depending on the degree of functionalization), leading to new collective processes.
- The material can be further functionalized with different organic molecules, imparting diverse properties based on the anchored molecules.
- Leaching processes involving receptors are minimized.
- Reversible reactions can be performed when the anchored organic molecules allow for it.

Depending on the nature of the interface between the organic and inorganic components, these materials can be classified into two categories: Class I materials are held together by weak bonds (hydrogen, van der Waals, or ionic bonds), while Class II materials feature strong chemical bonds (covalent or ionic-covalent bonds), potentially combined with the weak bonds characteristic of Class I.

Within this framework, enhanced sensing ensembles have been designed to improve sensitivity and selectivity for targets that are challenging to detect with conventional methods (Descalzo et al., 2006; Drechsler et al., 2004; Mancin et al., 2006; A. Verma & Rotello, 2005; Willner et al., 2007). These enhancements are particularly notable when using 3D-architected inorganic supports, such as nanoporous inorganic scaffolds, which exhibit superior properties compared to their planar counterparts. The new features offered include controlled access to specific regions, flow control within channels, and dual functionalization of the inner and outer regions of the material.

A more detailed description of these nanostructured materials will be provided below.

3.1. Types of porous materials

Porous materials are prevalent in our environment and play crucial roles in various aspects of daily life. The International Union of Pure and Applied Chemistry (IUPAC) classifies porous materials into three main categories: microporous (<2 nm), macroporous (>50 nm), and mesoporous (2-50 nm), which is the focus of our interest. These materials can be composed of a variety of solids, including oxides and non-oxides, and can be either crystalline or amorphous. The pores in these materials can manifest as cavities, channels, or interstices.

Microporous structures such as zeolites and metallophosphates were first synthesized nearly two centuries ago and remain essential in numerous industrial processes, particularly in catalysis, filtration, separation, biomedical regeneration, enzyme immobilization, drug delivery, and sensing (Carlsson et al., 2014; Cavenati et al., 2009; Jane et al., 2009; Kilian et al., 2007; Slowing et al., 2007; Vallet-Regí et al., 2008). In contrast, the industrial application of macroporous materials has seen a dramatic increase over the past decade.

Mesoporous materials, developed more recently, have garnered significant attention due to their large specific surface area and their applicability across a wide range of scientific and technological fields. The typical synthesis of these materials involves the use of organized self-assembling organic molecules or polymers, micellar solutions, lyotropic liquid crystals, or microemulsions, which act as structure-directing agents. The synthesis process is particularly critical, as the pore geometry directly influences the material's properties and potential applications (Wang et al., 2005). Advances in experimental techniques have enabled a degree of control over the desired architecture and final properties by adjusting synthetic parameters and reagents.

This thesis focuses on the utilization of porous anodic alumina (PAA) also known as nanoporous anodic alumina (NAA) when the pore size is smaller than 20 nm as a

mesoporous solid scaffold. Accordingly, the subsequent sections will explore the synthesis and functionalization of NAA supports.

3.2. Porous anodic alumina (PAA)

Porous anodic alumina (PAA) was initially discovered in the 1930s (Setoh & Miyata, 1932) but saw significant development between the 1950s and 1970s, (Keller et al., 1953; O'SULLIVAN JP & WOOD GC, 1970) resulting in various patented synthesis methods and applications (Bengough & Stuart, 1923; I. A. W. Smith, 1974). A major milestone occurred in 1995 when the formation of PAA with a highly ordered 2D hexagonal porous structure was confirmed, leading to an exponential increase in research and development interest, marked by a 75% increase in related publications from 1990 to 2005.

The first characterization of PAA by electron microscopy was conducted by Keller, who described it as arrays of hexagonally arranged nanometric pores, where the interpore distance is directly proportional to the anodization voltage (Setoh & Miyata, 1932). It has since been established that the shape and geometry of PAA largely depend on the anodization voltage or current intensity, with other factors such as anodization time, electrolyte type/concentration, pH, and temperature also playing crucial roles (Chen et al., 2008; W. Lee & Park, 2014; Zaraska et al., 2014, 2016). This characteristic structure can be seen below in Figure 7.

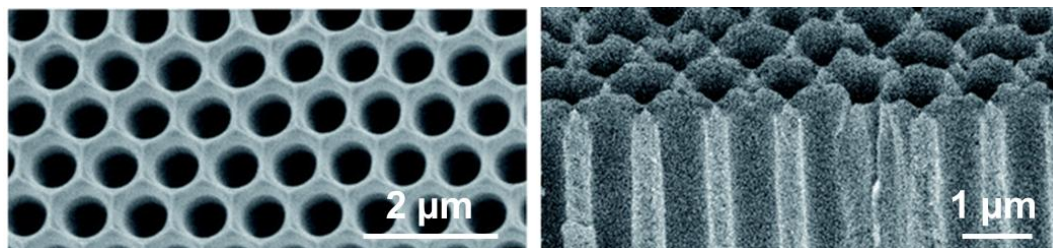


Figure 7. SEM image of highly ordered anodic porous alumina obtained at 400 V, showing (left) surface view and (right) cross-sectional view. Image adapted from (Yanagishita et al., 2021)

PAA has become a valuable tool in nanotechnology due to its broad range of applications, particularly in energy, nanofabrication, biotechnology, and notably, biosensing. Given its unique mechanical, electrical, and chemical properties, PAA is an ideal scaffold for implementing selected (bio)molecules. Its high surface area, thermal stability, hardness, biocompatibility, and transparency in the visible range make it suitable for developing hybrid materials used in molecular recognition and sensing (Jani et al., 2010).

Structurally, PAA can be described as an alumina matrix with hexagonally arranged cells containing cylindrical pores that grow perpendicularly to the substrate surface (W. Lee et al., 2006). It is typically produced by controlled anodization of aluminum surfaces in aqueous acids such as sulfuric, oxalic, and phosphoric acids (Ersching et al., 2012; Md Jani et al., 2013; Patermarakis & Masavetas, 2006). The ability to control pore size and shape is crucial for many applications, and the anodization process plays a vital role in achieving this.

In 1995, Masuda and Fukuda reported an optimized anodization process, (Masuda & Fukuda, 1995) which was further advanced by the nanoimprint process two years later, revolutionizing PAA production (Masuda et al., 1997). They proposed a two-step anodization procedure: the first step forms an irregular oxide layer that is removed,

leaving nanocaves that act as nucleation sites for the second anodization. This method allows for a more ordered hexagonal pore arrangement compared to other techniques like lithography, which are time-consuming and expensive (Zaraska et al., 2016). The two-step process is simple, cost-competitive, allows for controllable pore structures on the nanometric scale, and is easily scalable for industrial production (Eftekhari, 2008; A. P. Li et al., 1998).

Several theoretical models have been proposed to explain pore nucleation and growth in PAA, (Cheng & Ngan, 2015; Hoar & Mott, 1959; Patermarakis & Papandreadis, 1993) although a definitive explanation remains under debate. It is generally agreed that pore nucleation originates in the oxide thin film formed during the initial seconds of anodization, but the exact mechanisms vary. The models can be broadly categorized into those that consider the electric field (Diggle & Meek, 1974; Hoar & Mott, 1959; Van Overmeere et al., 2010) as the driving force and those that consider mechanical stress as it (Garcia-Vergara et al., 2006; Houser & Hebert, 2009). The former, supported by most of the scientific community, suggests that electric field-induced instability at specific sites generates localized increases in temperature and ionic conduction, leading to preferential oxide dissolution and pore formation/growth. In contrast, mechanical stress models propose that the significant volume expansion during oxide layer formation induces mechanical stress, promoting oxide flow from the bottom to the pore walls. Some models combine both electric and mechanical processes, suggesting that pore formation is driven by the electric field through the barrier layer, influenced by the plasticity of the barrier layer and stress relief during formation (B. He et al., 2006; S. Lee et al., 2013).

3.3. Anodic alumina functionalization

Functionalization, as defined, involves adding new functions, features, capabilities, or properties to a material by modifying its surface chemistry. Numerous studies have explored methods for functionalizing PAA surfaces (or NAA surfaces when

talking of pores less than 20 nm of diameter) to protect them from acidic environments and to impart specific functionalities. These techniques can be broadly categorized based on the medium in which the process is conducted (Figure 8)(Eckstein et al., 2018; Kumeria et al., 2014; Md Jani et al., 2013).

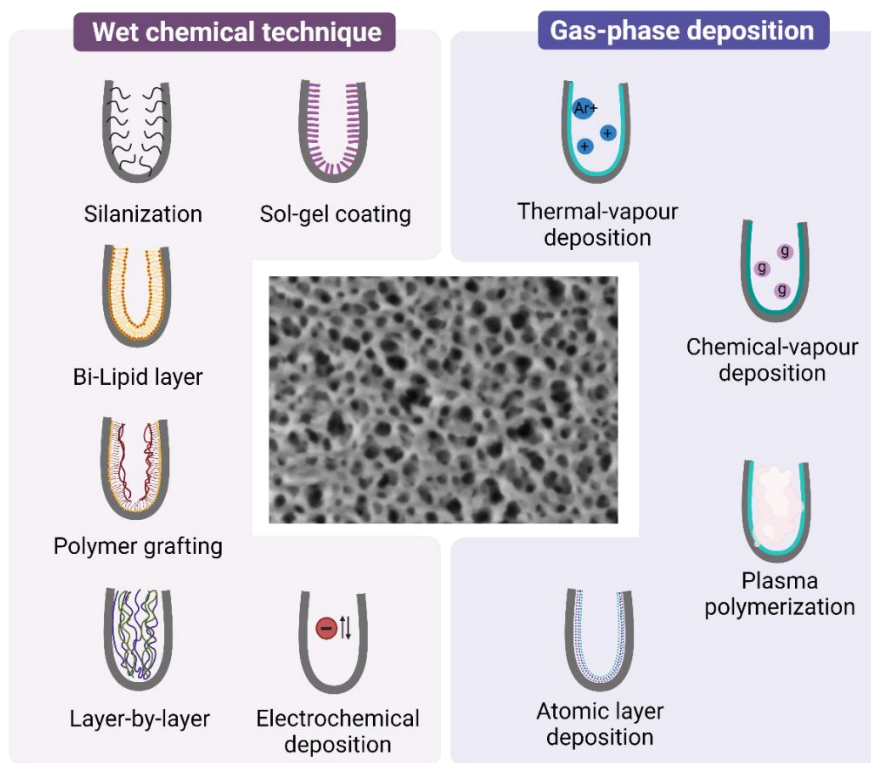


Figure 8. Overview of common gas phase and wet chemical techniques for functionalizing NAA surfaces.

a. **Physical/Gas Phase Deposition:** Techniques such as thermal vapor deposition, chemical vapor deposition (CVD), plasma polymerization, and atomic layer deposition (ALD) fall into this category. These methods are primarily used to deposit various

materials, including metals, metal oxides, nitrides, and carbon nanotubes, onto NAA surfaces.

b. Wet Chemical Modifications: This category includes self-assembly processes of silanes, organic and phosphonic acids, layer-by-layer deposition, polymer grafting, sol-gel processing, and electrochemical and electroless deposition. Unlike physical surface modifications, chemical surface modifications do not significantly alter the structural properties of the NAA substrate.

Chemical approaches often rely on forming self-assembled structures, resulting in uniform and extensive monolayers on the surface. Irregularities on the NAA surface, often due to anionic impurities from the electrolyte solutions used during fabrication, facilitate oxide attack, leading to the generation of surface hydroxyl groups that serve as anchorage points for functionalization. The main functionalization techniques are summarized below:

- ***Electrochemical and Electroless Deposition of Metals:***

In this deposition method, a monolayer is formed on a conducting surface (electrode) by depositing ions (anions or cations) from a solution into an electrolytic cell (Figure 9). The process requires three electrodes (working, counter, and reference) to facilitate electron movement and the oxidation and reduction reactions necessary for deposition. (Rodriguez & Tremiliosi-Filho, 2013) The quality of the resulting electrodeposition is influenced by several factors, including pre-treatment and cleaning of the metal surface, concentration of metal ions in the electrolyte, pH, agitation, voltage, temperature, electrolyte conductance, and addition agents.

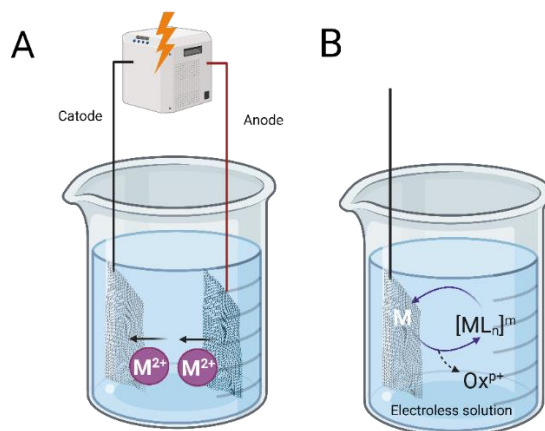


Figure 9. Illustration of a) electrochemical and b) electroless deposition for the functionalization of the NAA surface.

Electrochemical and electroless depositions offer certain advantages over other functionalization methods. They are significantly less expensive and more versatile, as they can be used to coat many samples simultaneously, including large pieces. Additionally, NAA functionalized using these procedures exhibits remarkable properties such as hardness, corrosion resistance, and excellent frictional characteristics.

- **Sol-Gel Chemistry:**

The sol-gel process is a functionalization technique that involves a hydrolysis reaction between the sol-precursor and the functional groups on the NAA surface (Figure 11). Initially, the substrate is exposed to the sol-precursor solution through methods such as immersion, dipping, or spin coating. This is followed by the evaporation of the solvent, leading to the formation of a glassy gel within the pores (Hench & West, 1990).

A "sol" refers to a colloidal solution that gradually transforms into a gel-like diphasic system, consisting of both liquid and solid phases. The morphologies of these phases can range from discrete particles to continuous polymer networks. During this

process, the sol undergoes a series of chemical reactions, leading to the formation of a solid network within the liquid medium. This network formation results in the gelation of the sol, developing a solid matrix that can effectively functionalize the NAA surface (Figure 10).

The sol-gel technique is highly versatile and can be tailored to impart a variety of functionalities to the NAA substrate, making it a valuable method for enhancing the properties of porous anodic alumina for diverse applications.

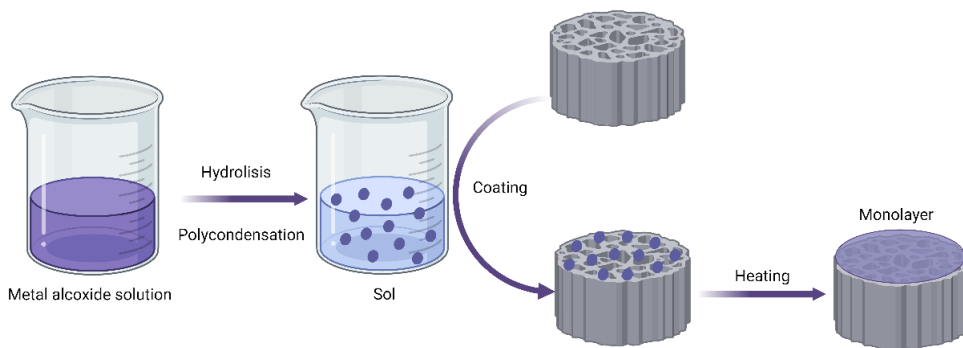


Figure 10. Illustration of sol-gel chemistry for NAA surface functionalization

The sol-gel method is an economical, low-temperature technique that enables the synthesis of high-purity, homogeneous, and multi-component structures with precise control over their structural properties, thermal stability, and surface reactivity (Hunks & Ozin, 2005; Lakshmi et al., 1997). This process facilitates the uniform deposition of small amounts of dopants, such as organic dyes and rare-earth elements, making it widely used in ceramics processing and manufacturing, either as a casting material or for producing very thin films of metal oxides for various applications. Sol-gel derived materials find applications in a wide range of fields, including optics, electronics, energy, space, biosensors, medicine, reactive materials, and separation technology.

- **Layer-by-Layer Deposition**

This technique involves the sequential immersion of a substrate into electrolyte solutions with opposite electrostatic charges (Figure 11). This method allows the precise formation of nanometric-scale electrolyte films with high resolution control. Key applications include tuning the transport properties of NAA membranes, attaching nanoparticles and biomolecules, and fabricating polyelectrolytic nanotubular structures using NAA as a template (Md Jani et al., 2013).

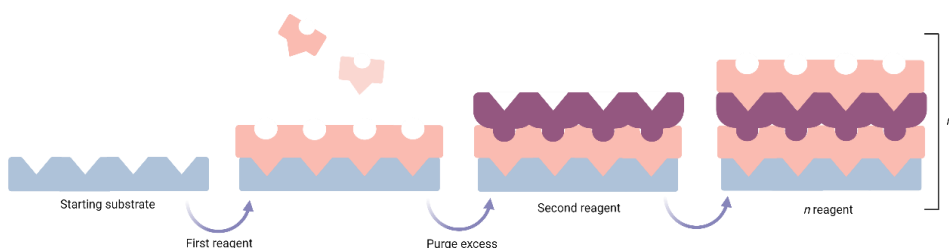


Figure 11. Diagram of NAA surface functionalization by the technique layer-by-layer deposition.

- **Functionalization with Organic and Phosphonic Acids**

Functionalization of NAA with organic and phosphonic acids is widely used to control wettability, enhance corrosion resistance, and ensure homogeneity of the formed layer. The process involves dip-coating to form a self-assembled monolayer (SAM) through chemical bonding of the acids with the hydroxyl groups on the NAA surface (Figure 12) (Alonso Frank et al., 2017; Queffélec et al., 2012). By varying the chain length, the surface properties can be finely tuned. These acids are compatible with a range of other organic functional groups, facilitating the attachment of additional organic/inorganic structures, such as nanoparticles, nanotubes, catalysts, and

biomolecules. Furthermore, this functionalization can be performed in various solvents, including water.

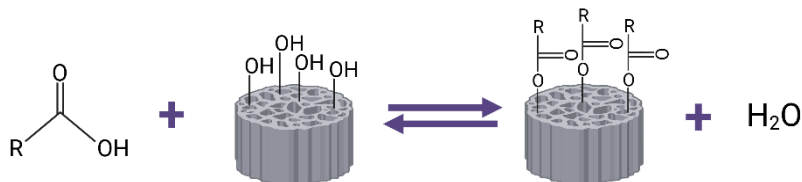


Figure 12. Schematic representation of the functionalization method for NAA surfaces with *n*-alkanoic acid.

- **Organosilane Modification of Aluminium Anodic Oxide (AAO)**

In this study, silanes are used to functionalize the NAA surface for biomolecule attachment. The method involves grafting organic molecules onto the NAA surface through spontaneous attachment and rearrangement from a liquid phase, forming self-assembled monolayers (SAMs). Organosilanes and phosphonates result in homogeneous layers on the alumina surface, enabling the addition of diverse reactive terminal functional groups, such as amine, isocyanate, carboxyl, epoxy, azide, halide, alkene, and alkyne. SAM formation occurs via the reaction with surface hydroxyl groups by simple incubation of the NAA substrate in a silane solution (Szczepanski et al., 2006). A schematic of silanization of hydroxylated NAA is shown in Figure 13.

By modifying the carbon chain length and terminal group, different functionalities can be imparted to the material. For instance, silanes with hydrophobic terminal groups like halides (e.g., trichloro-silanes and perfluoroalkyl-silanes) render the material hydrophobic, (Hendren et al., 2009; Ku et al., 2006; Odom et al., 2005) whereas silanes terminated with poly(ethylene glycol), amines, and epoxy groups significantly improve wettability, prevent biofouling, and enhance biocompatibility (La Flamme et al., 2007; S. W. Lee et al., 2005; K. C. Popat et al., 2004).

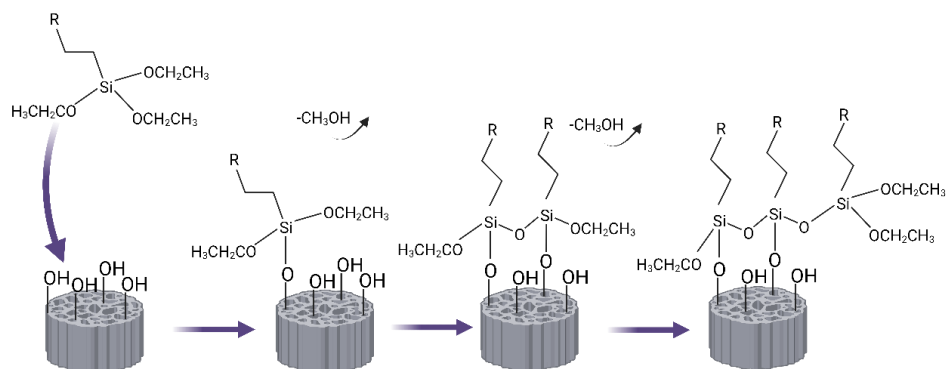


Figure 13. Representation of organosilane attachment and re-arrangement over NAA surfaces.

The most common application of organosilanes in material functionalization is forming an active layer for immobilizing other molecules or biomolecules, nanoparticles, polymers, quantum dots, or lipid bilayers, thereby providing functionality to hybrid organic-inorganic materials. They act as linkers, binding to the scaffold surface with one end and immobilizing specific bio-receptor molecules with the other. The terminal active groups dictate the conditions for receptor immobilization on the formed layer. Table 3 summarizes common organosilane reagents and the necessary reactions.

Table 3. Most common functionalizations of NAA with silanes and their chemical bond.

Organosilane	Terminal Group	Bond	Ref.
APTES	-NH ₂	Urea bond. Amide bond. Electrostatic interactions	(Sun et al., 2012; Yan et al., 2012)
ICPTS	-N=C=O	Urea bond.	(Yuan et al., 2012)

(3-azidopropyl) triethoxysilane / 3-Trimethylsiloxy-1-propyne	$-N_3 / -\equiv$	Huisgen cycloaddition	(X. He et al., 2012)
(3-mercaptopropyl) triethoxysilane	-SH	Thiol bond SH-Au bond	(Schloßbauer et al., 2012; Wu et al., 2013)
(3-iodopropyl) trimethoxysilane	-I / -Cl	Substitution reaction	(Díez et al., 2014)

Silanization, which covers a surface with organofunctional alkoxy silane molecules, is typically performed using (3-aminopropyl)triethoxysilane (APTES) and (3-isocyanatopropyl)triethoxysilane (ICPTS). Both share a similar chemical structure, differing only in the terminal active group—amine for APTES and isocyanate for ICPTS. The reaction mechanism for forming the surface monolayers is the same for both: hydrolysis of ethoxy groups converts alkoxy silanes into silanols, which rapidly condense with NAA surface hydroxyl groups to form the SAM (Figure 13) (Guy & Walker, 2016; Peña-Alonso et al., 2007).

Functionalizing NAA supports is a powerful approach for developing hybrid materials with new applications, particularly for immobilizing biomolecules on their surface, which is crucial for developing highly specific and sensitive sensing devices.

4. GATED MATERIALS

Gated materials are advanced materials that exhibit controlled access to their internal spaces, allowing them to selectively permit or block the passage of molecules, ions, or other substances. This gating mechanism is typically regulated by external stimuli,

such as changes in pH, temperature, light, magnetic or electric fields, and the presence of specific chemicals or biomolecules (Aznar et al., 2016; Sancenón et al., 2015). Gated materials are a key area of research in materials science due to their potential applications in various fields, including drug delivery, sensing, catalysis, and separation technologies.

Between gated materials it can be distinguished three main types divided by their porous structure and size. There are mesoporous materials, often used as hosts for gated systems due to their well-defined and tuneable pore structures. Examples include mesoporous silica and metal-organic frameworks (MOFs). When the porous structure is in the nanometer scale, we talk about nanoporous materials such as zeolites, which have small and precise pore sizes that can be modified to develop gating effects. Finally, there are also some polymeric materials that can undergo conformational changes in response to external stimuli, thereby acting as gates.

The integration of these 2D and 3D porous inorganic supports with (supra)molecular architectures has enabled the development of advanced nanodevices with numerous scientific and technological applications. Typically, gated materials comprise two primary components: (i) a responsive “gate-like” structure capable of “opening” or “closing” upon specific stimuli, and (ii) a porous inorganic support that can be loaded with various cargos.

The construction of gated materials involves the attachment of organic molecules, biomolecules, or supramolecules (varying in chemical nature, size, and shape) to the surface of a mesoporous inorganic scaffold. This configuration aims to regulate the diffusion of a cargo from the pores of the material to a solution, or vice versa, in response to predefined stimuli (Aznar et al., 2016). Generally, the pores are filled with specific cargos, while the outer surface is functionalized with (bio)molecules that control the release of the entrapped substances upon external stimulus application. Figure 14 illustrates a schematic of a gated material and its release mechanism.

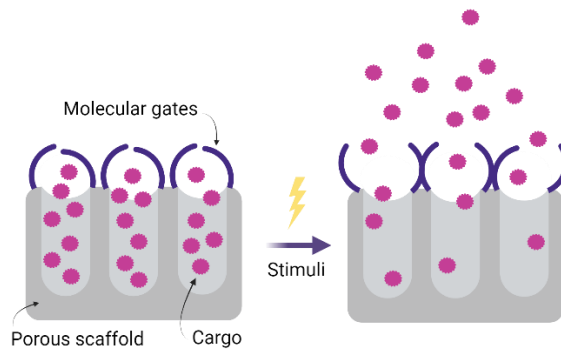


Figure 14. Illustration of a gated material

Research indicates that the primary applications of gated materials are in controlled release systems, particularly for biomedical purposes (Barreto et al., 2011; Doane & Burda, 2012; Z. Li et al., 2012; Stark, 2011). More recently, gated materials have gained attention for their potential in sensing and molecular recognition, showcasing a promising and versatile application area (Coll et al., 2013; Sancenón et al., 2015).

Key considerations in designing gated materials include selecting the stimulus that will trigger cargo release and choosing the molecular gate that will respond to this stimulus, facilitating mass transport. Depending on external stimuli, the gates can be categorized into five main types:

A. **Temperature-Responsive Gating:** Uses materials that alter their permeability with temperature fluctuations, useful for controlled release and thermal regulation applications (Lai et al., 2010).

B. **Light-Responsive Gating:** Incorporates photo-responsive molecules that change their configuration upon exposure to light, enabling precise control over the gating mechanism (Johansson et al., 2008; Lin et al., 2010).

C. **Magnetic/Electric Field-Responsive Gating:** Utilizes magnetic or electric fields to modulate the opening and closing of gates, often employed in smart sensing and actuation systems (C. Liu et al., 2009; Thomas et al., 2010).

D. **pH-Responsive Gating:** Involves materials that change their structure or surface charge in response to pH changes, commonly used in drug delivery to release drugs in specific parts of the body (Casasús et al., 2004; Cauda et al., 2010; Guo et al., 2010; Llopis-Lorente et al., 2017; Meng et al., 2010; A. Popat et al., 2012; Ruiz-Rico et al., 2017; Tian et al., 2017; Yang et al., 2005).

E. **Chemical/Biochemical-Responsive Gating:** Engages specific chemical reactions or interactions with biomolecules to trigger the gating mechanism, crucial for selective sensing and bio-responsive systems. Prevalent stimuli are oligonucleotides (Schlossbauer et al., 2010; Y. Zhang et al., 2012; C. L. Zhu et al., 2011), metal cations (Zhou et al., 2014), saccharides (Bernardos et al., 2010; Mal, Fujiwara, & Tanaka, 2003; Mal, Fujiwara, Tanaka, et al., 2003), small molecules (Aznar et al., 2011; Candel et al., 2011; Casasús et al., 2006; Choi et al., 2011; Schulz et al., 2011; Song & Yang, 2015; L. Zhang et al., 2014; Zhao et al., 2009), small redox active molecules (R. Liu et al., 2008; Mortera et al., 2009), enzymes (Bernardos et al., 2009; Park et al., 2009; Patel et al., 2008; Schlossbauer et al., 2009; Thornton & Heise, 2010), and peptides or proteins (Coll et al., 2011; Porta et al., 2011) among others. Gating mechanisms composed of biomolecules responsive to other biomolecules have gained significant importance because of their specificity, selectivity, and biocompatibility. They have been extensively utilized in drug delivery systems due to their well-documented advantages, such as targeted release, reduced side effects, and enhanced efficacy. Additionally, the application of biomolecule-gated materials in sensing protocols has garnered increasing attention recently.

In 2003, Fujiwara and colleagues (Mal, Fujiwara, & Tanaka, 2003) presented a pioneering study on gated materials utilizing MCM-41 mesoporous silica nanoparticles

(MSNs). These nanoparticles were loaded with the steroid cholestane and demonstrated the ability to photochemically control the uptake, storage, and release of the cargo (Figure 15B). The methodology involved filling the pores of the MSNs with cholestane, followed by the functionalization of the external surface with 7-[(3-triethoxysilyl)propoxy]coumarin. Upon irradiation with light of wavelengths exceeding 310 nm, the coumarin derivative undergoes a [2+2] photodimerization reaction, forming bulky cyclobutane dimers in an anti-head-to-head conformation. These dimers obstruct the pore entrance, thereby preventing the release of cholestane. The photodimerization is reversible; exposure to 250 nm irradiation reverts the dimers to their monomeric form, allowing for the release of cholestane. Similar control over pore accessibility was achieved with other cargo molecules, such as pyrene, phenanthrene, and progesterone, thereby demonstrating the versatility of this photochemically regulated system.

Other representative example of a gated material was reported by Stoddart, Zink, and co-workers (Hernandez et al., 2004) which reported the first example that used rotaxanes coupled with a redox reaction to design gated materials. In their research, the authors developed mesoporous silica nanoparticles (MSNs) loaded with $\text{Ir}(\text{ppy})_3$, modifying the surface with a 1,5-dioxynaphthalene (DNP) derivative. The nanopores were sealed through the formation of an inclusion complex between the DNP derivative and cyclobis(paraquat-p-phenylene) (CBPQT^{4+}). Upon reduction of CBPQT^{4+} with NaCNBH_3 , the inclusion complex was disrupted, leading to the release of the encapsulated dye.

Subsequently, the authors engineered a more intricate system wherein the CBPQT^{4+} ring could shuttle between a tetrathiafulvalene (TTF) unit and a DNP moiety (Mal, Fujiwara, Tanaka, et al., 2003), both connected by an oligoethylene glycol chain incorporating a rigid terphenylene spacer. In this supramolecular construct, CBPQT^{4+} exhibits a preference for the TTF station. However, oxidation of TTF using $\text{Fe}(\text{ClO}_4)_3$ to form a TTF^{2+} dication causes the CBPQT^{4+} ring to relocate to the DNP moiety. The addition of ascorbic acid subsequently reduces the TTF^{2+} back to its neutral state, prompting the

CBPQT⁴⁺ ring to return to the TTF station. This bistable [2]rotaxane unit was covalently attached to the MSNs by forming a carbamate linkage between the hydroxyl group of the [2]rotaxane and isocyanate groups on the silica surface. The material was then loaded with either Ir(ppy)₃ or Rhodamine B (RhB). Release kinetics of the gating system were examined in a PhMe (1:1) mixture for the iridium complex and in MeCN for RhB. Additionally, the authors engineered a hybrid material containing the dumbbell component of the [2]rotaxane but lacking the CBPQT⁴⁺ ring. This second material was incapable of controlling RhB release, resulting in the immediate diffusion of RhB into the solution. These findings confirmed the critical role of CBPQT⁴⁺ ring dynamics in regulating the transport of guest molecules from the nanopores to the surrounding solution.

This method is especially attractive due to its potential for harnessing endogenous reducing agents present within cells as natural triggers. The elevated levels of redox-active species associated with certain diseases, such as cancer, underscore the broad potential of redox-responsive capped systems in biomedical applications. The ability to selectively release therapeutic agents in response to specific intracellular conditions highlights the promise of these systems for targeted treatment strategies.

The following examples represented in Figure 15 illustrate the increasing complexity in the design of molecular gates, which integrate more sophisticated structures and allow the interconnection of multiple nanodevices with distinct gating mechanisms and encapsulated cargos.

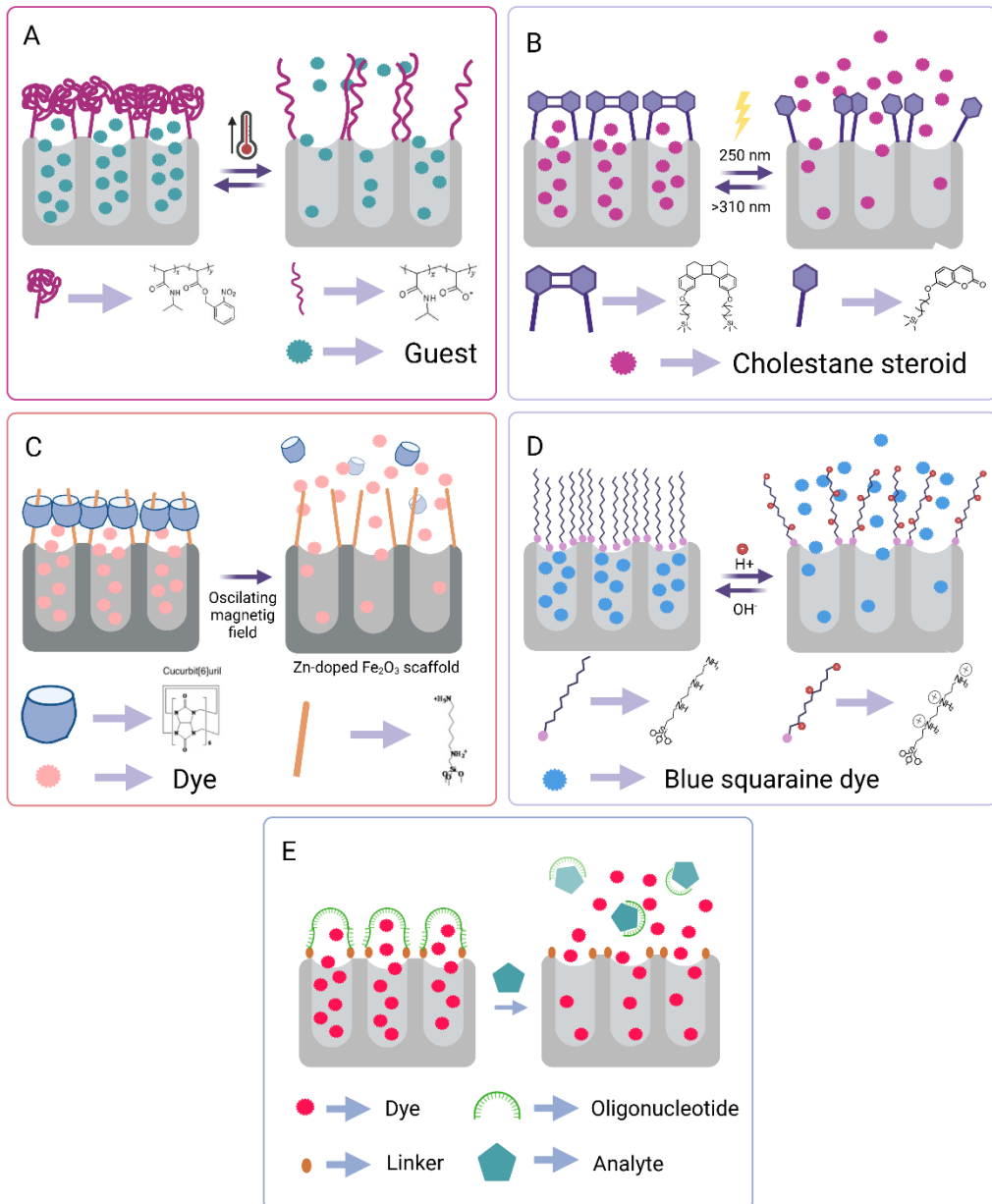


Figure 15. Schematic representation of gated materials controlled by temperature (A), light (B), magnetic field (C), pH (D) and biochemical interaction (E).

Over the years, gated ensembles have progressed from simple molecules or individual entities to intricate supramolecular structures with a large number of applications. Between such applications we can highlight the configuration of drug delivery systems, in which the gated materials can be used to encapsulate drugs and release them in a controlled manner at the target site, minimizing side effects and improving therapeutic efficiency (Kingsley et al., 2006). In addition to this, in relation to chemical processes regulation, gated catalytic materials can control the access of reactants to catalytic sites, enhancing selectivity and efficiency of catalytic reactions. Also, they can be used in separation technologies for example in filtration and purification processes where selective gating allows for the separation of specific components from a mixture (Aznar et al., 2016). Other use we have seen recently is the use of gated materials for environmental remediation, they can capture and release pollutants in response to environmental triggers, aiding in the cleanup of contaminated sites (Pete et al., 2021). Finally, gated materials have been used nowadays for sensing challenges, to detect specific analytes by a selective interaction with the sensing element (Sancenón et al., 2015). This use is the main theme of this thesis and what we are going to focus on.

Overall, gated materials represent a versatile and dynamic area of research with the potential to revolutionize numerous technological applications through their ability to provide controlled and responsive functionality. The development of gated materials faces several significant challenges, but future directions seem to focus on achieving precise control over gating mechanisms, even if it is a difficult task. Scalability results in another challenge, with scaling up production for industrial applications proving both difficult and costly. Additionally, ensuring the long-term stability and durability of gated materials under operational conditions is critical for their practical applications. Integrating these materials into existing technologies and systems seamlessly and cost-effectively is a key area of ongoing research.

5. IMPORTANCE OF GLOBAL INFECTIOUS DISEASE CONTROL

The concepts of pathogenicity and virulence are fundamental in the field of microbiology, shaping our understanding of the complex relationships between microorganisms and diseases. Since the pioneering work of Pasteur and Koch over a century ago, the identification of pathogens and the study of their virulence have become central to combat infectious diseases. These concepts have directed the focus of microbiologists, medical practitioners, and epidemiologists toward a selected group of microorganisms and viruses that represent a significant threat to human health. Despite the successes in developing antimicrobial agents, vaccines, and public health strategies, the persistence and emergence of infectious diseases in the modern era highlight the ongoing relevance and complexity of these concepts (Isenberg, 1988).

In the 20th century, advancements in hygiene, medical therapies, and the development of antibiotics significantly reduced the impact of many infectious diseases, especially in developed regions of the world. However, infectious diseases remain a significant global health challenge, representing the 30% of the leading causes of morbidity and mortality and 25% of deaths worldwide (Murray & Lopez, 2013). Recent years have seen a rise in emerging infectious diseases, many of which are linked to human activities that alter environments or spread pathogens to new geographical regions due to the global human and commercial transport (Jones et al., 2008; K. F. Smith et al., 2007, 2009; Taylor et al., 2001; Woolhouse & Gowtage-Sequeria, 2005). These developments underscore the need for a better understanding of pathogenicity and virulence, as well as the factors (both natural and anthropogenic) that influence the global distribution of diseases (K. F. Smith & Guégan, 2010).

The interconnections between human health and pathogenic microorganisms are intricate and far-reaching, influencing not only public health and medical advances but also food security, business, and economic stability. The ongoing emergence of new

pathogens and the re-emergence of old ones in new contexts require a holistic approach that integrates epidemiology, ecology, and socioeconomic factors. With a global population approaching 8.3 billion, including 800 million people living in underdeveloped conditions and around 2 billion lacking access to clean water or electricity, the need for improved strategies to control and contain infectious diseases is more urgent than ever (Facciola et al., 2023; Oren & Brown, 2023; Schulhof, 2007).

The study of pathogens and their virulence in combination with the research development in the diagnostic area remain critical in addressing the challenges caused by infectious diseases in the contemporary world. While significant progress has been made in reducing the impact of these diseases through medical and public health interventions, the persistence and emergence of new infectious threats highlight the complexity of the microbial world and its interactions with human societies. As we continue to confront these challenges, it is essential to refine our strategies, considering both the biological and environmental factors that shape the global landscape of infectious diseases. The lessons from the past century, combined with a forward-looking approach to emerging threats, will be key to safeguarding global health in the future.

5.1. Vegetal-infecting pathogens

Over the past fifty years, the field of plant pathology has undergone a significant transformation, shifting its focus from practical problem-solving to more specialized academic inquiries (Milgroom & Peever, 2003). This shift reflects the growing depth and complexity of our understanding of plant diseases and host-pathogen interactions. However, practical disease management remains a critical component of the field, ensuring that theoretical advances translate into real-world solutions. The constant influx of challenges underscores the dynamic and evolving nature of plant pathology, where old problems are often replaced by new ones, requiring continuous innovation and adaptation.

The potential for crop losses due to pests, diseases, and weeds is substantial, with estimates suggesting that up to 70% of global crop yields could be affected (Oerke & Dehne, 2004). However, effective crop protection practices have successfully reduced actual losses to around 30%. As global population growth and increasing demand for food exert pressure on agricultural systems, it is anticipated that crop production will need to double in the coming decades to meet these demands (Tilman, 1999). Achieving this goal will necessitate maintaining or improving the efficiency of crop protection strategies, which have historically relied heavily on the use of synthetic pesticides. From the 1990s, global pesticide use increased by an average of 4.4% annually and the the forecast is to exponentially increase these values over the coming years (Oerke & Dehne, 2004), reflecting the reliance on chemical interventions in combating agricultural pests and diseases.

However, the long-term sustainability of chemical-based crop protection strategies has come under scrutiny. Numerous studies have documented the negative effects of pesticides on human health, biodiversity, and even agricultural productivity itself (Wilson & Tisdell, 2001). These effects include the disruption of natural ecosystems, the elimination of beneficial organisms, and the development of resistance in target pest populations. As pests and pathogens evolve resistance to chemical treatments, the effectiveness of these strategies diminishes, leading to a vicious cycle of increasing pesticide use and decreasing efficacy (Gullino et al., 2000; Ma & Michailides, 2005; Urban & Lebeda, 2006). This growing resistance, coupled with environmental and health concerns, highlights the need for a paradigm shift in how we approach crop protection.

The impact of plant diseases on human well-being is a critical but often overlooked aspect of plant pathology. Agricultural losses due to pathogens can have profound effects on local economies, particularly in regions where agriculture is a primary source of livelihood. In such cases, the failure of a crop due to disease can lead to food insecurity, malnutrition, and economic hardship for smallholder farmers and their

communities. This is especially true in situations where crops lack genetic resistance to pathogens and effective chemical controls are not available. The resulting threats to economic and food security underscore the importance of developing resilient agricultural systems that can withstand the challenges caused by plant pathogens.

Land use changes remain a significant driver of pathogen emergence, even thousands of years after the advent of agrarian societies (Woolhouse & Gowtage-Sequeria, 2005). The conversion of natural ecosystems into agricultural land creates new opportunities for pathogens to spread and evolve, leading to the emergence of new diseases. This phenomenon is particularly pronounced in bacterial diseases, which are more strongly associated with land use changes than viral diseases. Additionally, zoonotic diseases (those that can be transmitted between animals and humans) are more influenced by these changes than non-zoonotic diseases (K. F. Smith & Guégan, 2010). These findings highlight the complex interplay between agriculture, land use, and disease emergence, emphasizing the need for integrated approaches to managing plant health.

Throughout their life cycles, plants are exposed to a wide range of environmental factors, including temperature fluctuations, moisture levels, soil quality, and interactions with other organisms such as weeds, insects, nematodes, and microorganisms (bacteria, fungi, and viruses). Each of these factors can have a significant impact on plant health, either beneficial or detrimental. Farmers and scientists must consider not only the biological interactions between plants and pathogens but also the economic and market forces that drive agricultural practices. While market trends influence agricultural decisions, the environment remains the most critical factor in determining the incidence and severity of plant diseases from year to year.

The properties of the agricultural landscape also play a significant role in shaping the genetic structure and function of pathogen populations. This, in turn, influences the ecological and evolutionary genetics of pathogens and the likelihood of disease

(re)emergence. The simultaneous effects of ecological changes and genetic evolution often drive the emergence and spread of plant diseases (Real et al., 2005). This phenomenon is particularly evident in cases where pathogen strains overcome plant disease resistance (Parlevliet, 2002) or where pathogens develop resistance to pesticides (Oerke & Dehne, 2004). Landscape properties can influence these processes by promoting high gene flow, which facilitates the spread of virulent strains, and by fostering high genetic diversity within pathogen populations, increasing the probability of virulent strain emergence.

Pathogens with high gene flow and genotype diversity pose greater risks than those with limited gene flow. Populations with high gene flow have a larger effective population size, increasing the likelihood of virulent (or resistant) mutants arising within the population. Moreover, these populations are more capable of spreading virulent mutants across large geographic areas (McDonald & Linde, 2002). Theoretically, it should be possible to reduce the risk of new virulent pathogen strains (or resistant strains) by designing management strategies that limit gene/genotype flow between pathogen populations. This would require identifying landscape features that restrict gene flow and determining the appropriate spatial scale for implementing management strategies (Plantegenest et al., 2007).

The relevance of plant disease outbreaks at the landscape level is increasingly recognized. This trend may be a consequence of the growing homogeneity of agricultural landscapes, driven by larger field sizes, uniform crop choices, and the artificial movement of pathogens between regions. In response, plant pathologists are employing the quantitative tools of landscape ecology to address these regional outbreaks. By extending the classic disease triangle (host-pathogen-environment) to encompass multiple spatial scales, they aim to manage plant diseases at the landscape level and protect crop health in a changing world (Moslonka-Lefebvre et al., 2011).

In conclusion, addressing the complex challenges posed by plant pathogens requires a multi-faceted approach that integrates cutting-edge scientific research, technological innovation, and sustainable agricultural practices. By leveraging our growing understanding of the ecological and evolutionary dynamics of pathogens, we can develop effective disease management strategies that protect crops, safeguard ecosystems, and ensure food security for future generations. The shift from traditional, chemical-based crop protection to a more holistic, landscape-scale approach represents a paradigm change that holds the promise of a more resilient and sustainable agricultural system. By fostering interdisciplinary collaboration and embracing the principles of landscape ecology, we can meet the challenges of plant disease management in an increasingly interconnected and rapidly changing world.

5.2. Animal-infecting pathogens

Emerging infectious diseases (EIDs) represent a significant challenge to global health and biosecurity in the 21st century. The increasing rate at which new pathogens are being identified, coupled with the complex interplay between human activities and ecological dynamics, underscores the need for robust and integrated surveillance systems. The identification of gaps in current surveillance mechanisms across humans, domestic animals, and wildlife, alongside the development of cost-effective strategies to address these gaps, is critical for early detection and control of zoonotic pathogens. These pathogens, which often cross species barriers, highlight the importance of coordinated global efforts to mitigate the risks associated with infectious diseases that do not respect national borders (Cleaveland et al., 2007; Kuiken et al., 2005).

The expert working groups should prioritize several tasks to strengthen global surveillance systems. Key among these tasks is identifying major gaps in existing surveillance frameworks and developing cost-effective methods to fill them. This includes implementing animal sampling in live animal markets, game farms, and points of entry, as

well as establishing systems for the proper preservation of samples from collection sites to laboratories. Additionally, addressing political barriers to effective surveillance, such as conflicting mandates among authorities, and integrating human and animal surveillance at both national and international levels, are essential steps. Facilitating the development and distribution of validated diagnostic tests for the rapid and sensitive detection of zoonotic pathogens across a wide range of potential host species is also critical. Encouraging research into the underlying mechanisms of disease emergence will contribute to innovative approaches to tackle these challenges (Kuiken et al., 2005).

Zoonotic pathogens, which naturally transmit between vertebrate hosts and humans, have been a consistent source of new infectious diseases throughout human history. Recent decades have seen a significant increase in the emergence of these pathogens, with over 30 new pathogens identified in the last 30 years (Woolhouse, 2002). The rate at which humans are encountering new infections appears unprecedented, reflecting the profound impact of anthropogenic factors on epidemiological transitions (Barrett et al., 1998; McMichael, 2004). The rise of EIDs, many of which involve wildlife hosts, suggests that animal-to-human transmission is a critical component in the emergence of new human diseases. (Cleaveland et al., 2007).

The predominance of viral pathogens among human and animal EIDs underscores the importance of maintaining expertise in virological techniques, improving antiviral treatments, and fostering collaboration between medical and veterinary virologists. The rapid international response to the SARS outbreak, facilitated by pre-existing knowledge of animal coronaviruses, exemplifies the value of such interdisciplinary cooperation. This collaborative approach led to the swift isolation, diagnosis, and characterization of the SARS virus, as well as a deeper understanding of its pathogenesis and immune response (Berger et al., 2004; Cavanagh, 2003, 2005). However, the frequent occurrence of host-switching events and the potential for small outbreaks to evade detection necessitate

improved diagnostic capabilities and communication in remote communities, where early detection could prevent large-scale epidemics (Shears, 2000a, 2000b).

The ongoing emergence of infectious diseases, particularly those of zoonotic origin, represents a formidable challenge to global health security. Addressing this challenge requires a multifaceted approach that includes strengthening surveillance systems, enhancing international cooperation, and advancing our understanding of the factors driving disease emergence. By identifying and addressing the gaps in current surveillance efforts, particularly in areas where human and animal health intersect, we can better anticipate and mitigate the risks that the EIDs represent. The integration of human and animal surveillance, combined with innovative diagnostic tools and interdisciplinary collaboration, will be key to improving our ability to detect, respond to, and control these threats. As the global community continues to confront both new and re-emerging infectious diseases, sustained commitment to these efforts will be essential to safeguarding public health and preventing future pandemics.

5.2.1. Pathogens and respiratory diseases

The lungs, like the skin, are continually exposed to the external environment. However, unlike the skin, the lungs serve as a critical gas exchange organ, with delicate membranes that must remain moist. Each day, the lungs are exposed to over 7,000 liters of air, necessitating robust protection against daily bombardment by particles, including dust, pollen, and pollutants, as well as viruses and bacteria. These pathogens represent a significant threat by potentially causing lung injury or invading the respiratory system to cause life-threatening infections.

Acute respiratory tract infections (RTIs) are the most common affliction in humans. In developed or industrialized countries, upper and lower RTIs are significant causes of disability and lost work or school days, with mortality generally low except among high-risk patients. However, in developing countries, respiratory infections are not

only a major cause of disability but also the leading cause of death in children under five years old. The clinical impact of respiratory viruses on humans is large. While various microorganisms, including viruses, bacteria, fungi, parasites, and protozoa, can infect the respiratory tract, only certain viruses and bacteria are common causes. Among these, Adenoviruses, Coronaviruses, Enteroviruses, Influenzaviruses, Respiratory Syncytial Virus (RSV), and certain classes of Herpesviruses, along with bacteria such as Streptococcus groups A, C, and G, *Arcanobacterium haemolyticum*, *Chlamydia pneumoniae*, and *Mycoplasma pneumoniae*, are notable (Denny Jr., 1995).

Inside these respiratory tract infections, upper respiratory tract infections (URTIs) are the most common medical complaints worldwide. In Europe, they account for half of all lost work time due to acute illness. Although largely self-limiting, these infections place a significant burden on primary care physicians and have a substantial economic impact on communities (Seaton et al., 2008). URTIs can lead to more severe lower respiratory tract infections (LRTIs), a global concern, particularly for millions of children in developing countries where the lack of antimicrobial therapy results in considerable mortality. In adults, URTIs can complicate into more severe LRTIs, such as pneumococcal pneumonia, which often follows viral catarrhal symptoms and is more prevalent during the winter months. The season of respiratory viral infections is also associated with increased asthma attacks and exacerbations of chronic respiratory conditions like chronic bronchitis and cystic fibrosis.

The Rhinovirus genus, belonging to the Picornaviridae family, contains over 100 antigenically distinct species and is the most common cause of the common cold, accounting for about 30% of cases. Coronaviruses, which make up the second most common group of cold-causing viruses, are pathogenic to humans and are the only members of the Coronaviridae family. (Seaton et al., 2008).

The emergence of SARS-CoV-2 and the ensuing COVID-19 pandemic profoundly impacted society, reshaping global health, economics, and public policies. Declared a pandemic by the World Health Organization (WHO) on March 11, 2020, COVID-19 quickly escalated into a global crisis, resulting in over 3 million cases and more than 200,000 deaths within its initial months. By 2023, the virus had claimed over 6 million lives, with millions more suffering long-term health effects. This devastating toll highlighted the interconnectedness of health and economics, exposing vulnerabilities in global preparedness and emphasizing the need for more robust epidemiological frameworks, particularly in low-income regions (Ashmore and Sherwood, 2023).

Health systems worldwide faced overwhelming costs, with governments allocating trillions to testing, vaccination campaigns, and emergency medical care. Testing technologies, including RT-PCR and rapid antigen tests, became central to controlling the virus's spread. RT-PCR tests, provided high sensitivity but required advanced laboratory infrastructure and skilled personnel, limiting their accessibility. Rapid antigen tests offered a more affordable alternative, ranging from 5-20€ per test, with faster results but reduced sensitivity. These disparities in cost and performance underscored significant inequalities in healthcare accessibility (Pak et al., 2020).

The high costs and limitations of existing diagnostic methods have driven the demand for innovative detection systems that are faster, cheaper, and more accessible. This global health crisis has revealed the urgency of improving detection systems and healthcare infrastructure, ensuring that populations worldwide are better prepared for emerging threats. Investing in accessible and innovative diagnostic solutions will be essential to advancing global health security and reducing the socioeconomic impact of future outbreaks.

In conclusion, respiratory tract infections, particularly those caused by viruses, represent a significant global health challenge, with varying impacts depending on

geographic and socioeconomic factors. Understanding the epidemiology and transmission of these pathogens is essential for developing effective prevention, control and treatment strategies, particularly in vulnerable populations where the burden of disease is greatest. Continued research and surveillance are crucial to mitigating the impact of these infections and improving global health outcomes.

6. REFERENCES

1. Abedi-Firoozjah, R., Ebdali, H., Soltani, M., Abdolahi-Fard, P., Heydari, M., Assadpour, E., Azizi-Lalabadi, M., Zhang, F., & Jafari, S. M. (2024). Nanomaterial-based sensors for the detection of pathogens and microbial toxins in the food industry; a review on recent progress. In *Coordination Chemistry Reviews* (Vol. 500). <https://doi.org/10.1016/j.ccr.2023.215545>
2. Adachi, T., & Nakamura, Y. (2019). Aptamers: A review of their chemical properties and modifications for therapeutic application. In *Molecules* (Vol. 24, Issue 23). <https://doi.org/10.3390/molecules24234229>
3. Akine, S., Utsuno, F., Piao, S., Orita, H., Tsuzuki, S., & Nabeshima, T. (2016). Synthesis, Ion Recognition Ability, and Metal-Assisted Aggregation Behavior of Dinuclear Metallohosts Having a Bis(Saloph) Macrocyclic Ligand. *Inorganic Chemistry*, 55(2). <https://doi.org/10.1021/acs.inorgchem.5b02288>
4. Alonso Frank, M., Meltzer, C., Braunschweig, B., Peukert, W., Boccaccini, A. R., & Virtanen, S. (2017). Functionalization of steel surfaces with organic acids: Influence on wetting and corrosion behavior. *Applied Surface Science*, 404. <https://doi.org/10.1016/j.apsusc.2017.01.199>
5. Ameen, S., Akhtar, M. S., Godbole, R., & Shin, H.-S. (2020). An Introduction to Nanoporous Materials. *Nanofluid Flow in Porous Media*.

6. Arya, A., Gangwar, A., & Kumar, A. (2019). Biosensors in animal biotechnology. In *Nanotechnology in Modern Animal Biotechnology: Concepts and Applications*. <https://doi.org/10.1016/B978-0-12-818823-1.00006-5>

7. Ashmore, P., & Sherwood, E. (2023). An overview of COVID-19 global epidemiology and discussion of potential drivers of variable global pandemic impacts. *Journal of Antimicrobial Chemotherapy*, 78(Supplement_2), ii2–ii11. <https://doi.org/10.1093/jac/dkad311>

8. Aznar, E., Mondragón, L., Ros-Lis, J. V., Sancenón, F., Marcos, M. D., Martínez-Máñez, R., Soto, J., Pérez-Payá, E., & Amorós, P. (2011). Finely Tuned Temperature-Controlled Cargo Release Using Paraffin-Capped Mesoporous Silica Nanoparticles. *Angewandte Chemie - International Edition*, 50(47). <https://doi.org/10.1002/anie.201102756>

9. Aznar, E., Oroval, M., Pascual, L., Murguía, J. R., Martínez-Máñez, R., & Sancenón, F. (2016). Gated Materials for On-Command Release of Guest Molecules. In *Chemical Reviews* (Vol. 116, Issue 2). <https://doi.org/10.1021/acs.chemrev.5b00456>

10. Bahadır, E. B., & Sezgintürk, M. K. (2016). Lateral flow assays: Principles, designs and labels. In *TrAC - Trends in Analytical Chemistry* (Vol. 82). <https://doi.org/10.1016/j.trac.2016.06.006>

11. Balzani, V. (1990). Supramolecular photochemistry. *Pure and Applied Chemistry*, 62(6). <https://doi.org/10.1351/pac199062061099>

12. Bangham, A. D., & Horne, R. W. (1964). Negative staining of phospholipids and their structural modification by surface-active agents as observed in the electron microscope. *Journal of Molecular Biology*, 8(5). [https://doi.org/10.1016/S0022-2836\(64\)80115-7](https://doi.org/10.1016/S0022-2836(64)80115-7)

13. Barreto, J. A., O'Malley, W., Kubeil, M., Graham, B., Stephan, H., & Spiccia, L. (2011). Nanomaterials: Applications in cancer imaging and therapy. *Advanced Materials*, 23(12). <https://doi.org/10.1002/adma.201100140>

14. Barrett, R., Kuzawa, C. W., McDade, T., & Armelagos, G. J. (1998). Emerging and Re-emerging Infectious Diseases: The Third Epidemiologic Transition. *Annual Review of Anthropology*, 27. <https://doi.org/10.1146/annurev.anthro.27.1.247>

15. Bengough, G. D., & Stuart, J. M. (1923). Improved process of protecting surfaces of aluminum and aluminum alloys. UK Patent.

16. Berger, A., Drosten, C., Doerr, H. W., Stürmer, M., & Preiser, W. (2004). Severe acute respiratory syndrome (SARS) - Paradigm of an emerging viral infection. In *Journal of Clinical Virology* (Vol. 29, Issue 1). <https://doi.org/10.1016/j.jcv.2003.09.011>

17. Bernardos, A., Aznar, E., Marcos, M. D., Martínez-Máñez, R., Sancenón, F., Soto, J., Barat, J. M., & Amorós, P. (2009). Enzyme-responsive controlled release using mesoporous silica supports capped with lactose. *Angewandte Chemie - International Edition*, 48(32). <https://doi.org/10.1002/anie.200900880>

18. Bernardos, A., Mondragón, L., Aznar, E., Marcos, M. D., Martínez-Máñez, R., Sancenón, F., Soto, J., Barat, J. M., Pérez-Payá, E., Guillem, C., & Amorós, P. (2010). Enzyme-responsive intracellular controlled release using nanometric silica mesoporous supports capped with "saccharides." *ACS Nano*, 4(11). <https://doi.org/10.1021/nn101499d>

19. Bhardwaj, H., Sumana, G., & Marquette, C. A. (2021). Gold nanobipyramids integrated ultrasensitive optical and electrochemical biosensor for Aflatoxin B1 detection. *Talanta*, 222. <https://doi.org/10.1016/j.talanta.2020.121578>

20. Callan, J. F., De Silva, A. P., & Magri, D. C. (2005). Luminescent sensors and switches in the early 21st century. In *Tetrahedron* (Vol. 61, Issue 36). <https://doi.org/10.1016/j.tet.2005.05.043>

21. Candel, I., Bernardos, A., Climent, E., Marcos, M. D., Martínez-Máñez, R., Sancenón, F., Soto, J., Costero, A., Gil, S., & Parra, M. (2011). Selective opening of nanoscopic capped mesoporous inorganic materials with nerve agent simulants; An application to design chromo-fluorogenic probes. *Chemical Communications*, 47(29). <https://doi.org/10.1039/c1cc12727f>

22. Carlsson, N., Gustafsson, H., Thörn, C., Olsson, L., Holmberg, K., & Åkerman, B. (2014). Enzymes immobilized in mesoporous silica: A physical-chemical perspective. In *Advances in Colloid and Interface Science* (Vol. 205). <https://doi.org/10.1016/j.cis.2013.08.010>

23. Casasús, R., Aznar, E., Marcos, M. D., Martínez-Máñez, R., Sancenón, F., Soto, J., & Amorós, P. (2006). New methods for anion recognition and signaling using nanoscopic gatelike scaffoldings. *Angewandte Chemie - International Edition*, 45(40). <https://doi.org/10.1002/anie.200602045>

24. Casasús, R., Marcos, M. D., Martínez-Máñez, R., Ros-Lis, J. V., Soto, J., Villaescusa, L. A., Amorós, P., Beltrán, D., Guillem, C., & Latorre, J. (2004). Toward the development of ionically controlled nanoscopic molecular gates. *Journal of the American Chemical Society*, 126(28). <https://doi.org/10.1021/ja048095i>

25. Cauda, V., Argyo, C., Schlossbauer, A., & Bein, T. (2010). Controlling the delivery kinetics from colloidal mesoporous silica nanoparticles with pH-sensitive gates. *Journal of Materials Chemistry*, 20(21). <https://doi.org/10.1039/b918590a>

26. Cavanagh, D. (2003). Severe acute respiratory syndrome vaccine development: Experiences of vaccination against avian infectious bronchitis coronavirus. In *Avian Pathology* (Vol. 32, Issue 6). <https://doi.org/10.1080/03079450310001621198>

27. Cavanagh, D. (2005). Coronaviridae: a review of coronaviruses and toroviruses. In *Coronaviruses with Special Emphasis on First Insights Concerning SARS*. https://doi.org/10.1007/3-7643-7339-3_1

28. Cavenati, S., Grande, C. A., Lopes, F. V. S., & Rodrigues, A. E. (2009). Adsorption of small molecules on alkali-earth modified titanosilicates. *Microporous and Mesoporous Materials*, 121(1–3). <https://doi.org/10.1016/j.micromeso.2009.01.012>

29. Chen, W., Wu, J. S., & Xia, X. H. (2008). Porous anodic alumina with continuously manipulated pore/cell size. *ACS Nano*, 2(5). <https://doi.org/10.1021/nn700389j>

30. Cheng, C., & Ngan, A. (2015). Theoretical pore growth models for nanoporous alumina. *Springer Series in Materials Science*, 219. https://doi.org/10.1007/978-3-319-20334-8_2

31. Choi, Y. L., Jaworski, J., Seo, M. L., Lee, S. J., & Jung, J. H. (2011). Controlled release using mesoporous silica nanoparticles functionalized with 18-crown-6 derivative. *Journal of Materials Chemistry*, 21(22). <https://doi.org/10.1039/c1jm11334h>

32. CLARK, L. C., WOLF, R., GRANGER, D., & TAYLOR, Z. (1953). Continuous recording of blood oxygen tensions by polarography. *Journal of Applied Physiology*, 6(3). <https://doi.org/10.1152/jappl.1953.6.3.189>

33. Cleaveland, S., Haydon, D. T., & Taylor, L. (2007). Overviews of pathogen emergence: Which pathogens emerge, when and why? In *Current Topics in Microbiology and Immunology* (Vol. 315). https://doi.org/10.1007/978-3-540-70962-6_5

34. Coll, C., Bernardos, A., Martínez-Máñez, R., & Sancenón, F. (2013). Gated silica mesoporous supports for controlled release and signaling applications. *Accounts of Chemical Research*, 46(2). <https://doi.org/10.1021/ar3001469>

35. Coll, C., Mondragón, L., Martínez-Máñez, R., Sancenón, F., Marcos, M. D., Soto, J., Amorós, P., & Pérez-Payá, E. (2011). Enzyme-mediated controlled release systems by anchoring peptide sequences on mesoporous silica supports. *Angewandte Chemie - International Edition*, 50(9). <https://doi.org/10.1002/anie.201004133>

36. de Castro, A. C. H., Alves, L. M., Siquieroli, A. C. S., Madurro, J. M., & Brito-Madurro, A. G. (2020). Label-free electrochemical immunosensor for detection of oncomarker CA125 in serum. *Microchemical Journal*, 155. <https://doi.org/10.1016/j.microc.2020.104746>

37. Demchenko, A. P. (2009). Introduction to fluorescence sensing. In *Introduction to Fluorescence Sensing*. <https://doi.org/10.1007/978-1-4020-9003-5>

38. Denny Jr., F. W. (1995). The clinical impact of human respiratory virus infections. *American Journal of Respiratory and Critical Care Medicine*, 152(4 Pt 2).

39. Descalzo, A. B., Martínez-Máñez, R., Sancenón, F., Hoffmann, K., & Rurack, K. (2006). The supramolecular chemistry of organic-inorganic hybrid materials. In *Angewandte Chemie - International Edition* (Vol. 45, Issue 36). <https://doi.org/10.1002/anie.200600734>

40. Díez, P., Sánchez, A., Gamella, M., Martínez-Ruiz, P., Aznar, E., De La Torre, C., Murguía, J. R., Martínez-Máñez, R., Villalonga, R., & Pingarrón, J. M. (2014). Toward the design of smart delivery systems controlled by integrated enzyme-based biocomputing ensembles. *Journal of the American Chemical Society*, 136(25). <https://doi.org/10.1021/ja503578b>

41. Diggle, J. W., & Meek, R. L. (1974). Oxides and Oxide Films. *Journal of The Electrochemical Society*, 121(2). <https://doi.org/10.1149/1.2402368>

42. Doane, T. L., & Burda, C. (2012). The unique role of nanoparticles in nanomedicine: Imaging, drug delivery and therapy. *Chemical Society Reviews*, 41(7). <https://doi.org/10.1039/c2cs15260f>

43. Drechsler, U., Erdogan, B., & Rotello, V. M. (2004). Nanoparticles: Scaffolds for molecular recognition. In *Chemistry - A European Journal* (Vol. 10, Issue 22). <https://doi.org/10.1002/chem.200306076>

44. Eckstein, C., Acosta, L. K., Pol, L., Xifré-Pérez, E., Pallares, J., Ferré-Borrull, J., & Marsal, L. F. (2018). Nanoporous Anodic Alumina Surface Modification by Electrostatic, Covalent, and Immune Complexation Binding Investigated by Capillary Filling. *ACS Applied Materials and Interfaces*, 10(12). <https://doi.org/10.1021/acsami.8b00572>

45. Eftekhari, A. (2008). Nanostructured Materials in Electrochemistry. In *Nanostructured Materials in Electrochemistry*. <https://doi.org/10.1002/9783527621507>

46. Ersching, K., Dorico, E., Da Silva, R. C., Zoldan, V. C., Isoppo, E. A., Viegas, A. D. C., & Pasa, A. A. (2012). Surface and interface characterization of nanoporous alumina templates produced in oxalic acid and submitted to etching procedures. *Materials Chemistry and Physics*, 137(1). <https://doi.org/10.1016/j.matchemphys.2012.08.058>

47. Facciola, A., Laganà, A., Genovese, G., Romeo, B., Sidoti, S., D'Andrea, G., Raco, C., Visalli, G., & Di Pietro, A. (2023). Impact of the COVID-19 pandemic on the infectious disease epidemiology. *Journal of Preventive Medicine and Hygiene*, 64(3). <https://doi.org/10.15167/2421-4248/jpmh2023.64.3.2904>

48. Fu, E., Liang, T., Ramachandran, S., Lutz, B., & Yager, P. (2011). Two-dimensional paper network format for amplified lateral flow assays. *15th International Conference on Miniaturized Systems for Chemistry and Life Sciences 2011, MicroTAS 2011*, 3.

49. Gale, P. A., & Quesada, R. (2006). Anion coordination and anion-templated assembly: Highlights from 2002 to 2004. In *Coordination Chemistry Reviews* (Vol. 250, Issues 23–24). <https://doi.org/10.1016/j.ccr.2006.05.020>

50. Garcia-Vergara, S. J., Iglesias-Rubianes, L., Blanco-Pinzon, C. E., Skeldon, P., Thompson, G. E., & Campestrini, P. (2006). Mechanical instability and pore generation in anodic alumina. *Proceedings of the Royal Society A: Mathematical, Physical and Engineering Sciences*, 462(2072). <https://doi.org/10.1098/rspa.2006.1686>

51. Gellman, S. H. (1997). Introduction: Molecular Recognition. *Chemical Reviews*, 97(5). <https://doi.org/10.1021/cr970328j>

52. Goyal, M., Ankush, Jangra, M. R., Batra, R., & Kumar, P. (2019). Aptamer-based biosensors for detection of environmental pollutants. In *Aptamers: Biotechnological Applications of a Next Generation Tool*. https://doi.org/10.1007/978-981-13-8836-1_10

53. Gullino, M. L., Leroux, P., & Smith, C. M. (2000). Uses and challenges of novel compounds for plant disease control. In *Crop Protection* (Vol. 19, Issue 1). [https://doi.org/10.1016/S0261-2194\(99\)00095-2](https://doi.org/10.1016/S0261-2194(99)00095-2)

54. Guo, W., Wang, J., Lee, S. J., Dong, F., Park, S. S., & Ha, C. S. (2010). A general pH-responsive supramolecular nanovalve based on mesoporous organosilica hollow nanospheres. *Chemistry - A European Journal*, 16(29). <https://doi.org/10.1002/chem.201000980>

55. Guy, O. J., & Walker, K. A. D. (2016). Silicon Carbide Biotechnology, Graphene Functionalization for Biosensor Applications. In *Silicon Carbide Biotechnology: A Biocompatible Semiconductor for Advanced Biomedical Devices and Applications: Second Edition*.

56. He, B., Son, S. J., & Lee, S. B. (2006). Shape-coded silica nanotubes for biosensing. *Langmuir*, 22(20). <https://doi.org/10.1021/la060187t>

57. He, X., Zhao, Y., He, D., Wang, K., Xu, F., & Tang, J. (2012). ATP-responsive controlled release system using aptamer-functionalized mesoporous silica nanoparticles. *Langmuir*, 28(35). <https://doi.org/10.1021/la302767b>

58. Hench, L. L., & West, J. K. (1990). The Sol-Gel Process. *Chemical Reviews*, 90(1). <https://doi.org/10.1021/cr00099a003>

59. Hendren, Z. D., Brant, J., & Wiesner, M. R. (2009). Surface modification of nanostructured ceramic membranes for direct contact membrane distillation. *Journal of Membrane Science*, 331(1–2). <https://doi.org/10.1016/j.memsci.2008.11.038>

60. Hernandez, R., Tseng, H. R., Wong, J. W., Stoddart, J. F., & Zink, J. I. (2004). An Operational Supramolecular Nanovalve. *Journal of the American Chemical Society*, 126(11). <https://doi.org/10.1021/ja039424u>

61. Hoar, T. P., & Mott, N. F. (1959). A mechanism for the formation of porous anodic oxide films on aluminium. *Journal of Physics and Chemistry of Solids*, 9(2). [https://doi.org/10.1016/0022-3697\(59\)90199-4](https://doi.org/10.1016/0022-3697(59)90199-4)

62. Houser, J. E., & Hebert, K. R. (2009). The role of viscous flow of oxide in the growth of self-ordered porous anodic alumina films. *Nature Materials*, 8(5). <https://doi.org/10.1038/nmat2423>

63. Hunks, W. J., & Ozin, G. A. (2005). Challenges and advances in the chemistry of periodic mesoporous organosilicas (PMOs). *Journal of Materials Chemistry*, 15(35–36). <https://doi.org/10.1039/b504511h>

64. Isenberg, H. D. (1988). Pathogenicity and virulence: another view. In *Clinical Microbiology Reviews* (Vol. 1, Issue 1). <https://doi.org/10.1128/CMR.1.1.40>

65. J. L. Atwood, J. L. S. (2004). *Encyclopaedia of Supramolecular Chemistry* (1st Ed.). Taylor & Francis Group.

66. Jane, A., Dronov, R., Hodges, A., & Voelcker, N. H. (2009). Porous silicon biosensors on the advance. In *Trends in Biotechnology* (Vol. 27, Issue 4). <https://doi.org/10.1016/j.tibtech.2008.12.004>

67. Jani, A. M. M., Kempson, I. M., Losic, D., & Voelcker, N. H. (2010). Dressing in layers: Layering surface functionalities in nanoporous aluminum oxide membranes. *Angewandte Chemie - International Edition*, 49(43). <https://doi.org/10.1002/anie.201002504>

68. Johansson, E., Choi, E., Angelos, S., Liong, M., & Zink, J. I. (2008). Light-activated functional mesostructured silica. *Journal of Sol-Gel Science and Technology*, 46(3). <https://doi.org/10.1007/s10971-007-1661-4>

69. Jones, K. E., Patel, N. G., Levy, M. A., Storeygard, A., Balk, D., Gittleman, J. L., & Daszak, P. (2008). Global trends in emerging infectious diseases. *Nature*, 451(7181). <https://doi.org/10.1038/nature06536>

70. Jung, I. Y., Lee, E. H., Suh, A. Y., Lee, S. J., & Lee, H. (2016). Oligonucleotide-based biosensors for in vitro diagnostics and environmental hazard detection. *Analytical and Bioanalytical Chemistry*, 408(10). <https://doi.org/10.1007/s00216-015-9212-2>

71. Keller, F., Hunter, M. S., & Robinson, D. L. (1953). Structural Features of Oxide Coatings on Aluminum. *Journal of The Electrochemical Society*, 100(9). <https://doi.org/10.1149/1.2781142>

72. Kilian, K. A., Böcking, T., Gaus, K., Gal, M., & Gooding, J. J. (2007). Peptide-modified optical filters for detecting protease activity. *ACS Nano*, 1(4). <https://doi.org/10.1021/nn700141n>

73. Kingsley, J. D., Dou, H., Morehead, J., & et al. (2006). Nanotechnology: A focus on nanoparticles as a drug delivery system. *Journal of Neuroimmune Pharmacology*, 1(3), 340–350. <https://doi.org/10.1007/s11481-006-9032-4>

74. Ku, A. Y., Ruud, J. A., Early, T. A., & Corderman, R. R. (2006). Evidence of ion transport through surface conduction in alkylsilane-functionalized nanoporous ceramic membranes. *Langmuir*, 22(20). <https://doi.org/10.1021/la0615591>

75. Kuiken, T., Leighton, F. A., Fouchier, R. A. M., LeDuc, J. W., Peiris, J. S. M., Schudel, A., Stöhr, K., & Osterhaus, A. D. M. E. (2005). Pathogen surveillance in animals. In *Science* (Vol. 309, Issue 5741). <https://doi.org/10.1126/science.1113310>

76. Kumar, N., & Kumbhat, S. (2016). Essentials in Nanoscience and Nanotechnology. In *Essentials in Nanoscience and Nanotechnology*. <https://doi.org/10.1002/9781119096122>

77. Kumeria, T., Santos, A., & Losic, D. (2014). Nanoporous anodic alumina platforms: Engineered surface chemistry and structure for optical sensing applications. In *Sensors (Switzerland)* (Vol. 14, Issue 7). <https://doi.org/10.3390/s140711878>

78. La Flamme, K. E., Popat, K. C., Leoni, L., Markiewicz, E., La Tempa, T. J., Roman, B. B., Grimes, C. A., & Desai, T. A. (2007). Biocompatibility of nanoporous alumina membranes for immunisolation. *Biomaterials*, 28(16). <https://doi.org/10.1016/j.biomaterials.2007.02.010>

79. Lai, J., Mu, X., Xu, Y., Wu, X., Wu, C., Li, C., Chen, J., & Zhao, Y. (2010). Light-responsive nanogated ensemble based on polymer grafted mesoporous silica hybrid nanoparticles. *Chemical Communications*, 46(39). <https://doi.org/10.1039/c0cc02914a>

80. Lakshmi, B. B., Patrissi, C. J., & Martin, C. R. (1997). Sol-Gel Template Synthesis of Semiconductor Oxide Micro- and Nanostructures. *Chemistry of Materials*, 9(11). <https://doi.org/10.1021/cm970268y>

81. Lee, S., Kim, D., Gillette, E., Oh, J., Han, S. W., & Lee, S. B. (2013). Anodized pore structural evolution of focused ion beam patterned Al: Direct analysis of branched nanopores and nanosacks. *Physical Chemistry Chemical Physics*, 15(26). <https://doi.org/10.1039/c3cp50630d>

82. Lee, S. W., Shang, H., Haasch, R. T., Petrova, V., & Lee, G. U. (2005). Transport and functional behaviour of poly(ethylene glycol)-modified nanoporous alumina membranes. *Nanotechnology*, 16(8). <https://doi.org/10.1088/0957-4484/16/8/059>

83. Lee, W., Ji, R., Gösele, U., & Nielsch, K. (2006). Fast fabrication of long-range ordered porous alumina membranes by hard anodization. *Nature Materials*, 5(9). <https://doi.org/10.1038/nmat1717>

84. Lee, W., & Park, S. J. (2014). Porous anodic aluminum oxide: Anodization and templated synthesis of functional nanostructures. In *Chemical Reviews* (Vol. 114, Issue 15). <https://doi.org/10.1021/cr500002z>

85. Lehn, J. M. (1988). Supramolecular chemistry - Scope and perspectives: Molecules - Supermolecules - Molecular devices. *Journal of Inclusion Phenomena*, 6(4). <https://doi.org/10.1007/BF00658981>

86. Li, A. P., Müller, F., Bimer, A., Nielsch, K., & Gösele, U. (1998). Hexagonal pore arrays with a 50-420 nm interpore distance formed by self-organization in anodic alumina. *Journal of Applied Physics*, 84(11). <https://doi.org/10.1063/1.368911>

87. Li, Z., Barnes, J. C., Bosoy, A., Stoddart, J. F., & Zink, J. I. (2012). Mesoporous silica nanoparticles in biomedical applications. *Chemical Society Reviews*, 41(7). <https://doi.org/10.1039/c1cs15246g>

88. Lin, Q., Huang, Q., Li, C., Bao, C., Liu, Z., Li, F., & Zhu, L. (2010). Anticancer drug release from a mesoporous silica based nanophotocage regulated by either a one- or two-photon process. *Journal of the American Chemical Society*, 132(31). <https://doi.org/10.1021/ja103415t>

89. Liu, C., Guo, J., Yang, W., Hu, J., Wang, C., & Fu, S. (2009). Magnetic mesoporous silica microspheres with thermo-sensitive polymer shell for controlled drug release. *Journal of Materials Chemistry*, 19(27). <https://doi.org/10.1039/b902985k>

90. Liu, R., Zhao, X., Wu, T., & Feng, P. (2008). Tunable redox-responsive hybrid nanogated ensembles. *Journal of the American Chemical Society*, 130(44). <https://doi.org/10.1021/ja8060886>

91. Livage, J., Henry, M., & Sanchez, C. (1988). Sol-gel chemistry of transition metal oxides. *Progress in Solid State Chemistry*, 18(4). [https://doi.org/10.1016/0079-6786\(88\)90005-2](https://doi.org/10.1016/0079-6786(88)90005-2)

92. Llopis-Lorente, A., Lozano-Torres, B., Bernardos, A., Martínez-Máñez, R., & Sancenón, F. (2017). Mesoporous silica materials for controlled delivery based on enzymes. *Journal of Materials Chemistry B*, 5(17). <https://doi.org/10.1039/c7tb00348j>

93. Ma, Z., & Michailides, T. J. (2005). Advances in understanding molecular mechanisms of fungicide resistance and molecular detection of resistant genotypes in phytopathogenic fungi. In *Crop Protection* (Vol. 24, Issue 10). <https://doi.org/10.1016/j.cropro.2005.01.011>

94. Mal, N. K., Fujiwara, M., & Tanaka, Y. (2003). Photocontrolled reversible release of guest molecules from coumarin-modified mesoporous silica. *Nature*, 421(6921). <https://doi.org/10.1038/nature01362>

95. Mal, N. K., Fujiwara, M., Tanaka, Y., Taguchi, T., & Matsukata, M. (2003). Photo-switched storage and release of guest molecules in the pore void of coumarin-modified MCM-41. *Chemistry of Materials*, 15(17). <https://doi.org/10.1021/cm0343296>

96. Malhotra, B. D., & Ali, M. A. (2017). Nanomaterials for Biosensors: Fundamentals and Applications. In *Nanomaterials for Biosensors: Fundamentals and Applications*. <https://doi.org/10.1016/C2015-0-04697-4>

97. Mancin, F., Rampazzo, E., Tecilla, P., & Tonellato, U. (2006). Self-assembled fluorescent chemosensors. *Chemistry - A European Journal*, 12(7). <https://doi.org/10.1002/chem.200500549>

98. Martínez-Máñez, R., & Sancenón, F. (2006). Chemodosimeters and 3D inorganic functionalised hosts for the fluoro-chromogenic sensing of anions. In *Coordination Chemistry Reviews* (Vol. 250, Issues 23–24). <https://doi.org/10.1016/j.ccr.2006.04.016>

99. Martinkova, P., Kostelnik, A., Valek, T., & Pohanka, M. (2017). Main streams in the construction of biosensors and their applications. In *International Journal of Electrochemical Science* (Vol. 12, Issue 8). <https://doi.org/10.20964/2017.08.02>

100. Masuda, H., & Fukuda, K. (1995). Ordered Metal Nanohole Arrays Made by a Two-Step Replication of Honeycomb Structures of Anodic Alumina. *Science*, 268(5216). <https://doi.org/10.1126/science.268.5216.1466>

101. Masuda, H., Yamada, H., Satoh, M., Asoh, H., Nakao, M., & Tamamura, T. (1997). Highly ordered nanochannel-array architecture in anodic alumina. *Applied Physics Letters*, 71(19). <https://doi.org/10.1063/1.120128>

102. McDonald, B. A., & Linde, C. (2002). The population genetics of plant pathogens and breeding strategies for durable resistance. *Euphytica*, 124(2). <https://doi.org/10.1023/A:1015678432355>

103. McMichael, A. J. (2004). Environmental and social influences on emerging infectious diseases: Past, present and future. *Philosophical Transactions of the Royal Society B: Biological Sciences*, 359(1447). <https://doi.org/10.1098/rstb.2004.1480>

104. Md Jani, A. M., Losic, D., & Voelcker, N. H. (2013). Nanoporous anodic aluminium oxide: Advances in surface engineering and emerging applications. In *Progress in Materials Science* (Vol. 58, Issue 5). <https://doi.org/10.1016/j.pmatsci.2013.01.002>

105. Meng, H., Xue, M., Xia, T., Zhao, Y. L., Tamanoi, F., Stoddart, J. F., Zink, J. I., & Nel, A. E. (2010). Autonomous in vitro anticancer drug release from mesoporous silica nanoparticles by pH-sensitive nanovalves. *Journal of the American Chemical Society*, 132(36). <https://doi.org/10.1021/ja104501a>

106. Milgroom, M. G., & Peever, T. L. (2003). Population biology of plant pathogens. In *Plant Disease* (Vol. 87, Issue 6). <https://doi.org/10.1094/PDIS.2003.87.6.608>

107. Mohr, G. J. (2005). Covalent bond formation as an analytical tool to optically detect neutral and anionic analytes. *Sensors and Actuators, B: Chemical*, 107(1 SPEC. ISS.). <https://doi.org/10.1016/j.snb.2004.06.039>

108. Morales, M. A., & Halpern, J. M. (2018). Guide to Selecting a Biorecognition Element for Biosensors. *Bioconjugate Chemistry*, 29(10). <https://doi.org/10.1021/acs.bioconjchem.8b00592>

109. Mortera, R., Vivero-Escoto, J., Slowing, I. I., Garrone, E., Onida, B., & Lin, V. S. Y. (2009). Cell-induced intracellular controlled release of membrane impermeable cysteine from a mesoporous silica nanoparticle-based drug delivery system. *Chemical Communications*, 22. <https://doi.org/10.1039/b900559e>

110. Moslonka-Lefebvre, M., Finley, A., Dorigatti, I., Dehnen-Schmutz, K., Harwood, T., Jeger, M. J., Xu, X., Holdenrieder, O., & Pautasso, M. (2011). Networks in plant epidemiology: From genes to landscapes, countries, and continents. In *Phytopathology* (Vol. 101, Issue 4). <https://doi.org/10.1094/PHYTO-07-10-0192>

111. Murray, C. J. L., & Lopez, A. D. (2013). Measuring the Global Burden of Disease. *New England Journal of Medicine*, 369(5). <https://doi.org/10.1056/nejmra1201534>

112. Naresh, V., & Lee, N. (2021). A review on biosensors and recent development of nanostructured materials-enabled biosensors. In *Sensors (Switzerland)* (Vol. 21, Issue 4). <https://doi.org/10.3390/s21041109>

113. Nguyen, H. H., & Kim, M. (2017). An Overview of Techniques in Enzyme Immobilization. *Applied Science and Convergence Technology*, 26(6). <https://doi.org/10.5757/asct.2017.26.6.157>

114. Odeh, F., Nsairat, H., Alshaer, W., Ismail, M. A., Esawi, E., Qaqish, B., Bawab, A. Al, & Ismail, S. I. (2020). Aptamers chemistry: Chemical modifications and conjugation strategies. In *Molecules* (Vol. 25, Issue 1). <https://doi.org/10.3390/molecules25010003>

115. Odom, D. J., Baker, L. A., & Martin, C. R. (2005). Solvent-extraction and Langmuir-adsorption-based transport in chemically functionalized nanopore membranes. *Journal of Physical Chemistry B*, 109(44). <https://doi.org/10.1021/jp0524983>

116. Oerke, E. C., & Dehne, H. W. (2004). Safeguarding production - Losses in major crops and the role of crop protection. *Crop Protection*, 23(4). <https://doi.org/10.1016/j.cropro.2003.10.001>
117. Oren, E., & Brown, H. E. (2023). Infectious disease epidemiology: An introduction. In *Infectious Disease Epidemiology: An Introduction*.
118. O'SULLIVAN JP, & WOOD GC. (1970). Morphology and mechanism of formation of porous anodic films on aluminum. *Proc Roy Soc Ser A Math Phys Sci*, 317(1731). <https://doi.org/10.1098/rspa.1970.0129>
119. Pak, A., Adegboye, O. A., Adekunle, A. I., Rahman, K. M., McBryde, E. S., & Eisen, D. P. (2020). Economic consequences of the COVID-19 outbreak: The need for epidemic preparedness. *Frontiers in Public Health*, 8, 241. <https://doi.org/10.3389/fpubh.2020.00241>
120. Park, C., Kim, H., Kim, S., & Kim, C. (2009). Enzyme responsive nanocontainers with cyclodextrin gatekeepers and synergistic effects in release of guests. *Journal of the American Chemical Society*, 131(46). <https://doi.org/10.1021/ja9061085>
121. Parlevliet, J. E. (2002). Durability of resistance against fungal, bacterial and viral pathogens; present situation. *Euphytica*, 124(2). <https://doi.org/10.1023/A:1015601731446>
122. Patel, K., Angelos, S., Dichtel, W. R., Coskun, A., Yang, Y. W., Zink, J. I., & Stoddart, J. F. (2008). Enzyme-responsive snap-top covered silica nanocontainers. *Journal of the American Chemical Society*, 130(8). <https://doi.org/10.1021/ja0772086>
123. Patermarakis, G., & Masavetas, K. (2006). Aluminium anodising in oxalate and sulphate solutions. Comparison of chronopotentiometric and overall kinetic response of growth mechanism of porous anodic films. *Journal of Electroanalytical Chemistry*, 588(2). <https://doi.org/10.1016/j.jelechem.2005.12.021>
124. Patermarakis, G., & Papandreadis, N. (1993). Study on the kinetics of growth of porous anodic Al₂O₃ films on Al metal. *Electrochimica Acta*, 38(15). [https://doi.org/10.1016/0013-4686\(93\)80119-K](https://doi.org/10.1016/0013-4686(93)80119-K)

125. Peña-Alonso, R., Rubio, F., Rubio, J., & Oteo, J. L. (2007). Study of the hydrolysis and condensation of γ -Aminopropyltriethoxysilane by FT-IR spectroscopy. *Journal of Materials Science*, 42(2). <https://doi.org/10.1007/s10853-006-1138-9>

126. Pete, A. J., Bharti, B., & Benton, M. G. (2021). Nano-enhanced Bioremediation for Oil Spills: A Review. *ACS ES&T Engineering*, 1(6), 928–946. <https://doi.org/10.1021/acsestengg.0c00217>

127. Plantegenest, M., Le May, C., & Fabre, F. (2007). Landscape epidemiology of plant diseases. In *Journal of the Royal Society Interface* (Vol. 4, Issue 16). <https://doi.org/10.1098/rsif.2007.1114>

128. Popat, A., Liu, J., Lu, G. Q., & Qiao, S. Z. (2012). A pH-responsive drug delivery system based on chitosan coated mesoporous silica nanoparticles. *Journal of Materials Chemistry*, 22(22). <https://doi.org/10.1039/c2jm30501a>

129. Popat, K. C., Mor, G., Grimes, C. A., & Desai, T. A. (2004). Surface modification of nanoporous alumina surfaces with poly(ethylene glycol). *Langmuir*, 20(19). <https://doi.org/10.1021/la049075x>

130. Porta, F., Lamers, G. E. M., Zink, J. I., & Kros, A. (2011). Peptide modified mesoporous silica nanocontainers. *Physical Chemistry Chemical Physics*, 13(21). <https://doi.org/10.1039/c0cp02959a>

131. Posthuma-Trumpie, G. A., & van Amerongen, A. (2012). Lateral flow assays. In *Antibodies Applications and New Development*. <https://doi.org/10.2174/978160805264611201010175>

132. Que, E. L., Domaille, D. W., & Chang, C. J. (2008). Metals in neurobiology: Probing their chemistry and biology with molecular imaging. In *Chemical Reviews* (Vol. 108, Issue 5). <https://doi.org/10.1021/cr078203u>

133. Queffélec, C., Petit, M., Janvier, P., Knight, D. A., & Bujoli, B. (2012). Surface modification using phosphonic acids and esters. In *Chemical Reviews* (Vol. 112, Issue 7). <https://doi.org/10.1021/cr2004212>

134. Real, L. A., Henderson, J. C., Biek, R., Snaman, J., Jack, T. L., Childs, J. E., Stahl, E., Waller, L., Tinline, R., & Nadin-Davis, S. (2005). Unifying the spatial population dynamics and molecular evolution of epidemic rabies virus. *Proceedings of the National Academy of Sciences of the United States of America*, 102(34). <https://doi.org/10.1073/pnas.0500057102>
135. Rodriguez, C. A. D., & Tremiliosi-Filho, G. (2013). Electrochemical Deposition. In *Encyclopedia of Tribology*. https://doi.org/10.1007/978-0-387-92897-5_700
136. Rogers, C. W., & Wolf, M. O. (2002). Luminescent molecular sensors based on analyte coordination to transition-metal complexes. In *Coordination Chemistry Reviews (Vols. 233–234)*. [https://doi.org/10.1016/S0010-8545\(02\)00023-1](https://doi.org/10.1016/S0010-8545(02)00023-1)
137. Ruiz-Rico, M., Pérez-Esteve, É., Lerma-García, M. J., Marcos, M. D., Martínez-Máñez, R., & Barat, J. M. (2017). Protection of folic acid through encapsulation in mesoporous silica particles included in fruit juices. *Food Chemistry*, 218. <https://doi.org/10.1016/j.foodchem.2016.09.097>
138. Rurack, K., & Martínez-Máñez, R. (2010). The Supramolecular Chemistry of Organic-Inorganic Hybrid Materials. In *The Supramolecular Chemistry of Organic-Inorganic Hybrid Materials*. <https://doi.org/10.1002/9780470552704>
139. Sajid, M., Kawde, A. N., & Daud, M. (2015). Designs, formats and applications of lateral flow assay: A literature review. *Journal of Saudi Chemical Society*, 19(6). <https://doi.org/10.1016/j.jscs.2014.09.001>
140. Sancenón, F., Pascual, L., Oroval, M., Aznar, E., & Martínez-Máñez, R. (2015). Gated Silica Mesoporous Materials in Sensing Applications. *ChemistryOpen*, 4(4). <https://doi.org/10.1002/open.201500053>
141. Schlossbauer, A., Kecht, J., & Bein, T. (2009). Biotin-avidin as a protease-responsive cap system for controlled guest release from colloidal mesoporous silica. *Angewandte Chemie - International Edition*, 48(17). <https://doi.org/10.1002/anie.200805818>

142. Schlossbauer, A., Sauer, A. M., Cauda, V., Schmidt, A., Engelke, H., Rothbauer, U., Zolghadr, K., Leonhardt, H., Bräuchle, C., & Bein, T. (2012). Cascaded photoinduced drug delivery to cells from multifunctional core-shell mesoporous silica. *Advanced Healthcare Materials*, 1(3). <https://doi.org/10.1002/adhm.201100033>

143. Schlossbauer, A., Warncke, S., Gramlich, P. M. E., Kecht, J., Manetto, A., Carell, T., & Bein, T. (2010). A programmable DNA-based molecular valve for colloidal mesoporous silica. *Angewandte Chemie - International Edition*, 49(28). <https://doi.org/10.1002/anie.201000827>

144. Scholthof, K. B. G. (2007). The disease triangle: Pathogens, the environment and society. *Nature Reviews Microbiology*, 5(2). <https://doi.org/10.1038/nrmicro1596>

145. Schulz, A., Woolley, R., Tabarin, T., & McDonagh, C. (2011). Dextran-coated silica nanoparticles for calcium-sensing. *Analyst*, 136(8). <https://doi.org/10.1039/c0an01009j>

146. Seaton, A., Seaton, D., & Leitch, A. G. (2008). Crofton and Douglas's Respiratory Diseases: Fifth Edition. In *Crofton and Douglas's Respiratory Diseases: Fifth Edition (Vols. 1–2)*. <https://doi.org/10.1002/9780470695999>

147. Setoh, S., & Miyata, A. (1932). Anodic film of aluminium. I and II. *Sci. Pap. Inst. Phys. Chem. Res.(Jpn.)*, 17(189).

148. Shears, P. (2000a). Communicable disease surveillance with limited resources: The scope to link human and veterinary programmes. *Acta Tropica*, 76(1). [https://doi.org/10.1016/S0001-706X\(00\)00081-4](https://doi.org/10.1016/S0001-706X(00)00081-4)

149. Shears, P. (2000b). Emerging and reemerging infections in Africa: The need for improved laboratory services and disease surveillance. In *Microbes and Infection (Vol. 2, Issue 5)*. [https://doi.org/10.1016/S1286-4579\(00\)00309-9](https://doi.org/10.1016/S1286-4579(00)00309-9)

150. Shen, Y., Zhang, Y., Gao, Z. F., Ye, Y., Wu, Q., Chen, H. Y., & Xu, J. J. (2021). Recent advances in nanotechnology for simultaneous detection of multiple pathogenic bacteria. In *Nano Today (Vol. 38)*. <https://doi.org/10.1016/j.nantod.2021.101121>

151. Slowing, I. I., Trewyn, B. G., Giri, S., & Lin, V. S. Y. (2007). Mesoporous silica nanoparticles for drug delivery and biosensing applications. *Advanced Functional Materials*, 17(8). <https://doi.org/10.1002/adfm.200601191>

152. Smith, I. A. W. (1974). PROCESS FOR PRODUCING AN ANODIC ALUMINUM OXIDE MEMBRANE. United States Patent.

153. Smith, K. F., Behrens, M., Schloegel, L. M., Marano, N., Burgiel, S., & Daszak, P. (2009). Reducing the risks of the wildlife trade. In *Science* (Vol. 324, Issue 5927). <https://doi.org/10.1126/science.1174460>

154. Smith, K. F., & Guégan, J. F. (2010). Changing geographic distributions of human pathogens. *Annual Review of Ecology, Evolution, and Systematics*, 41. <https://doi.org/10.1146/annurev-ecolsys-102209-144634>

155. Smith, K. F., Sax, D. F., Gaines, S. D., Guernier, V., & Guégan, J. F. (2007). Globalization of human infectious disease. *Ecology*, 88(8). <https://doi.org/10.1890/06-1052.1>

156. Song, N., & Yang, Y. W. (2015). Molecular and supramolecular switches on mesoporous silica nanoparticles. In *Chemical Society Reviews* (Vol. 44, Issue 11). <https://doi.org/10.1039/c5cs00243e>

157. Stark, W. J. (2011). Nanoparticles in biological systems. In *Angewandte Chemie - International Edition* (Vol. 50, Issue 6). <https://doi.org/10.1002/anie.200906684>

158. Sun, Y. L., Yang, B. J., Zhang, S. X. A., & Yang, Y. W. (2012). Cucurbit[7]uril pseudorotaxane-based photoresponsive supramolecular nanovalve. *Chemistry - A European Journal*, 18(30). <https://doi.org/10.1002/chem.201201083>

159. Szczepanski, V., Vlassioux, I., & Smirnov, S. (2006). Stability of silane modifiers on alumina nanoporous membranes. *Journal of Membrane Science*, 281(1–2). <https://doi.org/10.1016/j.memsci.2006.04.027>

160. Taniguchi, N. (1974). On the basic concept of “Nano-Technology.” The Basic Concept of “Nano-Technology”, Proceedings of the International Conference on Production Engineering Tokyo, Part II, Japan Society of Precision Engineering, Tokyo.

161. Taylor, L. H., Latham, S. M., & Woolhouse, M. E. J. (2001). Risk factors for human disease emergence. *Philosophical Transactions of the Royal Society B: Biological Sciences*, 356(1411). <https://doi.org/10.1098/rstb.2001.0888>

162. Thomas, C. R., Ferris, D. P., Lee, J. H., Choi, E., Cho, M. H., Kim, E. S., Stoddart, J. F., Shin, J. S., Cheon, J., & Zink, J. I. (2010). Noninvasive remote-controlled release of drug molecules in vitro using magnetic actuation of mechanized nanoparticles. *Journal of the American Chemical Society*, 132(31). <https://doi.org/10.1021/ja1022267>

163. Thornton, P. D., & Heise, A. (2010). Highly specific dual enzyme-mediated payload release from peptide-coated silica particles. *Journal of the American Chemical Society*, 132(6). <https://doi.org/10.1021/ja9094439>

164. Tian, B., Liu, S., Wu, S., Lu, W., Wang, D., Jin, L., Hu, B., Li, K., Wang, Z., & Quan, Z. (2017). pH-responsive poly (acrylic acid)-gated mesoporous silica and its application in oral colon targeted drug delivery for doxorubicin. *Colloids and Surfaces B: Biointerfaces*, 154. <https://doi.org/10.1016/j.colsurfb.2017.03.024>

165. Tilman, D. (1999). The Ecological Consequences of Changes in Biodiversity: A Search for General Principles. *Ecology*, 80(5). <https://doi.org/10.2307/176540>

166. Turner, M. G. (2005). Landscape ecology: What is the state of the science? In *Annual Review of Ecology, Evolution, and Systematics* (Vol. 36). <https://doi.org/10.1146/annurev.ecolsys.36.102003.152614>

167. Turro, N. J., Ramamurthy, V., & Scaiano, J. C. (2012). Modern Molecular Photochemistry of Organic Molecules. *Photochemistry and Photobiology*, 88(4). <https://doi.org/10.1111/j.1751-1097.2012.01178.x>

168. Urban, J., & Lebeda, A. (2006). Fungicide resistance in cucurbit downy mildew - Methodological, biological and population aspects. *Annals of Applied Biology*, 149(1). <https://doi.org/10.1111/j.1744-7348.2006.00070.x>

169. Vallet-Regí, M., Colilla, M., & Izquierdo-Barba, I. (2008). Bioactive mesoporous silicas as controlled delivery systems: Application in bone tissue regeneration. In *Journal of Biomedical Nanotechnology* (Vol. 4, Issue 1).

170. Van Overmeere, Q., Blaffart, F., & Proost, J. (2010). What controls the pore spacing in porous anodic oxides? *Electrochemistry Communications*, 12(9). <https://doi.org/10.1016/j.elecom.2010.06.010>

171. Verma, A., & Rotello, V. M. (2005). Surface recognition of biomacromolecules using nanoparticle receptors. In *Chemical Communications* (Issue 3). <https://doi.org/10.1039/b410889b>

172. Verma, N., & Kaur, G. (2019). Advances in the oligonucleotide-based biosensors for the detection of heavy metal contaminants in the environment. In *Tools, Techniques and Protocols for Monitoring Environmental Contaminants*. <https://doi.org/10.1016/B978-0-12-814679-8.00008-X>

173. Wang, X., Bu, X., & Feng, P. (2005). Porous Inorganic Materials. In *Encyclopedia of Inorganic and Bioinorganic Chemistry*. <https://doi.org/10.1002/9781119951438.eibc0264>

174. Willner, I., Basnar, B., & Willner, B. (2007). From molecular machines to microscale motility of objects: Application as “smart materials”, sensors, and nanodevices. *Advanced Functional Materials*, 17(5). <https://doi.org/10.1002/adfm.200601154>

175. Wilson, C., & Tisdell, C. (2001). Why farmers continue to use pesticides despite environmental, health and sustainability costs. *Ecological Economics*, 39(3). [https://doi.org/10.1016/S0921-8009\(01\)00238-5](https://doi.org/10.1016/S0921-8009(01)00238-5)

176. Woolhouse, M. E. J. (2002). Population biology of emerging and re-emerging pathogens. In *Trends in Microbiology* (Vol. 10, Issue 10). [https://doi.org/10.1016/S0966-842X\(02\)02428-9](https://doi.org/10.1016/S0966-842X(02)02428-9)

177. Woolhouse, M. E. J., & Gowtage-Sequeria, S. (2005). Host range and emerging and reemerging pathogens. *Emerging Infectious Diseases*, 11(12). <https://doi.org/10.3201/eid1112.050997>

178. Wu, S., Huang, X., & Du, X. (2013). Glucose- and pH-responsive controlled release of cargo from protein-gated carbohydrate-functionalized mesoporous silica

nanocontainers. *Angewandte Chemie - International Edition*, 52(21).
<https://doi.org/10.1002/anie.201300958>

179. Yan, H., Teh, C., Sreejith, S., Zhu, L., Kwok, A., Fang, W., Ma, X., Nguyen, K. T., Korzh, V., & Zhao, Y. (2012). Functional mesoporous silica nanoparticles for photothermal-controlled drug delivery in vivo. *Angewandte Chemie - International Edition*, 51(33).
<https://doi.org/10.1002/anie.201203993>

180. Yanagishita, T., Moriyasu, R., Ishii, T., & Masuda, H. (2021). Self-ordered anodic porous alumina with inter-hole spacing over 1.5 μm . *RSC Advances*, 11(6).
<https://doi.org/10.1039/d0ra10269e>

181. Yang, Q., Wang, S., Fan, P., Wang, L., Di, Y., Lin, K., & Xiao, F. S. (2005). pH-responsive carrier system based on carboxylic acid modified mesoporous silica and polyelectrolyte for drug delivery. *Chemistry of Materials*, 17(24).
<https://doi.org/10.1021/cm051198v>

182. Yuan, Q., Zhang, Y., Chen, T., Lu, D., Zhao, Z., Zhang, X., Li, Z., Yan, C. H., & Tan, W. (2012). Photon-manipulated drug release from a mesoporous nanocontainer controlled by azobenzene-modified nucleic acid. *ACS Nano*, 6(7).
<https://doi.org/10.1021/nn3018365>

183. Zaraska, L., Brudzisz, A., Wierzbicka, E., & Sulka, G. D. (2016). The effect of electrolyte change on the morphology and degree of nanopore order of porous alumina formed by two-step anodization. *Electrochimica Acta*, 198.
<https://doi.org/10.1016/j.electacta.2016.03.050>

184. Zaraska, L., Stępniewski, W. J., Jaskuła, M., & Sulka, G. D. (2014). Analysis of nanopore arrangement of porous alumina layers formed by anodizing in oxalic acid at relatively high temperatures. *Applied Surface Science*, 305.
<https://doi.org/10.1016/j.apsusc.2014.03.154>

185. Zeng, H., Fu, S., Yan, T., Yang, X., Liu, P., Xu, W., Dong, Q., & Li, J. (2020). Research advances of oligonucleotide aptamer-based biosensor for foodborne pathogen

detection. In *Food and Fermentation Industries* (Vol. 46, Issue 17). <https://doi.org/10.13995/j.cnki.11-1802/ts.024121>

186. Zhang, J. X. J., & Hoshino, K. (2018). *Molecular Sensors and Nanodevices: Principles, Designs and Applications in Biomedical Engineering*, Second Edition. In *Molecular Sensors and Nanodevices: Principles, Designs and Applications in Biomedical Engineering*, Second Edition. <https://doi.org/10.1016/C2017-0-02290-5>

187. Zhang, L., Li, Y., & Yu, J. C. (2014). Chemical modification of inorganic nanostructures for targeted and controlled drug delivery in cancer treatment. *Journal of Materials Chemistry B*, 2(5). <https://doi.org/10.1039/c3tb21196g>

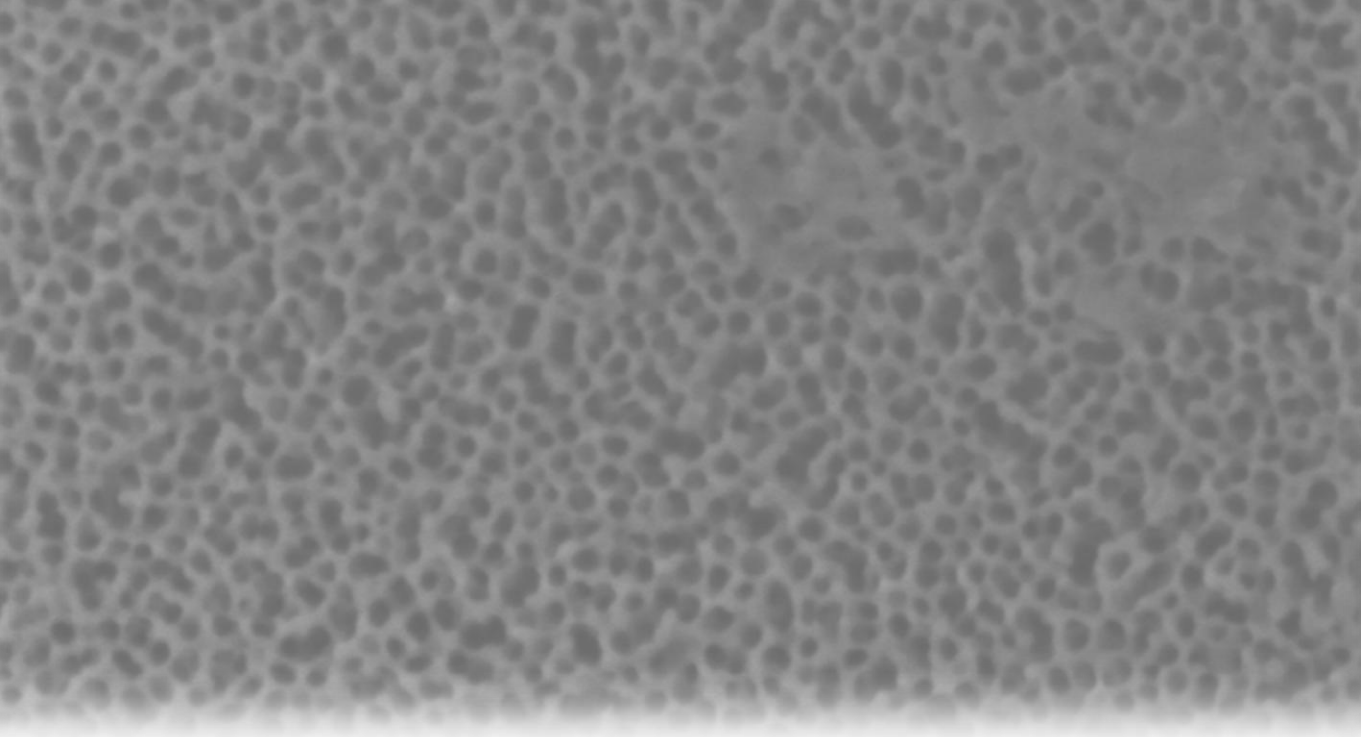
188. Zhang, Y., Yuan, Q., Chen, T., Zhang, X., Chen, Y., & Tan, W. (2012). DNA-capped mesoporous silica nanoparticles as an ion-responsive release system to determine the presence of mercury in aqueous solutions. *Analytical Chemistry*, 84(4). <https://doi.org/10.1021/ac202993p>

189. Zhao, Y., Trewyn, B. G., Slowing, I. I., & Lin, V. S. Y. (2009). Mesoporous silica nanoparticle-based double drug delivery system for glucose-responsive controlled release of insulin and cyclic AMP. *Journal of the American Chemical Society*, 131(24). <https://doi.org/10.1021/ja901831u>

190. Zhou, Y., Tan, L. L., Li, Q. L., Qiu, X. L., Qi, A. Di, Tao, Y., & Yang, Y. W. (2014). Acetylcholine-triggered cargo release from supramolecular nanovalves based on different macrocyclic receptors. *Chemistry - A European Journal*, 20(11). <https://doi.org/10.1002/chem.201304864>

191. Zhu, C. L., Lu, C. H., Song, X. Y., Yang, H. H., & Wang, X. R. (2011). Bioresponsive controlled release using mesoporous silica nanoparticles capped with aptamer-based molecular gate. *Journal of the American Chemical Society*, 133(5). <https://doi.org/10.1021/ja110094g>

192. Zukowski, K., Drozd, M., Ziółkowski, R., Pietrzak, M., Tokarska, K., Nowiński, A., & Malinowska, E. (2022). Lateral flow assays. In *Biosensors: Fundamentals, Emerging Technologies, and Applications*. <https://doi.org/10.1201/9781003189435-14>



Objectives

**Cover: FESEM image of functionalized NAA (self-produced image)*

Building on the concepts and terminology introduced earlier in this thesis, the focus of the research is directed towards the development of novel sensing systems based on gated materials. Specifically, four distinct gated systems supported on nanoporous anodic alumina (NAA) will be designed and developed for the detection of various viral and bacterial pathogens.

The global aim of this PhD thesis is to design, synthesize, and optimize novel gated nanodevices utilizing NAA films for the detection of specific targets. This primary objective is further divided into four specific goals:

- **Development of a DNA-capped NAA film system for detecting *Xylella fastidiosa* genomic DNA:** The first objective is to design a highly specific detection system for *Xylella fastidiosa*, a pathogen of significant concern in ecology and agriculture. By utilizing DNA as a capping agent on the NAA films, this system aims to achieve precise recognition and detection of the pathogen's genomic DNA.

- **Development of an antibody-gated NAA material for detecting *Mycobacterium tuberculosis*:** The third goal involves the development of an antibody-gated system specifically designed for the detection of *Mycobacterium tuberculosis*, a bacterial pathogen responsible for tuberculosis disease.

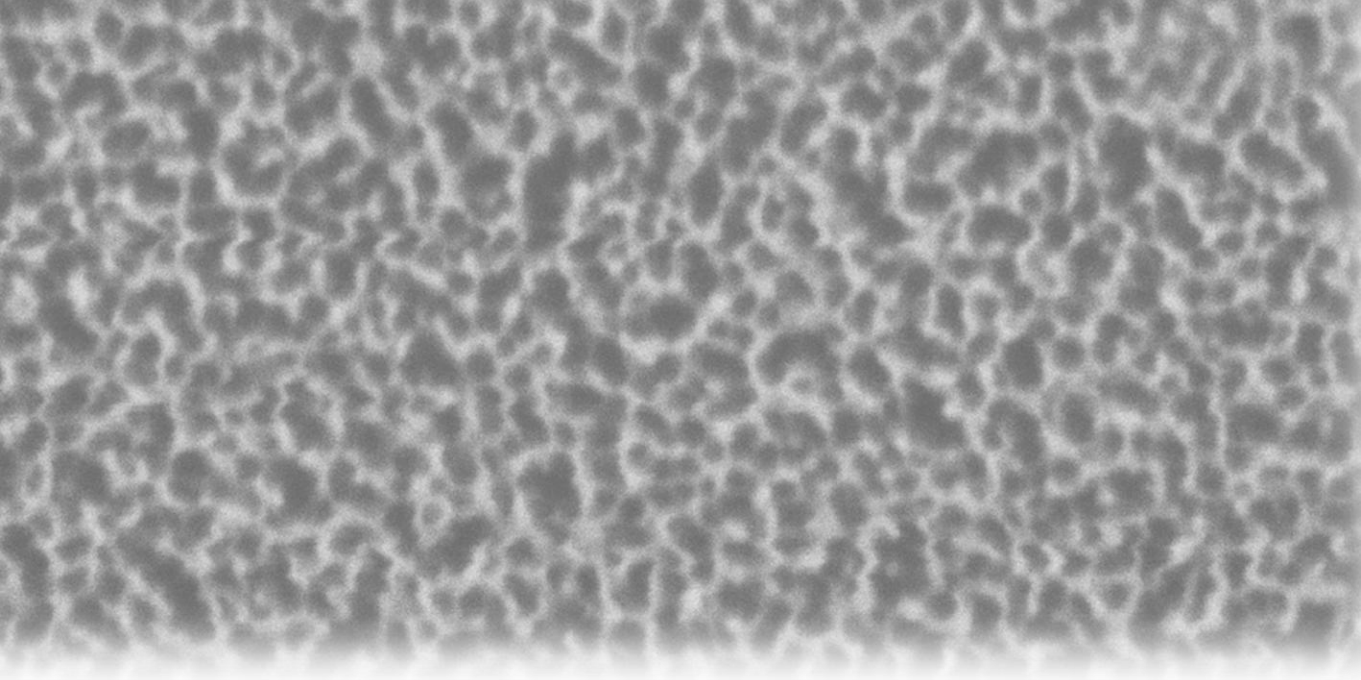
- **Design, synthesis, and evaluation of aptamer-capped NAA films for the early detection of SARS-CoV-2:** The second objective focuses on the development of an aptamer-based detection system for the virus SARS-CoV-2, the cause of the COVID-19. The early detection of this virus is crucial for the control of the spreading, and the proposed system seeks to offer high sensitivity and selectivity in identifying this pathogen.

- **Development of a new strategy that combines the CRISPR-Cas system with an DNA-gated NAA device for the specific detection of SARS-CoV-2 genetic material.** This

novel approach integrates the specificity of the CRISPR-Cas Systems for the detection of concrete oligonucleotidic sequences with the signal amplification of the NAA materials.

The following chapters provide a detailed discussion of the synthesis and characterization of these different gated materials, each synthesized to detect a specific analyte, ranging from whole cells and proteins to precise DNA sequences. Detailed discussions will cover the methods used to construct these systems, the selection and attachment of gating molecules, and the optimization of the materials for enhanced sensitivity and selectivity.

Moreover, this thesis will explore the release dynamics of the entrapped dye within these gated systems in the presence of their corresponding analytes. This investigation is crucial for understanding the efficiency and practicality of the gated materials in real-world applications. The studies will demonstrate how the interaction between the analyte and the gating mechanism triggers the controlled release of the dye, serving as a measurable signal for the presence of the target.



Chapter I | Advancements in Nanomaterial-Enhanced Biosensing for the Detection of *Xylella fastidiosa*

**Cover: FESEM image of raw NAA (self-produced image)*

Advancements in Nanomaterial-Enhanced Biosensing for the Detection of *Xylella fastidiosa*

Isabel Caballos^{abc}, Miguel Román-Écija^e, Blanca B Landa^e, Elena Aznar^{*abc} and Ramón Martínez-Mañez^{*abcd}

^a Instituto Interuniversitario de Investigación de Reconocimiento Molecular y Desarrollo Tecnológico (IDM), Universitat Politècnica de València, Universitat de Valencia, Spain.

^b Unidad Mixta de Investigación en Nanomedicina y Sensores. Universitat Politècnica de València, Instituto de Investigación Sanitaria La Fe (IISLAFE), Avenida Fernando Abril Martorell, 106, 46026, Valencia, Spain.

^c CIBER de Bioingeniería, Biomateriales y Nanomedicina (CIBER-BBN), Spain.

^d Joint Unit UPV-CIPF of Developmental Biology and Disease Models and Nanomedicine, Polytechnic University of Valencia (UPV)-Príncipe Felipe Research Center Foundation (CIPF), C/ Eduardo Primo Yúfera 3, 46012, Valencia, Spain.

^e Department of Crop Protection. Institute for Sustainable Agriculture (IAS), Consejo Superior de Investigaciones Científicas (CSIC), Córdoba, Spain.

*Corresponding authors. Email: elazgui@upvnet.upv.es; rmaez@qim.upv.es.

Research article under review

1. ABSTRACT

Xylella fastidiosa is a pathogenic bacterium that affects a variety of plants including trees, shrubs, herbs, and crops. Found in Europe, Asia, and South America, it has destroyed vast tracts of olive groves in Italy and caused the death of millions of coffee trees in Brazil. In this context, the development of rapid diagnostic tests is of interest aiming to alert of the presence of the pathogen and allowing a rapid intervention.

Here, a diagnostic sensor consisting of porous nanomaterial anodic alumina in combination with recognition oligonucleotides that can hybridize with the genomic material of *X. fastidiosa* is reported. When the bacteria are present, the nucleotide sequence combine with the target gene present in the genomic material and the porous material is uncapped, allowing the dye to be released into the medium. The system was fully characterized using scanning electron microscopy (HR-FESEM) and their atomic composition is determined by energy dispersive X-ray spectroscopy (EDXS). This technique allows a detection of a concentration of *X. fastidiosa* genomic material as low as $0.35 \text{ ng } \mu\text{l}^{-1}$ or $1.3 \cdot 10^5$ copies per μl . These findings support the advancement of precise diagnostic tools, enabling more responsive and sustainable agricultural practices to address the threats presented by *X. fastidiosa*.

- KEYWORDS: Nanoporous anodic alumina, *Xylella fastidiosa*, fluorometric sensor, direct detection.

2. INTRODUCTION

The bacterium *Xylella fastidiosa* is a xylem-colonizing, vector-borne, gram-negative, very slowly growing bacterium that was first properly identified as the cause of Pierce's disease (PD) in grapes (Kyrkou et al., 2018). However, it was not until 1987 that this bacterium was properly described, classified, and named *X. fastidiosa* by Wells et al (Wells et al., 1987). The characterization of *X. fastidiosa* culminated in whole-genome

sequencing from the *X. fastidiosa* citrus strain. *X. fastidiosa* was the first plant-pathogenic bacterium to have its entire genome sequenced. Sequences of three of *X. fastidiosa* strains (from almond, oleander, and citrus) are now available to consult (Simpson et al., 2000).

This bacterium has been found to be the cause of Pierce's disease (PD) of *Vitis vinifera* (a disease observed as early as 1884), and Brazilian pseudopeach disease (PPD) which was discovered in 1993 as the cause of citrus colorful chlorosis (CVC). Furthermore, this bacterium was found to be present in the *Prunus* genus causing many of the so-called leaf scorch diseases (Greco et al., 2021). Other species affected are *Acer spp.* (ornamental maple), *Carya illinoensis* (pecans tree), *Coffea arabica* (Arabica coffee plant, *X. fastidiosa* isolated in Brazil in 1995), *Hedera helix* (common ivy), *Platanum occidentalis* (American sycamore), *Quercus spp.* (oak) and *Ulmus Americana* (American elm). All of these diseases are not seed-borne and occur mainly in tropical/subtropical regions, although leaf scorch diseases also occur in colder climates, e.g. Oak leaf scorch in Canada (Purcell, 1997). *X. fastidiosa* is found in a latent state in many asymptomatic hosts which serve as an inoculum for vectors (Hopkins & Purcell, 2002; Wells et al., 1987). As we can observe, this bacterium represents a significant challenge due to its exceptionally wide host range, which comprises over 600 plant species spanning 63 diverse plant families (C. Castro et al., 2021).

Symptoms caused by *X. fastidiosa* depend mainly in the kind of host even if they share certain characteristics. The early symptoms are slight albinism or bronzing along the edges or tips of the leaves, which can increase and become waterlogged before browning and drying. These symptoms first appear on some branches and then on almost all leaves. The affected area is separated by a narrow yellow-green band, which is especially noticeable in autumn. Early defoliation occurs with the formation of new deformed leaves. Abnormally shaped fruit may also be formed, with internal and external discoloration of the stem, withering, abnormal growth, and ultimately death of the host.

Several pathogenic variants of this bacterium have been reported, and they are often host-specific. The following variants are listed: (i) *Xylella fastidiosa subsp. fastidiosa*, strain obtained from cultivated grapes, alfalfa, almond and maples. (ii) *X. fastidiosa subsp. Multiplex*, from peach, elm, plum, pigeon grape, sycamore and almond varieties. (iii) *X. fastidiosa subsp. Pauca*, from citrus varieties and possibly coffee varieties. (iv) *X. fastidiosa subsp. Sandyi*, a strain obtained from *Nerium oleander*. (v) *X. fastidiosa subsp. Tashk* from the ornamental tree *Chitalpa tashkentensis* (Vanhove et al., 2019; Rapticavoli et al., 2018).

Vectors are primarily sharpshooters, water hoppers, or applebugs (*Cicadidae*), which have no latent period and do not involve transovarial transmission of the bacteria (Di Serio et al., 2019). The pathogen persists within the adult vector and can multiply in the foregut. Possible local vectors in Europe are *Cicadella viridis* and *Philaenus spumarius* (grassland spitworm) (Farigoule et al., 2022).

The *Xylella fastidiosa* outbreak began in North America, where this bacterium is endemic. Only in the southwestern United States cause every year very severe outbreaks of grapevine Parkinson's disease resulting in annual crop losses of approximately US\$104 million, with growers spending around US\$50 million annually on preventative measures within the California viticulture industry (Burbank, 2022).

Before 2013, only sporadic instances of *X. fastidiosa* detection in Europe were reported, which were neither investigated nor deemed significant. The initial outbreak within the European Union occurred in 2013, affecting olive trees in the Italian region of Apulia, where *Xylella fastidiosa subsp. pauca* infections in olive orchards are projected to incur costs of up to €5.2 billion over the next 50 years if afflicted trees are not replaced (Ali et al., 2021). Genetic analysis linked the subspecies found to *X. fastidiosa* in Costa Rica, suggesting introduction via imported ornamental plants. Subsequently, *X. fastidiosa* was identified in France, with initial outbreaks in Corsica in 2015, Provence in 2019, and Occitania in 2020. In Spain, the first outbreak occurred in the Balearic Islands in 2016,

infesting more than 20 plant species, including vine, almond, olive, and fig. By December 2020, over 600 olive trees in the Balearic archipelago were infected, with the affected area expanding to 2292 hectares by 2021, resulting in the destruction of over 100,000 almond trees (Olmo et al., 2021). In 2016, a single olive tree in Madrid tested positive for the multiplex subspecies of *X. fastidiosa*, and three specimens of *Polygala myrtifolia* were detected as infected in an ornamental plant nursery in Almeria, although the bacterium has since been eradicated in this region (Loureiro et al., 2023).

Additional risks associated with *X. fastidiosa* in Europe include: (i) the bacterium's sporadic distribution within host tissues, often making detection challenging. (ii) insensitivity of detection techniques, as evidenced by low positivity rates in direct PCR assays. (iii) potential introduction via large-scale importations of wild grape rootstocks from America. (iv) the wide array of symptomless hosts, facilitating periodic introductions of the bacterium into Europe. (v) transmission by various *Cicadellidae* species, including certain European ones like *Cicadella viridis* and *P. spumarius*. (vi) uncertainty about the presence of vectors surviving winter as adults in Europe. (vii) overwintering of vectors unnoticed in adjacent woods and weeds, maintaining inoculum, and (viii) possible impact of recent climatic changes in the Mediterranean basin on vector populations (Cornara et al., 2017; Janse, 2010).

X. fastidiosa demands sophisticated detection methods to accurately identify and differentiate its strains from other phytopathogens as it represents a significant threat to agriculture. Traditional microscopy techniques, such as dark field or phase contrast microscopy, are essential due to the small and narrow dimensions of *X. fastidiosa* cells (0.2-0.4 x 1.0-4.0 µm). Traditional techniques involve investigating infected tissues in the sap/ooze of leaf veins, vessels of petioles, or trunk/branch vascular tissue where this bacterium usually can be found. Additional methods, including direct microscope visualization and acidified methanol immersion (infected roots show purplish spots within a minute or two where vessels contain bacteria), provide preliminary confirmation of

pathogen presence in fresh plant tissue. Strain differentiation is achieved through growth on PD2 and PW BCYE/CS-20 agar, complemented by serological techniques such as ELISA, PCR, and real-time PCR (Bragard et al., 2019).

Recent advancements in detection include the integration of Loop-Mediated Isothermal Amplification (LAMP) and Cas12a-based DNA Endonuclease-Targeted (DETECTR) CRISPR technology, as described by Gambley et al. (Farrall et al., 2023). This method enables specific detection of the *X. fastidiosa*-specific *rimM* gene within 10 min, showcasing rapid and accurate diagnostics. Amoia et al. (Amoia et al., 2023) presented a colorimetric LAMP protocol, demonstrating the potential for field application with a portable isothermal block. Moreover, ongoing research in ELISA technology continues to advance pathogen detection methods. Recently, Gorris et al. (Gorris et al., 2021) introduced a novel double antibody sandwich ELISA (DAS-ELISA) specifically designed for detecting *X. fastidiosa*. This assay exhibited a reliable sensitivity, detecting concentrations of 10^4 CFU ml⁻¹.

Biosensors are gaining a growing significance in biomarker detection, particularly those employing nanomaterials for signal enhancement. Among these nanomaterials, nanoporous anodic alumina (NAA) plays an important role in increasing biosensor sensitivity by facilitating biomolecule immobilization and signal amplification. Nanomaterials, particularly NAA, are highlighted for their role in fabricating gated nanomaterials, offering higher sensitivity and ease of functionalization (Caballos et al., 2023; Ribes et al., 2016). With their large surface-to-volume ratio, facilitate biomolecule immobilization and signal amplification. Combining nanomaterials with signalling molecules, such as radioactive species and fluorescent molecules, enhances signal intensity. NAA, due to its physical and chemical properties, can be engineered to produce various optical structures, offering versatility in analyte detection. These advancements enhance the reliability and accuracy of biosensor-based diagnostics.

DNA-based biosensors, utilizing oligonucleotide probes, offer numerous benefits such as high sensitivity, selectivity, rapidity, and a low detection limit. In this sense, the *acpP* gene emerges as a reliable marker for *X. fastidiosa* identification, integrating a 45-nucleotide probe in the final design of the biosensor.

Based on the above we report herein our results on the use of NAA loaded with rhodamine B and capped with a DNA sequence complementary to the *acpP* gene for *Xylella fastidiosa* detection. The presence of the *X. fastidiosa* genome induces pore uncapping and cargo delivery (Figure 1). The biosensor is characterized and tested in detecting the *X. fastidiosa* genome by evaluating the system's dynamic response, specificity, and sensitivity with synthetic single-stranded DNA (dsDNA) complementary molecules. The sensor is also tested in *X. fastidiosa* extracted genomic material and finally in almond tree samples, demonstrating its applicability for agricultural monitoring of *X. fastidiosa*. This research provides a simple portable aptasensor for *X. fastidiosa* detection, paving the way for future advancements in precision agriculture and sustainable crop management.

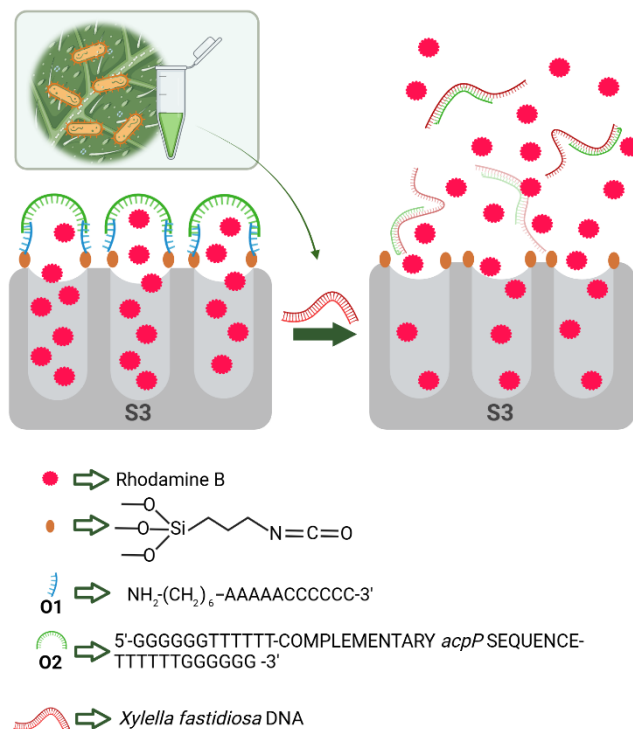


Figure 1. Scheme of fluorogenic sensors for *Xylella fastidiosa* DNA detection based on oligonucleotide gated NAA films loaded with rhodamine B.

3. RESULTS AND DISCUSSION

3.1. Design, synthesis, and characterization of the materials A schematic representation of the developed sensor and the procedures for its preparation is illustrated in Figure 2. The initial porous support of NAA (designated as S_0) was loaded with rhodamine B fluorophore by immersing NAA supports in a solution of RhB dissolved in acetonitrile, followed by gentle stirring at 50 rpm, resulting in the formation of S_1 . Following dye loading, the external surface of the NAA support underwent functionalization with isocyanate groups, leading to the formation of S_2 . This transformation was achieved through the reaction between aluminum hydroxyl (Al-OH) groups present at the external surface and 3-

(triethoxysilyl)propyl isocyanate, resulting in the formation of Al-O-Si bonds. During this process, NAA supports were positioned on the bottom surface of a sealed flask, ensuring that the porous films were oriented with their surfaces containing the pores facing upwards, thereby facilitating the interaction between the alumina surface and the agents dissolved in the liquid phase. Additionally, gentle stirring with an orbital stirrer promoted a more homogeneous environment for surface functionalization, thereby enabling the reproducible fabrication of sensors. Maintaining of very low humidity levels during these steps was imperative to prevent isocyanate hydrolysis and facilitate controlled coupling between the Al-OH groups at the external surface and 3-(triethoxysilyl)propyl isocyanate. Furthermore, this controlled humidity environment helped to prevent uncontrolled hydrolysis and condensation of alkoxysilane, which could otherwise lead to the formation of a solid phase on the external surface of the sensors. To avoid humidity, it was essential to use freshly prepared rhodamine B solutions for both synthesis and washing steps and employ a tightly sealed reaction flask. The surface functionalization with the alkoxysilane was also corroborated through electron microscopy and EDXS analysis, with an observed increase in silicon (Si), carbon (C), and nitrogen (N) atomic content following surface modification (as summarized in Table 1).

The isocyanate-modified NAA supports (S_2) underwent functionalization with oligonucleotide O_1 , which possesses an amine group, via urea linkages, resulting in the formation of S_3 . The oligonucleotide O_1 is characterized by a specific base sequence that enables subsequent hybridization with the capping oligonucleotides (O_2) containing the complementary DNA base sequence of the *acpP* gene of *X. fastidiosa*: 5'-TTTTTGGGGGGTTTCTCGGCGACAATTTTCTGACGCGCGCTTCGATGTCACTCATGGGGGGTTTTT-3'. Following the modification process, an increase in phosphorus (P), carbon (C), nitrogen (N), and oxygen (O) atomic content was observed, confirming the coupling of oligonucleotide to the NAA surface (Table 1).

In the last step, NAA supports were coated with oligonucleotide O_2 to produce sensors S_3-O_2 . These capping oligonucleotides contain two sequences at their ends that are complementary to oligonucleotides O_1 (see Figure 1). Confirmation of the removal of non-hybridized capping oligonucleotides O_2 and rhodamine B following the functionalization process was achieved by assessing the absorbance and fluorescence intensity of supernatants post-washing. Following this procedure, sensor S_3-O_2 was obtained. The final NAA-based sensor underwent further characterization via electron microscopy and EDXS analysis. Oligonucleotide O_2 possesses a three-dimensional structure with nanoscale dimensions and adopts a spatial arrangement on the alumina surface, effectively obstructing the pores and preventing the diffusion of the fluorophore from the porous material structure. At a macroscopic level, the oligonucleotide molecules form an organic layer on the inorganic porous support, as visualized in the electron microscopy images (Figure 3). Furthermore, an increase in phosphorus (P), carbon (C), nitrogen (N), and oxygen (O) atomic content was observed following surface coating. This organic-inorganic interphase served as a physical barrier that regulated the diffusion of the fluorophore between the porous solid support and the liquid medium. Upon the presence of complementary target oligonucleotides in the medium, hybridization with the gating oligonucleotides is expected to occur, inducing a displacement, unblocking the pores, and facilitating the release of the entrapped fluorophore (as further discussed below). Lastly, the surface morphology of alumina supports during the synthesis steps was also characterized by atomic force microscopy (refer to Figure S3 in the Supporting Information).

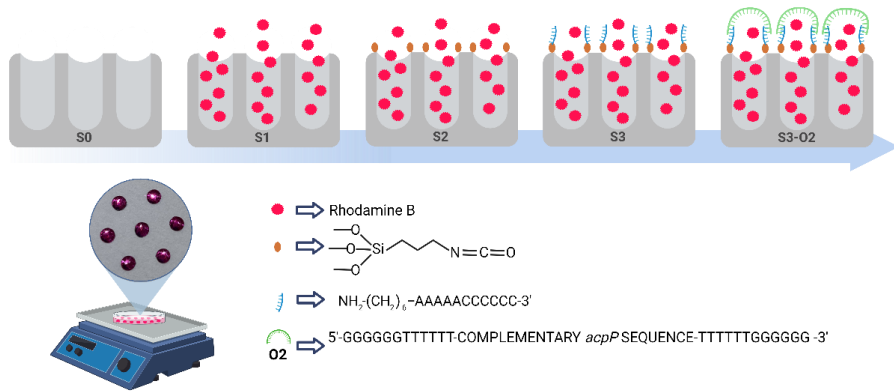


Figure 2. Schematic illustration of the synthesis steps of a fluorogenic sensor for the detection of *Xylella fastidiosa* DNA, which relies on oligonucleotide gated NAA films loaded with rhodamine B.

R

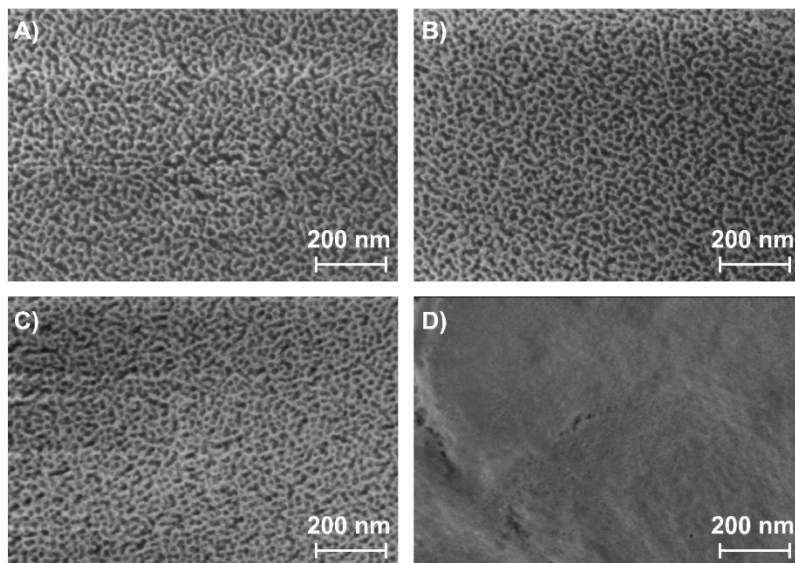


Figure 3. HR-FESEM images of NAA surfaces during synthesis steps (S_0 A); S_1 B); S_2 C); S_3 D); S_3-O_2 E).

	S ₀	S ₁	S ₂	S ₃	S ₃ -O ₂
C	0.84 ± 0.02	0.46 ± 0.01	0.35 ± 0.02	0.51 ± 0.02	1.14 ± 0.02
N	0	0.03 ± 0.00	0.03 ± 0.01	0.04 ± 0.01	0.13 ± 0.01
O	2.14 ± 0.04	2.89 ± 0.04	2.00 ± 0.04	2.13 ± 0.05	3.36 ± 0.06
Al	1.00 ± 0.02	1.00 ± 0.02	1.00 ± 0.02	1.00 ± 0.02	1.00 ± 0.02
Si	0	0	0.05 ± 0.01	0.02 ± 0.00	0.04 ± 0.00
P	0	0	0	0.01 ± 0.00	0.01 ± 0.00

Table 1. Relative atomic compositions respect to Al atoms of S₀, S₁, S₂, S₃, S₃-O₂ and used supports S₃-O₃ both blank (B, without stimulus) and with stimulus (oligonucleotide O₃) by EDXS analysis.

3.2. Release assays

Following the synthesis and characterization of the sensor, its ability to selectively release Rhodamine B in the presence of an oligonucleotide complementary to that used for capping was assessed. Consequently, NAA-based sensor S₃-O₂ were subjected to incubation with the corresponding complementary oligonucleotides O₃ (5'-ATTGATACTCCTAATTATGATGTGCAGAA-3') in PBS buffer, and the released Rhodamine B was quantified via fluorescence spectroscopy at 585 nm ($\lambda_{ex} = 555$ nm) using a plate reader. NAA sensor supports that were not incubated with oligonucleotides served as negative controls. The rhodamine B release profiles from are depicted in Figure 4. The rhodamine B release profiles are presented as variations in fluorescence intensity at different time versus the initial intensity ($I_t - I_0$) and divided by the initial intensity (I_0) to normalize the data. The results in Figure 4 are presented as the means and standard

deviations of measurements obtained from 6 distinct nanodevices incubated with PBS (black line) and 6 additional nanodevices incubated with the corresponding complementary oligonucleotide at a concentration of 10 μM (red line). Negligible rhodamine B release was observed from sensors employed as negative controls even after extended incubation times (up to 75 min), supporting the gating capability of the oligonucleotides on the NAA surface, which effectively block the pores and prevent dye diffusion. In contrast, a notable release of dye was observed from NAA $\text{S}_3\text{-O}_2$ disks incubated with the corresponding complementary oligonucleotide O_3 . The complementary oligonucleotide hybridized with the capping oligonucleotides O_2 on the NAA surface, thereby unblocking the pores and facilitating the diffusion of rhodamine B (Figure 4).

In a second validation step, the kinetics of rhodamine B delivery from support $\text{S}_3\text{-O}_2$ was investigated to validate the specific opening of the gated materials in the presence of *X. fastidiosa* genomic DNA. For this investigation, three independent gated supports of $\text{S}_3\text{-O}_2$ were individually immersed in hybridization buffer. Subsequently, 100 μL of previously denatured genomic DNA ($1 \text{ ng } \mu\text{L}^{-1}$) were added to one of the solutions, while 100 μL of buffer was added to the other as a negative control. To quantify the amount of delivered dye from the pores to the aqueous phase, the same methodology as previously described was employed. The results revealed that $\text{S}_3\text{-O}_2$ in hybridization buffer delivered a minimal amount of dye, accounting for less than 10% of the maximum dye released, indicating an effective capping of the pores. Conversely, in presence of *X. fastidiosa* genomic DNA, a significantly larger amount of rhodamine B was released. This behaviour of the nanomaterial demonstrates the ability of *X. fastidiosa* genomic DNA to uncap the pores and facilitate cargo delivery, as depicted in Figure 4.

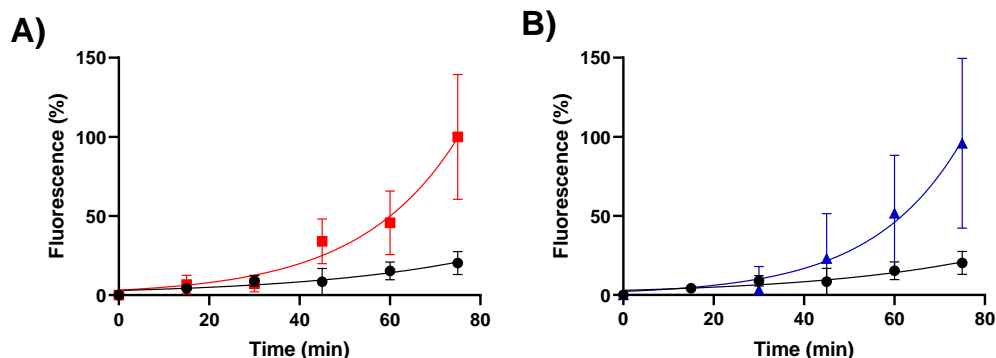


Figure 4. A) Rhodamine B delivery profile from S_3-O_2 incubated (red line) with the corresponding complementary oligonucleotide O_3 or with PBS (black line) and B) in the presence of 100 ng of denatured genomic DNA of *X. fastidiosa* in hybridization buffer (PBS, pH 7.5) (blue line) or only in hybridization buffer (black line) as negative control.

3.3. Stability evaluation in blank and inoculated competitive media

S_3-O_2 supports were also tested in a more competitive medium and cargo release experiments were performed with plant extract samples. For this purpose, different organic materials (leaves and branches) of the studied species were collected. These parts of the plant were chosen because they are known reservoirs for the bacteria. The plant extract was prepared following the protocol detailed in “Materials and Methods: Plant extracts preparation” and then S_3-O_2 supports were tested in presence of 500 μL of plant extract mixed with 500 μL of hybridization buffer (PBS). The release of Rhodamine B was measured at 75-minute incubation time, and it showed that the release was similar in all studied plant species, being able to hypothesize that the sensor will be functional not only in almond samples (as detailed below) but also in other species susceptible to *X. fastidiosa* infection (Figure 5A).

To further explore the capacity of the developed sensor, the performance of S_3-O_2 to detect the *acpP* gene of *X. fastidiosa* in the competitive medium of almond tree

extract was tested (Figure 5B). In these experiments, the rhodamine released was measured in presence of 0.1 ng mL^{-1} of extracted *X. fastidiosa* DNA in a matrix of 50% almond tree extract (after verifying that the extract was a negative to *X. fastidiosa*). This DNA concentration was selected as it is approximately twice the limit of detection of most reported diagnostic methods. The results showed that while a higher residual release was observed in competitive media compared to PBS, the measured fluorescence difference between negative and positive control (in the presence of the *X. fastidiosa* DNA) was comparable to the previous detailed above and achieved in PBS buffer.

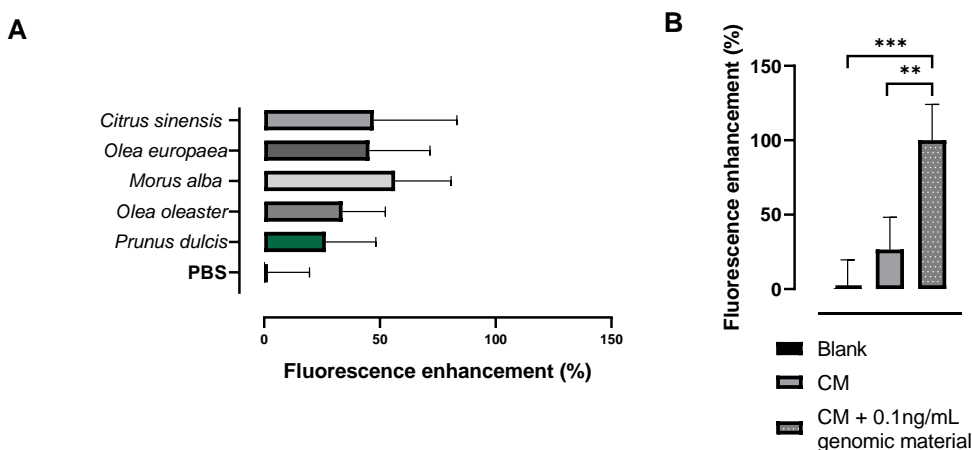


Figure 5. A) Media fluorescence intensity in the presence of different extracts in 50% PBS buffer after 75 min. B) Rhodamine B delivery from material S_3-O_2 evaluated in PBS buffer (blank), competitive media (50% almond tree extract in PBS) and in competitive media (CM) inoculated with *X. fastidiosa* DNA (concentration: 0.1 ng mL^{-1}) after a 75-minute incubation period.

3.4. Sensitivity studies

The sensitivity of the method was determined by performing experiments with S_3-O_2 at different concentrations of the extracted genomic material of *X. fastidiosa* in PBS (pH 7.5) and studying the generated response. For this purpose, 11 independent S_3-O_2

supports were immersed in hybridization buffer, and 100 μL of DNA suspension dilutions were added to each material, reaching a range of final concentrations between 0 (Blank) and 1 $\text{ng } \mu\text{L}^{-1}$. After 75 min, the total amount of rhodamine B diffused to the aqueous phase was measured by fluorescence. Results showed that delivered dye was directly related to the DNA concentration in PBS medium (Figure 6).

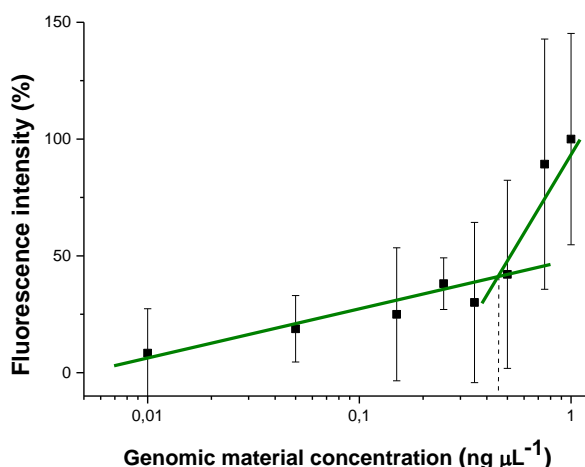


Figure 6. A) Rhodamine B released from solid $S_3\text{-O}_2$ in the presence of different concentrations of *Xylella fastidiosa* DNA in PBS buffer.

The limit of detection (LOD) was established at $0.35(\pm 0.12)$ $\text{ng } \mu\text{L}^{-1}$ for the experiments in PBS buffer. Given that each *Xylella fastidiosa* genome has an approximate weight of 2.7 femtograms, the number of genome copies per microliter can be calculated by dividing the concentration in grams by the genome weight. This calculation results in an estimated LOD of $129600(\pm 44400)$ copies μL^{-1} . These findings affirm the promising capability of these materials for fast and sensitive detection of oligonucleotides including the DNA base sequences of the *acpP* gene of *X. fastidiosa*. Notably, this method shows advantages of speed, simplicity, and independence from specialized instrumentation or databases. Furthermore, its potential for multiplexing is noteworthy, as it can be

effortlessly adapted for the detection of other relevant pathogens by simply adjusting the recognizing agent.

The low detection limits obtained are probably due to the advantageous interaction between the capping oligonucleotides and the *X. fastidiosa* genomic DNA, as well as the inherent signal amplification in the use of gated materials. Consequently, it has been documented that within these gated systems, a singular analyte molecule has the capability to prompt the delivery of a substantial quantity of dye molecules upon the opening of the pores. Indeed, other studies from our research group have determined that the quantity of delivered dye molecules can range from 10^4 to 10^{11} per molecule of DNA (Pla et al., 2020, 2021). In the present investigation, it has been estimated that 1 ng of genomic DNA could release an average of 10^9 molecules of rhodamine B, reinforcing the substantial signal amplification capability demonstrated herein.

3.5. Study of the system behavior with different sub-species of *Xylella fastidiosa*

In a step forward, the specific response of S_3-O_2 to the genomic material from different subspecies of *X. fastidiosa* was studied using genomic extractions of the subspecies *Xylella fastidiosa subsp. fastidiosa*, *Xylella fastidiosa subsp. multiplex* and *Xylella fastidiosa subsp. pauca* which are the most spread in European countries until this date (Loureiro et al., 2023). In these experiments, S_3-O_2 was submerged in almond tree extract in PBS (50% v.v) doped with 100 μL of dehybridized DNA ($1 \text{ ng } \mu\text{L}^{-1}$) from each subspecies of *X. fastidiosa* (Xf-fastidiosa, Xf-multiplex, Xf-pauca and Xf-morus) in 900 μL of hybridization buffer. The sensor S_3-O_2 was also tested in the presence of genomic DNA ($1 \text{ ng } \mu\text{L}^{-1}$) of *Curtobacterium flaccumfaciens strain XA2-10*, *Curtobacterium sp. BH-2-1-1*, *Staphylococcus capitis subsp. capitis*, *Staphylococcus warneri* and *Micrococcus luteus*. All these species have a wide host range and cause similar symptoms as *X. fastidiosa* so the infection manifestations can be mistakenly attributed. Released rhodamine B after 75 min

was measured by fluorescence as in previous experiments. As can be appreciated in Figure 7, S_3-O_2 responds to all studied subspecies of *X. fastidiosa*, whereas the additional bacteria displayed a lower cargo release.

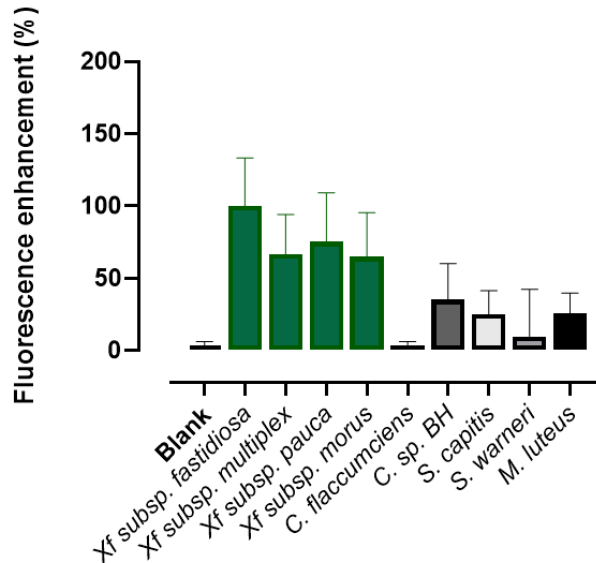


Figure 7. Media fluorescence intensity of rhodamine B in presence of the subspecies *Xf-fastidiosa*, *Xf-multiplex*, *Xf-pauca*, *Xf-morus* and the other interferent species. (1 ng mL^{-1}) ($N=6$). Control represents the delivery in almond tree extract without the stimulus after 75 min from the beginning of the experiment.

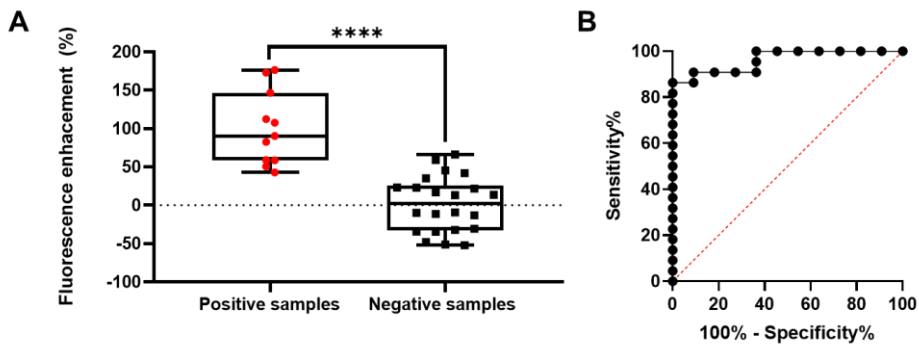
3.6. Detection of *Xylella fastidiosa* in real field samples

Given the increasing prevalence of infections attributed to *Xylella fastidiosa* worldwide, the urgent need for the development of rapid, sensitive, and trustworthy diagnostic techniques has become a critical challenge. In this context, the development of S_3-O_2 as diagnostic tool emerges as an alternative to existing techniques for the detection of *X. fastidiosa* in different crop samples. Nowadays, the most followed method

to detect *X. fastidiosa* infection is RT-PCR, which lasts at least 1-3 days between the sample collection and the final diagnosis.

In this section a validation of the S₃-O₂ sensor for the detection of *Xylella fastidiosa* in real tissue samples infected or not of *Prunus dulcis* (sweet almond tree), was carried out. Organic material was collected from crops from the Balearic Islands (Spain), from the locations of Lluçmajor, Villafranca and Benisalem. DNA testing of *Xylella fastidiosa* infection was done using multiplex real-time PCR assays for detection and identification of the bacterium presence in the different samples.

In our research, 44 almond extract samples from infected and non-infected trees were initially analyzed using the reference method (RT-PCR). 11 samples from the 33 were found positive. The 44 samples were analyzed also using the S₃-O₂ biosensor. For that purpose, two individual S₃-O₂ supports were immersed in 100 µL of the sample solution and 900 µL of hybridization buffer, followed by fluorescence measurement after 75 min. Figure 8A display the observed fluorescence obtained for positive and negative samples.



Sensor	Positive sample	Negative sample	True positive	True negative	False positive	False Negative	Sensitivity [%]	Specificity [%]	Positive predictive value [%]	Negative predictive value [%]
S ₃ -O ₂	11	22	10	20	2	1	90.9	90.9	84.6	95.7

Figure 8. A) Detection of X. fastidiosa in field samples of recovered tissue from the Balearic Islands using the developed sensor. B) The receiver-operating characteristic (ROC) curves for validation of sensor S₃-O₁ for detection of X. fastidiosa genetic material. C) Validation of the sensor with the 33 field samples.

The sensor S₃-O₂ was evaluated for its ability to distinguish between positive and negative samples, yielding a sensitivity of 90.9% and a specificity of 90.9%. Of the 11 positive samples tested, 10 were correctly identified as true positives, with one false negative, resulting in high sensitivity. Conversely, among the 22 negative samples, there were two false positives and zero true negatives, leading to a specificity of 90.9%. The positive predictive value (PPV) for S₃-O₂ was calculated at 84.6%, indicating that 84.6% of positive results were true positives. The negative predictive value (NPV) was 95.7%, meaning that 95.7% of negative results were accurately classified. These data suggest that S₃-O₂ demonstrates both high sensitivity and specificity, with reliable predictive values for both positive and negative sample detection (Figure 8C). This result illustrates the method's potential for applications because it improves in various aspects the current methods such as qPCR. Despite their high sensitivity and specificity, qPCR methodologies often need costly equipment and trained personnel, thus restricting their accessibility to many laboratories. In contrast, biosensors based on oligonucleotide-capped NAA offer numerous advantages: (i) they exhibit remarkable versatility in both cargo and capping DNA sequence selection; (ii) their preparation and testing costs are substantially lower compared to other techniques; (iii) the required equipment is simple, can be used everywhere and affordable for the majority of laboratories; and (iv) the analysis procedure is simplified, and obviates the need for sample treatments such as DNA extraction, amplification or culture. It should be highlighted that this finding is consistent with prior research, which has shown that genomic DNA is released into the extracellular medium and remains detectable (Pla et al., 2021).

4. CONCLUSION

In the research of biomarker analysis systems, nanomaterials have been used thanks to their numerous advantages such as a high surface-to-volume ratio, porosity, size and shape-dependent optical properties, and unique physicochemical characteristics. The incorporation of these features plays a crucial role in enhancing the analytical performance of biosensors. Furthermore, nano-enhanced biosensors for biomarker detection have emerged as an attractive area of research because of the coupling of the nanomaterial with biorecognition elements such as aptamers, enzymes, antibodies, or nucleic acids, giving some benefits in the diagnostic area such as rapid response time, cost-effectiveness, portability, and simplified preparation and determination procedures.

In the present study, the combination of nanoporous materials and a suitable oligonucleotide was employed to fabricate a sensitive, robust, and competitive fluorogenic sensor for detecting the *Xylella fastidiosa acpP* gene in PBS and competitive media (diluted plant extract). The probe comprises a NAA support previously loaded with the fluorescent dye rhodamine B and blocked with an oligonucleotide complementary to the specific *X. fastidiosa* sequence. Upon the presence of the specific *X. fastidiosa* sequence, the capping oligonucleotide is displaced, resulting in pore opening and fluorophore release. The probe exhibited a limit of detection of $0.75 \text{ ng } \mu\text{L}^{-1}$ in PBS buffer and demonstrates high selectivity for the specie *Xylella fastidiosa*, showing a poor response to the presence of other related pathogens. Applied to the identification of *X. fastidiosa* in real *Prunus dulcis* samples, the method yields excellent results in terms of sensitivity and predictive values. The proposed method is simple, rapid, portable, and can be easily adjusted using different reporters and capping sequences. This sensing approach may inspire the development of new simple tests with great potential for point-of-care pathogen testing and might results in a simple-to-use test in-site for the detection of *X. fastidiosa*.

5. MATERIALS AND METHODS

5.1. General techniques

Field Emission Scanning Electron Microscopy (FESEM) analysis was performed with a ZEISS Ultra 55 microscope (ZEISS, Oberkochen, Germany). Energy Dispersive X-ray spectroscopy (EDXS) analysis was obtained with the same equipment. Fluorescence spectroscopy was carried out on a BioTek Synergy H1 microplate reader (BioTek, Winooski, VT, USA).

5.2. Chemicals

Acetonitrile, (3-isocyanatopropyl) triethoxysilane, triethylamine (TEA), rhodamine B, phosphate buffered saline (PBS) were procured from Sigma-Aldrich Química (Madrid, Spain). Oligonucleotides O₁ (NH₂-(CH₂)₆-5'-AAAAACCCCC-3') and O₂ (5'-TTTTTGGGGGTTTCTCGGCGACAATTTTCTGACGCGCTTCGATGTCACTCATGGGGGTTTTT-3') were obtained from IDT (IA, USA). Nanoporous anodic alumina (NAA) foils were commercially obtained from InRedox® (CO, USA) featuring an alumina thickness of 10 ± 0.2 μm, a pore diameter of 5 ± 2 nm, and a pore density of 9 × 10¹¹ cm⁻². *X. fastidiosa* genomic DNA was acquired from the CECT service of the University of Valencia (Valencia, Spain). All materials were used as received.

5.3. Oligonucleotides design

The gen *acpP* was selected among the whole genome of *X. fastidiosa* because its specificity related to the specie and its conservation between the different subspecies of *X. fastidiosa*. This gene encodes the acyl carrier protein, responsible of the transportation of the growing fatty acid chain in fatty acid biosynthesis. It exhibits 100% coverage and specificity in the target species as indicated by the exploratory study conducted with the NCBI database. The recognition oligonucleotide (O₂) was designed to be complementary to this specific gene of the bacteria. The anchor sequence used between the

functionalized NAA and the recognition oligonucleotide is O₁: NH₂-(CH₂)₆-5'-AAAAAACCCCC-3'. The specific recognition sequence chosen to block the pores was O₂: 5'-TTTTTGGGGGGTTTCTCGGCGACAATTTTCTGACGCGCGCTTCGATGTCACTCATGGGGGGTTTTT-3'. This recognition oligonucleotide corresponds to the complementary sequence of a region of the *acpP* gene of *X. fastidiosa*.

5.4. Synthesis of support S₁

In a typical synthesis, NAA supports cut in disks of 2 mm were immersed in 8 mL of a mixture of rhodamine B solution in acetonitrile (6 mg, 1.57 mM, 8 mL). The suspension was stirred at room temperature for 24 h.

5.5. Synthesis of support S₂

Then an excess of (3- isocyanatopropyl)triethoxysilane (328 μL, 1.32 mmol) was added, and the final mixture was stirred at room temperature for 5.5 h. The resulting pink support (S₁) was slightly washed with the rhodamine B solution in acetonitrile (6 mg, 1.57 mM, 8 mL) three times and then dried and stored overnight at 4°C.

5.6. Synthesis of support S₃

Batches of 50 S₁ supports were immersed in a solution of rhodamine B in acetonitrile (262.5 μg, 1.57 mM, 4200 μL), TEA (24 μL) and 60 μL of oligonucleotide O₁ (at 100 μM concentration). Finally, the mixture was stirred 3h at room temperature to obtain material S₃.

5.7. Synthesis of support S₃-O₂

Support S₃ (in batches of 4 units) was immersed in a solution containing 195 μL of hybridization buffer (PBS, pH 7.5) and 55 μL of O₂ (100 μM). The mixture was stirred for 2h at room temperature. The resulting material was thoroughly washed with hybridization buffer (PBS, pH 7.5) to eliminate the unbounded oligonucleotide.

5.8. Characterization of the prepared supports

The prepared supports were characterized by FESEM and EDXS analysis. The nanostructure of the starting NAA support was assessed by FESEM. Images made by the Atomic Force Microscopy (AFM) were taken to assess the roughness of the porous materials and verify the images previously made with the other methods.

5.9. Release experiments of support S₃-O₂

To investigate the gating properties of S₃-O₂, two units of this material were immersed each in 1 mL of hybridization buffer (PBS, pH 7.5). To one of them, it was added 100 µL of the purified sequence complementary to the probe (to avoid anything that could interfere) at a concentration of 100 µM, while another 100 µL of water was added to the other device. Both experiments were maintained at 25°C, and, at certain times, aliquots were taken. The rhodamine B release was measured with the fluorimeter at 585 nm ($\lambda_{\text{exc}}=555$ nm).

Performance of S₃-O₂ with genomic DNA was studied using the same method, 100 µL of a *X. fastidiosa* genomic DNA in aqueous solution (0.1 ng mL⁻¹) was added to one of the supports after being subjected to a dehybridization treatment (5 min 90°C and 3 min 0°C), while 100 µL of water subjected to the same treatment was added to the other support as a negative control.

5.10. Plant extracts preparation

To prepare the almond extracts used in this study for the analysis in competitive media, whole branches obtained directly from the tree, as well as contaminated and healthy wood chips and sawdust, were utilized. If the pieces were too large, they were cut into smaller pieces and their surface bark was removed to expose the xylem. The different samples were weighed to ensure uniformity in the amount of material to be extracted. All materials were initially pressed dry, followed by the addition of 5 mL of extraction buffer

(PBS in our case), and allowed to soak for a few minutes. Once the material was thoroughly soaked, a second pressing was performed using the homogenizer Homex 7 tool (Bioreba, Reinach, Switzerland) in their respective approved extraction bags (from the same commercial brand). The homogenizer was used on each sample for approximately 30 sec. After repeating the process for all samples, the material was allowed to settle in the bags for 5 min, and using a pipette, all the buffer with extract was transferred and stored in the corresponding vials. In order to inactivate the bacterium, all the samples were frozen. The negative control samples used for the different experiments were obtained from almond trees and other species of the location of Córdoba (Spain), while the *X. fastidiosa* positive and negative samples (verified with the RT-PCR method) were obtained from crops from the locations of Lluçmajor, Villafranca y Benisalem (Balearic Islands, Spain).

5.11. Samples validation

Quantitative Polymerase Chain Reaction assays (qPCR) confirmed the presence of *Xylella fastidiosa* (subsp. *multiplex*) in all the positive almond samples studied. Mature branches and cuttings with attached mature leaves were sampled following the standard protocol of the European and Mediterranean Plant Protection Organization (EPPO) for *Xylella fastidiosa*: PM 7/24(3) (Camino et al., 2021). DNA extraction was performed using CTAB buffer from 0.5 g of xylem tissue samples. All samples were subjected of two qPCR assays in different times using the real-time PCR tests of Harper et al. (Harper et al., 2010) and Francis et al. (Francis et al., 2006).

5.12. Statistical analysis

Statistical analysis was carried out using the software GraphPad Prism 8. For the results analysis, a normalization process was carried out on the raw fluorescence data obtained by fluorometric analysis. For this purpose, the initial fluorescence data (at initial time point) were subtracted from the fluorescence value at each time point and divided

by the same initial fluorescence value. This normalization process was repeated for each fluorescence measure at each time point. This process was followed to obtain the Fluorescence (%) in Figure 4 and Figure 6.

For the rest of the graphs, the enhancement in fluorescence of *X. fastidiosa* samples compared to samples without *X. fastidiosa* genetic material was calculated. To do this, the previously calculated values (final intensity minus intensity at time 0 divided by intensity at time 0) was subtracted from the same calculated values of the negative control, so that the negative controls always remain zero and positive values represent the increase in fluorescence relative to this negative control.

All fluorescence values were normalized to percentage, with 100% being the highest intensity value. Results were considered statistically significant when *P*-value was <0.05.

6. REFERENCES

1. Ali, B. M., van der Werf, W., & Oude Lansink, A. (2021). Assessment of the environmental impacts of *Xylella fastidiosa* subsp. *pauca* in Puglia. *Crop Protection*, 142. <https://doi.org/10.1016/j.cropro.2020.105519>
2. Amoia, S. S., Minafra, A., Ligorio, A., Cavalieri, V., Boscia, D., Saponari, M., & Loconsole, G. (2023). Detection of *Xylella fastidiosa* in Host Plants and Insect Vectors by Droplet Digital PCR. *Agriculture (Switzerland)*, 13(3). <https://doi.org/10.3390/agriculture13030716>
3. Bragard, C., Dehnen-Schmutz, K., di Serio, F., Gonthier, P., Jacques, M. A., Jaques Miret, J. A., Justesen, A. F., MacLeod, A., Magnusson, C. S., Milonas, P., Navas-Cortés, J. A., Potting, R., Reignault, P. L., Thulke, H. H., van der Werf, W., Vicent Civera, A., Yuen, J., Zappalà, L., Makowski, D., ... Parnell, S. (2019). Effectiveness of in planta control

measures for *Xylella fastidiosa*. *EFSA Journal*, 17(5).
<https://doi.org/10.2903/j.efsa.2019.5666>

4. Burbank, L. P. (2022). Threat of *Xylella fastidiosa* and options for mitigation in infected plants. In *CAB Reviews: Perspectives in Agriculture, Veterinary Science, Nutrition and Natural Resources* (Vol. 2022, Issue 2022).
<https://doi.org/10.1079/cabireviews202217021>

5. Camino, C., Calderón, R., Parnell, S., Dierkes, H., Chemin, Y., Román-Écija, M., Montes-Borrego, M., Landa, B. B., Navas-Cortes, J. A., Zarco-Tejada, P. J., & Beck, P. S. A. (2021). Detection of *Xylella fastidiosa* in almond orchards by synergic use of an epidemic spread model and remotely sensed plant traits. *Remote Sensing of Environment*, 260.
<https://doi.org/10.1016/j.rse.2021.112420>

6. Castro, C., DiSalvo, B., & Caroline Roper, M. (2021). *Xylella fastidiosa*: A reemerging plant pathogen that threatens crops globally. *PLoS Pathogens*, 17(9).
<https://doi.org/10.1371/journal.ppat.1009813>

7. Cornara, D., Cavalieri, V., Dongiovanni, C., Altamura, G., Palmisano, F., Bosco, D., Porcelli, F., Almeida, R. P. P., & Saponari, M. (2017). Transmission of *Xylella fastidiosa* by naturally infected *Philaenus spumarius* (Hemiptera, Aphrophoridae) to different host plants. *Journal of Applied Entomology*, 141(1–2). <https://doi.org/10.1111/jen.12365>

8. Di Serio, F., Bodino, N., Cavalieri, V., Demichelis, S., di Carolo, M., Dongiovanni, C., Fumarola, G., Gilioli, G., Guerrieri, E., Picciotti, U., Plazio, E., Porcelli, F., Saladini, M., Salerno, M., Simonetto, A., Tauro, D., Volani, S., Zicca, S., & Bosco, D. (2019). Collection of data and information on biology and control of vectors of *xylella fastidiosa*. *EFSA Journal*, 16(5). <https://doi.org/10.2903/sp.efsa.2019.EN-1628>

9. Dupas, E., Briand, M., Jacques, M. A., & Cesbron, S. (2019). Novel Tetraplex Quantitative PCR Assays for Simultaneous Detection and Identification of *Xylella fastidiosa*

Subspecies in Plant Tissues. *Frontiers in Plant Science*, 10. <https://doi.org/10.3389/fpls.2019.01732>

10. Farigoule, P., Chartois, M., Mesmin, X., Lambert, M., Rossi, J. P., Rasplus, J. Y., & Cruaud, A. (2022). Vectors as Sentinels: Rising Temperatures Increase the Risk of *Xylella fastidiosa* Outbreaks. *Biology*, 11(9). <https://doi.org/10.3390/biology11091299>

11. Farrall, T., Abeynayake, S. W., Webster, W., Fiorito, S., Dinsdale, A., Whattam, M., Campbell, P. R., & Gambley, C. (2023). Development of a rapid, accurate, and field deployable LAMP-CRISPR-Cas12a integrated assay for *Xylella fastidiosa* detection and surveillance. *Australasian Plant Pathology*. <https://doi.org/10.1007/s13313-023-00954-4>

12. Francis, M., Lin, H., Rosa, J. C. La, Doddapaneni, H., & Civerolo, E. L. (2006). Genome-based PCR primers for specific and sensitive detection and quantification of *Xylella fastidiosa*. *European Journal of Plant Pathology*, 115(2). <https://doi.org/10.1007/s10658-006-9009-4>

13. Greco, D., Aprile, A., de Bellis, L., & Luvisi, A. (2021). Diseases Caused by *Xylella fastidiosa* in *Prunus* Genus: An Overview of the Research on an Increasingly Widespread Pathogen. In *Frontiers in Plant Science* (Vol. 12). <https://doi.org/10.3389/fpls.2021.712452>

14. Gorris, M. T., Sanz, A., Peñalver, J., López, M. M., Colomer, M., & Marco-Noales, E. (2021). Detection and diagnosis of *xylella fastidiosa* by specific monoclonal antibodies. *Agronomy*, 11(1). <https://doi.org/10.3390/agronomy11010048>

15. Harper, S. J., Ward, L. I., & Clover, G. R. G. (2010). Development of LAMP and real-time PCR methods for the rapid detection of *Xylella fastidiosa* for quarantine and field applications. *Phytopathology*, 100(12). <https://doi.org/10.1094/PHYTO-06-10-0168>

16. Hopkins, D. L., & Purcell, A. H. (2002). *Xylella fastidiosa*: Cause of Pierce's disease of grapevine and other emergent diseases. In *Plant Disease* (Vol. 86, Issue 10). <https://doi.org/10.1094/PDIS.2002.86.10.1056>
17. Janse, J. D. (2010). Diagnostic methods for phytopathogenic bacteria of stone fruits and nuts in COST 873. *EPP0 Bulletin*, 40(1). <https://doi.org/10.1111/j.1365-2338.2009.02356.x>
18. Kyrkou, I., Pusa, T., Ellegaard-Jensen, L., Sagot, M. F., & Hansen, L. H. (2018). Pierce's disease of grapevines: A review of control strategies and an outline of an epidemiological model. In *Frontiers in Microbiology* (Vol. 9, Issue SEP). <https://doi.org/10.3389/fmicb.2018.02141>
19. Loureiro, T., Mesquita, M. M., Dapkevicius, M. de L. E., Serra, L., Martins, Â., Cortez, I., & Poeta, P. (2023). *Xylella fastidiosa*: A Glimpse of the Portuguese Situation. In *Microbiology Research* (Vol. 14, Issue 4). <https://doi.org/10.3390/microbiolres14040108>
20. Olmo, D., Nieto, A., Borràs, D., Montesinos, M., Adrover, F., Pascual, A., Gost, P. A., Quetglas, B., Urbano, A., García, J. de D., Velasco-Amo, M. P., Olivares-García, C., Beidas, O., Juan, A., Marco-Noales, E., Gomila, M., Rita, J., Moralejo, E., & Landa, B. B. (2021). Landscape epidemiology of *xylella fastidiosa* in the balearic islands. *Agronomy*, 11(3). <https://doi.org/10.3390/agronomy11030473>
21. Purcell, A. H. (1997). *Xylella fastidiosa*, a regional problem or global threat? *Journal of Plant Pathology*, 79(2).
22. Rapicavoli, J., Ingel, B., Blanco-Ulate, B., Cantu, D., & Roper, C. (2018). *Xylella fastidiosa*: an examination of a re-emerging plant pathogen. *Molecular Plant Pathology*, 19(4). <https://doi.org/10.1111/mpp.12585>

23. Simpson, A. J. G., Reinach, F. C., Arruda, P., Abreu, F. A., Acencio, M., Alvarenga, R., Alves, L. M. C., Araya, J. E., Baia, G. S., Baptista, C. S., Barros, M. H., Bonaccorsi, E. D., Bordin, S., Bové, J. M., Briones, M. R. S., Bueno, M. R. P., Camargo, A. A., Camargo, L. E. A., Carraro, D. M., ... Setubal, J. C. (2000). The genome sequence of the plant pathogen *Xylella fastidiosa*: The *Xylella fastidiosa* consortium of the organization for nucleotide sequencing and analysis, Sao Paulo, Brazil. In *Nature* (Vol. 406, Issue 6792). <https://doi.org/10.1038/35018003>

24. Vanhove, M., Retchless, A. C., Sicard, A., Rieux, A., Coletta-Filho, H. D., de La Fuente, L., Stenger, D. C., & Almeida, R. P. P. (2019). Genomic diversity and recombination among *Xylella fastidiosa* subspecies. *Applied and Environmental Microbiology*, 85(13). <https://doi.org/10.1128/AEM.02972-18>

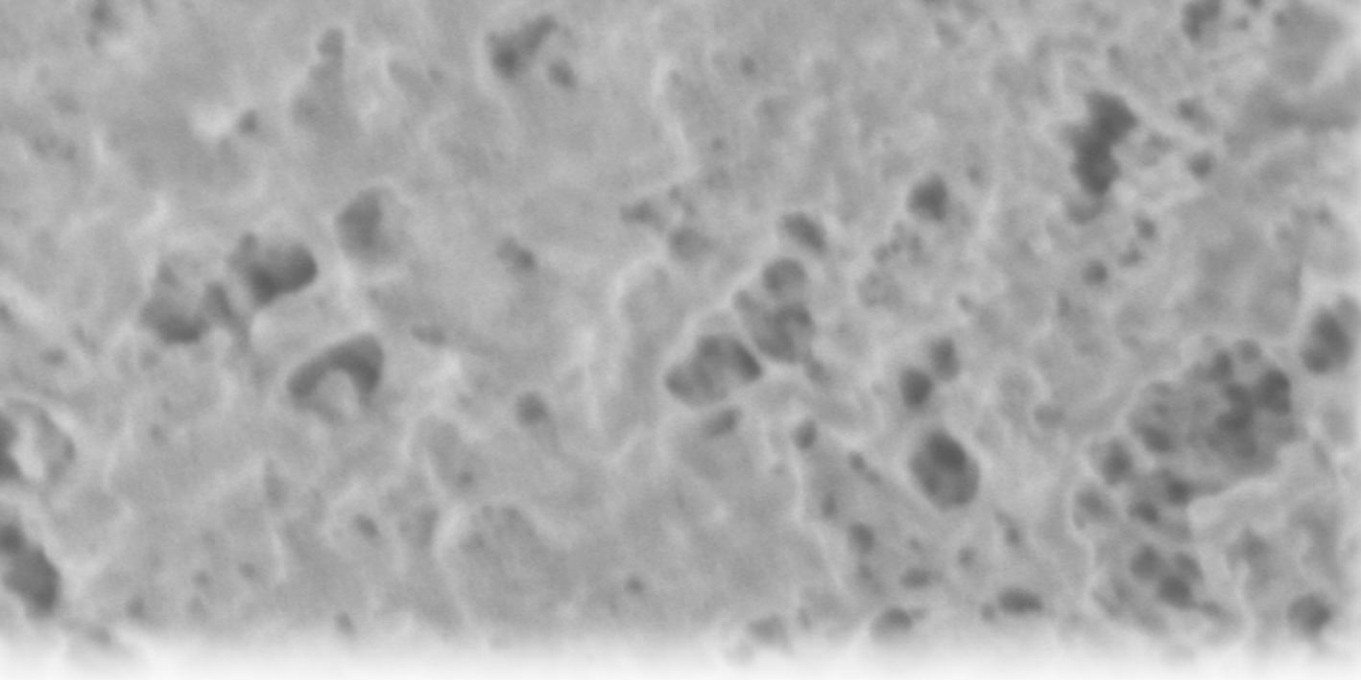
25. Waliullah, S., Hudson, O., Oliver, J. E., Brannen, P. M., Ji, P., & Ali, M. E. (2019). Comparative analysis of different molecular and serological methods for detection of *Xylella fastidiosa* in blueberry. *PLoS ONE*, 14(9). <https://doi.org/10.1371/journal.pone.0221903>

26. Wells, J. M., Raju, B. C., Hung, H.-Y., Weisburg, W. G., Mandelco-Paul, L., & Brenner, D. J. (1987). *Xylella fastidiosa* gen. nov., sp. nov: Gram-Negative, Xylem-Limited, Fastidious Plant Bacteria Related to *Xanthomonas* spp. *International Journal of Systematic Bacteriology*, 37(2). <https://doi.org/10.1099/00207713-37-2-136>

Acknowledgments

This research was supported by project PID2020-113256RA-I00 funded by MCIN/AEI /10.13039/501100011033, projects PID2021-126304OB-C41 and PID2021-126304OB-C41 funded by MCIN/AEI /10.13039/501100011033/ and by European Regional Development Fund - A way of doing Europe. Also, it is supported by project PDC2022-133576-C21 funded by MCIN/AEI /10.13039/501100011033 and by European Union Next

GenerationEU/ PRTR. Also, this study forms part of the Advanced Materials programme (MFA/2022/049) and was supported by MCIN with funding from European Union NextGenerationEU (PRTR-C17.11) and by Generalitat Valenciana. The project is also funded by the European Union. Views and opinions expressed are however those of the author(s) only and do not necessarily reflect those of the European Union or European Research Council. Neither the European Union nor the granting authority can be held responsible for them. This work was supported by the European Research Council (ERC) via Advanced Grant (101052997, EDISON). The project leading to this application has received funding from the European Union's Horizon 2020 research and innovation programme under grant agreement No 899708. This study was also supported by Generalitat Valenciana (CIPROM/2021/007). The work was also supported by Agència Valenciana de la Innovació (INNVA2-2021-2) and is susceptible to be co-founded by European Union. Part of the equipment used to develop this work was supported by Generalitat Valenciana (IDIFEDER/2021/044) and is susceptible to be co-founded through the Operational Programme of the European Regional Development Fund. I.C. thanks to Instituto de Salud Carlos III her postdoctoral fellowship (IFI21/0008). BioRender.com was used for the elaboration of some of the figures. The authors want to thank the Electron Microscopy Service at the UPV for support. This research was supported by CIBER - Consorcio Centro de Investigación Biomédica en Red- (CB06/01/2012), Instituto de Salud Carlos III, Ministerio de Ciencia e Innovación.

A grayscale FESEM image showing a porous, interconnected network of nanochannels, likely the capped Nanoporous Anodic Alumina (NAA) mentioned in the text. The structure consists of a dense array of interconnected, roughly rectangular or hexagonal pores, creating a complex, porous architecture.

Chapter II | Targeted Detection of *Mycobacterium tuberculosis* Using an Antibody-Coated Nanoporous Anodic Alumina Biosensor for MPT64 Antigen: A Novel Approach for Tuberculosis Screening

**Cover: FESEM image of capped NAA (self-produced image)*

Targeted Detection of *Mycobacterium tuberculosis* Using an Antibody-Coated Nanoporous Anodic Alumina Biosensor for MPT64 Antigen: A Novel Approach for Tuberculosis Screening

Isabel Caballos^{abc}, Ana Gil-Brusola^e, Ramón Martínez-Máñez^{abcd*} and Elena Aznar^{abc*}

^a Instituto Interuniversitario de Investigación de Reconocimiento Molecular y Desarrollo Tecnológico (IDM) Universitat de València–Universitat Politècnica de València, Camino de Vera s/n, 46022, Valencia, Spain.

^b Unidad Mixta de Investigación en Nanomedicina y Sensores, Universitat Politècnica de València – Instituto de Investigación Sanitaria La Fe, 46026 Valencia, Spain.

^c CIBER de Bioingeniería, Biomateriales y Nanomedicina (CIBER-BBN), Instituto de Salud Carlos III, 28029 Madrid, Spain.

^d Unidad Mixta UPV-CIPF de Investigación en Mecanismos de Enfermedades y Nanomedicina, Valencia, Universitat Politècnica de València, Centro de Investigación Príncipe Felipe, Valencia Spain

^e Servicio de Microbiología, Grupo Infección Grave, Hospital Politècnic i Universitari La Fe. Instituto de Investigación Sanitaria La Fe (IISLAFE), Avenida Fernando Abril Martorell, 106, 46026, Valencia, Spain.

*Corresponding authors: elazgui@upvnet.upv.es; rmaez@qim.upv.es.

Article under development

1. ABSTRACT

Tuberculosis (TB), ranking second only to COVID-19 as the deadliest infectious disease, is a chronic condition caused by *Mycobacterium tuberculosis*, where timely diagnosis and treatment are crucial for controlling its spread. This study introduces a cutting-edge biosensor for detecting *M. tuberculosis* MPT64 antigen, employing gated nanoporous anodic alumina (NAA) coated with a recognizing antibody. NAA material is loaded with rhodamine B and capped with this recognizing molecule only being able to open in the presence of the MPT64 *M. tuberculosis* protein thanks to the higher affinity for the target compared to the linker that holds it to the porous surface. When the target is present, the capping molecule displace, the pores open and this provokes to the specific release of rhodamine B to the medium for fluorescence measurement. The system is fully characterized at the physicochemical level by electron microscopy and spectroscopy. The biosensor achieved a detection limit (LOD) of 1.32 ± 1.02 nM (or 0.032 ± 0.025 mg L⁻¹) of the purified target and demonstrated high specificity through testing against various antigens from another viral pathogens and bacterial species. Its effectiveness was further validated with real samples, showing great potential as a rapid, sensitive, and precise tool for clinical TB diagnosis.

- KEYWORDS: gated materials, tuberculosis, mycobacterium tuberculosis, antibody, nanoporous anodic alumina.

2. INTRODUCTION

Tuberculosis (TB), caused by the bacterium *Mycobacterium tuberculosis*, is an ancient disease that continues to be one of the most significant global health challenges. Traces of TB have been found in the bones of Neolithic humans in Europe and in Egyptian mummies dating back to as early as 3700 BC, underscoring its deep-rooted presence in human history (Daniel, 2018; Ziskind & Halioua, 2007). Despite being a disease that is

theoretically curable, TB remains the most important communicable disease worldwide, particularly in developing regions where healthcare infrastructure is often inadequate.

The importance of early and accurate TB diagnosis cannot be overstated, particularly in the context of the disease's epidemiology. In the past, TB was thought to be transmitted genetically, a misconception that persisted even as the disease continued to spread. It was not until the work of epidemiologists like William Budd in the 19th century that the airborne nature of TB transmission began to be understood. Budd observed that phthisis (an old term for TB) caused significant mortality among African populations who had come into contact with Europeans, while those in the interior, with limited exposure to outsiders, were less affected (Rene & Dubos, 1953). This observation laid the groundwork for the understanding that TB is primarily transmitted through inhalation of airborne droplets containing the bacterium (Riley, 1974).

The dynamics of TB transmission underscore the importance of controlling the spread of the disease, particularly in settings with high rates of transmission. This emphasizes the need for effective infection control measures, particularly in healthcare settings where procedures like intubation, assisted ventilation, and bronchoscopy can increase the risk of transmission, especially among immunocompromised patients (Coleman et al., 2022; Ito, 2013).

Despite the significant advances in TB treatment since the introduction of effective chemotherapy in the 1950s (Kanabalan et al., 2021), the disease continues to pose a serious threat to global health. In developed countries, TB mortality has decreased, partly due to improved social conditions, public health measures, and the availability of effective treatment. However, the disease remains a leading cause of death in many developing regions, where healthcare systems are often overwhelmed and underfunded (Orgeur et al., 2024; Thaiss et al., 2012).

The World Health Organization (WHO) has repeatedly emphasized the critical nature of the TB epidemic since declaring it a global emergency in 1993. According to the WHO's 2023 Global TB Report, around 10.6 million people contracted TB in 2021, and tragically, 1.6 million people died from the disease (World Health Organization, 2023). Although TB has a relatively high treatment success rate of 85%, the challenge of accurately detecting *Mycobacterium tuberculosis* significantly complicates the control of the disease. In 2021, only 63% of pulmonary TB cases were confirmed, leading to delays in patient care and ongoing transmission, which perpetuates the global burden of TB. The rise of TB cases is particularly alarming when coupled with the HIV epidemic, which has had a profound impact on TB incidence (Nunn et al., 1994), especially in resource-limited settings where the provision of and access to healthcare services are often inadequate (Chai et al., 2018).

Historically, TB diagnosis has relied on traditional methods such as culture and smear microscopy (Inoue et al., 2011; Kim et al., 2013), which were developed after the bacterium was first identified by Robert Koch in 1882. Culture methods have been the gold standard for TB diagnosis due to their high sensitivity and specificity. However, *Mycobacterium tuberculosis* is a slow-growing bacterium, requiring 2–6 weeks to form visible colonies on egg-based media like Lowenstein-Jensen medium or on oleic acid-albumin agar (Koch & Mizrahi, 2018; Sakamoto, 2012). This long incubation period often results in delays in diagnosis, which can be detrimental to patient outcomes and public health efforts to control the spread of the disease.

Smear microscopy, another commonly used diagnostic tool, offers a faster and simpler method of detection. The technique involves staining sputum samples with Ziehl-Neelsen stain or fluorescent dyes such as auramine and rhodamine, which allows the visualization of acid-fast bacilli under a microscope (Wayne, 1982). However, while smear microscopy is quick and straightforward, it suffers from low sensitivity, particularly in samples with low bacterial loads or in patients with extrapulmonary TB. This limitation is

especially pronounced in settings where the quality of microscopy services may be variable due to a lack of trained personnel and resources (Natarajan et al., 2020).

To address these limitations, molecular diagnostic techniques such as Polymerase Chain Reaction (PCR) and Next-Generation Sequencing (NGS) have been developed (Beviere et al., 2023; Operario et al., 2017). PCR allows for the rapid amplification and detection of *M. tuberculosis* DNA from clinical samples, providing higher sensitivity than smear microscopy. NGS, on the other hand, offers a comprehensive analysis of the bacterial genome, enabling the detection of drug-resistant strains and providing valuable epidemiological data (Gu et al., 2019; Tang et al., 2010). However, these molecular methods are not without their drawbacks. PCR and NGS are time-consuming, labor-intensive, and expensive, making them less accessible in many parts of the world where TB is most prevalent (Grobbel et al., 2021). Additionally, these techniques are susceptible to cross-contamination, which can lead to false-positive results and complicate the diagnostic process. Given these challenges, there is an urgent need for the development of new diagnostic tools that are rapid, accurate, sensitive, and affordable. This is where the fields of nanotechnology and biosensors have shown great promise. Nanotechnology, the manipulation of materials at the nanoscale, has opened up new avenues for TB diagnostics (Bharti et al., 2022; Chopra et al., 2023; Grotz et al., 2018).

Among the various nanomaterials explored for the development of diagnostic tools, nanoporous anodic alumina (NAA) stands out due to its exceptional characteristics. NAA offers a high loading capacity, ease of surface modification, and cost-effective production through well-established techniques (Ribes et al., 2016). Besides, in recent years, NAA has been increasingly utilized to develop gated nanomaterials for biosensing applications. These systems are particularly advantageous as they release a reporter molecule only in the presence of the target pathogen or biomolecule, ensuring high specificity in detection. For instance, previous studies have demonstrated the effectiveness of oligonucleotide-gated NAA materials for the detection of the bacterium

Xylella fastidiosa in real samples (seen on Chapter III) or aptamer-capped mesoporous supports in detecting pathogens such as SARS-CoV-2 (Chapter IV of this thesis (Caballos et al., 2023)). These studies highlight the potential of gated materials in clinical diagnostics, yet their application to TB detection, remains unexplored.

One of the most promising gating mechanisms that can be integrated into porous supports for the development of functional sensory materials is the use of antibodies (Gao et al., 2022; Vikholm & Albers, 1998). Antibodies are large, Y-shaped proteins belonging to the immunoglobulin superfamily which are used by the immune system to identify and neutralize antigens such as bacteria and viruses, including those that cause disease. Antibodies possess a high binding affinity for specific target molecules. This precise binding ability makes antibodies highly suitable for use in biosensors, known as immunosensors, which are designed for the sensitive and accurate detection of pathogens. One of the defining features of antibodies is their ability to bind to a specific antigen with high affinity. This binding is mediated by the variable regions of the antibody, which can recognize unique epitopes on the target molecule. The strength and specificity of this interaction are determined by the sequence and structure of the antibody, which can be tailored to bind almost any target (Lipman et al., 2005). This versatility is a significant advantage in biosensor design, as antibodies can be produced to recognize a wide range of molecules, from small organic compounds to large proteins and even whole cells.

One of the primary advantages of using antibodies as recognition elements in biosensors is their unparalleled specificity. Antibodies can distinguish between closely related molecules, even differentiating between different isoforms of a protein or variations in glycosylation patterns. This high specificity minimizes the likelihood of cross-reactivity, leading to more accurate and reliable detection, which is particularly crucial in clinical diagnostics where false positives or negatives can have significant consequences. Another advantage, as mentioned before, is the high affinity of antibodies for their target

antigens. The strong binding interaction between an antibody and its antigen ensures that even low concentrations of the target molecule can be detected, enhancing the sensitivity of the biosensor. This high sensitivity is especially beneficial in applications where the analyte is present in trace amounts, such as in early disease detection or environmental monitoring.

The availability and diversity of antibodies also contribute to their widespread use in biosensor development. Antibodies can be generated against virtually any antigen, including those that are difficult to detect with other recognition molecules. The production of monoclonal antibodies, which are identical and target the same epitope, allows for consistent performance across different biosensor platforms. Additionally, advances in recombinant DNA technology have enabled the engineering of antibodies with enhanced stability, affinity, and specificity, further expanding their utility in biosensor applications (Borrebaeck, 2000).

In this study, we focus on the protein MPT64 as the target analyte. MPT64 plays a critical role in bacterial virulence and has been recognized as a potential biomarker for active tuberculosis (TB) disease, having been identified in the serum exosomes of TB patients through multiple reaction monitoring (MRM) (Cao et al., 2021)(Dahiya et al., 2019). One key advantage of targeting this secreted protein is that it allows for the antibody-analyte interaction without the need to lyse the bacterium. Additionally, MPT64 is specifically encoded in regions of difference, making it absent in most *Mycobacterium bovis* bacille Calmette–Guérin (BCG) substrains and non-tuberculous mycobacteria, which enhances the specificity of detection (Kamra et al., 2023).

Antibody-based biosensors have found applications across a broad spectrum of fields, including medical diagnostics, environmental monitoring, food safety, and biodefense. In medical diagnostics, these biosensors are used to detect biomarkers for various diseases, such as cancer, cardiovascular diseases, and infectious diseases. For

example, antibody-based biosensors are employed in point-of-care devices to rapidly detect proteins associated with specific diseases, like the work of Sannigrahi et al. (Sannigrahi et al., 2020) who developed a biosensor employing a magnetosome-anti-*Salmonella* antibody complex to detect lipopolysaccharide (somatic “O” antigen) and *Salmonella typhimurium* in real samples with a limit of detection of 0.001–0.1 $\mu\text{g mL}^{-1}$ (with a R^2 value of 0.960) for the lipopolysaccharide and 10^1CFU mL^{-1} of *S. typhimurium* in water and milk sample demonstrating its sensitivity.

We can find another example of the use of antibodies in the successful design of biosensors in the works of Shamsuddin et al. (Shamsuddin et al., 2021) who designed an antibody-based impedimetric biosensor with an ultrasensitive detection of carcinoembryonic antigen, an early colorectal cancer biomarker, down to fM levels. For this they used polyoctopamine, an amine-functionalised non-conducting polymer, as the transducer layer in an electrochemical biosensor where the antibodies were attached covalently setting the limit of detection at 11.76 fM which is significantly lower than the basal clinical levels of 25 pM.

Given the success of antibody-based detection systems in other fields, there is considerable potential in combining gated NAA materials with antibodies specifically designed to recognize the MPT64 protein of *Mycobacterium tuberculosis*. This combination could lead to the development of a highly specific and ultrasensitive biosensor for TB diagnostics. In this proposed system, NAA would be loaded with a fluorescent reporter dye, such as rhodamine B, and capped with an anti-MPT64 antibody that specifically binds to the protein. The antibody would serve as the gating mechanism, blocking the pores of the NAA and preventing dye release in the absence of the target protein. Upon encountering the MPT64 protein, the antibody would bind to the protein, causing it to uncouple from the NAA surface and thus opening the pores. This uncapping process would then trigger the release of the dye, producing a measurable signal that indicates the presence of *M. tuberculosis*. This method would not only ensure high

specificity but also allow for rapid responses, potentially enabling accurate TB diagnosis within a very short time frame. The potential of such a biosensor in clinical settings is vast and is particularly important in resource-limited settings, where traditional diagnostic methods may be too slow or cumbersome to be effective. Addressing the challenges of TB diagnosis is essential for reducing the global burden of the disease and achieving the goal of a TB-free society.

3. RESULTS AND DISCUSSION

3.1. Design, synthesis and characterization of gated NAA materials

To prepare the biosensor we used commercially available nanoporous anodic alumina (NAA) disks, each 2 mm in diameter (designated as M0). These disks were initially loaded with rhodamine B, a fluorescent molecule that would act as a detection reporter, and then the external surface of M0 was chemically modified by attaching 3-(triethoxysilyl)propyl isocyanate, producing the M1 material.

Subsequently, we selected a peptide sequence specifically designed to partially hybridize with the anti-MPT64 antibody and facilitate its attachment to the surface. The amine group located at one end of the amino acid chain was utilized to achieve this attachment. This amine group was employed to covalently bind the peptide to the M1 material via urea bond formation with the isocyanate groups, resulting in the development of the gated NAA solid, designated as M2.

The selection of the most effective peptide for interaction with the anti-MPT64 antibody was performed using an ELISA assay. This method allowed us to evaluate the binding affinities of three peptides (P1, P2, and P3) designed based on specific regions of the MPT64 protein, targeting its external domains for enhanced interaction potential. As shown in Figure 2A, the selected regions of the MPT64 antigenic protein, along with their

respective amino acid sequences, were utilized to synthesize the peptides. The ELISA results (Figure 2B) revealed that peptide P1 exhibited the highest absorbance values, indicating superior affinity for the anti-MPT64 antibody compared to P2 and P3. This enhanced binding capacity underscores P1 as the optimal candidate for molecular gate linkage. The data also demonstrated the antibody's high specificity for the MPT64 target (C+) across varying concentrations (5, 10, 15, and 20 $\mu\text{g}/\text{mL}$), while minimal baseline absorbance was observed with a random, unrelated peptide (C-). These findings confirm the suitability of peptide P1 for the intended biosensing application.

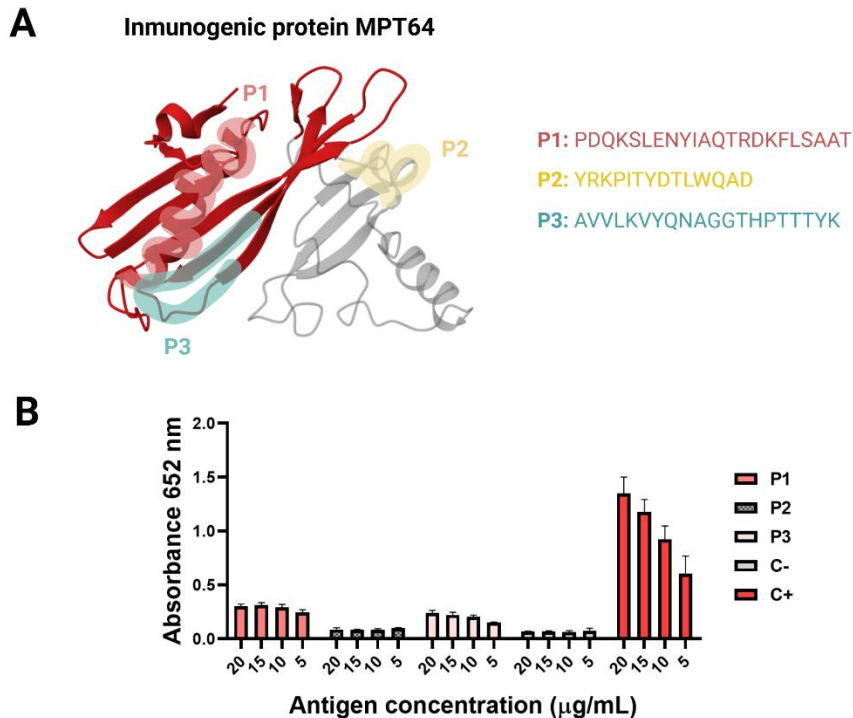


Figure 2. A) Selected regions of the MPT64 antigenic protein from *M. tuberculosis* and their respective amino acid sequences used for synthesizing anchor peptides. B) ELISA-based evaluation of peptide binding affinities, showing the superior performance of peptide P1 compared to P2 and P3 in binding the anti-MPT64 antibody. Data include absorbance values at increasing concentrations (5–20 $\mu\text{g}/\text{mL}$) for the target peptide (C+)

and baseline values for a random peptide (C-). Results are presented as means \pm standard errors (N = 4).

In the final step, the M2 material was exposed to a solution of anti-MPT64 antibody in PBS. This process allowed the antibody to interact with the peptide and capping the pores. This forms an organic layer over the pores. This layer is sufficiently bulky to obstruct the pore entrances, effectively preventing the release of the encapsulated dye. Consequently, the final material, designated as M3, was obtained (as illustrated in Figure 3).

To characterize the materials at each stage—M0, M1, M2, and M3—we employed field emission scanning electron microscopy (FESEM), atomic force microscopy (AFM), and energy-dispersive X-ray spectroscopy (EDXS). The original M0 material appeared as small silvery disks, while the final M3 material took on a pinkish hue due to the rhodamine B loading. FESEM images of M0 revealed its porous structure, that is maintained until material M3, that demonstrated a dense capping layer covering the pores. We can also be seen in the FESEM images that the attached peptide is not big enough to cover the pores.

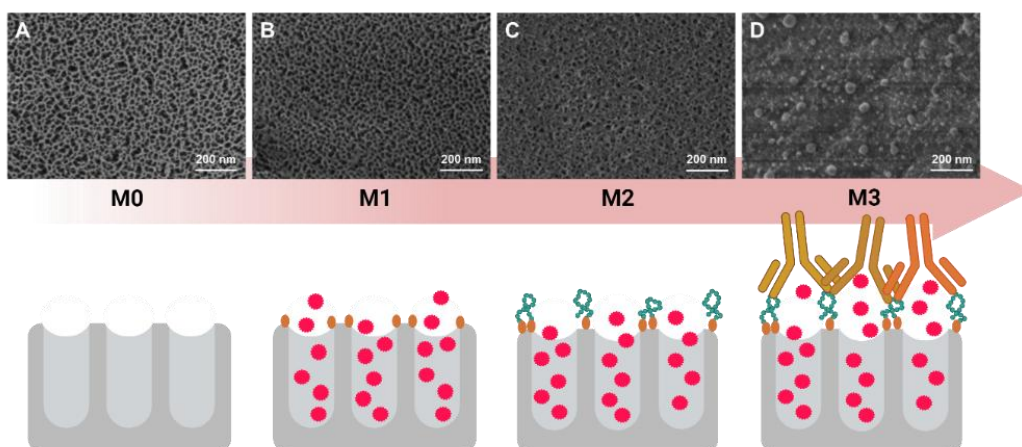


Figure 3. Physicochemical characterization of oligonucleotide-capped NAA. A) FESEM image of the material surface before capping, showing the nanopores (M0 material). B) The material was loaded with rhodamine B to produce a red fluorescence signal if rhodamine B is released to the medium. C) FESEM image of the material surface after covalent capping with the specific peptide (M2 material). And D) FESEM image of the final M3 material capped with the anti-MPT64 antibody. Scale bar of 200 nm.

AFM provided a three-dimensional view of the material surfaces, as shown in Figure 4. It can be seen how the roughness diminishes as the synthesis steps advance. EDXS analysis confirmed the successful synthesis of the various materials by quantifying atomic content. The carbon content in the M1 material increased due to the rhodamine B loading, while the M3 and M4 materials this increase is even higher due to the attachment of the organic molecules. The M3 material exhibited the highest carbon content, corresponding to the presence of the capping antibody, which also led to increased nitrogen levels (Table 1).

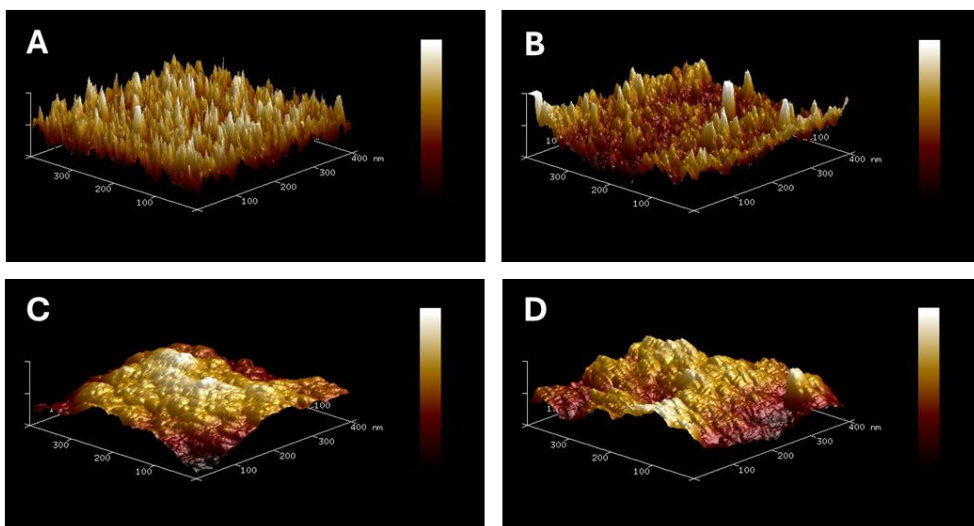


Figure 4. AFM images of the synthesized solids. A) corresponds to M0, B) to M1, C) to material M2 and D) to final material M3.

Table 1. Relative atomic compositions represented by atomic percentage (with respect to the total) of the M0, M1, M2, and M3 materials determined by EDXS.

Element	M0	M1	M2	M3
C	12.82 ± 0.41	17.07 ± 0.39	35.51 ± 0.52	35.75 ± 0.46
N	2.40 ± 0.3	3.33 ± 0.28	5.37 ± 0.45	6.64 ± 0.41
O	46.03 ± 0.34	45.69 ± 0.33	33.01 ± 0.42	34.93 ± 0.39
Al	38.75 ± 0.3	32.16 ± 0.26	20.71 ± 0.27	16.49 ± 0.21
Si	0.00 ± 0.05	1.74 ± 0.07	3.64 ± 0.11	3.47 ± 0.1

3.2. Purified antigen-triggered cargo release

We carried studies on the delivery of the rhodamine B from M3 in the absence and in the presence of the purified MPT64 protein at a final concentration of 10 nM. The reactions were carried out at 25°C, and fluorescence was measured at various time intervals to monitor the release of rhodamine B into the medium as a result of the recognition between the antibodies capping the material and the target protein MPT64. After 1 hour, the presence of the protein resulted in a 3.2-fold increase in fluorescence compared with the delivery observed in its absence (Figure 5).

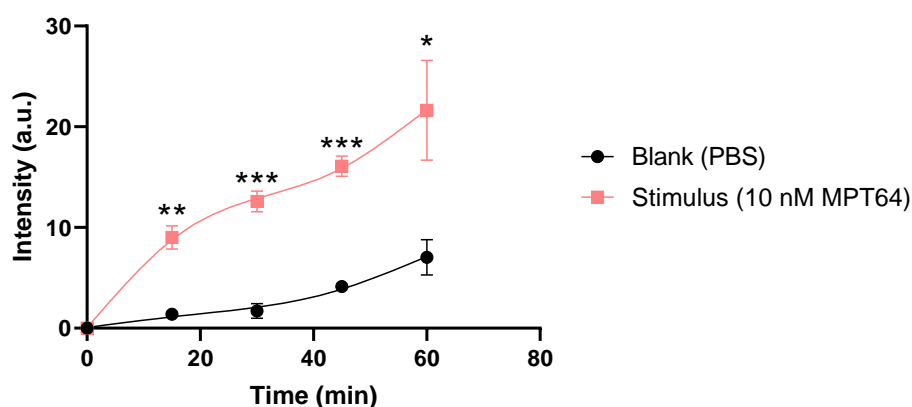


Figure 5. Rhodamine B release profiles from M3 in the presence (colored line) or not (black line) of the target MPT64 protein at 25 °C for 60 min. Represented data corresponds to means \pm standard errors ($n = 3$). *Statistically significant change (Welch's t -test, $P < 0.05$). AU, arbitrary units.

3.3. Specificity and sensitivity assays

In a further assay, we confirmed that biosensor M3 was indeed specific for recognizing the MPT64 protein. To do this, we performed parallel release assays: in one assay, the MPT64 protein was added to M3, while in the others, we introduced 10 nM concentrations of various proteins associated with respiratory viruses that can cause

symptoms similar than early-stage tuberculosis. The interfering proteins tested included the G glycoprotein from the respiratory syncytial virus (RSV), the Spike protein from SARS-CoV-2, and the nucleoproteins from Influenza A and B viruses, all at a final concentration of 10 nM. The reactions were conducted at 25°C, and fluorescence was measured after 60 minutes. Our results demonstrated a significant release of rhodamine B exclusively in the presence of the target MPT64 protein, with no notable release observed in the presence of the other proteins, indicating a high level of specificity and minimal off-target effects (Figure 6).

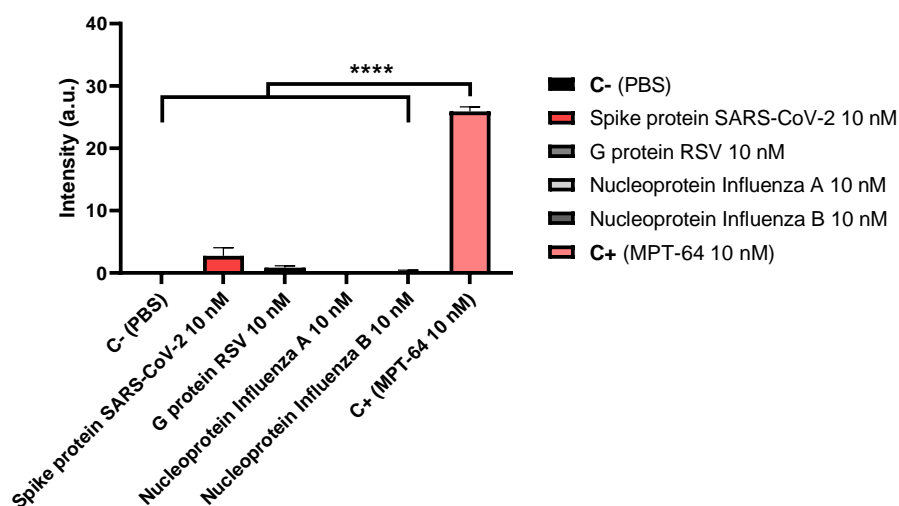


Figure 6. Rhodamine B release in the presence of different interferent proteins (10 nM, at 25 °C for 60 min) using the M3 material. The SARS-CoV-2 Spike protein, the RSV glycoprotein G and the nucleoproteins of Influenza A and B were considered, as well as one negative control (just PBS) and one positive control with 10 nM of the target analyte MPT64.

To evaluate the sensitivity of the M3 detection method, experiments were conducted using various concentrations of MPT64. For this purpose, 8 individual M3 materials were immersed in hybridization buffer, followed by the addition of 100 µL of

protein suspension dilutions, resulting in final concentrations ranging from 0 to 10 nM. After an incubation period of 60 minutes, the amount of rhodamine B released into the aqueous phase was quantified through fluorescence measurements. The results demonstrated a direct correlation between the concentration of MPT64 and the amount of dye released (Figure 7).

The limit of detection (LOD) for the system was determined by graphically identifying the intersection point between the baseline fluorescence and the positively sloped response curve. Using this technique, it was obtained a LOD of 1.32 ± 1.02 nM (or 0.032 ± 0.025 mg L⁻¹). This LOD is significantly lower than those typically reported by molecular techniques used for MPT64 detection, 0.032 mg L⁻¹ compared with 2.5 mg L⁻¹ reported by the works of Zhu et al. (C. Zhu et al., 2012) who performed an ELISA assay (based on antibody recognition) for the detection of MPT64.

Compared to current molecular techniques like DNA amplification or sequencing, our oligonucleotide-capped nanoporous anodic alumina biosensor offers several distinct advantages: (i) the capping DNA sequences and cargo can be easily customized; (ii) the overall cost of preparation and testing is lower; (iii) the required equipment is simple, widely available, and affordable for most laboratories; and (iv) the process is faster and more straightforward, eliminating the need for DNA extraction and amplification. As a result, this assay could serve as a practical and efficient alternative for the rapid and accurate detection of *M. tuberculosis*.

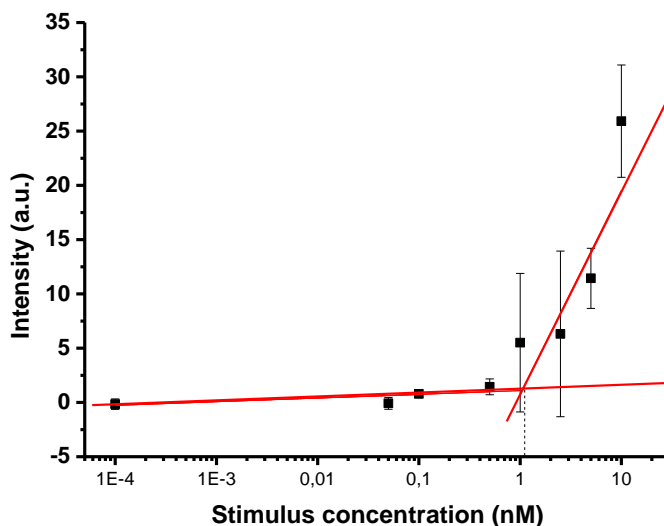


Figure 7. Dye release from solid M3 in the presence of different amounts of MPT64 in PBS.

3.4. Detection of *M. tuberculosis* in competitive media and clinical samples

To further assess the system's robustness, the performance of M3 was tested in a clinically relevant medium: fluid from sputum collected from a healthy individual using collecting tube and diluted in hybridization buffer (PBS). In this experiment, 100 μL of MPT64 100 nM was added to 900 μL of the different sputum dilutions. As shown in Figure 10, the presence of MPT64 in this complex medium led to the selective displacement of the antibody, resulting in pore uncapping and dye release. While a slightly higher baseline fluorescence was observed in all the diluted sputum medium tested compared to the buffer alone, the fluorescence signal in the presence of the purified protein remained comparable to that achieved in PBS buffer (Figure 8).

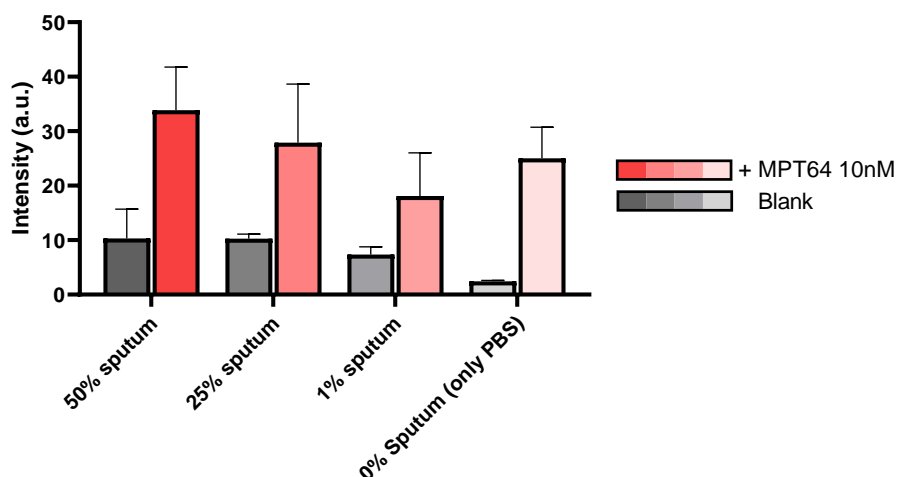


Figure 8. Rhodamine B delivery from material M3 in PBS (Negative control) and in the presence of different concentrations of sputum sample diluted in PBS. The grey bars represent the media without any stimulus and the coloured bars represent the media of the sputum samples inoculated with MPT64 10 nM.

To further validate our detection system, a small-scale analytical assay was conducted. The samples provided by the microbiology department of Hospital Universitari i Politècnic La Fe were grown in liquid MGIT™ medium, which is specifically designed for detecting *Mycobacterium tuberculosis* complex. This medium contains modified Middlebrook 7H9 broth, to which the MGIT™ growth supplement is added, creating optimal conditions for the proliferation of most mycobacteria. Contaminating bacteria are inhibited by the inclusion of a mixture of antibiotics. The presence and growth of bacteria, including mycobacteria, are detected by the fluorescence emitted from the tube, which increases as the bacteria consume oxygen and replace it with carbon dioxide in the medium.

Given that the samples can be grown in this medium, it was essential to first verify that the medium did not interfere with our biosensor. To do this, we conducted a series

of dye release experiments from M3 using the pure culture medium. In one set of experiments, the medium was inoculated with 10 nM of the MPT64 protein, while another set served as a negative control. This was performed in triplicate to ensure reproducibility. Additionally, we repeated the assay after diluting the culture medium to 10% concentration with PBS to determine if reducing the concentration of the medium would decrease the nonspecific release observed in comparison to the controls in pure PBS.

This approach allowed us to assess whether the culture medium influenced the specificity and selectivity of our detection system, particularly in the presence of the target protein MPT64. As we can see in Figure 9, the presence of the medium enlarges the unspecific dye release from the pores but there is a significant difference between the Blank bar (depicted in black) and the release when the stimulus is present (depicted in grey).

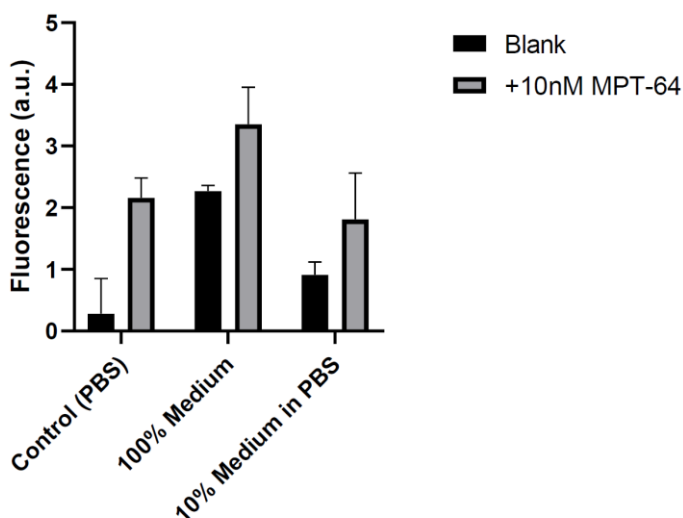


Figure 9. Dye release from solid M3 at different concentrations of the MGIT™ medium. The black bars represent the release when there is no stimulus present in the

medium and the grey bar represents the delivery in medium inoculated with 100 μL of MPT64 100 nM in a final volume of 1 mL. The error bars correspond to the standard deviation of the means ($N=3$).

Detecting the protein MPT64 from *M. tuberculosis* directly in clinical samples is essential for integrating the probe into medical practice effectively. Therefore, the ability of the sensing materials to identify the MPT64 protein in samples from infected patients was evaluated (Figure 10). The current standard for TB detection in most hospitals is RT-qPCR, a method that requires complex equipment, trained personnel, and at least two hours to produce results. In this study, samples from TB positive and negative patients at Hospital Universitari i Politècnic La Fe were analysed using both RT-qPCR and the M3 material (see Experimental Section for details). A total of 20 patients participated in the study. Of these, 10 patients were diagnosed with TB, while the remaining 10, who were hospitalized for other reasons, served as the negative control group.

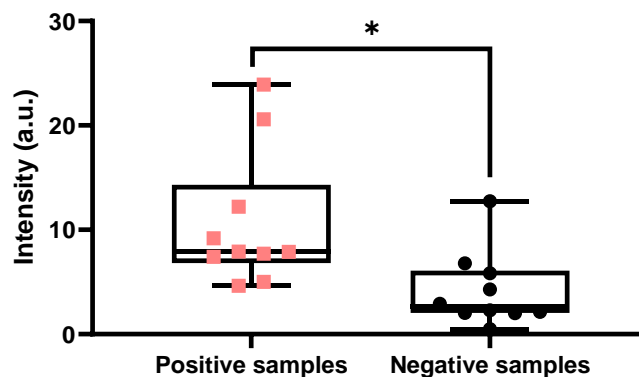


Figure 10. Measurement of dye release in presence of diluted liquid culture samples. The scatter plot represents how levels are lower in negative samples ($N = 10$) (black dots) than in samples tested positive for the presence of *M. tuberculosis* ($N = 10$) (colored dots) establishing a discrimination limit in 5 fluorescence units.

Additionally, a final validation experiment was conducted using positive culture samples from patients infected with other species from the *Mycobacterium* genus, specifically *Mycobacterium abscessus* and *Mycobacterium intracellulare*. Detection assays were performed in triplicate using the final gated material. Individual supports were immersed in 950 μL of PBS buffer, and 50 μL of each sample was added to the respective supports. After 60 minutes, the release of rhodamine B was measured, with the results presented in Figure 11. The data indicate a selective response to *M. tuberculosis*.

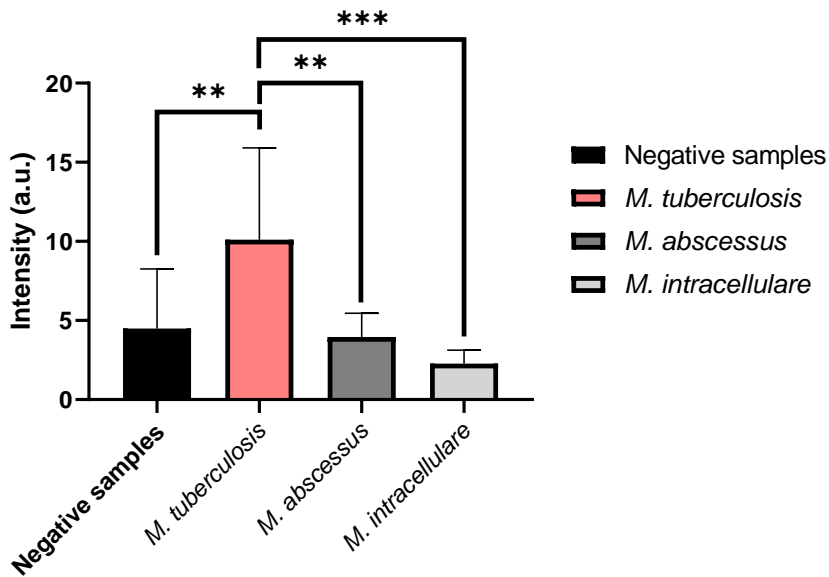


Figure 11. The release of Rhodamine B from probe M3 was tested using samples infected with the *M. tuberculosis*, *M. abscessus* and *M. intracellulare* as well as the negative control of the same mycobacterium growth medium without any grown bacterium.

4. CONCLUSIONS

The development of new strategies for the sensitive and rapid detection of *Mycobacterium tuberculosis* is essential for improving diagnostics in tuberculosis (TB) cases, especially in clinical settings where early intervention is critical. In this study, we report the preparation of a peptide- and antibody-capped nanoporous anodic alumina (NAA) sensor loaded with rhodamine B as a fluorescent indicator for the detection of the MPT64 protein from *M. tuberculosis*. The synthesis process involved modifying NAA disks with a peptide sequence specifically designed to interact with the anti-MPT64 antibody, resulting in a responsive, selective system that operates by controlled dye release. The resulting material, M3, demonstrated the ability to block dye release in the absence of the target protein, while effectively releasing rhodamine B upon interaction with the MPT64 protein, thus confirming a selective gating mechanism.

When exposed to purified MPT64 protein in a controlled assay, the M3 material responded with an increase in fluorescence intensity, demonstrating the sensor's high sensitivity and specificity for *M. tuberculosis* detection. The results showed a notable 3.2-fold increase in fluorescence in the presence of MPT64 protein at 10 nM, with minimal release observed in the absence of the target. Moreover, specificity tests conducted with proteins from common respiratory viruses (e.g., RSV, SARS-CoV-2, and Influenza A and B) confirmed that the M3 material did not respond significantly in the presence of other proteins, reinforcing the sensor's specificity for *M. tuberculosis*. Moreover, the biosensor displayed a detection limit (LOD) as low as 1.32 nM, a value notably lower than typical molecular diagnostic methods such as PCR. Unlike PCR and other conventional detection techniques, our sensor does not require DNA amplification, complex equipment, or lengthy processing times, allowing it to produce results within 60 minutes and simplifying the overall workflow. This rapid and selective detection of the MPT64 protein underscores the potential of the M3 material as a practical diagnostic tool.

The robustness of this gated NAA material was further evaluated in real clinical matrices, including diluted sputum samples and liquid culture media. Results showed that while complex media slightly increased background fluorescence, the presence of the MPT64 protein in these competitive environments still led to significant pore opening and dye release. These findings support the application of this sensor in complex biological samples without extensive pretreatment. Tests with additional *Mycobacterium* species confirmed selective dye release in samples containing *M. tuberculosis*, further validating the sensor's selectivity.

In conclusion, this study suggests that gated materials incorporating specific biochemical recognition elements, such as antibodies, offer an innovative approach for the rapid, easy, and reliable detection of *M. tuberculosis*. The M3 material presents a portable and cost-effective alternative to traditional diagnostic methods, demonstrating high sensitivity, selectivity, and the potential to significantly expedite TB diagnostics in clinical settings. Furthermore, the simplicity of this system positions it as a promising diagnostic tool for use in resource-limited settings, where rapid, accessible TB detection is critical.

5. MATERIALS AND METHODS

5.1. Reagents

(3-Triethoxysilyl)propylisocyanate, acetonitrile, rhodamine B, triethylamine (TEA), and TRIS(hydroxymethyl)aminomethane (TRIS) were sourced from Sigma-Aldrich Química (Madrid, Spain). Nanoporous anodic alumina supports were obtained commercially from InRedox® (CO, USA). The anti-MPT64 antibody (ab193435) and purified recombinant *Mycobacterium tuberculosis* MPT64 protein (ab226277) were purchased from Abcam (Danaher Corporation, Cambridge, UK) and used without further modification. Peptides were commercially synthesized by Nzytech (Lisbon, Portugal).

5.2. Material characterization

A ZEISS Ultra 55 microscope was utilized for Field Emission Scanning Electron Microscopy (FSEM) and Energy Dispersive X-ray spectroscopy (EDXS) analyses. Fluorescence spectroscopy measurements were conducted using a Synergy H1 microplate reader (BioTek, Winooski, VT, USA).

5.3. Linker peptide design

To design the molecular linker that attaches the antibody to the surface of the material, we employed a manual screening technique. We used the UniProt database to analyze the spatial conformation of the MPT64 protein, identifying its main and most exposed domains. From these domains, we extracted the corresponding amino acid sequences and synthesized peptides based on them. In total, four peptides were synthesized from four different regions of the MPT64 protein. These peptides were then tested using an ELISA assay to evaluate their affinity with the anti-MPT64 antibody. The goal was to select a peptide with sufficient affinity to hold the antibody in place while still being able to dissociate in the presence of the full MPT64 protein.

5.4. ELISA peptides assay

To assess the affinity of each peptide for the anti-MPT64 antibody, we performed a direct ELISA assay. We prepared each peptide at various concentrations to observe the interaction without saturating the system. Specifically, 100 μL of each peptide was added to the wells at concentrations of 2, 5, 10, and 20 $\mu\text{g mL}^{-1}$, followed by gentle agitation at 4°C overnight. This step was done in quadruplicate for each sample.

After the peptides were adsorbed onto the plate, we manually washed the wells by removing the solution and flicking the plate over a sink after each wash. Next, 200 μL of blocking buffer was added to each well, the plate was covered, and it was placed on a shaker at 4°C overnight.

The following morning, each well was washed three times with wash buffer. Then, 100 μL of the primary antigen, diluted in blocking buffer to a concentration of $1 \mu\text{g mL}^{-1}$, was added. The plate was covered and incubated for 24 hours at 4°C . Afterward, the wells were washed three times, and the secondary antibody conjugated to the HRP enzyme was added at a concentration of $0.001 \mu\text{g mL}^{-1}$, followed by another overnight incubation at 4°C .

The next day, after washing the plate three times, it was ready for measurement. We added 100 μL of enzyme substrate solution to each well, incubated with gentle agitation for 3 minutes, and then added stop solution to each well, shaking for 1 minute. Finally, the plate was read at an absorption wavelength of 650 nm using a plate reader to obtain the data.

5.5. Synthesis of solids

To synthesize solid M1, 25 individual NAA supports, each with a diameter of 2 mm, were submerged in an 8 mL rhodamine B solution in acetonitrile (6 mg, 1.57 mM). This mixture was stirred continuously for 24 hours to ensure efficient pore loading. Afterward, the surface of the supports was functionalized by adding (3-triethoxysilyl)propylisocyanate (1.32 mmol, 328 μL) and stirring the reaction for 5 hours and 30 minutes. The supports were then dried and stored overnight at 4°C .

Next, M1 was immersed in a solution containing the specific peptide sequence (P1), rhodamine B (262.5 μg , 1.57 mM, 350 μL), and triethylamine (2 μL) in acetonitrile for 3 hours, resulting in solid M2. This material was then further treated by immersing it in hybridization buffer (1X PBS, pH 7.4) containing the anti-MPT64 antibody (AB) to produce the sensing material M3. To optimize the capping conditions of these gated materials for maximum performance, different concentrations of the capping antibody were tested: 0.025, 0.125, 0.225, and 0.325 μM of AB. The final reaction volume was set at 400 μL of hybridization buffer, and the mixtures were agitated at 25°C for 180 minutes. Finally, the

resulting materials were rinsed with hybridization buffer to remove any unbound antibody and excess rhodamine B.

5.6. Cargo quantification

To determine the amount of rhodamine B that could be loaded into the pores, two independent M3 supports were immersed in 1 mL of hybridization buffer. One support was heated to 90°C and stirred for 60 minutes to force the pores to open and release their maximum cargo, while the other support was stirred at 25°C for the same duration to serve as a control. The released fluorophore was measured at an emission wavelength of 575 nm, with excitation at 555 nm. The concentration of released dye was quantified by referencing a calibration curve generated with known concentrations of rhodamine B. This experiment was performed in triplicate for accuracy.

5.7. Detection protocol

To evaluate the ability of the materials to detect the MPT64 protein, the fluorescence emission of rhodamine B, released from the inner mesoporous structure, was measured both in the presence and absence of purified MPT64 protein. Two separate M3 supports were each immersed in 900 μL of hybridization buffer. One of the supports received 100 μL of MPT64 solution (1 ng μL^{-1} , Abcam, UK), while the other was treated with 100 μL of hybridization buffer as a control. Both samples were stirred at 25°C, with aliquots taken periodically. The released rhodamine B was then detected by fluorescence spectroscopy at 575 nm ($\lambda_{\text{exc}} = 555$ nm). The experiment was conducted in triplicate to ensure reproducibility. The experiment was repeated using 900 μL of competitive media, specifically sputum samples collected from a healthy patient, at various dilutions. The sputum was diluted in PBS to concentrations of 50%, 25%, and 1%. For each dilution, two different release assays were conducted: one to test the release in the absence of the stimulus, and the other to test the release in the presence of the stimulus. In the first assay, one independent M3 support were immersed in 1 mL of the diluted sputum. In the

second assay, 900 μL of the same concentration of diluted sputum was mixed with 100 μL of purified MPT64 protein at a concentration of 100 nM and the release from M3 was tested. This was repeated by triplicate.

5.8. Quantification curve of MPT64 protein recognition

The response of the solid M3 to different concentrations of MPT64 was studied. For that, 24 independent supports of the M3 material were submerged in a solution containing 100 μL of different dilutions of MPT64 (from 0 to 10 nM) and volume was completed until 1 mL with hybridization buffer (diluting the protein concentrations 1:10). Solutions were stirred at 25 $^{\circ}\text{C}$ and released rhodamine B was determined at 575 nm ($\lambda_{\text{exc}} = 555 \text{ nm}$) after 60 min.

5.9. Specificity

To further evaluate the specificity of the anti-MPT64 antibody for its target, we conducted a release assay comparing the response of the M3 material to the presence of purified MPT64 protein at a concentration of 10 nM against other proteins from various respiratory pathogens. In this experiment, six different supports were used. The first support served as a negative control and was tested in a medium containing only PBS. The second support was exposed to a medium with the G protein from the respiratory syncytial virus (RSV) at a concentration of 10 nM. The third support was tested in PBS containing the Spike protein from SARS-CoV-2 at 10 nM. The fourth and fifth supports were exposed to the nucleoproteins of Influenza A and B viruses, respectively, each at the same concentration of 10 nM. The final support acted as a positive control, with MPT64 protein added to the medium at a concentration of 10 nM.

This experimental design allowed us to assess the selectivity of the anti-MPT64 antibody by comparing its response to MPT64 with its response to proteins from other respiratory pathogens.

To further evaluate the selectivity of M3, we conducted release assays on real samples infected with other *Mycobacterium* species. Following the same procedure used for testing positive samples for *M. tuberculosis* (as described later), 50 μL of culture from each species was added to 950 μL of PBS, yielding a final volume of 1 mL. This assay included five different cultures from five distinct patients for each *Mycobacterium* species (*Mycobacterium abscessus* and *Mycobacterium intracellulare*), with each sample analysed in duplicate. The release of rhodamine B was then quantified using fluorescence detection ($\lambda_{\text{exc}} = 555 \text{ nm}$, $\lambda_{\text{em}} = 585 \text{ nm}$).

5.10. Validation in competitive media

To evaluate the potential of sensing material M3 for detecting varying concentrations of MPT64 in more realistic conditions, the culture medium used for storing *Mycobacterium tuberculosis* samples was tested. This culture medium is specifically designed to allow the growth of only those bacteria belonging to the genus *Mycobacteria*. Various concentrations of the culture medium were diluted in hybridization buffer, with each concentration tested in triplicate in a final volume of 1 mL. Following incubation at 25°C for 60 minutes, the release of rhodamine B was measured by analyzing the fluorescence emission at 575 nm ($\lambda_{\text{exc}} = 555 \text{ nm}$).

5.11. MPT64 detection in patient samples

In the final stage of the study, the nanodevice's performance was evaluated using human sputum samples and compared to the reference method, RT-qPCR. Samples were collected from patients suspected of having a TB infection at the Hospital Universitari i Politècnic La Fe in Valencia, following approval from the relevant ethics committees. To ensure privacy, patient data were anonymized. The samples were cultivated in the previously mentioned culture medium for at least 24 hours before testing.

For the assessment of M3, samples were tested in duplicate. Each M3 support was immersed in 950 μL of PBS, followed by the addition of 50 μL of the cultivated sample (5%), resulting in a final volume of 1 mL per vial. As with previous experiments, the release of rhodamine B was measured by fluorescence after 60 minutes ($\lambda_{\text{exc}} = 555 \text{ nm}$).

6. REFERENCES

1. Bharti, A., Verma, Y., Dubey, A., Swamy, M., & Singh, A. P. (2022). Prospects and application of nanotechnology for diagnosis of tuberculosis in livestock: A review. *Indian Journal of Animal Research*, 56(10). <https://doi.org/10.18805/IJAR.B-3841>
2. Beviere, M., Reissier, S., Penven, M., Dejoies, L., Guerin, F., Cattoir, V., & Piau, C. (2023). The role of next-generation sequencing (NGS) in the management of tuberculosis: Practical review for implementation in routine. *Pathogens*, 12(8). <https://doi.org/10.3390/pathogens12080978>
3. Borrebaeck, C. A. K. (2000). Antibodies in diagnostics - From immunoassays to protein chips. *Immunology Today*, 21(8), 364–370. [https://doi.org/10.1016/S0167-5699\(00\)01683-2](https://doi.org/10.1016/S0167-5699(00)01683-2)
4. Caballos, I., Aranda, M. N., López-Palacios, A., Pla, L., Santiago-Felipe, S., Hernández-Montoto, A., Tormo-Mas, M. Á., Pemán, J., Gómez-Ruiz, M. D., Calabuig, E., Sánchez-Sendra, B., Francés-Gómez, C., Geller, R., Aznar, E., & Martínez-Mañez, R. (2023). Aptamer-Capped Nanoporous Anodic Alumina for SARS-CoV-2 Spike Protein Detection. *Advanced Materials Technologies*, 8(11). <https://doi.org/10.1002/admt.202201913>
5. Cao, X. J., Li, Y. P., Wang, J. Y., Zhou, J., & Guo, X. G. (2021). MPT64 assays for the rapid detection of *Mycobacterium tuberculosis*. *BMC Infectious Diseases*, 21(1). <https://doi.org/10.1186/s12879-021-06022-w>
6. Chai, Q., Zhang, Y., & Liu, C. H. (2018). *Mycobacterium tuberculosis*: An adaptable pathogen associated with multiple human diseases. *Frontiers in Cellular and Infection Microbiology*, 8(May). <https://doi.org/10.3389/fcimb.2018.00158>

7. Chopra, H., Mohanta, Y. K., Rauta, P. R., Ahmed, R., Mahanta, S., Mishra, P. K., Panda, P., Rabaan, A. A., Alshehri, A. A., Othman, B., Alshahrani, M. A., Alqahtani, A. S., al Basha, B. A., & Dhama, K. (2023). An insight into advances in developing nanotechnology-based therapeutics, drug delivery, diagnostics and vaccines: Multidimensional applications in tuberculosis disease management. *Pharmaceuticals*, 16(4). <https://doi.org/10.3390/ph16040581>

8. Coleman, M., Martinez, L., Theron, G., Wood, R., & Marais, B. (2022). *Mycobacterium tuberculosis* transmission in high-incidence settings—New paradigms and insights. *Pathogens*, 11(11). <https://doi.org/10.3390/pathogens11111228>

9. Dahiya, B., Khan, A., Mor, P., Kamra, E., Singh, N., Gupta, K. B., Sheoran, A., Sreenivas, V., & Mehta, P. K. (2019). Detection of *Mycobacterium tuberculosis* lipoarabinomannan and CFP-10 (Rv3874) from urinary extracellular vesicles of tuberculosis patients by immuno-PCR applicable to this manuscript. *Pathogens and Disease*, 77(5). <https://doi.org/10.1093/femspd/ftz049>

10. Daniel, T. M. (2018). The bioarchaeology of tuberculosis: A global view on a reemerging disease. *The American Journal of Tropical Medicine and Hygiene*, 73(3). <https://doi.org/10.4269/ajtmh.2005.73.649>

11. Gao, S., Guisán, J. M., & Rocha-Martin, J. (2022). Oriented immobilization of antibodies onto sensing platforms: A critical review. *Analytica Chimica Acta*, 1189. <https://doi.org/10.1016/j.aca.2021.338907>

12. Grobbel, H. P., Merker, M., Köhler, N., Andres, S., Hoffmann, H., Heyckendorf, J., Reimann, M., Barilar, I., Dreyer, V., Hillemann, D., Kalsdorf, B., Kohl, T. A., Sanchez Carballo, P., Schaub, D., Todt, K., Utpatel, C., Maurer, F. P., Lange, C., & Niemann, S. (2021). Design of multidrug-resistant tuberculosis treatment regimens based on DNA sequencing. *Clinical Infectious Diseases*, 73(7). <https://doi.org/10.1093/cid/ciab359>

13. Grotz, E., Tateosian, N., Amiano, N., Cagel, M., Bernabeu, E., Chiappetta, D. A., & Moretton, M. A. (2018). Nanotechnology in tuberculosis: State of the art and the

challenges ahead. *Pharmaceutical Research*, 35(11). <https://doi.org/10.1007/s11095-018-2497-z>

14. Gu, W., Miller, S., & Chiu, C. Y. (2019). Clinical Metagenomic Next-Generation Sequencing for Pathogen Detection. *Annual Review of Pathology: Mechanisms of Disease*, 14. <https://doi.org/10.1146/annurev-pathmechdis-012418-012751>

15. Inoue, M., Tang, W. Y., Wee, S. Y., & Barkham, T. (2011). Audit and improve! Evaluation of a real-time probe-based PCR assay with internal control for the direct detection of *Mycobacterium tuberculosis* complex. *European Journal of Clinical Microbiology and Infectious Diseases*, 30(1). <https://doi.org/10.1007/s10096-010-1059-z>

16. Ito, K. (2013). Tuberculosis in the elderly. *Japanese Journal of Chest Diseases*, 72(5). <https://doi.org/10.5505/solunum.2012.17894>

17. Kamra, E., Prasad, T., Rais, A., Dahiya, B., Sheoran, A., Soni, A., Sharma, S., & Mehta, P. K. (2023). Diagnosis of genitourinary tuberculosis: detection of mycobacterial lipoarabinomannan and MPT-64 biomarkers within urine extracellular vesicles by nano-based immuno-PCR assay. *Scientific Reports*, 13(1). <https://doi.org/10.1038/s41598-023-38740-3>

18. Kanabalan, R. D., Lee, L. J., Lee, T. Y., Chong, P. P., Hassan, L., Ismail, R., & Chin, V. K. (2021). Human tuberculosis and *Mycobacterium tuberculosis* complex: A review on genetic diversity, pathogenesis, and omics approaches in host biomarker discovery. *Microbiological Research*, 246. <https://doi.org/10.1016/j.micres.2020.126674>

19. Kim, J., Lee, J., Lee, K. I., Park, T. J., Kim, H. J., & Lee, J. (2013). Rapid monitoring of CFP-10 during culture of *Mycobacterium tuberculosis* by using a magnetophoretic immunoassay. *Sensors and Actuators, B: Chemical*, 177. <https://doi.org/10.1016/j.snb.2012.11.011>

20. Koch, A., & Mizrahi, V. (2018). *Mycobacterium tuberculosis*. *Trends in Microbiology*, 26(6). <https://doi.org/10.1016/j.tim.2018.02.012>

21. Lipman, N. S., Jackson, L. R., Trudel, L. J., & Weis-Garcia, F. (2005). Monoclonal versus polyclonal antibodies: Distinguishing characteristics, applications, and information resources. *ILAR Journal*, 46(3). <https://doi.org/10.1093/ilar.46.3.258>
22. Natarajan, A., Beena, P. M., Devnikar, A. V., & Mali, S. (2020). A systemic review on tuberculosis. *Indian Journal of Tuberculosis*, 67(3). <https://doi.org/10.1016/j.ijtb.2020.02.005>
23. Nunn, P. P., Elliott, A. M., & McAdam, K. P. W. J. (1994). Impact of human immunodeficiency virus on tuberculosis in developing countries. *Thorax*, 49(5). <https://doi.org/10.1136/thx.49.5.511>
24. Operario, D. J., Koepfel, A. F., Turner, S. D., Bao, Y., Pholwat, S., Banu, S., Foongladda, S., Mpagama, S., Gratz, J., Ogarkov, O., Zhadova, S., Heysell, S. K., & Houpt, E. R. (2017). Prevalence and extent of heteroresistance by next-generation sequencing of multidrug-resistant tuberculosis. *PLoS ONE*, 12(5). <https://doi.org/10.1371/journal.pone.0176522>
25. Orgeur, M., Sous, C., Madacki, J., & Brosch, R. (2024). Evolution and emergence of *Mycobacterium tuberculosis*. *FEMS Microbiology Reviews*, 48(2). <https://doi.org/10.1093/femsre/fuae006>
26. Rene, & Dubos, J. (1953). The White Plague. Tuberculosis, Man and Society. *Southern Medical Journal*, 46(8). <https://doi.org/10.1097/00007611-195308000-00035>
27. Ribes, À., Xifré-Pérez, E., Aznar, E., Sancenón, F., Pardo, T., Marsal, L. F., & Martínez-Máñez, R. (2016). Molecular gated nanoporous anodic alumina for the detection of cocaine. *Scientific Reports*, 6. <https://doi.org/10.1038/srep38649>
28. Riley, R. L. (1974). Airborne infection. *The American Journal of Medicine*, 57(3). [https://doi.org/10.1016/0002-9343\(74\)90140-5](https://doi.org/10.1016/0002-9343(74)90140-5)
29. Sakamoto, K. (2012). The pathology of *Mycobacterium tuberculosis* infection. *Veterinary Pathology*, 49(3). <https://doi.org/10.1177/0300985811429313>
30. Sannigrahi, S., Arumugasamy, S. K., Mathiyarasu, J., & K, S. (2020). Magnetosome-anti-Salmonella antibody complex based biosensor for the detection of

Salmonella typhimurium. *Materials Science and Engineering C*, 114. <https://doi.org/10.1016/j.msec.2020.111071>

31. Shamsuddin, S. H., Gibson, T. D., Tomlinson, D. C., McPherson, M. J., Jayne, D. G., & Millner, P. A. (2021). Reagentless Affimer- and antibody-based impedimetric biosensors for CEA-detection using a novel non-conducting polymer. *Biosensors and Bioelectronics*, 178. <https://doi.org/10.1016/j.bios.2021.113013>

32. Tang, Y., Wang, H., Xiang, J., Chen, Y., He, W., Deng, N., & Yang, H. (2010). A sensitive immunosorbent bio-barcode assay combining PCR with icELISA for detection of gonyautoxin 2/3. *Analytica Chimica Acta*, 657(2). <https://doi.org/10.1016/j.aca.2009.10.045>

33. Thaiss, W. M., Thaiss, C. C., & Thaiss, C. A. (2012). Recent developments in the epidemiology and management of tuberculosis - new solutions to old problems? *Infection and Drug Resistance*, 5(1). <https://doi.org/10.2147/idr.s27604>

34. Vikholm, I., & Albers, W. M. (1998). Oriented immobilization of antibodies for immunosensing. *Langmuir*, 14(14). <https://doi.org/10.1021/la971412x>

35. Wayne, L. G. (1982). Microbiology of tubercle bacilli. *American Review of Respiratory Disease*, 125(3 II). <https://doi.org/10.1164/arrd.1982.125.3P2.31>

36. World Health Organization. (2023). *Global tuberculosis report 2023*.

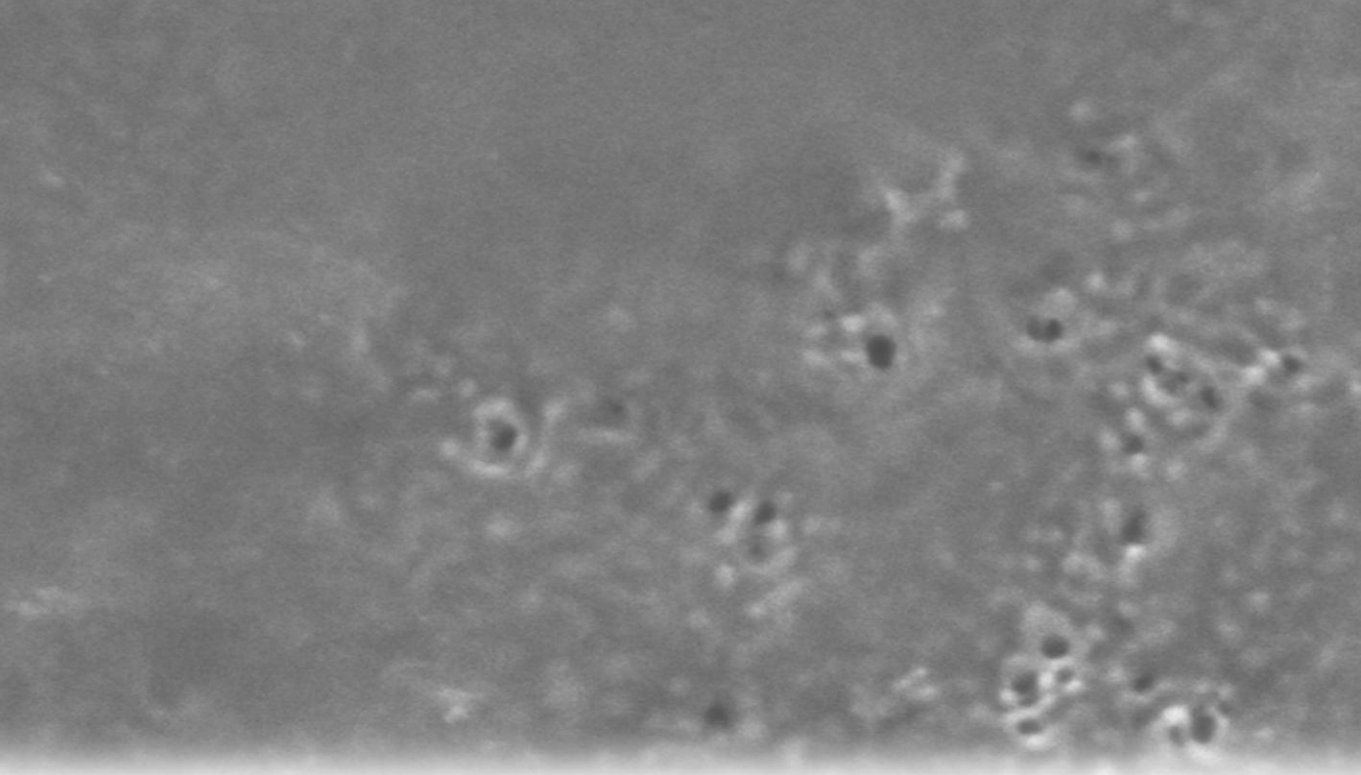
37. Zhu, C., Liu, J., Ling, Y., Yang, H., Liu, Z., Zheng, R., Qin, L., & Hu, Z. (2012). Evaluation of the clinical value of ELISA based on MPT64 antibody aptamer for serological diagnosis of pulmonary tuberculosis. *BMC Infectious Diseases*, 12. <https://doi.org/10.1186/1471-2334-12-96>

38. Ziskind, B., & Halioua, B. (2007). Tuberculosis in ancient egypt. *Revue Des Maladies Respiratoires*, 24(10). [https://doi.org/10.1016/S0761-8425\(07\)78506-6](https://doi.org/10.1016/S0761-8425(07)78506-6)

Acknowledgements

We thank PID2021-126304OB-C41 (to R. M.-M.) from the Ministerio de Ciencia, Innovación y Universidades and AEI/10.13039/501100011033 (the former co-financed by

the NextGenerationEU Fund and the latter by the European Regional Development Fund), and CIPROM/2021/007 (to R. M.-M.) from the Generalitat Valenciana. G. R. acknowledges support from the CSIC PTI Salud Global (through the NextGenerationEU Fund, regulation 2020/2094) and R. M.-M. from the CIBER, Instituto de Salud Carlos III (group CB07/01/2012). I. C. thanks the Instituto de Salud Carlos III for her predoctoral fellowship (IFI21/00008).



Chapter III | Aptamer-Capped Nanoporous Anodic Alumina for SARS-CoV-2 Spike Protein Detection

**Cover: FESEM image of capped NAA (self-produced image)*

Aptamer-Capped Nanoporous Anodic Alumina for SARS-CoV-2 Spike Protein Detection

Isabel Caballos^{a,b,c}, M. Nieves Aranda^{a,b}, Alba López-Palacios^{a,b,c}, Luis Pla^{a,b,c}, Sara Santiago-Felipe^{a,b,c}, Andy Hernández-Montoto^{a,b,c}, María Ángeles Tormo-Mas^{d}, Javier Pemán^e, María Dolores Gómez-Ruiz^e, Eva Calabuig^e, Ron Geller^f, Beatriz Sánchez-Sendra^e, Clara Francés-Gómez^e, Elena Aznar^{a,b,c*}, and Ramón Martínez-Máñez^{a,b,c*}*

^a Instituto Interuniversitario de Investigación de Reconocimiento Molecular y Desarrollo Tecnológico, Universitat Politècnica de València, Universitat de València, Camino de Vera s/n, 46022, Valencia, Spain.

^b Unidad Mixta de Investigación en Nanomedicina y Sensores. Universitat Politècnica de València, Instituto de Investigación Sanitaria La Fe (IISLAFE), Avenida Fernando Abril Martorell, 106, 46026, Valencia, Spain

^c CIBER de Bioingeniería, Biomateriales y Nanomedicina (CIBER-BBN), Spain.

^d Grupo Infección Grave, Hospital Universitari i Politècnic La Fe, Instituto de Investigación Sanitaria La Fe (IISLAFE), Avenida Fernando Abril Martorell, 106, 46026, Valencia, Spain.

^e Unidad de Enfermedades Infecciosas, Hospital Politècnic i Universitari La Fe. Instituto de Investigación Sanitaria La Fe (IISLAFE), Avenida Fernando Abril Martorell, 106, 46026, Valencia, Spain

^f I2SysBio, Universidad de Valencia-CSIC. Calle del Catedrático Agustín Escardino 9, 46980, Paterna, Spain.

*Corresponding authors: elazgi@upvnet.upv.es, rmaez@qim.upv.es, tormo_man@iislafe.es.

Published online: March 20, 2023

(Reprinted with permission from ACS Nano, 2024, November 6. © American Chemical Society 2023)

1. ABSTRACT

The COVID-19 pandemic, which began in 2019, has highlighted the importance of testing and tracking infected individuals as a means of mitigating the spread of the virus. In this context, the development of sensitive and rapid methods for the detection of SARS-CoV-2, the virus responsible for COVID-19, is crucial. Here, a biosensor based on oligonucleotide-gated nanomaterials for the specific detection of SARS-CoV-2 spike protein is presented. The sensing system consists of a nanoporous anodic alumina disk loaded with the fluorescent indicator rhodamine B and capped with a DNA aptamer that selectively binds the SARS-CoV-2 spike protein. The system is initially evaluated using pseudotype virus systems based on vesicular stomatitis virus carrying different SARS-CoV-2 S-proteins on their surface. When the pseudotype virus is present, the cap of the solid is selectively removed, triggering the release of the dye from the pore voids to the medium. The nanodevice demonstrated its ability to detect pseudotype virus concentrations as low as $7.5 \cdot 10^3$ PFU mL⁻¹. In addition, the nanodevice is tested on nasopharyngeal samples from individuals suspected of having COVID-19.

- KEYWORDS: SARS-CoV-2, aptamer, gated material, optical sensor, nanomaterials

2. INTRODUCTION

Coronavirus disease 2019 (COVID-19) caused by SARS-CoV-2 coronavirus has rapidly spread all over the world resulting in a global pandemic, counting with more than 613 million SARS-CoV-2-infected confirmed cases and more than 6500000 reported deaths worldwide until September 2022 (Johns Hopkins University & Medicine, 2022). The main symptoms caused by this positive-stranded RNA virus are similar to acute respiratory infection, like cough, fever, loss of taste and smell and difficulty breathing. The most exposed population are elderly people, adolescents, infants, and people with the compromised immune system (Das et al., 2020). The high capacity of dissemination of the

virus requires to identify the presence of SARS-CoV-2 in an accurate and rapid way. This is desirable not only for the identification of infected patients but also for the detection of asymptomatic and presymptomatic people (Ji et al., 2020; Hashemi et al. 2021). To manage with this global concern, it is necessary to provide the society with a wide collection of different systems that could afford the massive demand of tests releasing the appropriate information. Given the global impact of COVID-19, there is a need for the development of highly accurate approaches for the rapid identification of biomarkers of SARS-CoV-2 infection in patient samples, including ribonucleic acid (RNA), antigens, antibodies, or directly the whole virus.

The real-time quantitative reverse transcription polymerase chain reaction (RT-qPCR) is currently the standard test to detect this virus. This approach often requires laboratory facilities, trained personnel, expensive instrumentation, and the assay takes hours to provide a result. In addition, RT-qPCR is not always available in underdeveloped and developing countries where the vast population lives in the backcountry (Guglielmi et al., 2020). Besides, considering the increasing infection rate, PCR methods are not sufficient to cover the current testing demand. Another commonly used approach is serological testing, which is not recommended when the viral load is very low, for example in the early stages of the infection, since the serological antibodies will not be present until a couple of weeks after the initial viral infection (Huang et al., 2021). In contrast, antigen detection systems, which rely on the identification of a specific immunogenic component of a pathogen, typically a polysaccharide molecule or a protein, as a means of detecting the presence of the pathogen, have gained general approval thanks to their detection speed, simplicity, low cost, and accuracy. The drawback of the technique is that current sensitivity levels are still poor leading to a high variability and low performance depending on the manufactured brand. Antigen detection systems are usually used as screening tests for example in large groups or as a previous exploratory test before the realization of a more accurate molecular and/or serologic assay (Pavia et al., 2021). Based on the above, it can be concluded that there is still room to develop a test that combines

the sensitivity and accuracy of the PCR methods and the low-priced and rapid antigen detection procedures in order to deal with the spread of the virus and control potential new outbreaks (Liu et al., 2020; Bhalla et al., 2020).

Recently, biosensors targeting pathogens or infection biomarkers based on nanotechnology have become more and more popular owing to their capacity to supply accurate, sensitive, and reliable results, revolutionizing the healthcare industry. Multiple reported designs have demonstrated that it is possible to obtain numerous benefits from the combination of the usefulness and versatility of nanomaterials with the recognition properties of sensitive and highly selective biomolecules (Bellan et al., 2011). On this point, some new approaches have been extensively applied in the development of sensing systems with a huge variety of applications, which enhanced the sensitivity of already available detection systems. Among the great variety of nanomaterials available to develop sensitive biosensors, nanoporous anodic alumina (NAA) offers easy modification of the surface, high loading capacity and its production can be easily arranged by standard production techniques that are cost-competitive (Ribes et al., 2017). In the last years, NAA have been used to develop gated nanomaterials for biosensing applications. In those systems, only the target pathogen or biomolecule induces the release of the entrapped reporter (Ribes et al., 2016; Pla et al., 2020 and Ahmad et al., 2019). For example, we have previously reported oligonucleotide-capped mesoporous supports for the detection of *Staphylococcus aureus* (Pla et al., 2020) and *Candida auris* DNA in blood culture specimens from infected individuals, bringing gated materials into clinical settings and showing their enormous potential in clinical settings (Pla et al., 2021).

Among the possible gating mechanism that can be implemented on porous supports to configure a functional sensory material, aptamers have demonstrated excellent performances. Aptamers consist of small peptide molecules or more commonly oligonucleotide sequences having high specific binding affinity for their target molecules leading a precise and accurate detection. Aptamers can be easily implemented to any

specific design through surface activation or modification by chemical treatment using appropriate linkers and coupling agents (Iliuk et al., 2011 and Seok Kim et al., 2016). As a consequence, such small proteins or oligonucleotides have been widely used to develop sensing systems known as aptasensors. Due to their high stability, purity, and reversibility under harsh environmental conditions with vast availability of target specific linkers, such devices are being now used as novel diagnostics devices (Kumar et al, 2020).

Biosensors based on aptamers have been demonstrated to be a highly effective analytical tool for the rapid diagnosis of infections, with high sensitivity and specificity. In the case of SARS-CoV-2 detection, Zhang et al. (Liu et al., 2020) developed a system for the detection of SARS-CoV-2 that utilizes aptamer probes that bind to a specific protein target, bringing together a ligation DNA region in close proximity and initiating ligation-dependent qPCR amplification. Another example has been reported by Sandall et al. (Farrow et al., 2020) who described the development of a system based on the use of an intrinsic silicon thin film transistor functionalized with aptamers that specifically bind to the SARS-CoV-2 spike protein. Also, several examples using nanomaterials and aptamers to recognize SARS-CoV-2 targets have been described. For example, Tabrizi and coworkers developed a photoelectrochemical aptasensor based on graphitic carbon nitride combined with CdS quantum dots and chitosan to obtain a nanocomposite which is further functionalized with a RBD spike domain sensitive aptamer (Amouzadeh Tabrizi et al., 2021). In another approach, Ray et al. took advantage of distance-dependent nanoparticle surface energy transfer phenomena to detect spike protein by fluorescence quenching induced thanks to aptamer-functionalized gold nanostars (Pramanik et al., 2021).

Taking into account literature reports, it can be envisioned the potential of combining the excellent performance of gated materials and aptamers to configure a functional nanomaterial for SARS-COV-2 infection biomarkers recognition. Based on this premise, herein we report a method for highly ultrasensitive and specific detection of

SARS-CoV-2-associated antigens, in particular the spike protein receptor-binding domain, based on aptamer-capped gated NAA. In our design, NAA supports were first loaded by diffusion with the fluorescent reporter dye rhodamine B, followed by the capping with an aptamer that specifically binds with the spike protein of SARS-CoV-2 virus. As a capping system the aptamer described by Yang et al. (Song et al., 2020) was selected due to its suitable properties like the absence of secondary structures formation, molecular weight, and target affinity. Once the system is arranged, the capping aptamer inhibits dye release blocking the pores. Only in the presence of SARS-CoV-2 spike protein, the capping aptamer is displaced (thanks to the specific hybridization between aptamer and protein), uncapping the pores and allowing dye release. The capped sensing aptasensor was also tested using pseudotype virus systems based on vesicular stomatitis virus (VSV) carrying different SARS-CoV-2 S-proteins on the surface. Finally, the system has been tested in patient samples. The prepared materials are found to respond rapidly, allowing accurate detection in buffer and nasopharyngeal samples in just one hour.

3. RESULTS AND DISCUSSION

3.1. Synthesis and characterization of gated NAA

In our proposed system, pores of NAA were filled with the fluorescent reporter rhodamine B and the outer surface was chemically modified by the attachment of (3-triethoxysilyl)propylisocyanate, to give support S1. Then, two oligonucleotides NH₂-(CH₂)₆-5'-AAA AAA CCC CCC-3' (O1) and 5'-TTT TTG GGG GGC AGC ACC GAC CTT GTG CTT TGG GAG TGC TGG TCC AAG GGC GTT AAT GGA CAG GGG GGT TTT T-3'(O2) were used to obtain a capped nanomaterial through strong covalent and hydrogen bonding interactions. First, O1, which is designed to recognize and hybridize with the sequence 3'-TTT TGG GGG G-5' included in O2, was covalently anchored by the formation of urea bonds with the isocyanate moieties present in S1 to obtain support S2. In a second step, O2, which contains the specific aptamer sequence to recognize SARS-CoV-2 spike protein

(i.e. 5'-CAG CAC CGA CCT TGT GCT TTG GGA GTG CTG GTC CAA GGG CGT TAA TGG ACA-3'), was employed to block the pores of S2 by hybridization with O1, obtaining the final sensing gated nanomaterial S3 (see Experimental Section for further details). The dsDNA O1-O2 ensemble on the external surface of the inorganic scaffold is expected to be bulky enough to block pores and inhibit dye delivery. In contrast, in the presence of the target spike SARS-CoV-2, the capping aptamer will recognize the SARS-CoV-2 spike protein. This would lead to a displacement of the O2 sequence from the surface of the functional material, resulting in cargo release (Figure1).

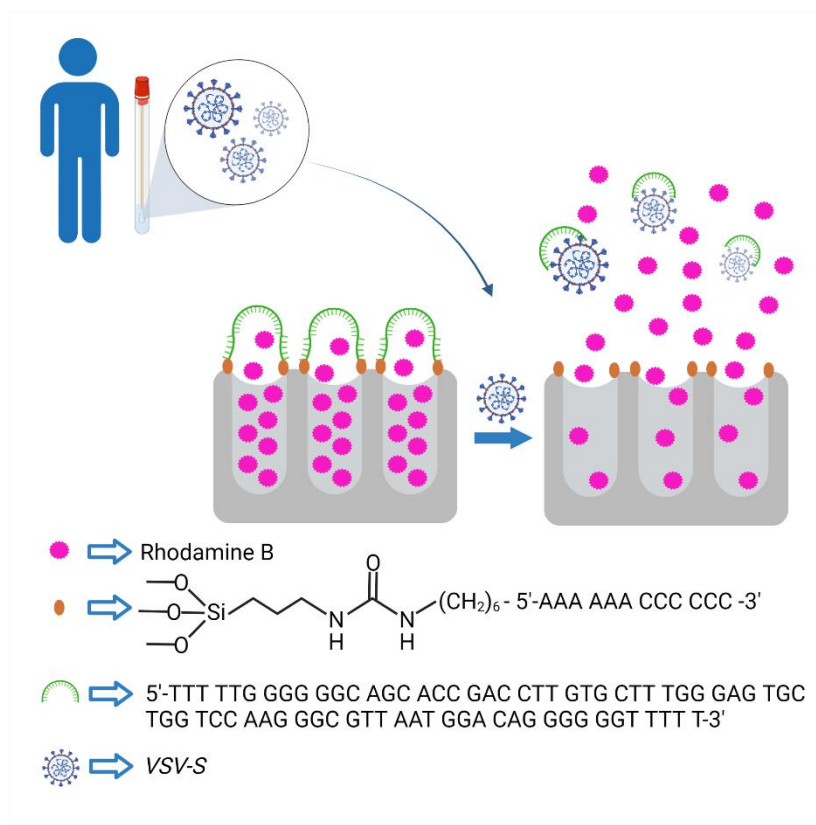


Figure 1. Scheme of the gated NAA material S3 selectiveness for the recognition of SARS-CoV-2 spike protein. In the absence of the virus protein, pores are blocked while

the presence of SARS-CoV-2 S protein induced aptamer displacement and delivery of the entrapped dye.

Raw NAA material, S1, S2 and S3 were characterized by FESEM and EDX analyses. Commercially available NAA supports are composed of anodic aluminum oxide films grown on a 0.1 mm thick aluminum layer with a pore density of $9 \cdot 10^{11} \text{ cm}^{-2}$. Pore entrance has a funnel-like shape which progressively shifts from a larger size (20-30 nm) at the top of the funnel to a 5 nm size at the end. The pores are as long as 10 μm . As material was cut in discs of 2 mm of diameter. The appearance of the initial material was a silver small disc while final S3 support acquired pink color (due to the loading of the dye) as depicted in the insets of Figure 2. Representative FESEM images of the starting NAA scaffold showed the porous structure described above (Figure 2A). Besides, images of S3 evidenced the presence of a dense capping layer on the top of the pores (Figure 2B) confirming a compact pore capping.

Organic content in S2 and S3 was analyzed by energy-dispersive X-ray spectroscopy (Table). As expected, high carbon content (C/Al 4.771) was found in solid S1, due to the high loading capacity of NAA material. Solid S2 showed a decrease of carbon content due to the experimental conditions for O1 attachment, which do not prevent a partial cargo release (C/Al 0.353). Finally, solid S3 maintained a similar organic matter content. Likewise, a higher P/Al and N/Al content from the capping oligonucleotide in the final material was confirmed.

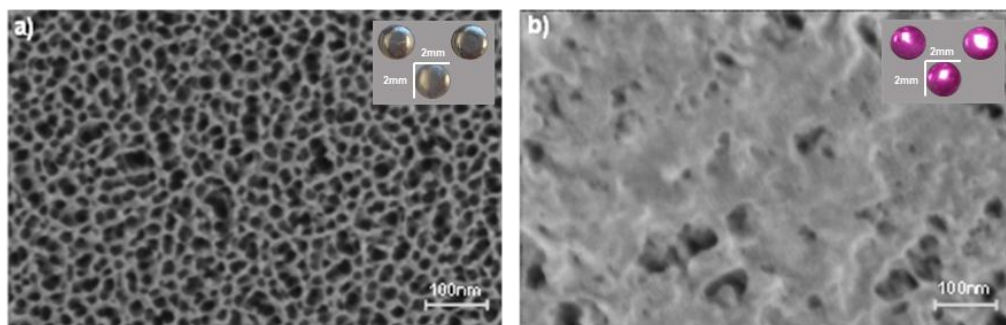


Figure 2. FESEM images of NAA support (a) and solid **S3** (b). Insets: photographs of the corresponding solids.

Table 1. Atomic elements relation in the different prepared solids.

	C/Al	N/Al	P/Al
S0	0.16 ± 0.00	-	-
S1	4.77 ± 0.10	0.74 ± 0.02	-
S2	0.35 ± 0.00	0.05 ± 0.00	0.00 ± 0.00
S3	0.35 ± 0.01	0.06 ± 0.00	0.01 ± 0.01

Maximum amount of rhodamine B that can be released from the final material to the solution was also quantified by extraction experiments. As a result, a deliverable rhodamine B content was calculated to be ca. $0.33 \mu\text{g mL}^{-1}$.

3.2. Release assays

To demonstrate the opening mechanism of the material in a first approach, the controlled release from the material to the solution was studied in the presence and absence of the purified SARS-CoV-2 spike protein, which constitutes the target of the capping aptamer. To carry out this study, two independent gated supports of the S3 solid were separately submerged in hybridization buffer. Then, $100 \mu\text{L}$ of purified SARS-CoV-2 spike protein ($1 \text{ ng } \mu\text{L}^{-1}$) were added to the solution and $100 \mu\text{L}$ of TRIS buffer was added

to the other one. To quantify the amount of the delivered dye from the pores to the aqueous phase, the fluorescence of the supernatant solution was measured at predetermined times. Figure 3A shows the rhodamine B delivery profile from solid S3 in the absence and presence of the SARS-CoV-2 spike protein. When S3 is placed only in hybridization buffer it delivers a very low amount of dye (less than 10% of the maximum dye delivered), which indicates a tight pore closure (Figure 3A, curve 1). On the contrary, when S3 is placed in a solution where the SARS-CoV-2 spike is present, a much larger amount of rhodamine B is released (10-fold at 60 min, Figure 3A, curve 2).

In a next step, we validated the system using a model closer to clinical samples, demonstrating that the system can recognize a complete virus that expresses the target protein of SARS-CoV-2 on its surface. Research using pathogens classified as high biosafety levels, such as SARS-CoV-2, is complicated by the inherent difficulty of working under biosafety level 3 conditions. Hence, model systems are often preferred for many applications. Pseudotype virus systems provide such models. These are based on the use of a low biosafety level virus in which the viral envelope protein is deleted from the genome and replaced with that of a pathogenic virus, either by supplying it in trans or by encoding it within the viral genome. These systems have proved valuable for assaying entry mechanisms of diverse viruses, evaluation of neutralizing antibodies levels, discovery of antivirals, and as vaccines (Millet et al., 2019). Moreover, as the pseudotype virus encodes a functional entry glycoprotein of a virus of interest, these can be used to safely and rapidly evaluate detection systems.

Based on the above, to simulate the presence of the virus in the sample we used a pseudotype virus system as a model system based on vesicular stomatitis virus (VSV) carrying different SARS-CoV-2 S-proteins on the surface (VSV-S). These VSV pseudotype viruses have been shown to enter cells in an analogous manner to SARS-CoV-2 but facilitate the evaluation of the system (Case et al., 2020). We employed both a replication competent VSV encoding the Wuhan spike protein in place of its glycoprotein G (VSV-S),

which grows to high titer, and replication incompetent VSV where the spike protein from different variants was supplied in trans (see Experimental Section for further details). The viruses were named depending on the SARS-CoV-2 variant genome they were carrying as VSV-Alpha, VSV-Beta, VSV-Gamma and VSV-Delta.

The behavior of two independent S3 materials in hybridization buffer were studied in the presence of 100 μL of VSV-S pseudotype or VSV (without S-protein) and the amount of rhodamine B released to the solution was recorded by measuring the emission band at different times at 575 nm ($\lambda_{\text{exc}} = 555 \text{ nm}$) (Figure 3b). It was observed that SARS-CoV-2 spike protein (purified or attached to the pseudotyped virus) uncapped the pores and induce cargo delivery as represented in Figure 3.

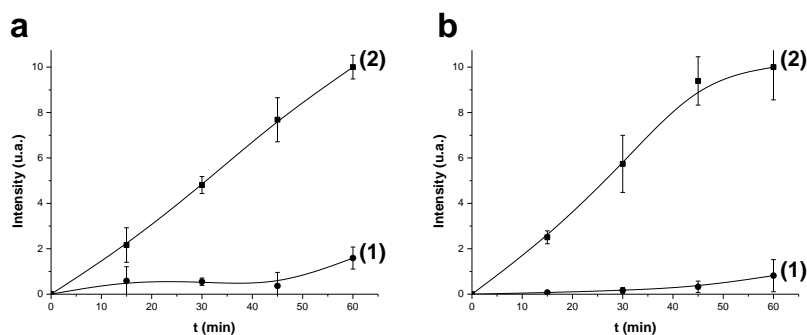


Figure 3. Rhodamine B delivery from the pores of material S3 in TRIS buffer (pH 7.5) at different periods of time. Plot (a) indicates dye release in the lack of any stimulus (1) and in presence of target purified spike protein at a concentration of $1 \text{ ng } \mu\text{L}^{-1}$ (2). Plot (b) illustrates cargo delivery in the presence of VSV-S ($2.5 \cdot 10^4 \text{ PFU mL}^{-1}$) (2) and in presence of VSV without any spike on its surface ($2.5 \cdot 10^4 \text{ PFU mL}^{-1}$) (1).

3.3. Sensitivity and specificity studies

The sensitivity of the method was determined by performing experiments with S3 at different concentrations of VSV-S and studying the generated response. For that, 11 independent S3 supports were immersed in hybridization buffer, and 100 μL of virus

suspension dilutions were added to each material, reaching a range of final concentrations between 10^3 and $5 \cdot 10^5$ PFU mL^{-1} . After 60 min, the total amount of rhodamine B diffused to the aqueous phase was measured by fluorescence. Results showed that delivered dye was directly related to the VSV-S concentration (Figure 4). Remarkably, a LOD in the range of those usually reported by instrumental techniques used for SARS-CoV-2 detection (see Table S1) was observed; nevertheless, this method is faster, simpler, and do not require specialized instrumentation or database. In addition to this, it can be highlighted its capacity of being multiplexed, using the same technology for future relevant pathogens just adjusting the recognizing agent (Pfefferle et al., 2020 and Mak et al., 2020).

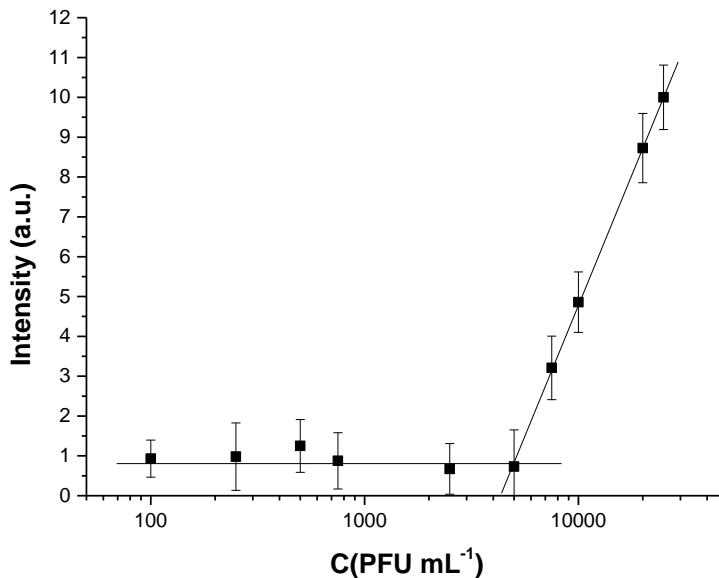
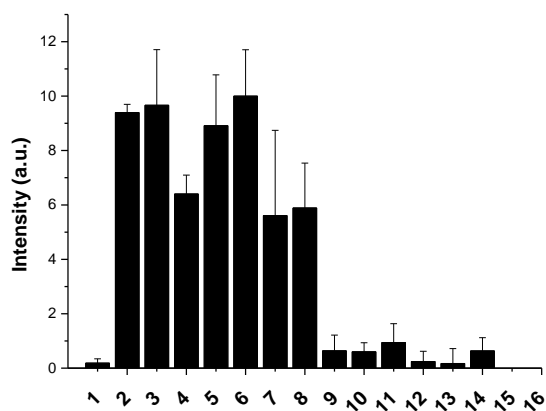


Figure 4. Dye release from solid S3 in the presence of different amounts of VSV-S in TRIS buffer.

In a step forward, the selectivity of S3 to detect the spike protein of SARS-CoV-2 was tested (Figure 5). In these experiments, the response of S3 was assessed in the

presence of 100 μL of the purified spike protein (1 ng mL^{-1}) and eight drugs in 900 μL of hybridization buffer. These drugs are commonly found in samples since they are commonly prescribed for the treatment of common illnesses or chronic diseases. As it can be observed, only the presence of the SARS-CoV-2 spike protein (or mixtures SARS-CoV-2 spike protein + drug) were able to trigger a notable rhodamine B release while the presence of the drugs alone induced poor uncapping and cargo delivery, indicating a high selective response of S3.



1	Blank	8	SP + Tiotropium $0,5 \text{ mg mL}^{-1}$
2	Spike protein (SP)	9	Salbutamol $0,1 \text{ mg mL}^{-1}$
3	SP + Salbutamol $0,1 \text{ mg mL}^{-1}$	10	Acetaminophen $0,1 \text{ mg mL}^{-1}$
4	SP + Acetaminophen $0,1 \text{ mg mL}^{-1}$	11	Acetylsalicylic acid $0,05 \text{ mg mL}^{-1}$
5	SP + Acetylsalicylic acid $0,05 \text{ mg mL}^{-1}$	12	Enoxaparin $0,1 \text{ mg mL}^{-1}$
6	SP + Enoxaparin $0,1 \text{ mg mL}^{-1}$	13	Levotyroxine $0,025 \text{ mg mL}^{-1}$
7	SP + Levotyroxine $0,025 \text{ mg mL}^{-1}$	14	Tiotropium $0,5 \text{ mg mL}^{-1}$

Figure 5. Media fluorescence intensity in the presence of drug interferences alone or in combination with the viral spike protein ($1 \text{ ng } \mu\text{L}^{-1}$) in TRIS buffer after 60 min.

3.4. Detection of VSV-S in competitive media and inoculated clinical samples

In addition, to evaluate the robustness of the system, the behavior of S3 in the presence of $100 \mu\text{L}$ of $2.5 \cdot 10^5 \text{ PFU mL}^{-1}$ of VSV-S was evaluated in $900 \mu\text{L}$ of a clinically relevant media, as it is a nasopharyngeal fluid obtained from the use of a collection swab in 5 mL of hybridization buffer (TRIS). As it is depicted in Figure 6, the presence of VSV-S also produced a selective displacement of the aptamer, pore uncapping and dye delivery in this competitive medium. In this case, although a higher residual release was observed in competitive media than in buffer the measured fluorescence in the presence of the virus was comparable to that achieved in TRIS buffer.

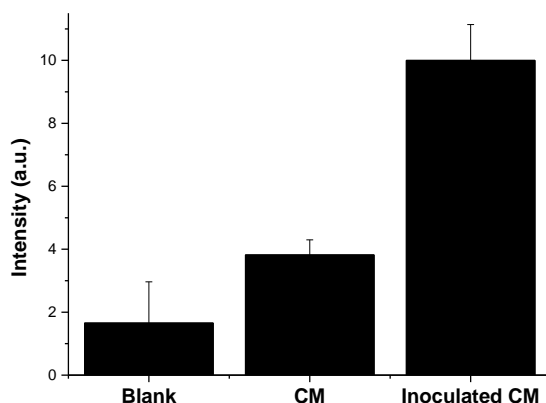


Figure 616. Delivery of rhodamine B from material S3 in TRIS (Blank) in the presence of the stimulus, in competitive media (CM) and competitive media inoculated with VSV-S (concentration: $2.5 \cdot 10^4 \text{ PFU mL}^{-1}$) after 60 minutes.

In a further attempt, a small analytical assay was performed. Taking into account the usual SARS-CoV-2 concentration in nasopharyngeal samples (an average of $7 \cdot 10^6 \text{ PFU mL}^{-1}$ per sample until the fifth day of infection and a maximum of $7.11 \cdot 10^8$ copies per swab

(Wölfel et al., 2020)), aliquots of negative nasopharyngeal samples were inoculated with different amounts of the pseudotyped virus VSV-S ($5 \cdot 10^3$ to $4 \cdot 10^4$ PFU mL⁻¹) to emulate SARS-CoV-2 infected samples. Then, 100 μ L of each sample was added to an eppendorf tube containing the S3 support and 900 μ L of hybridization buffer. After 60 min at 25 °C rhodamine B released from pores was monitored at 575 nm ($\lambda_{\text{exc}} = 555$ nm). Experimental points (Figure 7) show that the obtained signal is proportional to the concentration of VSV-S. The possibility of obtaining an approximation of the virus concentration in the samples is of interest in a clinical context, as it might allow differentiating patients with a high viral load and who may need a different treatment than others with a lower load. Moreover, preliminary studies carried out to assess the stability of aptamer-gated nanomaterials have demonstrated that the aptasensor can be stored up to 8 weeks without any changes in their sensing performance (Ribes et al., 2017).

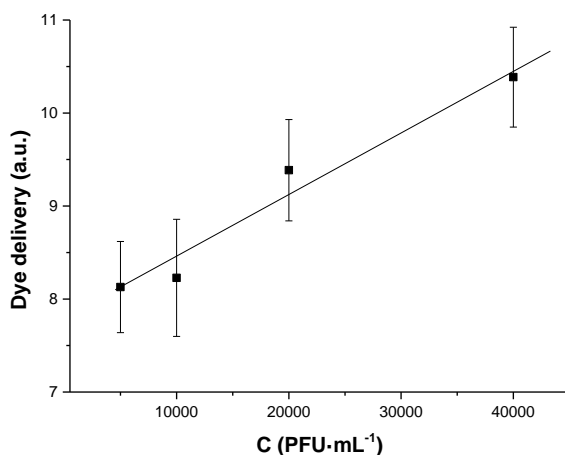


Figure 7. Dye release from solid S3 in the presence of increasing amounts of VSV-S in clinical sample.

3.5. Study of the system behavior with different S proteins from different SARS-CoV-2 variants of concern

In a step forward, the response of S3 to S protein from different SARS-CoV-2 variants of concern were studied using pseudotyped VSV carrying the different S protein variants Alpha, Beta, Gamma and Delta (i.e. VSV-Alpha, VSV-Beta, VSV-Gamma and VSV-Delta), which are the most spread in European countries until December 2021. In each experiment, S3 was submerged in a nasopharyngeal sample doped with the pseudotyped virus carrying a spike protein with the corresponding genome of the variant of concern (VSV-Alpha, VSV-Beta, VSV-Gamma and VSV-Delta). Released rhodamine B after 60 min was measured by fluorescence as in previous experiments. As can be appreciated in Figure 8, S3 responds to all studied variants, giving hope to the detection of new coming variants of the virus using S3.

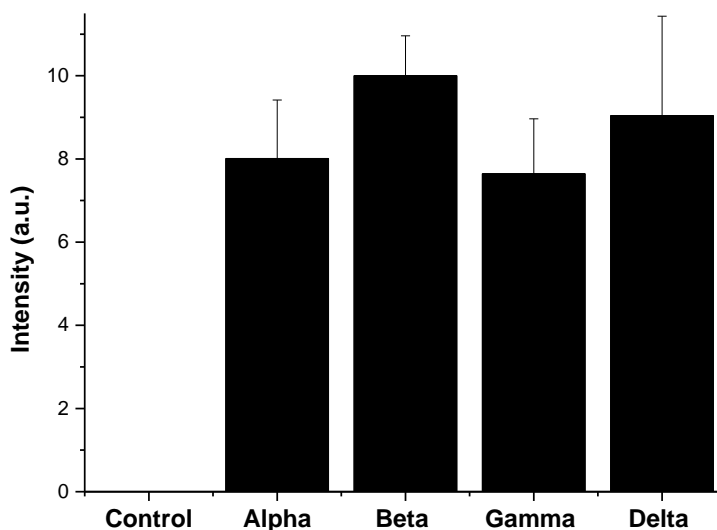


Figure 8. Media fluorescence intensity of rhodamine B in presence of VSV-Alpha, VSV-Beta, VSV-Gamma and VSV-Delta. ($2.5 \cdot 10^4$ PFU mL^{-1}). Control represents the delivery

in the nasopharyngeal sample without the stimulus after 60 minutes from the beginning of the experiment.

4. CONCLUSION

Rapid and accurate detection of SARS-CoV-2 infections is crucial for preventing new outbreaks and ensuring appropriate treatment. Therefore, the development of new approaches for the simple and rapid identification of this virus is essential in clinical practice. As demonstrated in this study, nanoporous materials can be combined with aptamers to develop a useful fluorescence-based biosensor for the detection of the SARS-CoV-2 spike protein in a competitive environment. The nanoporous anodic alumina (NAA) scaffold constitutes the biosensor, this support has been loaded with rhodamine B and capped with an aptamer specific to the SARS-CoV-2 spike protein. Upon exposure to the spike protein or SARS-CoV-2 pseudotypes, the capping aptamer is displaced, the pores open, and the fluorophore is released. The biosensor exhibits a limit of detection of 7.5×10^3 PFU mL⁻¹ in TRIS buffer and 2×10^4 PFU mL⁻¹ in nasopharyngeal samples collected in TRIS media, which is comparable to the performance of other state-of-the-art SARS-CoV-2 detection systems. In addition, the biosensor demonstrates high selectivity for the SARS-CoV-2 spike protein and is not affected by other interfering substances. The proposed method was successfully applied to the identification of SARS-CoV-2 virus pseudotypes in artificially inoculated clinical samples and nasopharyngeal samples from COVID-19 patients. It is efficient in terms of sensitivity and predictive values and is fast, simple, and portable. It can also be easily modified by incorporating different reporters and capping sequences. This approach to sensing may also provide inspiration for the development of new simple tests for point-of-care pathogen testing.

5. MATERIALS AND METHODS

5.1. General Techniques

A ZEISS Ultra 55 microscope was employed to perform Field Emission Scanning Electron Microscopy (FSEM) and Energy Dispersive X-ray spectroscopy (EDX) analyses. Measurements of fluorescence spectroscopy were carried out on a Synergy H1 microplate reader (BioTek, Winooski, VT, USA).

5.2. Reactives and reagents

(3-triethoxysilyl)propylisocyanate, acetonitrile, rhodamine B, triethylamine (TEA) and TRIS(hydroxymethyl)aminomethane (TRIS) were acquired from Sigma-Aldrich Química (Madrid, Spain). Nanoporous anodic alumina supports were commercially obtained from InRedox® (CO, USA). Oligonucleotides were purchased in Integrated DNA Technologies, Inc. (IA, USA) and used without further purification.

5.3. Oligonucleotides Design

The aptamer sequence was obtained from the literature (for additional information regarding the aptamer employed on this subject, see reference ^[23]) and were acquired from IDT by Danaher Corporation (Leuven, Belgium). The specific sequences chosen to cap the pores were O1: 5'-AAA AAA CCC CCC-3'; O2: 5'-TTT TTG GGG GGC AGC ACC GAC CTT GTG CTT TGG GAG TGC TGG TCC AAG GGC GTT AAT GGA CAG GGG GGT TTT T-3'.

5.4. Synthesis of solids

To synthesize solid S1, 25 independent NAA supports of 2 mm of diameter were submerged in a rhodamine B solution in CH₃CN (6 mg, 1.57 mM, 8 mL), which was mixed for 24 h to facilitate the loading of pores. Then surface functionalization was accomplished

by the addition of (3-triethoxysilyl)propylisocyanate (1.32 mmol, 328 μL) and stirring the mixture during 5 h 30 min. Finally, the material was dried overnight at room temperature. S1 was immersed in a solution of the corresponding nucleotide sequence (O1) in the rhodamine B (262.5 μg , 1.57 mM, 350 μL) and TEA (2 μL) solution in CH_3CN to obtain solid S2, hereafter the same solids were immersed one second time in hybridization buffer (20 mM TRIS-HCl, 37.5 mM MgCl_2 , pH 7.5) with the DNA aptamer (O2) to obtain the sensing solid S3. Optimization of capping conditions were carried out for the resulting gated materials to achieve the best performance. Amounts of capping oligonucleotide were 50 μL of O1 (10 μM), 10 μL of O2 (100 μM). Final volume of reaction was established in 125 μL of hybridization buffer and mixtures were agitated at 25 $^\circ\text{C}$ for 120 min. Lastly, the obtained materials were rinsed with hybridization buffer to eliminate the unbounded oligonucleotide and any excess of rhodamine B.

5.5. Cargo quantification

To calculate the amount of the rhodamine B that can be loaded in the pores, a pair of independent supports of solid S3 were submerged in 1 mL of hybridization buffer. Then, one of them was stirred at 90 $^\circ\text{C}$ during 60 min to force the opening of the pores and the maximum cargo release, and the other was maintained in agitation at 25 $^\circ\text{C}$ during 60 min as a control. The delivered fluorophore was measured at 575 nm ($\lambda_{\text{exc}} = 555 \text{ nm}$), and the quantification of final released dye was undertaken using a calibration curve with different concentrations of rhodamine B. The experiment was done by triplicate.

5.6. Virus obtention

To generate the replication competent vesicular stomatitis virus carrying the S protein of the Wuhan SARS-CoV-2 strain, we replaced the G gene in a plasmid encoding the antigenome of VSV with an additional GFP transcriptional unit (Andreu-Moreno et al., 2020) with the Wuhan spike sequence lacking the C-terminal 21 amino acids to facilitate virus production. The virus was then rescued as previously described (Andreu-Moreno et

al., 2020) but using induced BHK-G43 cells which express the G protein of VSV (Hanika et al., 2005). The virus was then amplified for 1 passage on Vero cells. Replication incompetent VSV carrying different S proteins were produced as previously described (Gozalbo-Rovira et al., 2020). The genotype of the S proteins relative to the Wuhan S sequences were: Alpha, mutations H69Del, V70Del, Y144Del, N501Y, A570D, D614G, P681H, T716I, S982A and D1118H; Beta, mutations D80A, L241Del, L242Del, A243Del, E484K, N501Y, D614G, and A701V; Gamma, mutations L18F, T20N, P26S, D138Y, R190S, K417T, E484K, N501Y, D614G, H655Y, T1027I and V1176F; and Delta, mutations T19R, F157Del, R158Del, L452R, T478K, D614G, P681R and D950N. All viruses were purified by centrifugation at 50,000g for 4 hours and resuspended in DMEM All viruses were maintained in the same media at -80°C.

5.7. Detection protocol

The ability of the materials to detect spike protein and VSV-S was assessed by the fluorescence emission response of the reporter rhodamine B diffused from the inner mesoporous structure in the presence and in the absence of SARS-CoV-2 spike protein. For that, two independent supports of the material S3 were separately submerged in 900 μL of hybridization buffer each. Then, 100 μL of purified spike protein (1 $\text{ng } \mu\text{L}^{-1}$, Sinobiological, Beijing, China) were added to one of the supports of each pair of S3 solids whereas 100 μL of hybridization buffer were transferred to the other. All solutions were stirred at 25 °C and aliquots were collected periodically. The experiment was done by triplicate and released rhodamine B was detected by fluorescence spectroscopy at 575 nm ($\lambda_{\text{exc}} = 555 \text{ nm}$). In a step forward, a similar release assay was performed but using 100 μL of VSV-S ($2,5 \cdot 10^5 \text{ PFU mL}^{-1}$) to one of the supports of S3. The solutions were stirred as well at 25°C.

5.8. Quantification curve of SARS-CoV-2 spike protein recognition

The response of the solid S3 to different concentrations of VSV expressing the coronavirus spike protein on the surface was studied. For that, eleven independent supports of the S3 material were submerged in a solution containing 100 μL of different dilutions of VSV-S (from 10^4 to $5 \cdot 10^6$ PFU mL^{-1}) and volume was completed until 1 mL with hybridization buffer (diluting the virus concentrations 1:10). Solutions were stirred at 25 $^{\circ}\text{C}$ and released rhodamine B was determined at 575 nm ($\lambda_{\text{exc}} = 555$ nm) after 60 min.

5.9. Selectivity

To evaluate the selectivity of the system, dye release experiments were carried out by adding to independent supports of each material S3 a known concentration of different drugs commonly used in several treatments (levothyroxine, 0.025 mg mL^{-1} ; acetylsalicylic acid, 0.05 mg mL^{-1} ; salbutamol, 0.1 mg mL^{-1} ; paracetamol, 0.1 mg mL^{-1} ; enoxaparin, 0.1 mg mL^{-1} and tiotropium, 0.05 mg mL^{-1}). In the same experiment, 100 μL of SARS-CoV-2 spike protein (1 ng mL^{-1}) was used as a positive control and 100 μL of hybridization buffer as a negative control. The final volume was completed to 1 mL with hybridization buffer and mixed for 60 min at 25 $^{\circ}\text{C}$. Released rhodamine B was determined by fluorescence ($\lambda_{\text{exc}} = 555$ nm, $\lambda_{\text{em}} = 585$ nm).

5.10. Validation in competitive media

The potential use of the sensing material S3 to detect different concentrations of VSV-V in more realistic samples was tested. Therefore, the virus obtained as we mention before were diluted to the concentration of $2,5 \cdot 10^4$ PFU mL^{-1} . Then, human nasopharyngeal samples were collected from healthy donors with the help of a swab and kept in 5 mL of hybridization buffer. The samples were artificially inoculated with the concentration of prepared before. Finally, 100 μL of each sample were added to four independent S3 supports submerged in 900 μL of hybridization buffer. After 60 min at 25

°C the delivered rhodamine B was determined according to the obtained fluorescence emission at 575 nm ($\lambda_{\text{exc}} = 555 \text{ nm}$).

5.11. Study of the system behavior with different VSV-S variants

To assess the responsiveness of the system to the constant changing of SARS-CoV-2 that have naturally occurred during all the pandemic, different virus variants were tested with independent S3 supports. Thus, VSV carrying the different S protein variants Alpha, Beta, Gamma and Delta, which are the most spread in European countries until December 2021, were used. All the different four variants were diluted to a concentration of $2,5 \cdot 10^4 \text{ PFU mL}^{-1}$, meanwhile the control essay was performed containing no virus. All viruses were first diluted in TRIS media and then 100 μL of each one was added to 900 μL of competitive media (nasopharyngeal sample) containing a final volume of 1 mL each Eppendorf tube. Released rhodamine B after 60 min was measured by fluorescence as in previous experiments ($\lambda_{\text{exc}} = 555 \text{ nm}$).

6. REFERENCES

1. Ahmad, A., Spencer, J. E., Lockhart, S. R., Singleton, S., Petway, D. J., & Bagarozzi, D. A. (2019). Rapid molecular detection of fungal pathogens in clinical specimens. *Mycoses*, 62(6), 513-520.
2. Amouzadeh Tabrizi, M., Nazari, L., & Acedo, P. (2021). Detection of biomolecules using innovative biosensor technology. *Sensors and Actuators B: Chemical*, 345, 130377.
3. Bellan, L. M., Wu, D., & Langer, R. S. (2011). Nanotechnology and biomedical research integration. *Wiley Interdisciplinary Reviews: Nanomedicine and Nanobiotechnology*, 3(3), 229-245.

4. Bhalla, N., Pan, Y., Yang, Z., & Payam, A. F. (2020). Nanoparticle-based biosensors: Recent advances and challenges. *ACS Nano*, 14(8), 7783-7791.

5. Case, J. B., Rothlauf, P. W., Chen, R. E., Liu, Z., Zhao, H., Kim, A. S., Bloyet, L. M., Zeng, Q., Tahan, S., Droit, L., Ilagan, M. X. G., Tartell, M. A., Amarasinghe, G., Henderson, J. P., Miersch, S., Ustav, M., Sidhu, S., Virgin, H. W., ... Whelan, S. P. J. (2020). CRISPR diagnostics for COVID-19 detection. *Cell Host & Microbe*, 28(4), 475-485.

6. Das, C. M., Guo, Y., Yang, G., Kang, L., Xu, G., Ho, H.-P., & Yong, K.-T. (2020). Nanotechnology for enhanced clinical diagnostics. *Advanced Theory and Simulations*, 3, 2000185.

7. Gozalbo-Rovira, R., Gimenez, E., Latorre, V., Francés-Gómez, C., Albert, E., Buesa, J., Marina, A., Blasco, M. L., Signes-Costa, J., Rodríguez-Díaz, J., & Navarro, D. (2020). Evaluating biosensors for COVID-19 diagnostics. *Journal of Clinical Virology*, 131, 104611.

8. Guglielmi, G. (2020). Impact of new diagnostics on disease control. *Nature*, 583, 506-507.

9. Hanika, A., Larisch, B., Steinmann, E., Schwegmann-Weßels, C., Herrler, G., & Zimmer, G. (2005). Viral detection in clinical virology. *Journal of General Virology*, 86(6), 1455-1460.

10. Hashemi, S. A., Golab Behbahan, N. G., Bahrani, S., Mousavi, S. M., Gholami, A., Ramakrishna, S., Firoozsani, M., Moghadami, M., Lankarani, K. B., & Omidifar, N. (2021). Advances in biosensing for viral detection. *Biosensors and Bioelectronics*, 171, 112731.

11. Huang, L., Ding, L., Zhou, J., Chen, S., Chen, F., Zhao, C., Xu, J., Hu, W., Ji, J., Xu, H., Xu, H., & Liu, G. L. (2021). Development of biosensors for infectious disease detection. *Biosensors and Bioelectronics*, 171, 112685.
12. Iliuk, A. B., Hu, L., & Tao, W. A. (2011). Enhancing biosensor sensitivity through innovative technology. *Analytical Chemistry*, 83(12), 4440-4447.
13. Ji, T., Liu, Z., Wang, G., Guo, X., Khan, S. A., Lai, C., Chen, H., Huang, S., Xia, S., Chen, B., Chen, Y., & Zhou, Q. (2020). Detecting SARS-CoV-2 using biosensor technology. *Biosensors and Bioelectronics*, 166, 112455.
14. Johns Hopkins University & Medicine. (n.d.). New COVID-19 cases worldwide. Retrieved from <https://coronavirus.jhu.edu/>
15. Kim, Y. S., Ahmad Raston, N. H., & Gu, M. B. (2016). Novel nanomaterials in biosensor development. *Biosensors and Bioelectronics*, 76, 2-12.
16. Kumar, R., Nagpal, S., Kaushik, S., & Mendiratta, S. (2020). Virus diagnosis and monitoring tools. *VirusDisease*, 31(1), 97-105.
17. Liu, R., He, L., Hu, Y., Luo, Z., & Zhang, J. (2020). Nanostructures in chemical sensing applications. *Chemical Science*, 11(46), 12157-12164.
18. Mak, G. C., Cheng, P. K., Lau, S. S., Wong, K. K., Lau, C. S., Lam, E. T., Chan, R. C., & Tsang, D. N. (2020). Clinical virology innovations in biosensor usage. *Journal of Clinical Virology*, 129, 104500.
19. Millet, J. K., Tang, T., Nathan, L., Jaimes, J. A., Hsu, H. L., Daniel, S., & Whittaker, G. R. (2019). Structural analysis of viral proteins with advanced imaging. *Journal of Visualized Experiments*, 145. <https://doi.org/10.3791/59010>

20. Pavia, C. S., & Plummer, M. M. (2021). Infection and immunity research advances. *Journal of Microbiology, Immunology and Infection*, 54(5), 776-780.

21. Pfefferle, S., Reucher, S., Nörz, D., & Lütgehetmann, M. (2020). COVID-19 diagnostics and epidemiological response. *Eurosurveillance*, 25(9). <https://doi.org/10.2807/1560-7917.ES.2020.25.9.2000152>

22. Pla, L., Aviñó, A., Eritja, R., Ruiz-Gaitán, A., Pemán, J., Friaza, V., Calderón, E. J., Aznar, E., Martínez-Máñez, R., & Santiago-Felipe, S. (2020). Applications of DNA-based biosensors. *Journal of Fungi*, 6(4), 292.

23. Pla, L., Santiago-Felipe, S., Tormo-Mas, M. Á., Pemán, J., Sancenón, F., Aznar, E., & Martínez-Máñez, R. (2020). Innovations in chemical biosensing. *Sensors and Actuators B: Chemical*, 320, 128281.

24. Pla, L., Santiago-Felipe, S., Tormo-Mas, M. Á., Ruiz-Gaitán, A., Pemán, J., Valentín, E., Sancenón, F., Aznar, E., & Martínez-Máñez, R. (2021). Emerging biosensors for pathogen detection. *Emerging Microbes & Infections*, 10(1), 407-415.

25. Pramanik, A., Gao, Y., Patibandla, S., Mitra, D., McCandless, M. G., Fassero, L. A., Gates, K., Tandon, R., & Ray, P. C. (2021). Nanotechnology in viral diagnostics. *The Journal of Physical Chemistry Letters*, 12(9), 2166-2171.

26. Ribes, À., Aznar, E., Bernardos, A., Marcos, M. D., Amorós, P., Martínez-Máñez, R., & Sancenón, F. (2017). Nanostructured systems in biosensor development. *Chemistry – A European Journal*, 23(35), 8581-8589.

27. Ribes, À., Santiago-Felipe, S., Bernardos, A., Marcos, M. D., Pardo, T., Sancenón, F., Martínez-Máñez, R., & Aznar, E. (2017). Chemical sensors for pathogen detection. *ChemistryOpen*, 6(6), 653-662.

28. Ribes, À., Xifré-Pérez, E., Aznar, E., Sancenón, F., Pardo, T., Marsal, L. F., & Martínez-Mañez, R. (2016). Use of porous materials in biosensing. *Scientific Reports*, 6, 38649.

29. Song, Y., Song, J., Wei, X., Huang, M., Sun, M., Zhu, L., Lin, B., Shen, H., Zhu, Z., & Yang, C. (2020). Novel approaches in analytical chemistry for viral detection. *Analytical Chemistry*, 92(15), 9895-9900.

30. Wölfel, R., Corman, V. M., Guggemos, W., Seilmaier, M., Zange, S., Müller, M. A., Niemeyer, D., Jones, T. C., Vollmar, P., Rothe, C., Drosten, C., & Wendtner, C. (2020). COVID-19 molecular diagnostics. *Nature*, 581(7809), 465-469.

31. Seok Kim, Y., Ahmad Raston, N. H., & Bock Gu, M. (2016). Developments in biosensor applications for diagnostics. *Biosensors and Bioelectronics*, 76, 2-11.

32. Andreu-Moreno, I., & Sanjuán, R. (2020). Dynamics of virus-host interactions. *mBio*, 11(5), e02156.

Acknowledgments

This study was supported by the Spanish Government (projects RTI2018-100910-B-C41, PID2021-126304OB-C41 and SAF2017-82251-R (MCUI/AEI/FEDER, UE)), the Generalitat Valenciana (project no.2 RD 180/2020, PROMETEO/2018/024, CIPROM/2021/007), Supera COVID-19 Fund (DIACOVID project), the Universitat Politècnica de València–Instituto de Investigación Sanitaria La Fe (IIS-LaFe) (SARS-COV-2-SEEKER project) and by the European Commission –NextGenerationEU, through CSIC's Global Health Platform (PTI Salud Global) to Ron Geller. Ron Geller holds a Ramon y Cajal fellowship from the Spanish Ministerio de Economía y Competitividad (RYC-2015-17517).
Figure 1 done with BioRender.com

Ethical Committee approval

The present work has been developed with the approval of projects 2020-112-1, 2020-465-1, 2020-528-1 and 2021-012-1 by Medicaments Research Ethics Committee – CEIm of Hospital Universitari i Politècnic La Fe and by the approval of project P05_25_02_21 from the Research Ethics Committee of Universitat Politècnica de València. The informed consent of all participating subjects has been obtained. The study conforms to recognized standards, such as the Declaration of Helsinki.

Conflicts of interest

There are no conflicts to declare.

7. SUPPORTING INFORMATION

Figure S1. TEM images of the raw NAA support.

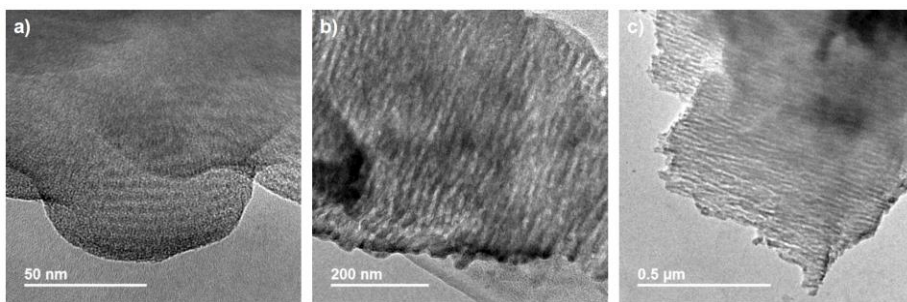


Figure S2. FESEM images of the material after use. A) reflects the surface of a nanosensor which has been tested in presence of the SARS-CoV-2 Spike protein. B) corresponds to the device surface that acts as a negative control (in the absence of the Spike protein).

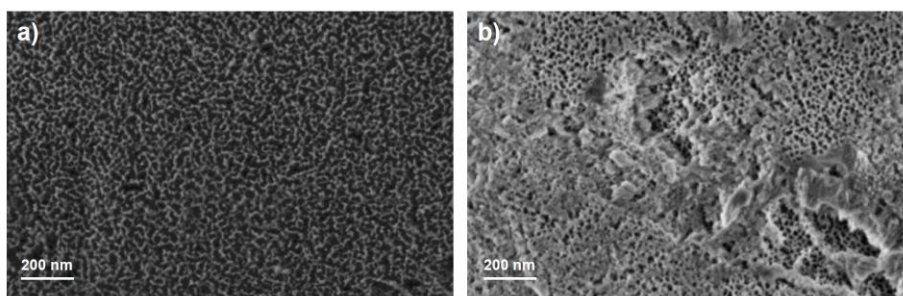


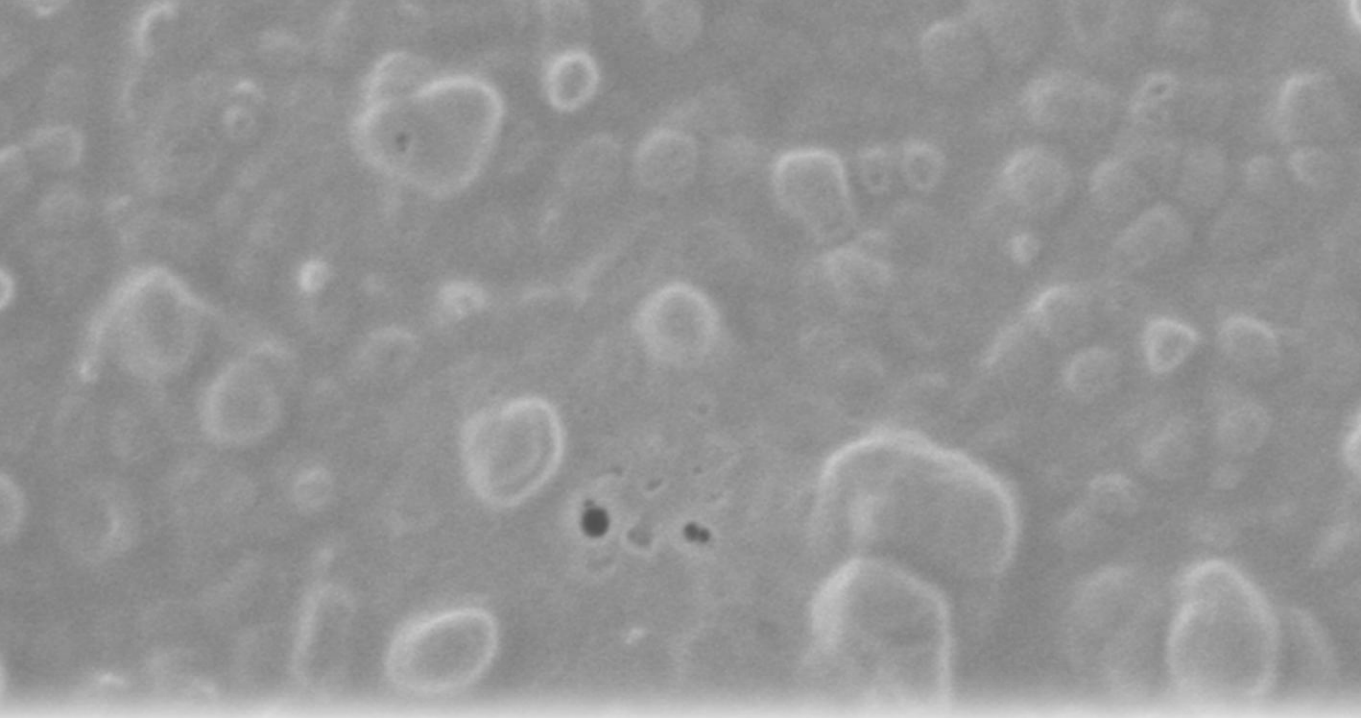
Table S1. List of commercial tests to detect SARS-CoV-2

*Sample collected with a nasopharyngeal swab according to each manufacturer guidelines.

Assay	Manufacturer/ Distributor	LOD (PFU/mL)	Principle	Time to result	Ref
ActivXpress + COVID-19 Ag Complete Kit	Edinburgh Genetics Ltd	1.0×10^4	Colloidal gold	5–20 min	[1]
Biocredit COVID-19 Ag	Rapidgen Inc	5.0×10^4	Colloidal gold	0 min	[1]
Bioeasy 2019-nCoV Ag	Shenzhen Bioeasy Biotechnology	5.0×10^3	Fluorescence	10 min	[1]
ESPLINE SARS-CoV-2	Fujirebio Diagnostics Inc	5.0×10^2	Colloidal gold	30 min	[1]
Rapid SARS-CoV-2 Antigen test card	Boson Diagnostics/Excalibur Healthcare Services	2.5×10^4	Colloidal gold	15 min	[1]

GENEDIA W COVID-19 Ag	Green Cross Medical Science	1.0×10^4	Colloidal gold	5–10 min	[1]
iChroma COVID-19 Ag Test	Boditech Medical Inc	1.0×10^4	Fluorescence	12 min	[1]
Innova SARS-CoV-2 Antigen Rapid	Innova Medical Group Ltd	1.0×10^3	Colloidal gold	15 min	[1]
SARS-CoV-2 Antigen Rapid Test Kit	Joysbio Biotechnology Ltd	2.5×10^2	Colloidal gold	15–20 min	[1]
Mologic COVID-19 Ag Test device	Mologic Ltd	5.0×10^3	Colloidal gold	10 min	[1]
NowCheck COVID-19 Ag test	Bionote Inc./Mologic Ltd	5.0×10^3	Colloidal gold	15–30 min	[1]
Coronavirus Ag Rapid Test	Zhejiang Orient Gene Biotech Ltd	1.0×10^3	Colloidal gold	10–15 min	[1]
Panbio COVID-19 Ag Rapid Test	Abbott Rapid Diagnostics	5.0×10^3	Colloidal gold	15 min	[1]
Respi-Strip COVID-19 Ag	Coris Bioconcept	2.5×10^5	Colloidal gold	15–30 min	[1]
SARS-CoV-2 Rapid Antigen Test	SD Biosensor Inc./Roche Diagnostics)	5.0×10^2	Colloidal gold	15–30 min	[1]
Standard F COVID-19 Ag FIA	SD Biosensor Inc	2.5×10^4	Fluorescence	15–30 min	[1]
Standard Q COVID-19	SD Biosensor Inc	5.0×10^3	Colloidal gold	15 min	[1]
Sure-Status COVID-19 Antigen Card Test	Premier Medical Corporation	5.0×10^2	Colloidal gold	15–20 min	[1]
Wondfo 2019-nCoV Antigen Test	Guangzhou Wondfo Biotech Co	2.5×10^3	Colloidal gold	10–15 min	[1]
qCovid-19 RT-qPCR	qgenomics	7.5×10^3	Fluorescence	24 hours	[2]

Biotinylated DNA aptamer on silver nanoparticles	Scientific research	3.8×10^4	Surface Enhanced Raman Scattering	7 min	[3]
NAA loaded with rhodamine B and capped with anti-spike protein aptamer	Scientific research	7.5×10^3	Fluorescence	Less than 1 hour	This paper



Chapter IV | Nucleic Acid Detection with Gated Nanoporous Anodic Alumina and CRISPR-Cas12a

**Cover: FESEM image of capped NAA (self-produced image)*

Nucleic Acid Detection with Gated Nanoporous Anodic Alumina and CRISPR-Cas12a

Isabel Caballos^{a,b}, Alejandro Requena-Menéndez^d, Roser Montagud-Martínez^d, Andy Hernández-Montoto^a, David Navarro^{e,f}, Ramón Martínez-Máñez^{a,b,c}, Elena Aznar^{a,b*}, and Guillermo Rodrigo^{d*}*

^a Instituto Interuniversitario de Investigación de Reconocimiento Molecular y Desarrollo Tecnológico (IDM) Universitat de València–Universitat Politècnica de València, Camino de Vera s/n, 46022, Valencia, Spain.

^b Unidad Mixta de Investigación en Nanomedicina y Sensores. Universitat Politècnica e València, Instituto de Investigación Sanitaria La Fe (IIS La Fe), Valencia Spain.

^c Unidad Mixta de Investigación en Mecanismos de Enfermedades y Nanomedicina, Universitat Politècnica de València – Centro de Investigación Príncipe Felipe (CIPF), 46012 Valencia, Spain.

^d Institute for Integrative Systems Biology (I2SysBio), CSIC – Universitat de València, 46980 Paterna, Spain.

^e Microbiology Service, Clinic University Hospital, INCLIVA Biomedical Research Institute, 46010 Valencia, Spain.

^f Department of Microbiology, School of Medicine, Universitat de València, 46010 Valencia, Spain.

*Corresponding authors: Guillermo.rodrido@csic.es, rmaez@qim.upv.es.

Publication under review.

1. ABSTRACT

Nanostructured materials appropriately functionalized are increasingly being recognized as effective tools in diagnostic and therapeutic applications. Yet, their interface with biotechnological systems needs to be extended to boost a plethora of biomedical applications. Here, we combined stimuli-responsive gated nanoporous anodic alumina (NAA) with the CRISPR-Cas12a technology to develop a rapid and precise nucleic acid detection system. NAA material is loaded with rhodamine B and capped with arbitrary ssDNA. The system is fully characterized at the physicochemical level by electron microscopy and spectroscopy. The general-purpose and specific dsDNA detection relies on the programmability of the RNA-guided Cas12a nuclease. The collateral catalytic activity of the nuclease is exploited to uncap the NAA material, leading to the specific release of rhodamine B to the medium for fluorescence measurement. Signal transduction is characterized through the engineered interface with synthetic dsDNA molecules. The applicability of the system is illustrated by detecting in a simple manner the SARS-CoV-2 genome from clinical samples in 1h and with high accuracy. A recombinase polymerase amplification process running isothermally is used for RNA-to-dsDNA transformation. This work shows a new promising approach for the development of accessible and effective diagnostic tools in the fight against infectious diseases.

- **KEYWORDS.** nanobiotechnology, nanostructured materials, controlled release, SARS-CoV-2, CRISPR diagnostics.

2. INTRODUCTION

Infectious agents (mainly, viruses and bacteria) represent an omnipresent threat that has waded humanity with multiple outbreaks causing public health crises, being the most recent the coronavirus disease 2019 (COVID-19) pandemic, caused by severe acute respiratory syndrome coronavirus 2 (SARS-CoV-2) (Zhu et al., 2020). In the global world of

today, infectious agents have an unprecedented capacity of spread both in terms of geographic expansion and speed, (Smith et al., 2007) which jeopardizes national healthcare systems. It is therefore imperative in an emergency scenario to leverage rapid detection protocols and set up a large network of point of care (POC) testing settings (St John, 2010).

Clinical diagnoses of infectious diseases rely on culture-based approaches and polymerase chain reaction (PCR). Nowadays, reverse transcription quantitative PCR (RT-qPCR) is the gold standard diagnostic technique in the clinic (Yang and Rothman, 2004), because it allows having pathogenic titers, in addition to warrant high sensitivity and specificity. However, the protocols are often slow and cumbersome, especially when pathogen characterization is desired. Moreover, they require expensive equipment and well-trained personnel, which hinders a massive testing action at multiple locations.

The development of reliable POC testing tools is important in order to set up a wide diagnostic line to complement RT-qPCR-based diagnoses (both within the healthcare system and at the personal level). Early and frequent detection of infections upon an outbreak becomes invaluable for adopting containment measures to reduce transmission, especially if asymptomatic individuals are detected, and timely therapeutic interventions are established to mitigate severe and fatal outcomes, which are mainly prevalent in the elderly population (Larremore et al., 2021). In this regard, nanotechnological advances are giving rise to specific, sensitive, and smart nanodevices with great potential in the biosensing field (Welch et al., 2021).

Nanostructured materials with high surface-to-volume ratio capable of delivering various types of cargo molecules in substantial amounts are appealing for diagnostic and therapeutic applications (Aznar et al., 2016; Alberti et al., 2015). These materials typically involve a cargo-containing inorganic porous support and a highly-tunable surface that allows the immobilization of diverse biological elements (*e.g.*, nucleic acids, enzymes, or

antibodies) through covalent or non-covalent bonds. The attached elements act as molecular gates (or gatekeepers), blocking the pores and preventing the release of the previously loaded cargo (typically fluorogenic dyes for diagnostics). As a result, these materials are responsive to specific analytes interacting with the gatekeeper, leading to reversible or irreversible structural changes that trigger cargo release.

Among the inorganic porous supports, nanoporous anodic alumina (NAA) has gained significant attention in recent years (Rajeev et al., 2018). They are fabricated by self-ordering electrochemical anodization, which leads to have nanochannel arrays in a simple, scalable, and cost-effective manner which contrasts with fabrication by conventional lithographic techniques (Chen et al., 2001). These nanostructured materials stand out for their mechanical, optical, and electrical properties (Vojkuvka et al., 2012; Marsal et al., 2009), as well as their thermal stability and biocompatibility (La Flamme et al., 2007). Moreover, the abundance of hydroxyl groups on their nanochannels facilitates efficient biofunctionalization through alkoxy silane chemistry. All these properties have enabled the development and application of NAA materials for the detection of viral particles (virions) (Nguyen et al., 2009), bacterial cells (Pla et al., 2020), proteins (*e.g.*, immunoglobulin) (Alvarez et al., 2009), nucleic acids (Ribes et al., 2019), and small molecules (Ribes et al., 2016). For that, the surface of the devices was functionalized with antibodies, high-affinity aptamers, or complementary oligonucleotides. Notably, recent strategies have allowed detecting the genome of diverse pathogens (Ribes et al., 2019; Hernández-Montoto et al., 2023) and even genetic biomarkers such as microRNAs (Garrido-Cano et al., 2021). Porous nanomaterials have also allowed going beyond the simple detection model to the implementation of biocomputing schemes (Wen et al., 2012).

Notwithstanding, the development of novel strategies in which the very same functionalized NAA material was capable of detecting a variety of targets, while maintaining the specificity and sensitivity, would represent a significant advance in POC

diagnostics. Not being constrained by a particular application, the gated NAA device could be routinely produced and stored for when needed. Here, we intend to exploit clustered regularly interspaced short palindromic repeat (CRISPR) systems (*viz.*, the RNA-guided adaptive immune system in prokaryotes against viruses) (Barrangou et al., 2007) in combination with gated NAA materials to develop a novel detection platform. In recent years, CRISPR systems have been repurposed for nucleic acid detection (Kaminski et al., 2021), as well as for gene regulation and editing (McCarty et al., 2020). Some CRISPR-associated (Cas) proteins, such as Cas12a, display a collateral catalytic activity upon DNA target recognition that allows digesting oligonucleotides present in the medium (usually in the form of fluorogenic probes for diagnostics) (Chen et al., 2018). This feature could be exploited to interface CRISPR systems with oligonucleotide-capped NAA materials, where the cargo of the material would be released once the CRISPR-Cas12a complex had recognized the nucleic acid of interest and, in turn, had indiscriminately cleaved the capping oligonucleotides.

A CRISPR-based detection usually requires a pre-amplification process of the nucleic acid of interest, although some systems have been developed for a direct recognition (Fozouni et al., 2021). A key aspect in POC detection lies in operating at a constant and low temperature, then avoiding thermocycling. A variety of isothermal amplification methods have been developed for nucleic acid detection (Zhao et al., 2015), such as recombinase polymerase amplification (RPA), which allows operating at temperatures in the 37-42 °C range (Piepenburg et al., 2006). Such methods exploit primer-directed enzyme-nucleic acid interactions and polymerization. Of relevance, they have been applied to detect the genomes of pathogenic bacteria (Hara-Kudo et al., 2005) and viruses including SARS-CoV-2 (Ganguli et al., 2020). Nonetheless, spurious amplifications due to the presence of contaminants or closely related nucleic acid sequences, as well as the lack of standardized protocols, limit the precision of these methods. Thus, the implementation of a subsequent CRISPR-based step results highly beneficial to increase specificity and even sensitivity.

In the following, we present our results on the use of gated NAA materials responding to Cas12a for specific nucleic acid detection. We characterized the resulting material by means of high-resolution techniques of microscopy and spectroscopy. We used rhodamine B to load it, thereby measuring the release by fluorescence in a quantitative and time-resolved manner. As a proof of principle, we here focused on the detection of the SARS-CoV-2 genome. For that, we programmed Cas12a with a CRISPR RNA (crRNA) targeting the N gene of the virus. We assessed the dynamic response of the system, as well as its specificity and sensitivity, with synthetic double-stranded DNA (dsDNA) molecules. Finally, we collected clinical samples of infected patients with SARS-CoV-2 to test the detection ability of the engineered system.

3. RESULTS AND DISCUSSION

3.1. Design, synthesis, and characterization of gated NAA materials

Starting from commercially available NAA scaffolds cut into disks of 2 mm diameter (S0 material), we loaded the pores with rhodamine B (S1 material), a fluorogenic molecule serving as reporter of the detection. We then chemically modified the outer surface by the attachment of 3-(triethoxysilyl)propyl isocyanate to generate S2 material. Subsequently, a single-stranded DNA (ssDNA) molecule of arbitrary sequence and modified in their 5' and 3' ends with amine moieties was chosen to minimize secondary structure. We exploited these amino groups to covalently anchor the oligonucleotide by means of the formation of urea bonds with isocyanate moieties present in S2 material. As a result, we obtained a gated NAA solid, termed S3 material. The oligonucleotide ensemble on the surface of the inorganic scaffold was expected to be bulky enough to block the pores and prevent rhodamine B delivery.

To obtain a quantitative physicochemical picture, S0, S1, S2, and S3 materials were characterized by field emission scanning electron microscopy (FESEM), atomic force

microscopy (AFM), and energy dispersive X-ray spectroscopy (EDXS). The appearance of the initial S0 solid was of a silvery small disk, while the final S3 solid acquired a pinkish tone due to the loading with rhodamine B. Representative FESEM images of the S0 material showed the porous structure described above, while the images of the S3 material evidenced the presence of a dense capping layer on the top of the pores (Figure 1A,B; see also Figure S1 in Supporting Information to have a comparative view of the S1 and S2 materials). AFM images resolved the three-dimensional aspect the different material surfaces (Figure S2, Supporting Information). In addition, EDXS analyses served to quantify the atomic content and confirm the appropriate synthesis of the different materials. Due to the cargo molecules loaded into the material, the carbon content of the S1 solid increased from the raw material. The isocyanate attachment to generate the S2 solid did not prevent a partial cargo release, reflected in a slight decrease in carbon content. The S3 solid showed the highest carbon content due to the capping oligonucleotides, which was also reflected in the highest nitrogen and phosphorous content (Figure 1C).

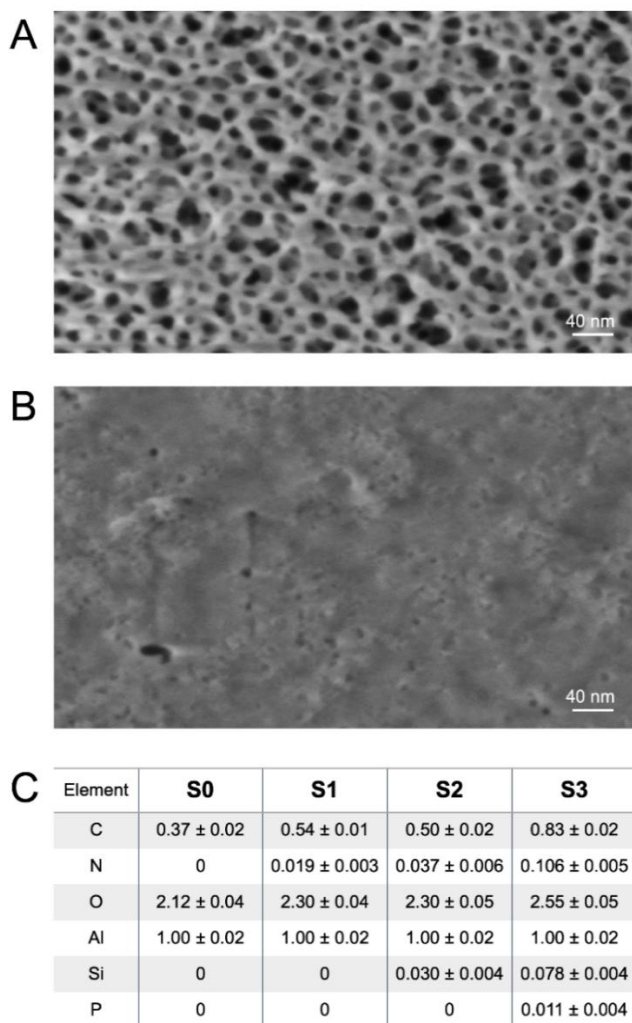


Figure 1. Physicochemical characterization of oligonucleotide-capped NAA. A) FESEM image of the material surface before capping, showing the nanopores (S0 material). The material was loaded with rhodamine B to produce a red fluorescence signal if rhodamine B is released to the medium. B) FESEM image of the material surface after covalent capping with oligonucleotides (ssDNA) of arbitrary sequence (S3 material). Scale bar of 40 nm. Bottom, relative atomic compositions (with respect to Al atoms) of the S0, S1, S2, and S3 materials determined by EDXS.

To demonstrate that the gated NAA material exhibited a controlled release mechanism, we used a nonspecific deoxyribonuclease (DNase) able to digest both dsDNA and ssDNA molecules (Sutton et al., 1997). The fluorescence level of the aqueous phase determined the amount of delivered dye from the uncapped nanopores. The S3 material was incubated with 1 ng mL^{-1} DNase I from bovine pancreas at $25 \text{ }^{\circ}\text{C}$ and fluorescence was monitored with time (Figure 2A). After 1 h, we found a 3.5-fold dynamic range. Next, we investigated the physicochemical change suffered by the material. FESEM images illustrated exposure of the nanopores to the medium upon incubation with the nuclease (Figure 2B,C). In terms of atomic composition, EDXS analyses showed a 38% reduction in carbon content, 38% reduction in nitrogen content, and 16% reduction in phosphorous content (Figure S3, Supporting Information), which agrees with a loss of capping oligonucleotides and cargo molecules.

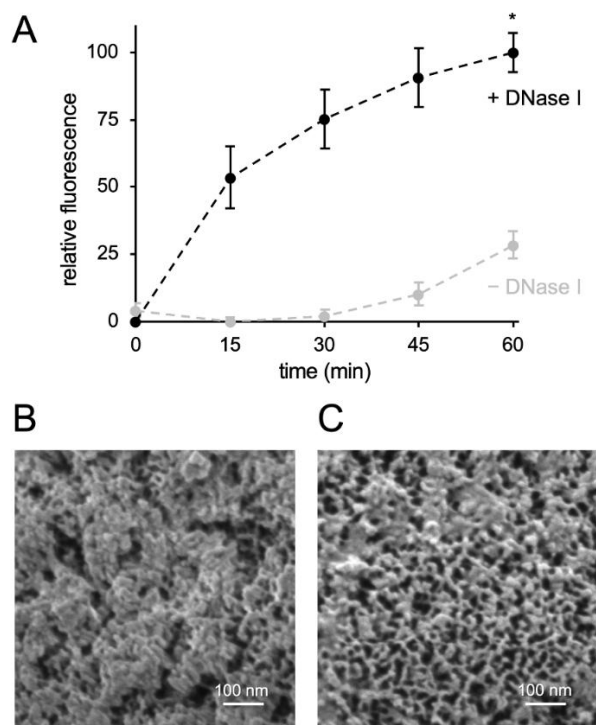


Figure 2. Functional characterization of oligonucleotide-capped NAA. A) Rhodamine B release dynamics with and without DNase I (1 ng/mL, at 25 °C for 60 min). Represented data correspond to means \pm standard errors ($n = 3$). *Statistically significant change (Welch's t -test, $P < 0.05$). B) FESEM image of the material surface after blank incubation. C) FESEM image of the material surface after incubation with DNase I. Scale bar of 100 nm.

3.2. CRISPR-Cas12a regulation of cargo release

To interface the aforementioned NAA material with the CRISPR-Cas12a system *in vitro*, we considered the Cas12a from *Lachnospiraceae* bacterium. This Cas12a variant has demonstrated excellent activity for both dsDNA primary targeting and subsequent ssDNA *trans*-cleavage (Chen et al., 2018). As a case study, we focused on detecting the SARS-CoV-2 genome. To this end, we considered a previously designed crRNA able to target a

dsDNA fragment complementary to the N gene (Marqués et al., 2021), which can be generated by PCR with the Centers for Disease Control and Prevention (CDC) N1 primers. In this amplicon, there is a suitable protospacer adjacent motif (PAM) for Cas12a recognition, whose sequence reads TTTG (Figure 3A). The crRNA was *in vitro* transcribed and incubated with a commercial preparation of Cas12a to form the ribonucleoprotein.

We performed CRISPR-Cas12a reactions with the S3 material and a synthetic dsDNA molecule mimicking the N1 amplicon. Reactions occurred at 25 °C and fluorescence was measured at different time points to assess the release of rhodamine B to the medium due to the *trans*-cleavage of the oligonucleotides capping the material (Figure 3B). After 1 h, we found that the dsDNA presence (ON state) led to a 2.4-fold increase in fluorescence (with respect to the OFF state), confirming the proposed signal transduction mechanism (Figure 3C; see also Figure S4A in Supporting Information). We also noticed some nonspecific intrinsic release from the material, arguably due to some nanopores not fully capped. The dynamic response reached a plateau in less than 30 min, and a first-order kinetic model was used to fit the data (Mircioiu et al., 2019).

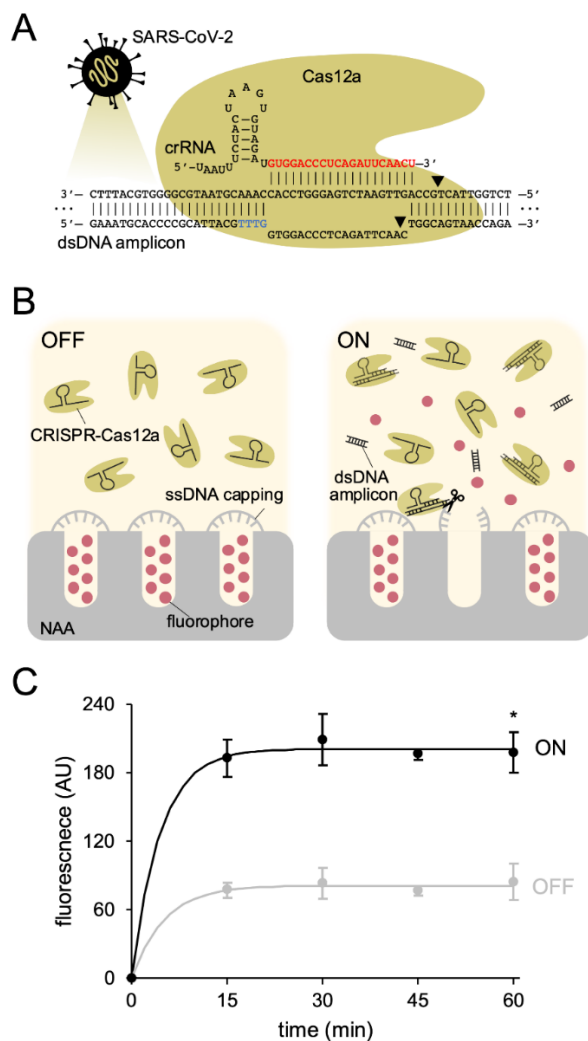


Figure 3. Interfacing CRISPR-Cas12a-based detection with NAA-based rhodamine B release. A) Scheme of the CRISPR-Cas12a ribonucleoprotein targeting the N1 dsDNA amplicon of SARS-CoV-2. The spacer of the crRNA is shown in red and the PAM in blue. B) Scheme of the oligonucleotide-capped NAA-based rhodamine B release by the collateral activity of Cas12a upon targeting the dsDNA amplicon (ON state). When the dsDNA amplicon is absent (OFF state), the capping oligonucleotides keep rhodamine B within the NAA particle (S3). C) Rhodamine B release dynamics based on the collateral activity of

*Cas12a (100 nM) upon targeting synthetic N1 dsDNA molecules (500 nM, at 25 °C for 60 min). Represented data correspond to means \pm standard errors ($n = 3$). Solid lines correspond to adjusted theoretical models [$F = F_{\infty}(1 - e^{-kt})$, where $F_{\infty} = 201.2$ AU and $k = 0.227 \text{ min}^{-1}$ in the ON state, and $F_{\infty} = 81.4$ AU and $k = 0.198 \text{ min}^{-1}$ in the OFF state]. *Statistically significant change (Welch's t-test, $P < 0.05$). AU, arbitrary units.*

In addition, we decided to investigate the effect of temperature, as this physical variable might serve for fine-tuning purposes. We measured the dynamic response of the system at 31 and 37 °C, finding greater release of rhodamine B to the medium as temperature increased (Figure 4). After 1 h at 37 °C, we quantified a 4.3-fold change with respect to a blank reaction without target dsDNA, which represents an enhancement of 79% from 25 °C. The nonspecific intrinsic release from the material only increased marginally with temperature. Despite the typical habitat of *L. bacterium* is the mammalian gut (Meehan et al., 2014), the activity of its Cas12a has been shown almost constant in the 25-37 °C range *in vitro* (Fuchs et al., 2022). Thus, we attributed such enhancement to an increase in the diffusivity of the CRISPR-Cas12a complex following statistical mechanics principles (Miller et al., 1924), thereby leading to more collisions with the gated NAA material.

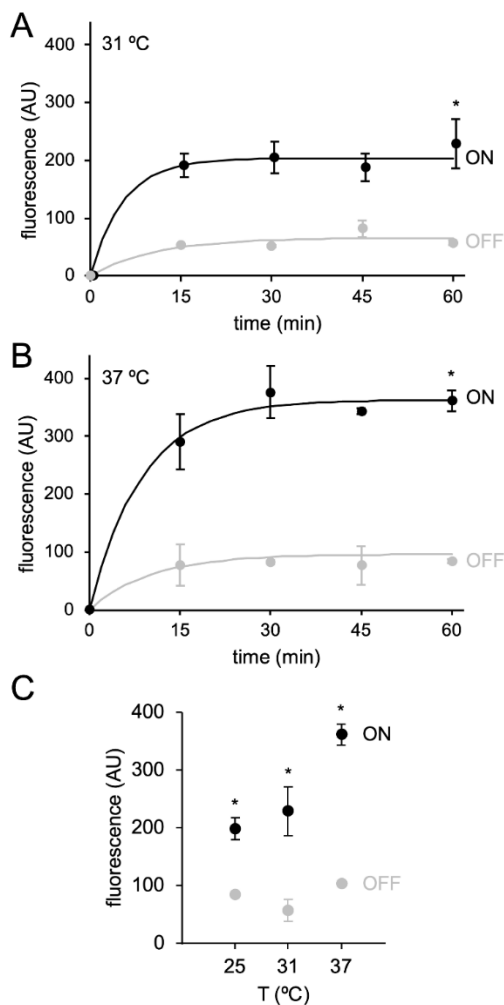


Figure 4. Effect of temperature on the dynamic response. A, B) Rhodamine B release dynamics at different temperatures (31 and 37 °C) upon incubating the S3 material with CRISPR-Cas12a ribonucleoproteins and synthetic N1 dsDNA molecules. Represented data correspond to means \pm standard errors ($n = 3$). Solid lines correspond to adjusted theoretical models [$F = F_{\infty}(1 - e^{-kt})$], where $F_{\infty} = 203.6$ AU and $k = 0.185$ min^{-1} at 31 °C in the ON state, $F_{\infty} = 66.1$ AU and $k = 0.091$ min^{-1} at 31 °C in the OFF state, $F_{\infty} = 362.8$ AU and $k = 0.115$ min^{-1} at 37 °C in the ON state, and $F_{\infty} = 96.3$ AU and $k = 0.098$ min^{-1} at 37 °C in the OFF state]. C) Scatter plot between rhodamine B release and

temperature (incubation for 60 min). *Statistically significant change (Welch's *t*-test, $P < 0.05$). AU, arbitrary units.

3.3. Specificity and sensitivity assays

To evaluate the specificity of our detection system, we synthesized additional dsDNA molecules mimicking SARS-CoV-2 amplicons generated by PCR with the CDC N2 primers targeting the N gene, the Charité E-Sarbeco primers targeting the E gene, and custom designed primers targeting the S gene (Figure S5, Supporting Information). Then, we conducted CRISPR-Cas12a reactions with the S3 material, using the crRNA targeting the N1 amplicon. Reactions occurred at 25 °C and a single fluorescence measurement was done after 30 min. Our results revealed a significant release of rhodamine B to the medium only in the intended case, with no apparent off-target effects (Figure 5A). Even though all amplicons contained suitable PAMs to be recognized by Cas12a, the non-complementarity of the crRNA prevented the formation of the ternary complex and then the activation of the collateral catalytic activity of the nuclease. Thanks to appropriate crRNA designs, the CRISPR-Cas12a system has been exploited to discriminate sequences harboring mutations in both the protospacer and the PAM (Marqués et al., 2021; Yang et al., 2022), so further work could explore this extreme with the interface here implemented with the NAA material.

To assess the sensitivity of the system, we performed a set of CRISPR-Cas12a reactions with the S3 material and increasing concentrations of the target dsDNA molecule (0, 1, 10, 100, and 500 nM), corresponding to the N1 amplicon. As before, reactions occurred at 25 °C. We only observed substantial release of rhodamine B to the medium at target concentrations of 500 nM (Figure 5B). In that favorable condition, we estimated the formation of 100 nM activated nuclease for *trans*-cleaving ssDNA molecules. It is important to note that because the S3 solid remains at the bottom of the tube, only those activated Cas12a nucleases in the vicinity of the material surface can

hydrolyze the capping oligonucleotides. Using a calibration line established from control solutions, we determined the release of about 2.1 μM rhodamine B in the ON state, highlighting a signal amplification of 21-fold from the nuclease to the reporter. Of note, in these new experiments, we found a larger dynamic range of 4.2-fold. Arguably, the use of a distinct batch of particles, which could have a different load of rhodamine B and a different layer of capping oligonucleotides, could explain this variation from our previous results. Yet, the behavior from particle to particle was highly comparable within a given batch. In this regard, continued efforts to scale up and homogenize the production of functional materials are important for biomedical applications (Núñez et al., 2018).

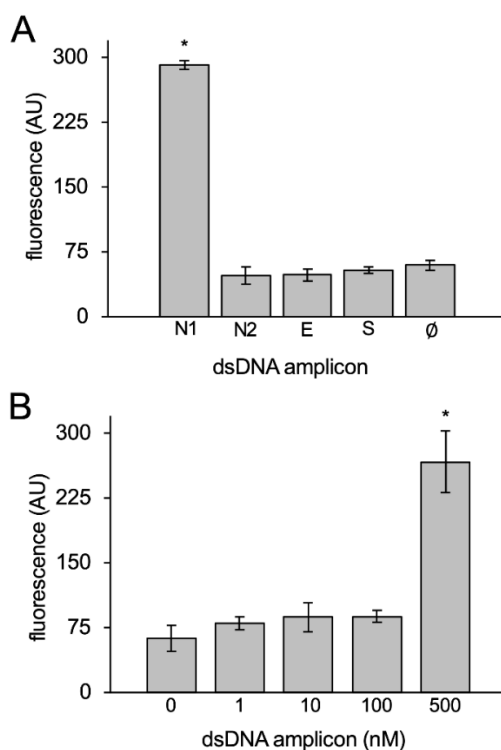


Figure 5. Specificity and sensitivity analyses. A) Rhodamine B release in the presence of different dsDNA molecules (500 nM, at 25 °C for 30 min) using the S3 material. The SARS-CoV-2 N (N1 and N2 regions), E, and S genes were considered. B) Rhodamine B

*release in the presence of increasing amounts of synthetic N1 dsDNA molecules (at 25 °C for 30 min). Represented data correspond to means ± standard errors (n = 3). *Statistically significant change (Welch's t-test, P < 0.05). AU, arbitrary units.*

3.4. Detection of SARS-CoV-2 in clinical samples

We designed an experimental test based on the application of a CRISPR-Cas12a ribonucleoprotein and a gated NAA material aimed to detect the SARS-CoV-2 RNA genome from clinical samples. Nasopharyngeal swab samples from different hospitalized patients were collected, and RT-qPCR assays were performed to confirm the infection by SARS-CoV-2 in a subset of them (Figure S6, Supporting Information). In our devised assay, the first step is an RT-RPA reaction. This allows producing dsDNA amplicons at a suitable concentration from the virus genome in the case of positive samples. In a second step, the S3 material and preassembled CRISPR-Cas12a ribonucleoproteins are mixed with the RT-RPA product for the specific dsDNA detection (Figure 6A). The resulting protocol is streamlined, not needing RNA extraction, sample concentration, or intermediate purification.

To perform RT-RPA reactions against SARS-CoV-2, we extended the CDC N1 primers by their 3' ends, so that the resulting product was the very same N1 amplicon (note that RPA requires longer primers than PCR) (Piepenburg et al., 2006). Specifically, the RT-RPA reaction occurred at 42 °C for 30 min, followed by the CRISPR-NAA reaction at 25 °C for additional 30 min. Our results showed a highly significant response in terms of rhodamine B delivery. On average, we found an 11.4-fold change in fluorescence between positive and negative samples (Figure 6B), which allowed discriminating infected patients with precision. We also noticed much higher fluorescence levels than with synthetic dsDNA molecules, which was attributed to the elements present in the RPA buffer, such the ssDNA-binding protein (Figure S4B, Supporting Information).

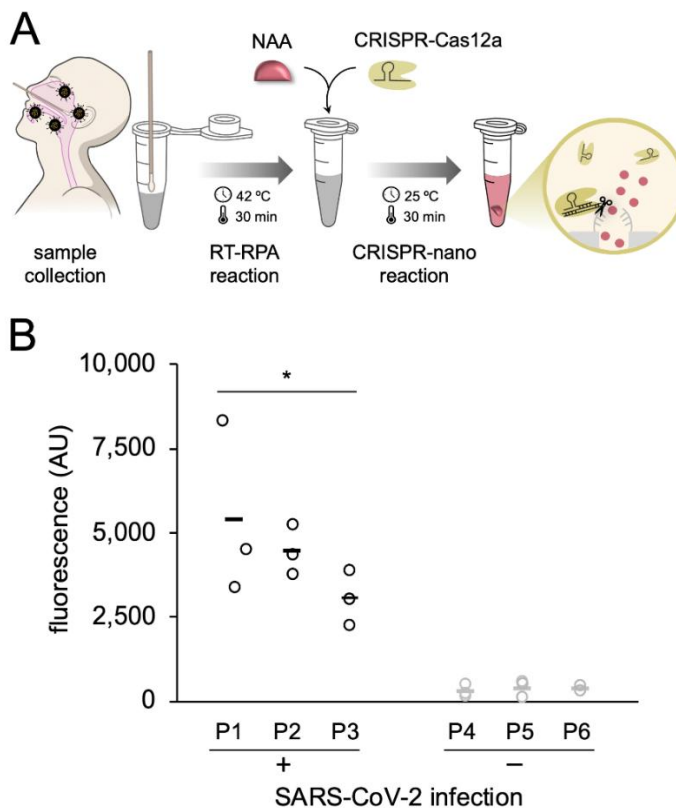


Figure 6. SARS-CoV-2 detection in clinical samples with oligonucleotide-capped NAA and CRISPR-Cas12a ribonucleoproteins. A) Scheme of the diagnostic method. RT-RPA was used to amplify the SARS-CoV-2 RNA genome from a nasopharyngeal swab in the form of dsDNA (N1 region; at 42 °C for 30 min). Then, a single S3 material and pre-assembled CRISPR-Cas12a ribonucleoproteins were added to the reaction for the specific detection of the N1 dsDNA amplicon (at 25 °C for 30 min). B) Rhodamine B release based on the collateral activity of Cas12a (100 nM) upon targeting the N1 dsDNA amplicon (RPA primers at 480 nM). Patients P1, P2, and P3 were diagnosed as positive for SARS-CoV-2 infection by RT-qPCR. Patients P4, P5, and P6 were diagnosed as negative by RT-qPCR ($C_T > 40$). Represented data correspond to technical replicates from patient samples (means marked with horizontal lines). *Statistically significant change (Welch's t-test, $P < 0.05$). AU, arbitrary units.

To detect another pathogen of interest following our development, it would only be necessary to redesign the crRNA, which is an easy task. Avoiding the need to synthesize a new NAA material for each new target could represent an advantage compared to previous work (Hernández-Montoto et al., 2023). In principle, nothing prevents using an alternative isothermal amplification method (Zhao et al., 2015). We decided to use RPA due to the low temperature requirement (in the 37-42 °C range) and the simplicity of the primer design. In previous work, the Cas12a nuclease was exploited to process ssDNA-modified gold nanoparticles aimed to obtain a colorimetric readout (Zhang et al., 2021; Ma et al., 2021) or magnetic nanoparticles immobilizing an enzyme through an ssDNA linker to produce a compound easily detectable with commercial electrochemical devices (*e.g.*, glucometer) (Liu et al., 2021). Accordingly, the NAA material might be loaded with glucose rather than rhodamine B, thereby avoiding the use of a fluorometer. Of relevance, we envision that NAA materials might be capped as well with RNA oligonucleotides. In this case, the RNA-guided Cas13a ribonuclease (RNase) would be used, as this protein displays a collateral catalytic activity over RNA molecules upon RNA target recognition (Gootenberg et al., 2017). Nonetheless, such a material might also be a target for Cas12a, as recent work has revealed certain *trans*-cleavage activity over RNA of this DNase (Li et al., 2022). In this regard, probing the functional versatility of the CRISPR systems for the controlled release of arbitrary cargo molecules from NAA materials represents one way to engineer a new variety of nanobiotechnological devices.

4. CONCLUSIONS

The development of diagnostic systems capable of detecting infectious agents in a confident, specific, sensitive, portable, and rapid manner, without the need for expensive equipment and highly trained personnel, is crucial to support epidemiological containment and allow early therapeutic interventions. Herein, we have expanded the nucleic acid (pathogen genome) detection toolbox by engineering a novel system that

combines NAA materials and the CRISPR-Cas12a technology. In brief, an oligonucleotide-capped NAA material was responsive to the collateral catalytic activity of a Cas12a nuclease upon dsDNA recognition. The specificity of the detection relied on the exquisite sequence recognition ability of the RNA-guided Cas12a nuclease. The sensitivity, when dealing with clinical samples, was based on the RPA efficiency and the signal amplification obtained with the NAA material. Importantly, we demonstrated that a human respiratory virus can be detected from clinical samples with high accuracy (dynamic range of the response of >10-fold). Hence, the devised system displays POC testing potential. In sum, having coupled inorganic (NAA), organic, and biological chemistry (CRISPR) with success, our results prompt exciting prospects in the field of nanobiotechnology to devise diagnostic, therapeutic, and even theranostic applications (Lammers et al., 2011).

5. MATERIALS AND METHODS

5.1. Reagents

Commercially available NAA scaffolds are composed of anodic aluminum oxide films grown on a 0.1 mm thick aluminum layer with a pore density of $9 \cdot 10^{11} \text{ cm}^{-2}$. Cavities present a funnel-like shape, which progressively shifts from a size of 20-30 nm at the top of the funnel (pore entrance) to a size of about 5 nm at the end. The pores are typically 10 μm long. The NAA on Al foils (25×75 mm) used in this work were provided by InRedox with the following physical characteristics: alumina thickness of $10 \pm 0.2 \mu\text{m}$, pore diameter of $5 \pm 2 \text{ nm}$, pore density of $9 \cdot 10^{11} \text{ cm}^{-2}$, and porosity of $15 \pm 2\%$. Chemical reagents such as rhodamine B or tris(hydroxymethyl)aminomethane (Tris) were provided by Merck.

The ssDNA oligonucleotide to cap the material was obtained from IDT, with the sequence TACGCAAGGCGAATCTACCCTACGCAAGGCGAATCTACCC. This arbitrary sequence was chosen to minimize any secondary structure potentially interfering with the

detection. The 5' and 3' terminals were functionalized with a primary amine (NH₂) for conjugation with the isothiocyanate label. The spacer used was (CH₂)₆ in both cases, which is hydrophobic. The 3'-NH₂ modification prevents a premature degradation by 3'→5' exonucleases typically found in biological samples. Amino modifications were used in post-coupling reactions (attachment to surfaces).

A purified preparation of *L. bacterium* Cas12a was obtained from IDT. Besides, the crRNA to target the SARS-CoV-2 N1 amplicon, whose sequence reads UAAUUUCUACUAAGUGUAGAUGUGGACCCUCAGAUUCAACU, was generated by *in vitro* transcription with the TranscriptAid T7 high yield transcription kit (Thermo) from a DNA template. The crRNA was purified using the RNA clean and concentrator column (Zymo) and quantified in a NanoDrop spectrophotometer (Thermo).

5.2. Material characterization

High resolution FESEM was used to image the microstructure of the material. NAA particles were fixed by carbon cement. Images were captured with a GeminiSEM 500 microscope (Zeiss) operating at 1 kV. The elemental composition of the analyzed surfaces was determined by EDXS using an X-ray detector coupled to the microscope. AFM in tapping mode was used to measure the surface topography. Images were obtained with a MultiMode 8-HR platform (Bruker).

5.3. Material preparation for release assays

NAA particles (disks with diameter of 2 mm, 25 units) were immersed in a rhodamine B solution in acetonitrile (1.5 mM, 8 mL) and incubated at 25 °C for 24 h using an orbital stirrer at 50 rpm to load the nanopores. Then, for surface functionalization, 1 mL 3-(triethoxysilyl)propyl isocyanate was added and the mixture was stirred for 5.5 h. NAA particles were rinsed with rhodamine B in acetonitrile and air dried on paper. To cap the material, NAA particles (50 units) were soaked in a rhodamine B solution in

acetonitrile (1.5 mM, 4.3 mL), followed by the addition of an aqueous solution of the oligonucleotide bearing amine groups in the ends (100 μM , 625 μL) and 25 μL triethylamine. The mixture was incubated at 25 $^{\circ}\text{C}$ for 3 h using an orbital stirrer at 50 rpm. NAA particles were washed with rhodamine B in acetonitrile and air dried on paper.

To verify the functionalization of the materials, a single NAA particle was incubated in 1 mL buffer A (20 mM Tris and 37.5 mM MgCl_2) with and without DNase I from bovine pancreas (1 ng mL^{-1} , Merck). DNase I can hydrolyze the oligonucleotides present in the surface and then open the nanopores. Reactions were incubated at 25 $^{\circ}\text{C}$ for 1 h at 700 rpm using a thermoshaker (Grant-Bio). At scheduled times (15, 30, 45, and 60 min), aliquots of 100 μL were taken for fluorescence measurements. Red fluorescence measurements were performed in a Synergy H1 microplate reader (BioTek; excitation at 555 nm and emission reception at 575 nm).

5.4. CRISPR-Cas12a-based detection

Prior to the detection assay, the CRISPR-Cas12a ribonucleoprotein was formed by mixing the crRNA (625 nM) and Cas12a (500 nM) at room temperature for 30 min, and NAA particles were washed with the reaction buffer composed by 10 mM Tris-HCl (pH 7.9), 50 mM NaCl, and 10 mM MgCl_2 (termed buffer C). In a 2 mL tube (Axygen), 500 nM synthetic dsDNA mimicking the SARS-CoV-2 N1 amplicon was mixed with 100 nM CRISPR-Cas12a ribonucleoprotein for a total volume of 200 μL (adjusted with buffer C). A single NAA particle was added to the reaction, which was incubated at 25, 31, or 37 $^{\circ}\text{C}$ for 1 h with shaking at 500 rpm in a Thermomixer (Eppendorf). An aliquot of 20 μL was extracted every 15 min to load a 384 well microplate (black, transparent bottom; Falcon) to measure red fluorescence (from rhodamine B release) in a CLARIOstar Plus fluorometer (BMG; excitation at 557 nm and emission reception at 604 nm). To test the sensitivity of the system, different concentrations of synthetic SARS-CoV-2 N1 amplicon were considered: 1, 10, 100, and 500 nM. To test the specificity of the system, CRISPR-Cas12a-based

detection reactions were carried out with additional synthetic SARS-CoV-2 amplicons: N2, E, and S (always at 500 nM).

5.5. Patient samples

Nasopharyngeal swab samples were collected from six different patients in the Clinic University Hospital of Valencia (Spain). Three of them resulted positive for SARS-CoV-2 infection after RT-qPCR in the hospital, whereas the other three resulted negative. Samples were inactivated through the action of proteinase K followed by a heat shock (5 min at 60 °C) before proceeding with the research study. No RNA extraction was performed. The study received approval from the ethics committee of the Clinic University Hospital of Valencia (order #2020/221).

5.6. Nucleic acid amplification by RT-RP

The TwistAmp basic kit (TwistDX) was employed. 480 nM RPA N1 forward and reverse primers, 500 U RevertAid reverse transcriptase (Thermo), and 50 U RiboLock RNase inhibitor (Thermo) were mixed with 29.5 µL rehydration buffer to reach a total volume of 45.4 µL (adjusted with RNase-free water). The TwistAmp basic reaction pellet was then resuspended with the resulting volume, and 2 µL patient sample was added. To initiate the reaction, 7 mM magnesium acetate was introduced. Reactions were incubated at 42 °C for 30 min in a Thermomixer (Eppendorf), with intermittent shaking at 300 rpm for 10 s every 2 min.

5.7. SARS-CoV-2 detection in patient samples

A single NAA particle was introduced into the reaction tube (Axygen) with 40 µL RT-RPA final product (in the form of dsDNA) and 100 nM preassembled CRISPR-Cas12a ribonucleoprotein for a total volume of 50 µL, which was incubated at 25 °C for 30 min.

Red fluorescence (from rhodamine B release) was measured in a CLARIOstar Plus fluorometer (BMG) after completing the reaction.

5.8. RT-qPCR validation

The TaqPath 1-step RT-qPCR master mix, CG (Applied) was used. In a microplate (Applied), 2 μL patient sample was mixed with 500 nM CDC N1 primers, 125 nM probe (SARS-CoV-2 RUO kit, IDT), and the RT-qPCR mix to achieve a total volume of 20 μL . The microplate was then loaded into a real-time PCR system (QuantStudio 3, Applied), and the following protocol was employed: an initial step of 53 $^{\circ}\text{C}$ for 10 min for RT, 95 $^{\circ}\text{C}$ for 2 min for RT inactivation, followed by 40 cycles of 95 $^{\circ}\text{C}$ for 3 s for denaturation and 60 $^{\circ}\text{C}$ for 30 s for annealing and extension. Samples with cycle threshold (C_T) values lower than 40 were considered positive for SARS-CoV-2 infection.

6. REFERENCES

1. Alberti, S., Soler-Illia, G. J., & Azzaroni, O. (2015). Capabilities of hybrid nanomaterials. *Chemical Communications*, 51(30), 6050–6075.
2. Alvarez, S. D., Li, C. P., Chiang, C. E., Schuller, I. K., & Sailor, M. J. (2009). Reflective colorimetric detection of toxic gases using nanoporous Si photonic crystals. *ACS Nano*, 3(11), 3301–3307.
3. Aznar, E., Oroval, M., Pascual, L., Murguía, J. R., Martínez-Máñez, R., & Sancenón, F. (2016). Nanogated materials in sensing applications. *Chemical Reviews*, 116(9), 561–718.
4. Barrangou, R., Fremaux, C., Deveau, H., Richards, M., Boyaval, P., Moineau, S., Romero, D. A., & Horvath, P. (2007). CRISPR provides acquired resistance against viruses in prokaryotes. *Science*, 315(5819), 1709–1712.

5. Chen, J. S., Ma, E., Harrington, L. B., da Costa, M., Tian, X., Palefsky, J. M., & Doudna, J. A. (2018). CRISPR-Cas12a target binding unleashes indiscriminate single-stranded DNase activity. *Science*, 360(6387), 436–439.
6. Chen, Y., & Pepin, A. (2001). Electrophoretic manipulation of single DNA molecules in nanofabricated channels. *Electrophoresis*, 22(9), 187–207.
7. Fozouni, P., Son, S., de León Derby, M. D., Knott, G. J., Gray, C. N., D’Ambrosio, M. V., Zhao, C., Switz, N. A., Kumar, G. R., Stephens, S. I., Boehm, D., Tsou, C. L., Shu, J., Bhuiya, A., Armstrong, M., Harris, A. R., Chen, P. Y., Osterloh, J. M., Meyer-Franke, A., ... Fletcher, D. A. (2021). Direct detection of SARS-CoV-2 using CRISPR-Cas13a and a mobile phone. *Cell*, 184(2), 323–333.e9.
8. Fuchs, R. T., Curcuru, J. L., Mabuchi, M., Noireterre, A., Weigele, P. R., Sun, Z., & Robb, G. B. (2022). High-throughput CRISPR-Cas13-based diagnostics for viral detection. *Communications Biology*, 5, 325.
9. Ganguli, A., Mostafa, A., Berger, J., Aydin, M. Y., Sun, F., Stewart de Ramirez, S. A., Varela, E., Cunningham, B. T., King, W. P., & Bashir, R. (2020). Rapid isothermal amplification and portable detection system for SARS-CoV-2. *Proceedings of the National Academy of Sciences*, 117(39), 22727–22735.
10. Garrido-Cano, I., Pla, L., Santiago-Felipe, S., Simón, S., Ortega, B., Bermejo, B., Lluch, A., Cejalvo, J. M., Eroles, P., & Martínez-Máñez, R. (2021). Development of a point-of-care biosensor for breast cancer diagnosis. *ACS Sensors*, 6(3), 1022–1029.
11. Gootenberg, J. S., Abudayyeh, O. O., Lee, J. W., Essletzbichler, P., Dy, A. J., Joung, J., Verdine, V., Donghia, N., Daringer, N. M., Freije, C. A., Myhrvold, C., Bhattacharyya, R. P., Livny, J., Regev, A., Koonin, E. V., Hung, D. T., Sabeti, P. C., Collins, J. J., & Zhang, F. (2017). Nucleic acid detection with CRISPR-Cas13a/C2c2. *Science*, 356(6336), 438–442.

12. Hernández-Montoto, A., Aranda, M. N., Caballos, I., López-Palacios, A., Tormo-Mas, M. Á., Pemán, J., Prieto Rodríguez, M., Picornell, C., Aznar, E., & Martínez-Mañez, R. (2023). CRISPR-Cas biosensors in clinical applications. *Advanced Healthcare Materials*, 12, 2203326.
13. Kaminski, M. M., Abudayyeh, O. O., Gootenberg, J. S., Zhang, F., & Collins, J. J. (2021). CRISPR-based diagnostics for infectious disease detection. *Nature Biomedical Engineering*, 5(6), 643–656.
14. Larremore, D. B., Wilder, B., Lester, E., Shehata, S., Burke, J. M., Hay, J. A., Tambe, M., Mina, M. J., & Parker, R. (2021). Test sensitivity is secondary to frequency and turnaround time for COVID-19 screening. *Science Advances*, 7(1), eabd5393.
15. La Flamme, K. E., Popat, K. C., Leoni, L., Markiewicz, E., LaTempa, T. J., Roman, B. B., Grimes, C. A., & Desai, T. A. (2007). Nanostructure-mediated drug delivery for cancer therapeutics. *Biomaterials*, 28(18), 2638–2645.
16. Li, J., Luo, T., He, Y., Liu, H., Deng, Z., Bu, J., Zhong, S., & Yang, Y. (2022). Recent advancements in CRISPR-based diagnostics. *Chemical Communications*, 58(18), 2540–2543.
17. Liu, R., Hu, Y., He, Y., Lan, T., & Zhang, J. (2021). New insights into molecular biosensors and applications. *Chemical Science*, 12(24), 9022–9030.
18. Ma, L., Peng, L., Yin, L., Liu, G., & Man, S. (2021). Recent progress in CRISPR biosensors for disease diagnosis. *ACS Sensors*, 6(10), 2920–2927.
19. Marsal, L. F., Vojkuvka, L., Formentin, P., Pallarés, J., & Ferré-Borrull, J. (2009). Optical sensors using porous materials. *Optical Materials*, 31(6), 860–864.

20. McCarty, N. S., Graham, A. E., Studená, L., & Ledesma-Amaro, R. (2020). CRISPR-based systems for genetic control. *Nature Communications*, 11(1), 1281.
21. Meehan, C. J., & Beiko, R. G. (2014). Genome analysis using bioinformatics. *Genome Biology and Evolution*, 6(3), 703–713.
22. Miller, C. C., & Walker, J. (1924). The distribution of pressure in a fluid flow. *Proceedings of the Royal Society A*, 106(740), 724–749.
23. Mircioiu, C., Voicu, V., Anuta, V., Tudose, A., Celia, C., Paolino, D., Fresta, M., Sandulovici, R., & Mircioiu, I. (2019). Novel methods in drug delivery systems. *Pharmaceutics*, 11(3), 140.
24. Nguyen, B. T. T., Koh, G., Hui, S. L., Chua, A. J. S., Ng, M. M. L., & Toh, C. S. (2009). Enhanced pathogen detection using biosensors. *Analytical Chemistry*, 81(17), 7226–7234.
25. Núñez, R. N., Veglia, A. V., & Pacioni, N. L. (2018). Microchemistry applications in biosensing. *Microchemical Journal*, 141, 110–117.
26. Piepenburg, O., Williams, C. H., Stemple, D. L., & Armes, N. A. (2006). DNA amplification technology. *PLOS Biology*, 4(7), e204.
27. Pla, L., Santiago-Felipe, S., Tormo-Mas, M. Á., Pemán, J., Sancenón, F., Aznar, E., & Martínez-Máñez, R. (2020). Development of novel chemical sensors for pathogen detection. *Sensors and Actuators B: Chemical*, 320, 128281.
28. Rajeev, G., Prieto Simon, B., Marsal, L. F., & Voelcker, N. H. (2018). Healthcare applications of nanomaterials. *Advanced Healthcare Materials*, 7(4), 1700904.

29. Ribes, À., Aznar, E., Santiago-Felipe, S., Xifre-Perez, E., Tormo-Mas, M. Á., Pemán, J., Marsal, L. F., & Martínez-Máñez, R. (2019). Biosensors for point-of-care applications. *ACS Sensors*, 4(5), 1291–1298.
30. Ribes, À., Xifré-Pérez, E., Aznar, E., Sancenón, F., Pardo, T., Marsal, L. F., & Martínez-Máñez, R. (2016). Advanced nanomaterials in medical diagnostics. *Scientific Reports*, 6, 38649.
31. Smith, K. F., Sax, D. F., Gaines, S. D., Guernier, V., & Guégan, J. F. (2007). Ecological perspectives on infectious disease emergence. *Ecology*, 88(8), 1903–1910.
32. St John, A. (2010). Clinical chemistry in the diagnosis of disease. *Clinical Biochemistry Review*, 31(3), 111–119.
33. Sutton, D. H., Conn, G. L., Brown, T., & Lane, A. N. (1997). Structural studies of RNA-protein complexes. *Biochemical Journal*, 321(3), 481–486.
34. Vojkuvka, L., Santos, A., Pallarès, J., Ferré-Borrull, J., Marsal, L. F., & Celis, J. P. (2012). Surface coatings and their applications in biosensing. *Surface and Coatings Technology*, 206(7), 2115–2124.
35. Wen, Y., Xu, L., Li, C., Du, H., Chen, L., Su, B., Zhang, Z., Zhang, X., & Song, Y. (2012). Chemical sensors using nanoporous materials. *Chemical Communications*, 48(50), 8410–8412.
36. Welch, E. C., Powell, J. M., Clevinger, T. B., Fairman, A. E., & Shukla, A. (2021). Multifunctional nanostructured materials. *Advanced Functional Materials*, 31(15), 2104126.

37. Yang, J., Barua, N., Rahman, M. N., Li, C., Lo, N., Yeong, K. Y., Tsang, T. F., Tan, H. S., Hossain, M. S., & Tang, J. W. (2022). Molecular spectrum of infectious diseases. *Microbiology Spectrum*, 10(3), e03260-22.

38. Yang, S., & Rothman, R. E. (2004). Laboratory diagnostics for infectious diseases. *The Lancet Infectious Diseases*, 4(6), 337–348.

39. Zhang, W. S., Pan, J., Li, F., Zhu, M., Xu, M., Zhu, H., Yu, Y., & Su, G. (2021). CRISPR-based viral diagnostics for point-of-care applications. *Analytical Chemistry*, 93(9), 4126–4133.

40. Zhu, N., Zhang, D., Wang, W., Li, X., Yang, B., Song, J., Zhao, X., Huang, B., Shi, W., Lu, R., Niu, P., Zhan, F., Ma, X., Wang, D., Xu, W., Wu, G., Gao, G. F., & Tan, W. (2020). A novel coronavirus from patients with pneumonia in China, 2019. *The New England Journal of Medicine*, 382(8), 727–733.

Acknowledgements

We thank M. C. Marqués (I2SysBio) for her help with preliminary experiments. This work was supported by the grant AP2020-38 (to E. A. and G. R.) from the Universitat de València and Instituto de Investigación Sanitaria La Fe (VLC-Biomed program), the grants PDC2022-133941-I00 (to G. R.) and PID2021-126304OB-C41 (to R. M.-M.) from the Ministerio de Ciencia, Innovación y Universidades and AEI/10.13039/501100011033 (the former co-financed by the NextGenerationEU Fund and the latter by the European Regional Development Fund), and the grants GVA-COVID19/2021/036 (to G. R.) and CIPROM/2021/007 (to R. M.-M.) from the Generalitat Valenciana. G. R. acknowledges support from the CSIC PTI Salud Global (through the NextGenerationEU Fund, regulation 2020/2094) and R. M.-M. from the CIBER, Instituto de Salud Carlos III (group CB07/01/2012). I. C. thanks the Instituto de Salud Carlos III for her predoctoral fellowship (IFI21/00008). A. R.-M. and I. C. have contributed equally to this work.

Competing interests

The authors declare no competing financial interests.

7. SUPPORTING INFORMATION

Figure S117. High-resolution FESEM images to show the change of the NAA surface during the synthesis process. A) S0 material (raw). B) S1 material. C) S2 material. Arrows indicate residues produced upon functionalization with 3-(triethoxysilyl)propyl isocyanate. D) S3 material (final). Windowed area shows a surface region completely covered by the capping oligonucleotides. Scale bars of 200 nm.

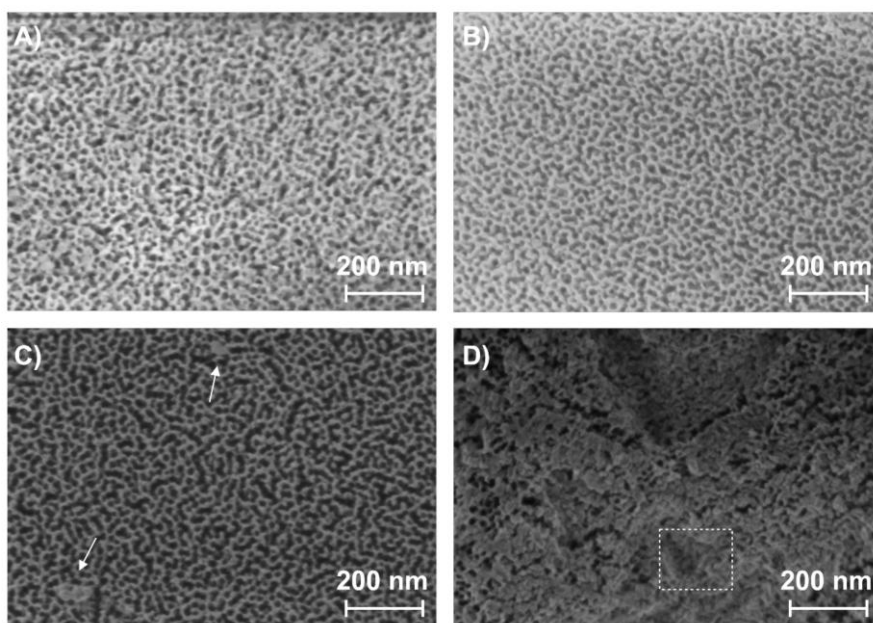


Figure S218. AFM images to show the topography of the different NAA surfaces during the synthesis process. A) S0 material (raw). B) S1 material. C) S2 material. D) S3 material (final).

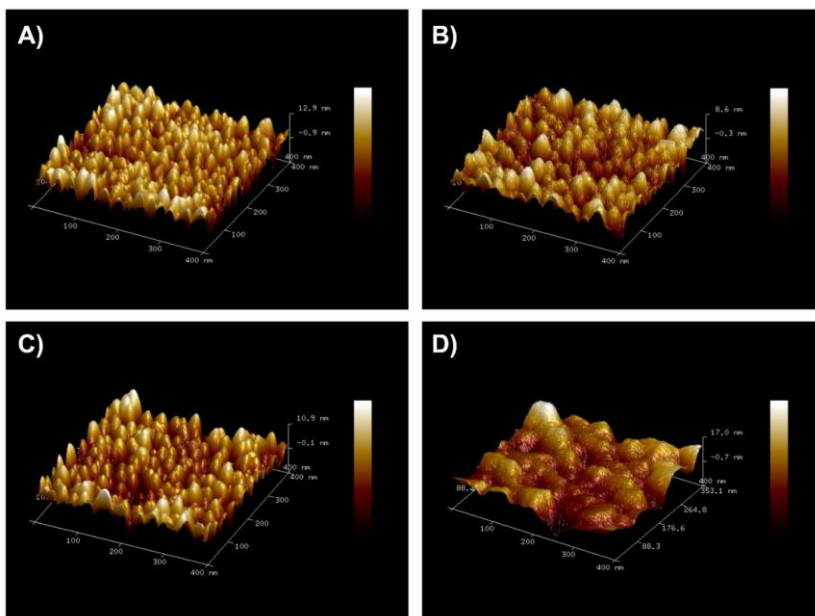


Figure S3. EDXS analysis of the S3 material upon incubation with DNase I. The change in relative weight and atomic composition (with respect to Al) was calculated. One material was incubated with DNase I and another with just buffer A. For all elements, DNase I led to a loss of material.

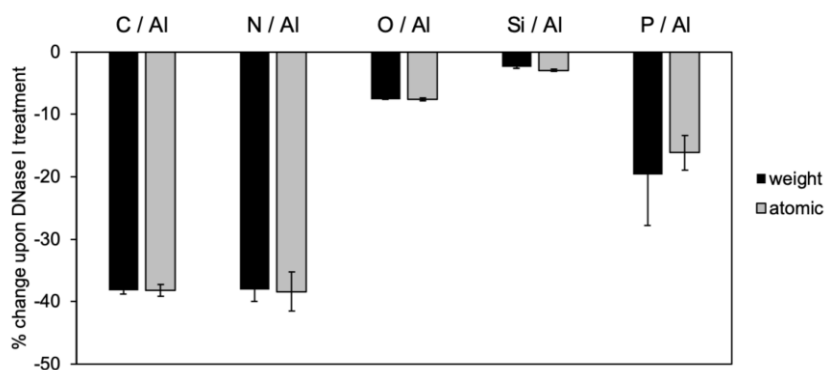


Figure S4. Absolute fluorescence signals of rhodamine B release from the nanostructured material (S3) incubated with CRISPR-Cas12a ribonucleoproteins and synthetic N1 dsDNA molecules (at 25 °C for 60 min). Represented data correspond to means \pm standard errors ($n = 3$). *Statistically significant change (Welch's t-test, $P < 0.05$). AU, arbitrary units.

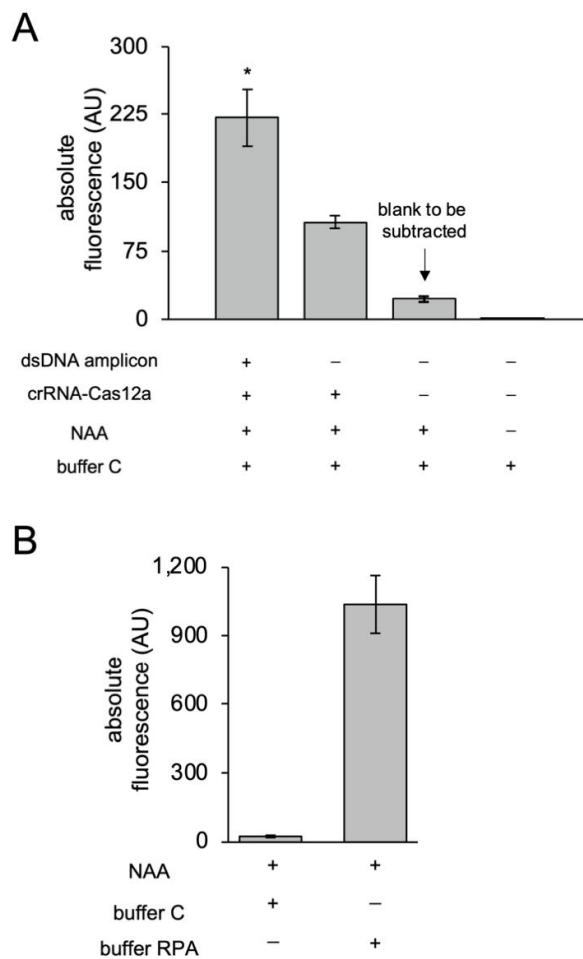


Figure S519. dsDNA amplicon sequences considered in this work. They come from the N (N1 and N2), E, and S genes of SARS-CoV-2. The RPA primers to obtain these products are

GACCCCAAATCAGCGAAATGCACCCCGCA (forward) and GTTCTCCATTCTGTTACTGCCAGTTGAAT (reverse) for N1,

TTACAAACATTGGCCGCAAATTGCACAATTTGC (forward) and GCGCGACATTCCGAAGAACGCTGAAGC (reverse) for N2,

ACAGGTACGTTAATAGTTAATAGCGT (forward) and ATATTGCAGCAGTACGCACACA (reverse) for E, and CGCCAATGTTACTTGGTTCCATGCTATACATGTC (forward) and AGGACAGGGTTATCAAACCTCTTAGTACCAT (reverse) for S.

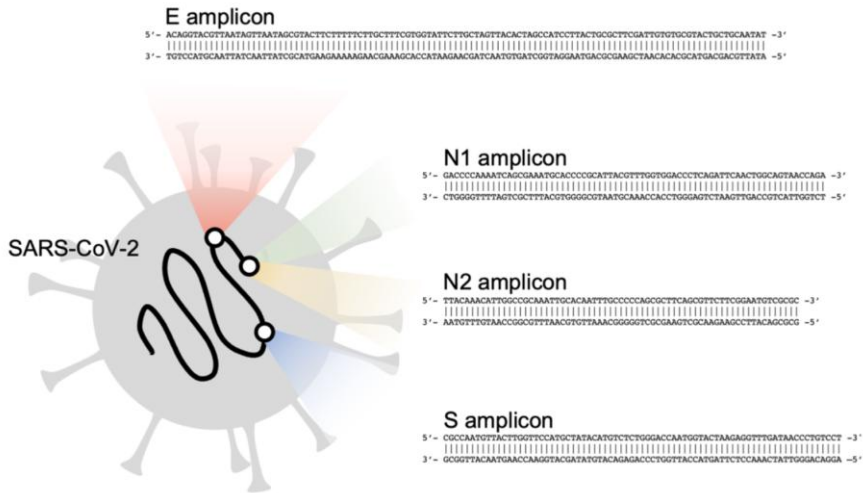
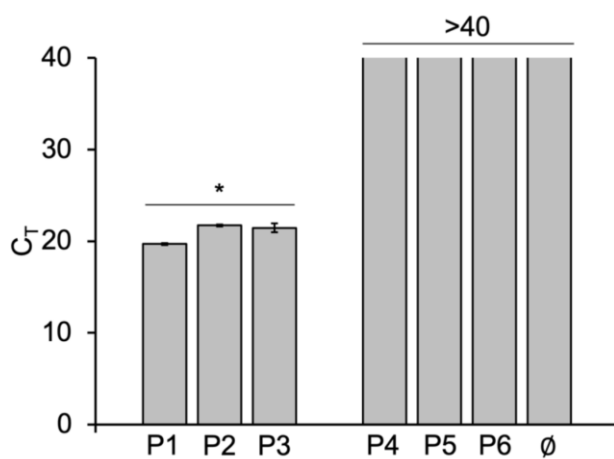
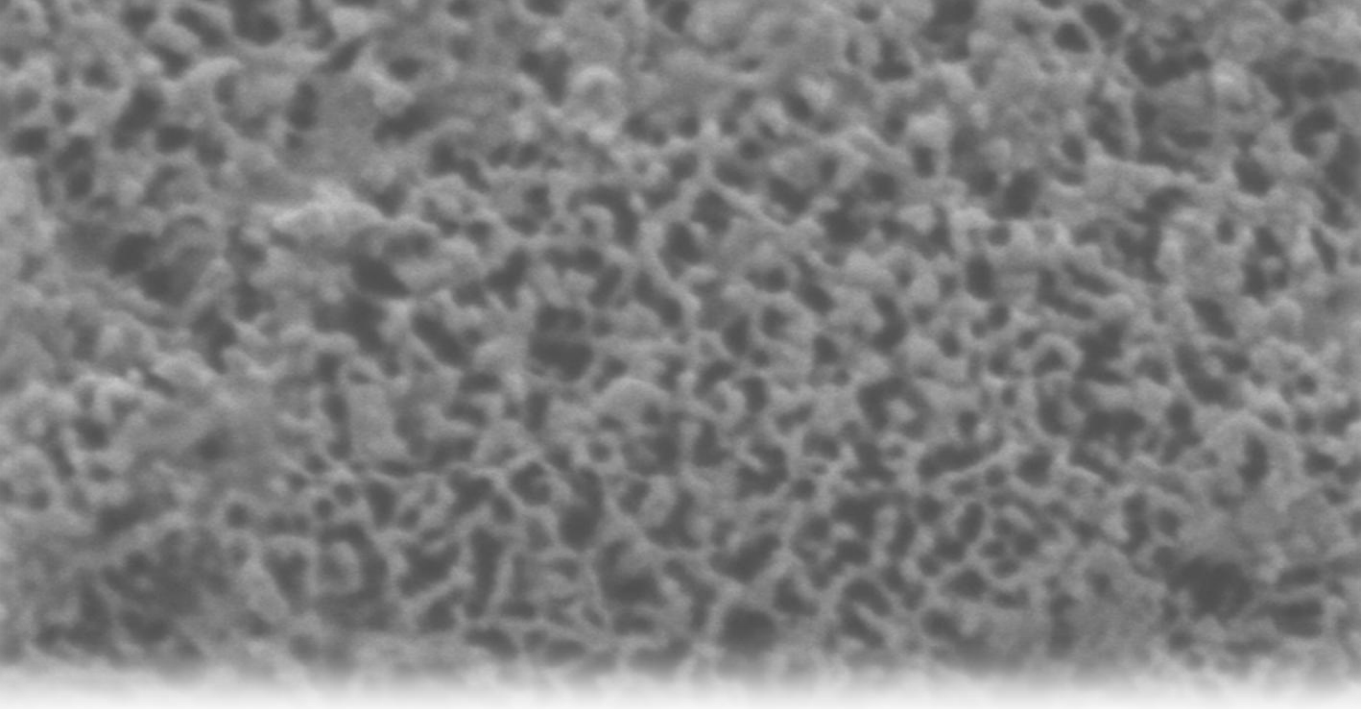


Figure S6. RT-qPCR characterization of clinical samples. Top, cycle threshold (CT) values obtained from clinical samples of different patients. Samples with CT < 40 were considered as positive for SARS-CoV-2 infection. Represented data correspond to means \pm standard errors ($n = 3$, technical replicates from a patient sample). *Statistically significant change (Welch's ttest, $P < 0.05$). Bottom, features of the different patient samples used in this work, including type, targeted region, diagnosis in the hospital, and the CT value obtained in our lab.



Patient	Sample type	Targeted region	Diagnosis (hospital)	C _T (lab)
P1	nasopharyngeal swab	N1	Positive	19.7
P2	nasopharyngeal swab	N1	Positive	21.7
P3	nasopharyngeal swab	N1	Positive	21.4
P4	nasopharyngeal swab	N1	Negative	>40
P5	nasopharyngeal swab	N1	Negative	>40
P6	nasopharyngeal swab	N1	Negative	>40
∅	water	N1		>40



Discussion

**Cover: FESEM image of functionalized NAA (self-produced image)*

The quest for reliable tools capable of rapidly and selectively detecting specific biomolecules remains a critical objective, particularly in fields requiring swift, quantifiable results, such as clinical diagnostics and environmental monitoring. Gated systems have proven highly advantageous, utilizing unique structural and functional characteristics that allow for the efficient loading and controlled release of molecules like dyes, fluorescent indicators, and even therapeutic agents in response to specific analytes. This versatility positions gated systems as highly adaptable tools suitable for a broad spectrum of applications in medicine, agriculture, environmental analysis, and beyond. Among these, nanoporous anodic alumina (NAA) systems have emerged as exceptionally promising platforms for diagnostics, as they offer favorable physicochemical properties such as structural stability, tunable porosity, and ease of functionalization, enabling precise biomolecular recognition.

This PhD thesis has contributed to this rapidly evolving field by designing, synthesizing, and characterizing advanced gated nanodevices based on NAA films that respond selectively to biomolecules through functionalization with various molecular gates. These detection systems share a foundational design: the functionalization of NAA surfaces with DNA, aptamers, antibodies, or CRISPR-Cas systems to achieve highly specific biomolecule detection. This tailored functionalization enables controlled diffusion of encapsulated reporter molecules when target analytes are present, ensuring precise, selective, and sensitive detection.

The thesis addresses critical applications across multiple fields, highlighting the versatility and adaptability of gated NAA systems. For example, the development of a DNA-capped NAA film for detecting *Xylella fastidiosa* DNA is particularly relevant for environmental and agricultural applications. This pathogen poses a severe threat to agriculture globally, affecting crops such as olive, grapevine, and citrus. The high specificity achieved by the DNA-gated NAA material underscores its potential as a practical diagnostic tool for early and selective detection of *Xylella fastidiosa* in ecological

and agricultural settings, providing critical support for pest control and biodiversity conservation.

In the area of infectious disease diagnostics, an aptamer-capped NAA system was developed for the early detection of SARS-CoV-2, enabling a rapid and sensitive response to the virus. This system is designed to detect the virus at low concentrations, offering high sensitivity and selectivity, which is crucial for controlling virus spread during pandemic outbreaks. The potential applications of this system in pandemic preparedness and public health surveillance represent an important advancement in the rapid detection and containment of viral diseases, as it provides a cost-effective, accessible alternative to conventional molecular techniques.

Furthermore, antibody-gated NAA materials were developed to detect *Mycobacterium tuberculosis*, the causative agent of tuberculosis, one of the world's leading infectious diseases. This device exhibited high specificity and minimal non-specific interactions, offering a robust solution for tuberculosis diagnostics that bypasses the limitations of traditional methods, such as the need for complex equipment or extended processing times.

Finally, this thesis explores a cutting-edge approach by integrating CRISPR-Cas technology with DNA-gated NAA for the precise detection of SARS-CoV-2 genetic material. This novel system leverages the exceptional specificity of CRISPR-Cas targeting for oligonucleotide sequences with the signal amplification capabilities of NAA, achieving highly specific and amplified detection of SARS-CoV-2. This combination of CRISPR technology and NAA materials establishes a new paradigm for the detection of viral genetic material, offering a powerful alternative to PCR-based diagnostics that can be adapted to detect a wide variety of genetic targets.

Overall, the gated NAA materials developed in this thesis exhibit multiple advantageous characteristics:

1. **High Versatility:** Each of these systems can be modified to detect a range of bioanalytes, supporting the potential for multiplex detection via functionalization with distinct molecular gates. This modular design could enable simultaneous detection of multiple pathogens or biomarkers in a single assay, vastly enhancing the diagnostic capacity and applicability of these systems for public health and environmental monitoring.
2. **Rapid Response Times:** With response times under one hour, these systems enable faster decision-making than traditional diagnostic methods that often require extended incubation or complex processing steps. This rapid response is crucial for applications where time-sensitive intervention is necessary, such as pandemic outbreak monitoring and agricultural pest management.
3. **Robustness in Complex Matrices:** These systems were rigorously validated in complex sample matrices, including clinical samples, water, and serum, highlighting their stability and effectiveness in real-world applications. The robustness of gated NAA materials in complex environments underscores their potential for deployment in various fields without requiring extensive sample preparation.
4. **Signal Amplification Capacity:** The gated NAA materials offer significant signal amplification, where even minimal analyte presence can trigger substantial dye release, obviating the need for additional DNA amplification or extensive sample manipulation typically required in traditional molecular assays. This amplification ability ensures reliable detection at lower analyte concentrations, supporting applications in early diagnostics and low-biomarker-level scenarios.
5. **Cost-Effectiveness and Accessibility:** The systems developed in this research are designed to be user-friendly and affordable, making them accessible to laboratories and facilities with limited resources. The simplicity of these devices,

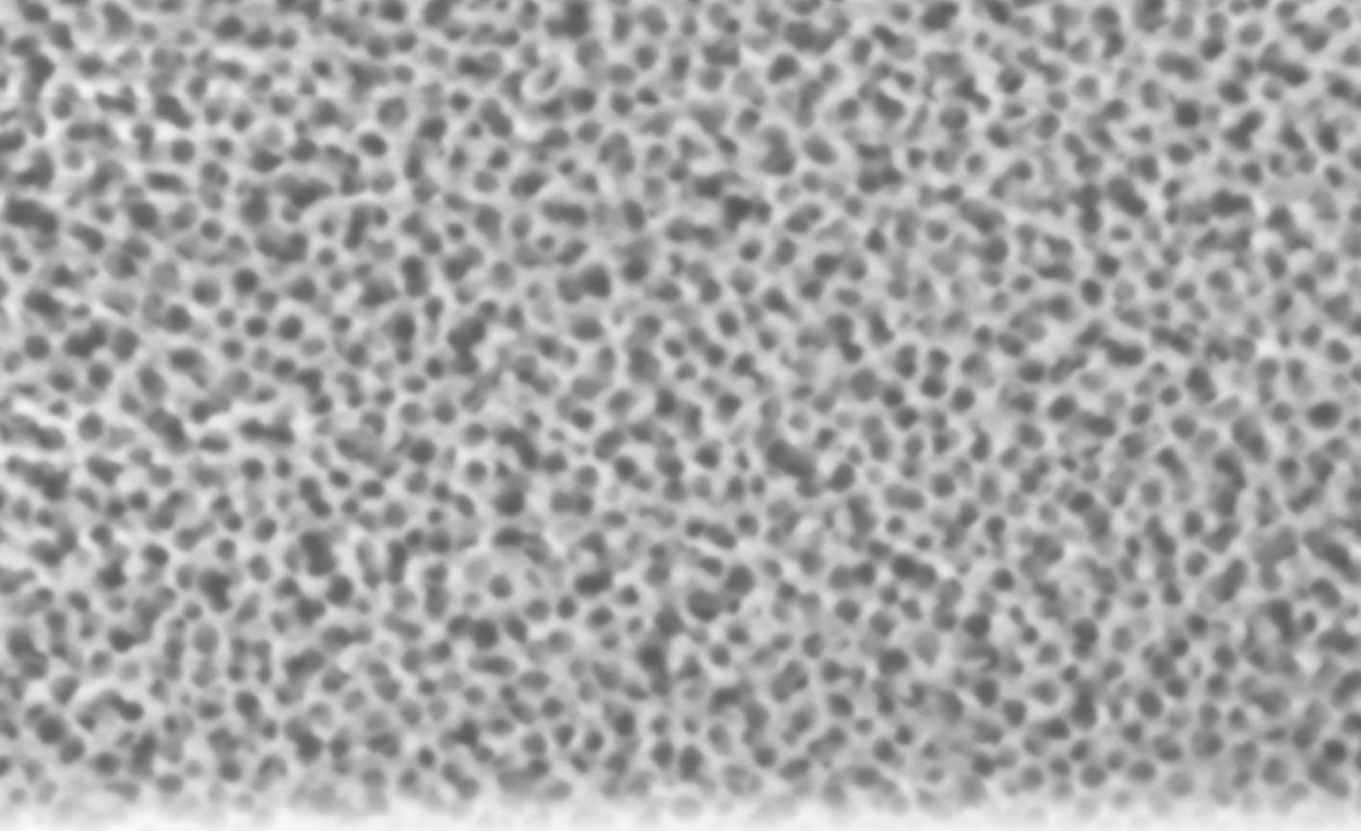
combined with their portability and low equipment requirements, positions them as practical solutions for point-of-care diagnostics and decentralized testing environments.

These achievements underscore the versatility of gated NAA systems, which transcend traditional bioanalytical applications. For instance, in Chapter 1, the DNA-gated NAA system developed for detecting *Xylella fastidiosa* in agricultural settings demonstrates its potential as a diagnostic tool to protect crop health and biodiversity. Chapter 2's aptamer-based device for SARS-CoV-2 detection illustrates the system's relevance to pandemic preparedness. Chapter 3's antibody-gated sensor for *Mycobacterium tuberculosis* offers an effective solution for tuberculosis diagnostics, and Chapter 4's dual-material device for RSV expands the versatility of detection across multiple respiratory pathogens. Chapter 7 integrates CRISPR-Cas with NAA, setting a new standard for precision viral diagnostics.

Looking to the future, the potential for further development and clinical validation of these nanodevices is immense. Clinical trials, optimization for large-scale production, and integration into existing diagnostic workflows will be essential for transitioning these technologies into routine use. These nanodevices could provide scalable, highly sensitive, and rapid alternatives to conventional diagnostic techniques, particularly in resource-limited settings, where cost-effective and accessible diagnostics are crucial.

Future research should also focus on expanding the applications of gated NAA materials to detect other significant pathogens, such as those causing zoonotic diseases or chronic infections. Additionally, improving the multiplexing capacity of these devices to enable simultaneous detection of multiple pathogens would further increase their utility. Efforts to enhance the reusability and storage stability of these sensors could also improve their practicality in diverse field conditions.

In summary, the contributions of this PhD thesis represent an advance in the development of high-performance, versatile, and accessible detection systems. The innovative use of gated NAA materials for the rapid, selective detection of biomarkers and pathogens holds tremendous potential to transform diagnostics in agriculture, medicine, and environmental monitoring. By bridging the gap between complex laboratory diagnostics and user-friendly, cost-effective testing solutions, these nanodevices can play a pivotal role in improving public health, food security, and environmental protection globally.



Conclusions

**Cover: FESEM image of raw NAA (self-produced image)*

This Ph.D. thesis has contributed to the biomedical field by designing new hybrid nanosensors to overcome some of the main limitations in the current methods of pathogen detection. Specifically, the conclusions acquired from this work are:

- I. Selective recognition materials have been successfully developed, each capable of specifically identifying the intended target pathogen.
- II. All materials demonstrated sensitivity comparable to or superior to existing technologies, proving effective in detecting pathogens at low concentrations.
- III. The use of molecular gates (DNA, aptamers and antibodies) enabled a tailored approach for each pathogen, enhancing specificity and minimizing cross-reactivity.
- IV. Each detection system maintained high stability and functionality within complex real-world samples, indicating robustness and reliability in practical applications.
- V. The integration of nanoporous anodic alumina (NAA) as a support material across different sensing systems provided a versatile platform compatible with various biological entities, facilitating adaptation for multiple diagnostic targets.
- VI. The systems developed exhibit rapid response times, allowing for detection in under one hour, which is advantageous for time-sensitive diagnostic and environmental monitoring applications.
- VII. Signal amplification was effectively achieved through controlled release mechanisms, allowing for the detection of minimal quantities of analyte without the need for DNA replication or complex pre-treatments.
- VIII. The materials developed are cost-effective and suitable for non-specialized personnel, making them accessible for widespread use in clinical and field diagnostics.
- IX. Environmental and clinical applications were successfully validated, with specific systems proving applicable for pathogenic detection in plant and human infectious disease diagnostics.

CONCLUSIONS

- X. These advances contribute meaningfully to the fields of molecular recognition and diagnostics, offering portable, sensitive, and adaptable tools that may serve as a foundation for future diagnostic kit development.

Taken together, the results evidence the potential of using gated materials to address unmet diagnostic needs, paving the way for the development of faster, more sensitive, and highly specific sensors that can meet the demands of societies increasingly exposed to emerging pathogens and environmental risks.